

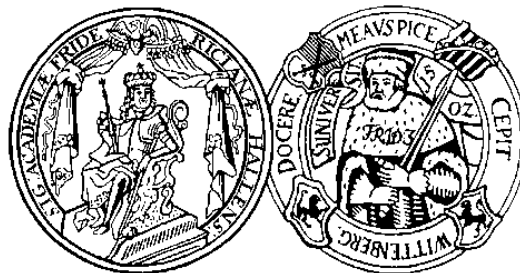
Investigations on the Human Myt1 Kinase: Substrate Studies, Assay Development and Inhibitor Screening

Dissertation

zur Erlangung des akademischen Grades eines
Doktors der Naturwissenschaften
(Dr. rer. nat.)

vorgelegt der
Naturwissenschaftlichen Fakultät I - Biowissenschaften

Martin-Luther-Universität Halle-Wittenberg



von

Alexander Rohe

geboren am 06.11.1985 in Saarbrücken

Gutachter:

1. Prof. Dr. W. Sippl
2. Prof. Dr. M. Schutkowski
3. Prof. Dr. M. Jung

Halle (Saale), 28. August 2013

Tag der Verteidigung: 15. Januar 2014

Durchgeführt am Institut für Pharmazie, Abteilung Medizinische Chemie,
Martin-Luther-Universität Halle-Wittenberg

Gutachter: Prof. Dr. W. Sippl,
Martin-Luther-Universität Halle-Wittenberg

Zweitgutachter: Prof. Dr. M. Schutkowski,
Martin-Luther-Universität Halle-Wittenberg

Drittgutachter: Prof. Dr. M. Jung,
Albert-Ludwigs-Universität Freiburg i. Br.

Table of Contents

Table of Contents	V
Abbreviations and Symbols	IX
List of Figures	XV
List of Tables.....	XVII
1. Introduction.....	1
2. Theoretical Background.....	3
2.1. Kinases	3
2.1.1. From Structure to Molecular Function.....	3
2.1.2. Kinase Inhibition.....	4
2.1.3. Selectivity in Kinase Inhibition.....	8
2.1.4. Kinase Inhibitor Drug Resistance	11
2.2. Myt1, a Wee Family Kinase.....	11
2.2.1. Structural Features	11
2.2.2. Myt1 and its Physiological Role	13
2.2.2.1. Cell Cycle in General and G2/M in Particular.....	13
2.2.2.2. Myt1 in Regulation of Mitotic Entry	16
2.2.2.3. Intracellular Membrane Dynamics and Mitotic Exit	17
2.2.2.4. Checkpoint Recovery and Maintaining G2-Arrest	18
2.2.2.5. Meiosis.....	19
2.2.3. Myt1 as a Potential Drug Target in Cancer Therapy	19
2.3. Target-Based Drug Discovery and Virtual Screening.....	21
3. Aim of the Work.....	25
4. Materials and Methods.....	27
4.1. Devices and Equipment.....	27
4.2. Consumables	28
4.3. Reagents	29
4.4. Buffers and Solutions	34

4.5.	Kinase Preparation	35
4.5.1.	Myt1 (full-length).....	35
4.5.1.1.	Cell Culture	35
4.5.1.2.	Vital Stain and Cell Counting	35
4.5.1.3.	Transfection and Harvesting	36
4.5.1.4.	Isolation of Protein	36
4.5.2.	Myt1 (kinase domain).....	37
4.6.	Statistics and General Data Analysis	37
4.7.	BCA-Assay	38
4.8.	Peptide Quantitation	39
4.9.	SDS-PAGE	39
4.10.	Western Blot.....	40
4.11.	Dot Blot	41
4.12.	TCA Precipitation	41
4.13.	<i>In vitro</i> Kinase Reactions Utilizing Protein Substrates.....	41
4.14.	Fluorescence Polarization: Background and Analysis	42
4.15.	Fluorescence Polarization Immunoassay (FPIA).....	43
4.16.	pTyr FP Immunoassay (FPIA II)	44
4.17.	LanthaScreen Binding Assay	44
4.17.1.	Instrumentational Setup and Data Analysis.....	44
4.17.2.	Tracer Titrations	45
4.17.3.	Inhibitor Studies.....	45
4.18.	Synthesis and Characterization of DasAFITC	46
4.19.	CMC Determination Assays.....	47
4.20.	DasAFITC Assay Procedure	48
4.20.1.	Kinase Concentration and Incubation Time	48
4.20.2.	Kinase Binding Assays	48
4.20.3.	Anisotropy Data Analysis.....	49

4.21.	Microarray Assays	49
4.22.	Solid Phase Peptide Synthesis	50
5.	Results and Discussion	53
5.1.	Substrate Studies	53
5.2.	TR-FRET Based Binding Assay: LanthaScreen	60
5.2.1.	Assay Development: LanthaScreen (Adaption to Myt1).....	60
5.2.2.	LanthaScreen Inhibition Data	63
5.2.3.	LanthaScreen: Limitations and Drawbacks	66
5.2.4.	Docking Studies	68
5.3.	FP Based Kinase Binding Assay: DasAFITC-Assay	70
5.3.1.	Synthesis and Characterization of a Suitable Tracer.....	71
5.3.2.	Assay Development: DasAFITC Assay.....	73
5.3.2.1.	CMC Determination and Assay Buffer	73
5.3.2.2.	Microplates and Tracer Concentration	77
5.3.2.3.	Construction of Binding Isotherms.....	77
5.3.2.4.	Time Dependence and Assay Performance	79
5.3.2.5.	Assay Validation.....	81
5.3.3.	Inhibitor Screening.....	83
5.3.3.1.	Identifying False-Positives: Flavonoids as Examples.....	83
5.3.3.2.	Virtual Screening	85
5.3.3.3.	Glycotriazoles	89
5.3.4.	DasAFITC Assay: Conclusion, Limitations, Drawbacks	89
5.3.5.	Affinity of ATP to Myt1	90
5.4.	Glycoglycerolipids as Myt1 Inhibitors?	92
5.5.	Advanced Substrate Studies	96
5.5.1.	Peptide Microarray Studies	96
5.5.2.	A Homogenous FP Based pTyr Assay (FPIA II).....	101
5.5.3.	Solution Phase Verification of Peptidic Substrates.....	104

6. Summary and Perspectives.....	113
Bibliography	115
Appendix	137
Sequence Alignment and Modeling.....	137
Chemical Structures of Selected Screening Compounds.....	140
DasAFITC: ¹ H-NMR.....	144
DasAFITC: ¹³ C-NMR.....	144
DasAFITC: HR-MS	145
DasAFITC: HPLC	145
Analytics of Peptides Synthesized in this Work: HPLC and MS	146
Top 50 Peptides per Slide from Microarray Experiments	148
MS/MS: Phospho-Peptides	159
Abstract / Zusammenfassung.....	163
Danksagung	165
Publikationen.....	165
Curriculum Vitae	169
Eigenständigkeitserklärung	171

Abbreviations and Symbols

Å	Ångström
Abl1	Abelson murine leukemia viral oncogene homolog 1
Ac	Acetyl
ACE	Angiotensin-converting enzyme
ACN	Acetonitrile
AcOH	Acetic acid
ADP	Adenosine-5'-diphosphate
AP	Alkaline phosphatase
ATP	Adenosine-5'-triphosphate
BCA	Bicinchoninic acid
BCIP	5-Bromo-4-chloro-3-indolyl phosphate
Bcr	breakpoint cluster region protein
BLAST	Basic local alignment search tool
Boc	<i>tert</i> -Butyloxycarbonyl
BSA	Bovine serum albumine
Btk	Bruton's tyrosine kinase
BuOH	Butanol
C	Crosslinking
CAK	Cdk-activating kinase
CAPS	<i>N</i> -cyclohexyl-3-aminopropanesulfonic acid
Cdc	Cell division control protein
Cdk	Cyclin-dependent kinase
CHAPS	3-[(3-Cholamidopropyl)dimethylammonio]-1-propanesulfonate
Chk	Checkpoint kinase
Ci	Curie
CMC	Critical micelle concentration
CV	Coefficient of variation
Cyc	Cyclin
CycA	Cyclin A
CycB	Cyclin B
δ	Chemical shift (NMR)
DBU	1,8-Diazabicyclo[5.4.0]undec-7-ene
DIPEA	Diisopropyl ethylamine
DMEM	Dulbecco's modified Eagle's medium
DMF	Dimethyl formamide

DMSO	Dimethyl sulfoxide
DNA	Deoxyriboneucleic acid
D-PBS	Dulbecco's PBS
DPH	1,6-Diphenyl-1,3,5-hexatriene
DPPA	Diphenyl phosphoryl azide
DTT	Dithiothreitol
ϵ	Molar absorptivity coefficient
EC ₅₀	Concentration at 50% effect
ECL	Enhanced chemoluminescence
EDTA	Ethylendiamintetraacetic acid
EGFR	Epidermal growth factor receptor
EGTA	Ethyleneglycol-bis(2-aminoethyl ether)-tetraacetic acid
EIA	Enzyme immunoassay
ER (cell)	Endoplasmic reticulum
ER (FRET)	Emission ratio
ESI	Electrospray ionization
EtOAc	Ethyl acetate
EtOH	Ethanol
F	Dilution factor (cell counting)
F5M	Fluorescein-5-maleimide
f_b	Bound fraction (FP)
FCS	Fetal calf serum
f_f	Free fraction (FP)
FITC	Fluorescein-5-isothiocyanate
Fmoc	9-Fluorenylmethoxycarbonyl
FP	Fluorescence polarization
FPIA	Fluorescence polarization immunoassay
FRET	Förster resonance energy transfer
5-FU	5-Fluorouracil
G	Gini coefficient
g (centrifuge)	Relative centrifugal force
g (fluorescence)	Quantum yield enhancement factor
G-phase	Gap phase
GAPDH	Glyceraldehyde-3-phosphate dehydrogenase
GGL	Glycoglycerolipid
GK	Gatekeeper
GST	Glutathione S-transferase

HEK	Human embryonic kidney
HEPES	4-(2-Hydroxyethyl)-1-piperazineethanesulfonic acid
HIV	Human immunodeficiency virus
HPLC	High performance liquid chromatography
HR-MS	High resolution mass spectrometry
HRP	Horseradish peroxidase
HSP90	Heat shock protein 90
HTS	High throughput screening
I	Index (microarray read-out)
I_{\parallel}	Fluorescence intensity parallel to the polarization plane of the exciting light
I_{\perp}	Fluorescence intensity perpendicular to the polarization plane of the exciting light
IC_{50}	Concentration at 50% inhibition
IMAC	Immobilized metal ion affinity chromatography
IPTG	Isopropyl- β -D-thiogalactopyranosid
K	Calibration factor (FP)
KBA	Kinase binding assay buffer A
KBB	Kinase binding assay buffer B
K_d	Dissociation constant
K_i	Inhibition constant
K_m	Michaelis constant
LB	Lysogeny broth
M-phase	Mitotic phase
MALDI	Matrix-assisted laser desorption ionization
MAPK	Mitogen-activated protein kinase
MBHA	4-Methyl-benzhydrylamine
MD	Molecular dynamics
MeOH	Methanol
MLU	Martin-Luther-University
MPF	Maturation promoting factor / M-Phase promoting factor
MPLC	Medium pressure liquid chromatography
MS	Mass spectrometry
mTOR	Mammalian target of rapamycin
μ	Arithmetic mean value
Myt1	Membrane-associated tyrosine- and threonine-specific Cdc2-inhibitory kinase

NBT	Nitro blue tetrazolium
NMR	Nuclear magnetic resonance spectroscopy
OD	Optical density
P	Polarization
PAGE	Polyacrylamide gel electrophoresis
Pbf	Pentamethyl-2,3-dihydrobenzofuran-5-sulfonyl
PBS	Phosphate buffered saline
PD	Pyrido [2,3-d]pyrimidine
Pd/C	Palladium on activated charcoal
PDB	Protein data bank
PDGFR	Platelet-derived growth factor receptor
Pin1	Peptidylprolyl cis/trans isomerase NIMA-interacting 1
PKA	Protein kinase A
PMT	Photo multiplier tube
PVDF	Polyvinylidene difluoride
PyBOP	Benzotriazol-1-yl-oxytripyrrolidinophosphonium hexafluorophosphate
QM/MM-GBSA	Quantum Mechanics/ Molecular Mechanics Generalized Born Surface Area
QQ-Plot	Quantile-Quantile-plot
QSAR	Quantitative structure–activity relationship
r	Anisotropy
r_b	Intrinsic anisotropy of bound probe
r_f	Intrinsic anisotropy of free probe
Δr_{\max}	Maximum difference (anisotropy)
Rb	Retinoblastoma-associated protein
RIA	Radio immunoassay
RMSD	Root mean square deviation
RNA	Ribonucleic acid
RNAi	RNA interference
RPM	Revolutions per minute
s	Kinase selectivity score
SD	Standard deviation
SDS	Sodium dodecyl sulfate
SEM	Standard error of mean
σ	Standard deviation
SPPS	Solid phase peptide synthesis

TBS	Tris-buffered saline
tBu	<i>tert</i> -Butyl
TCA	Trichloroacetic acid
TEMED	<i>N,N,N',N'</i> -Tetramethyl ethylenediamine
TFA	Trifluoroacetic acid
TGS	Tris-glycine-SDS
THF	Tetrahydrofuran
TLC	Thin layer chromatography
TRF	Time-resolved fluorescence
TR-FRET	Time-resolved FRET
Tris	2-Amino-2-hydroxymethyl-propane-1,3-diol
Trt	Trityl
TX100	Triton X-100
V	Total volume (cell counting)
VS	Virtual screening
Wee1	Wee1A protein kinase
Z	Arithmetic mean (cell counting)

Proteinogenic amino acids

A - Ala - Alanine	M - Met - Methionine
C - Cys - Cysteine	N - Asn - Asparagine
D - Asp - Aspartate	P - Pro - Proline
E - Glu - Glutamate	Q - Gln - Glutamine
F - Phe - Phenylalanine	R - Arg - Arginine
G - Gly - Glycine	S - Ser - Serine*
H - His - Histidine	T - Thr - Threonine*
I - Ile - Isoleucine	V - Val - Valine
K - Lys - Lysine	W - Trp - Tryptophane
L - Leu - Leucine	Y - Tyr - Tyrosine*

*lower-case 'p' before serine, threonine or tyrosine and their abbreviations denotes phosphorylation.

List of Figures

FIG. 1: GENERAL STRUCTURE OF A KINASE DOMAIN (HERE: MYT1; PDB: 3P1A).....	4
FIG. 2: SCHEMATIC REPRESENTATION OF DASATINIB, A TYPE I INHIBITOR, BOUND TO THE TYROSINE KINASE SRC (A) AND A SCHEMATIC REPRESENTATION OF A TYPE II INHIBITOR BOUND TO THE TYROSINE KINASE SRC (B).	6
FIG. 3: COMPARISON OF THE HYDROPHOBIC BACK POCKETS OF KINASES HAVING A LARGE PHE (A) OR A SMALL THR (B) GATEKEEPER RESIDUE.....	7
FIG. 4: CURRENT UNDERSTANDING OF DIRECT PHOSPHORYLATION-DRIVEN REGULATION OF CDK1/CYCB.	16
FIG. 5: A GENERAL WORKFLOW FOR A TARGET-BASED DRUG DISCOVERY PROCESS.	23
FIG. 6: PHOSPHORYLATION OF CDK1 (A) AND CDK1/CYCB1 (MPF, B) BY THE HUMAN MYT1 KINASE.	54
FIG. 7: ASSESSMENT OF THE ANALYTICAL PERFORMANCE OF BOTH FPIA ANTIBODY SETUPS WITH (A) ANTI-P ^{TYR15} - CDK1-ANTIBODY AND (B) ANTI-P ^{TYR} -ANTIBODY.	55
FIG. 8: RESULTS OF FPIA IN TERMS OF ACCEPTANCE OF PEPTIDIC SUBSTRATES OF MYT1 ^{FL} AND THE KINASE DOMAIN ONLY (MYT1 ⁷⁵⁻³⁶²).	56
FIG. 9: DOT BLOT RESULTS USING ANTI-P ^{THR14} -CDK1 ANTIBODY AS PRIMARY ANTIBODY.	57
FIG. 10: WEE1-SUBSTRATE (A) AND MYT1-SUBSTRATE COMPLEX (B) DERIVED FROM THE LAST SNAPSHOT (50 NS) OF MD SIMULATION.....	59
FIG. 11: TRACER TITRATIONS USING TRACER 236 (A) AND TRACER 178 (B) IN PRESENCE OF COMPETITOR PD166285 OR VEHICLE (DMSO) AT 15 nM MYT1 ^{FL}	61
FIG. 12: DISPLACEMENT CURVE FOR THE POSITIVE CONTROL PD166285 USING THE ESTABLISHED LANTHASCREEEN ASSAY PROTOCOL.....	62
FIG. 13: MYT1 ^{FL} INHIBITOR TITRATIONS WITH DASATINIB (A) AND STAUROSPORINE (B) IN THE LANTHASCREEEN KINASE BINDING ASSAY.....	64
FIG. 14: CHEMICAL STRUCTURES OF PD166285, TYRPHOSTIN AG 1478 AND DASATINIB.	65
FIG. 15: ILLUSTRATION OF SPECTROSCOPIC COMPOUND INTERFERENCE WITH THE LANTHASCREEEN ASSAY.....	66
FIG. 16: GENERAL STRUCTURE OF THE TESTED GLYCOTRIAZOLE SERIES AND TWO SCREENING HITS THEREOF.....	67
FIG. 17: GOLD DOCKING SOLUTION OF COMPOUND PD166285 IN THE BINDING POCKET OF MYT1 (A) AND A SCHEMATIC REPRESENTATION OF THE INTERACTIONS BETWEEN COMPOUND PD166285 AND THE RESIDUES IN THE BINDING POCKET OF MYT1 (B)..	68
FIG. 18: GOLD DOCKING SOLUTION OF DASATINIB IN THE ATP-BINDING POCKET OF MYT1 (A) AND A SCHEMATIC REPRESENTATION OF THE INTERACTIONS BETWEEN DASATINIB AND THE RESIDUES IN THE ATP-BINDING POCKET OF MYT1 (B).	69
FIG. 19: ASSAY PRINCIPLE OF THE DASAFITC-BASED ANISOTROPY KINASE BINDING ASSAY.	70
FIG. 20: SYNTHESIS OF DASAFITC, A FLUORESCHEIN-LABELED DASATINIB-DERIVATIVE.	71
FIG. 21: FLUORESCENCE CHARACTERIZATION OF DASAFITC BY 3D SCAN IN A CONTOUR PLOT (A). EMISSION SCANS AT 330 NM INDICATE THAT DASAFITC HAS INHERENT FRET PROPERTIES (B).	72
FIG. 22: FLUORESCENCE ANISOTROPY (A) AND QUANTUM YIELD (B) CHANGES ON INSERTION OF THE PROBE DASAFITC INTO MICELLES AND THE EFFECTS ON CMC DETERMINATIONS (C, D).	74
FIG. 23: CHANGE IN ANISOTROPY (A) AND FLUORESCENCE INTENSITY (B) UPON KINASE TITRATION.	78

FIG. 24: TIME COURSE OF THE ASSOCIATION OF KINASE TRACER AND MYT1.....	80
FIG. 25: DETERMINATION OF THE Z'-FACTOR: A REPRESENTATIVE RESULT OF A PLATE CONTAINING DASATINIB CONTROLS (N=44) AND VEHICLE CONTROLS (N=44).	80
FIG. 26: EXEMPLARY IC ₅₀ CURVES FOR DASATINIB WITH ABL1 AND BTK.....	81
FIG. 27: IC ₅₀ CURVES FOR IDENTIFIED MYT1 INHIBITORS.....	82
FIG. 28: IC ₅₀ CURVES FOR THE THREE HIT COMPOUNDS DERIVED FROM VIRTUAL SCREENING.	88
FIG. 29: CHEMICAL STRUCTURES OF THREE HIT COMPOUNDS IDENTIFIED VIA VIRTUAL SCREENING.	88
FIG. 30: DISPLACEMENT CURVE FOR ATP OBTAINED IN THE DASAFITC-ASSAY.....	91
FIG. 31: ILLUSTRATION OF THE FULL-LENGTH MYT1 SEQUENCE AND RESPECTIVE FUNCTION OF SELECTED REGIONS. .	94
FIG. 32: TEST OF GGL1 IN THE DASAFITC-BASED BINDING ASSAY.	94
FIG. 33: REPRESENTATIVE WESTERN BLOT RESULTS FOR INVESTIGATIONS ON THE INHIBITORY PROPERTIES OF GLYCOGLYCEROLIPID GGL1 ON FULL-LENGTH MYT1.	95
FIG. 34: NAHTMAN-PLOT FOR MICROARRAYS AS A MEANS OF IDENTIFYING FALSE POSITIVES FROM ANTIBODY CONTROL SLIDES.	98
FIG. 35: ALIGNED DOT PLOTS AND QUANTILE-QUANTILE-PLOTS OF THE NORMALIZED RESPONSE INDEX FOR THE INDIVIDUALLY ASSESSED MICROARRAY CHIPS AFTER INCUBATION WITH WEE1 AND MYT1.....	98
FIG. 36: VENN-PLOT OF POTENTIAL PEPTIDE SUBSTRATES IDENTIFIED IN MICROARRAY EXPERIMENTS FOR WEE1 AND MYT1.....	99
FIG. 37: THEORETICAL CONSIDERATIONS IN TERMS OF MOLECULAR WEIGHT OF THE PROBE IN FP-BASED IMMUNOASSAYS.	101
FIG. 38: FPIA II: TITRATION OF THE FLUORESCENT PROBE WITH ANTIBODY.	103
FIG. 39: TITRATION OF ANTIBODY-PROBE COMPLEXES WITH DIFFERENT PHOSPHO PEPTIDES.	103
FIG. 40: VALIDATION OF SUBSTRATES EFS_HUMAN_302 (A) AND A002-D_747 (B) BY INHIBITION PROFILE. .	108
FIG. 41: SEQUENCE COMPARISON OF A 13-MERIC PEPTIDE DERIVED FROM CDK1 (CDK1 ⁹⁻²¹ , A) WITH A002-D_747 (B) AND EFS_HUMAN_302 (C).	110
FIG. 42: SEQUENCE ALIGNMENT OF CDK2 (PDB CODE 1QMZ), WEE1 (PDB CODE 1X8B) AND MYT1 (PDB CODE 3PIA).....	137
FIG. 43: RMSD PLOTS OBTAINED FROM MD SIMULATION OF WEE1-TY AND MYT1-TY.	137
FIG. 44: INTERACTION OF TY SUBSTRATE RESIDUES (GLN8, LYS9, GLU12, THR14 AND TYR15) WITH MYT1 (A) AND WEE1 (B).	138
FIG. 45: COMPARISON OF THE OVERALL STRUCTURE OF WEE1 (PDB CODE 1X8B) AND MYT1 (PDB: 3P1A).	138
FIG. 46: COMPARISON OF THE BINDING MODE OF DASATINIB IN THE BINDING POCKET OF DIFFERENT KINASES.....	139

List of Tables

TABLE 1: SDS-PAGE: CONSTITUTION OF 12% SEPARATING GELS AND 4% STACKING GELS.	39
TABLE 2: TIME-RESOLVED FLUORESCENCE SETTINGS FOR PERFORMING LANTHASCREEN KINASE BINDING ASSAYS.....	45
TABLE 3: COMPARISON OF MYT1 AND WEE1 CONCERNING SUBSTRATE ACCEPTANCE.....	58
TABLE 4: TEST OF COMMON KINASE INHIBITORS FOR EFFECTS ON HUMAN MYT1 KINASE.....	63
TABLE 5: CMC VALUES OF SELECTED DETERGENTS AND COMPARISON WITH CMC VALUES FROM LITERATURE.	75
TABLE 6: COMPARISON OF K_D ESTIMATIONS BASED ON OBTAINED ANISOTROPY CURVES AND CALCULATED BOUND FRACTION WITH VALUES REPORTED IN LITERATURE.....	79
TABLE 7: DETERMINED INHIBITION PROFILE FOR ABL1 AND BTK, AND COMPARISON WITH LITERATURE DATA.....	81
TABLE 8: INHIBITION PROFILE OF MYT1 OBTAINED BY THE DASAFITC-ASSAY.....	82
TABLE 9: RESULTS FOR FIVE COMPOUNDS SUGGESTED BY VIRTUAL SCREENING.	87
TABLE 10: TESTED GLYCOGLYCEROLIPIDS.	92
TABLE 11: POTENTIAL PEPTIDE SUBSTRATES IDENTIFIED FOR WEE1 IN ALPHABETICAL ORDER.	100
TABLE 12: POTENTIAL PEPTIDE SUBSTRATES IDENTIFIED FOR MYT1 IN ALPHABETICAL ORDER.....	100
TABLE 13: EVALUATION OF POTENTIAL PEPTIDIC SUBSTRATES IN <i>IN VITRO</i> KINASE REACTIONS USING THE FPIA II...	105

1. Introduction

Enzymes are biochemical catalysts and essential regulators of metabolism, differentiation and proliferation of every single cell [1]. Not surprisingly, as one of the largest groups of enzymes [2], kinases play a physiological role of particular importance, and dysfunction of kinases has been associated with various diseases. For example, the chromosomal mutation [(t9;22)(q34;q11)], known as the Philadelphia chromosome, leads to the related fusion oncoprotein Bcr-Abl [3-5]. Deregulated tyrosine kinase activity of Bcr-Abl is the biochemical characteristic of chronic myeloid leukemia (CML) [6-8]. In 2001, approval and introduction of the selective inhibitor imatinib (Glivec[®], Gleevec[®]) was celebrated as the magic bullet against CML [7, 9-10].

However, selective inhibitors are valuable tools not only for correcting pathological states but also for the elucidation of biochemical and cellular functions. Selective inhibition of a kinase is physiologically more meaningful than knockout of the respective kinase gene, e.g. by RNA interference [11-12].

The Wee-kinase family, particularly Wee1 and Myt1, are crucial regulators of the cell cycle and have repeatedly been suggested as potential drug targets [12-15]. Inhibition of these kinases may abrogate cellular protection mechanisms, selectively leading to apoptosis in rapidly proliferating cancer cells.

In 2009, the introduction of the first selective Wee1 inhibitor, MK-1775, offered the possibility of proving this concept [16]. By now, MK-1775 is in phase-II clinical trials [17] and medicinal as well as biological research has progressed significantly because the available inhibitor renders experimental verification of given hypotheses possible (e.g. [18-22]).

In contrast, for Myt1, no selective inhibitors are known. At the beginning of the work described herein, there was hardly any information on compounds affecting Myt1. Two reports mentioned the assaying of some known ATP-competitive kinase inhibitors against Myt1 but the results were contradictory [23-24]. Rational development of selective inhibitors requires profound knowledge on a molecular level. The identification of chemical structures affecting the target protein is a major step to gaining insights into these molecular mechanisms and is prerequisite to realizing substances that provide both potency and selectivity.

Thus, inhibitors are indispensable for assessing the actual biological role and druggability of a given target protein.

2. Theoretical Background

To set the stage, background knowledge about the structure and function of kinases and general ways of kinase inhibition are concisely summarized in the following. Subsequently, the present knowledge on the biological role of Myt1 and the rationale for the development of Myt1 inhibitors are presented.

2.1. Kinases

Genes encoding for kinases comprise one of the largest families within the human genome [2] and, altogether, 539 kinase genes are known so far [25]. Functionally, kinases catalyze the transfer of the γ -phosphate group of ATP to a given acceptor group. Protein kinases, for instance, use serine, threonine, tyrosine or histidine residues as acceptor groups (throughout this thesis, the term 'kinases' equals 'protein kinases'). Phosphorylation can affect proteins in a number of ways: It acts as a means of activation or inactivation, alters binding to other proteins, or changes subcellular localization. Through the activity of the kinases' counterparts, the phosphatases, this process is fully reversible, giving this post-translational modification a switch-like character [26]. Therefore, kinases are involved in intertwined networks and feedback loops, most often in a redundant manner, to control cellular functions [27-28].

2.1.1. *From Structure to Molecular Function*

Besides functional aspects, the molecular structure within the kinase family is also very similar. As an example, the crystal structure of the catalytic domain of the Myt1 kinase (PDB: 3P1A) is shown in Fig. 1.

The kinase domain of any kinase consists of two lobes: an N-terminal lobe, mainly consisting of β -sheets, and a C-terminal lobe, dominated by α -helical structure elements. Both parts are linked via a hinge region containing the binding motif for the adenine moiety of ATP. The carbohydrate core and the phosphate groups are coordinatively locked into position by a divalent magnesium ion and a conserved lysine residue [29]. Features differing between kinases, such as the gatekeeper residue and other non-conserved regions, are of major importance for kinase inhibition and will be discussed in more detail in the following sections.

As a further general kinase feature, an activation loop containing the conserved DFG-motif is of major importance for the actual catalytic mechanism.

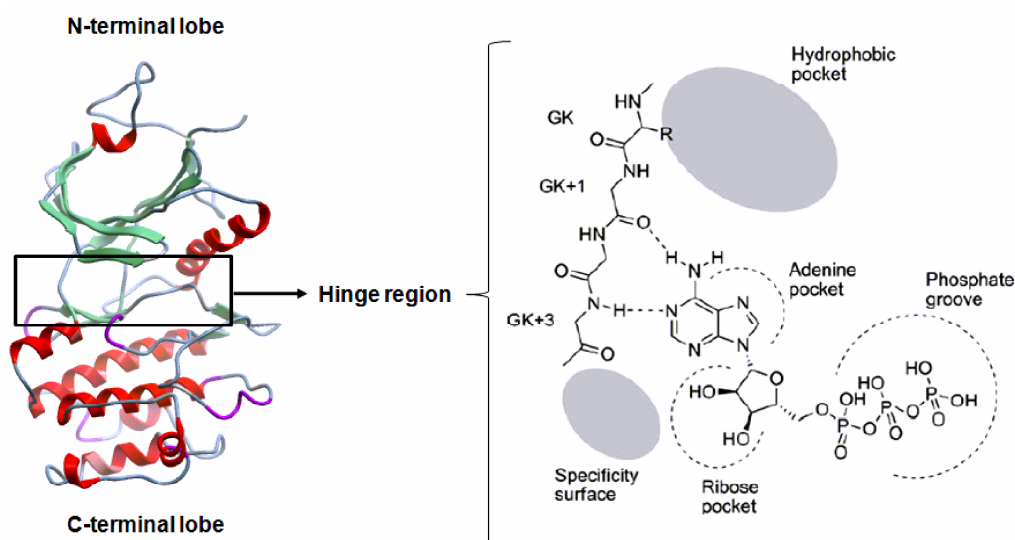


Fig. 1: General structure of a kinase domain (here: Myt1; PDB: 3P1A). On the left, the two lobes can be seen, connected via a hinge region that is responsible for ATP binding as shown exemplarily on the right in the Traxler model [30]. GK: Gatekeeper residue. Grey shading indicates non-conserved regions. Adapted with permission from [31]. Copyright 2010 American Chemical Society.

Insights into the catalytic course of events of phosphoryl transfer were gained by structural elucidation of the catalytic subunit of protein kinase A (PKA) in complex with ADP, magnesium ions, aluminium fluoride and substrate peptide [32]: The aluminium fluoride in its planar geometry forms a trigonal bipyramidal coordination with the oxygen atoms of the donor and acceptor groups, mimicking the transition state of an actual phosphoryl transfer.

The aspartyl residue of the DFG-motif coordinates a magnesium ion that, in turn, coordinatively adjusts the phosphate groups of ATP. The recipient hydroxyl function, as a nucleophile, attacks the γ -phosphate group of ATP, which, when transferred, passes through a trigonal bipyramidal transition state. Other amino acid residues in the active site help increase the nucleophilicity of the initial attacking acceptor functionality, such as a further conserved aspartate residue that may aid by deprotonating the substrate hydroxyl function [33]. Taken together, the reaction rate is increased by orders of magnitude so that the requirements of a switch-like regulation can be met.

2.1.2. Kinase Inhibition

Generally, there are three ways to inhibit a kinase:

- Substrate-site targeting inhibitors disrupt the protein-protein interaction between the kinase and its direct downstream target. Historically, there has been a problem in obtaining druglike, small molecule substrate mimetics,

since these protein-protein binding sites are usually solvent-exposed and rather featureless surface patches [34]. Notwithstanding, some successful examples of substrate-site ligands were reported in the literature (e.g. [35-36]). These inhibitors usually provide only micromolar potency. However, since they do not need to compete with millimolar levels of ATP inside the cell but with rather low concentrations of protein substrates, acceptable *in vivo* potency can arise from surprisingly low levels of affinity compared to ATP-competitive inhibitors [37].

- Allosteric inhibitors, sometimes referred to as type III inhibitors, target a site different from substrate or co-substrate binding site, even though they may bind in spatial proximity to it (reviewed in [38]). So far, there are relatively few examples of allosteric inhibitors, but there has been a consistent effort to develop such inhibitors [39].
- ATP-competitive inhibitors displace the co-substrate from its binding site.

The majority of the small-molecule inhibitors that have been developed target the ATP binding site, including all approved and marketed kinase inhibitors (as of July 2013). With respect to the conformation adopted by the conserved DFG-motif that controls the kinase activation state [33], ATP-competitive inhibitors can be further divided in two subgroups: type I and type II inhibitors. Type I inhibitors target the active kinase conformation, where the aspartate residue in the DFG-motif faces the ATP-binding cleft while the phenylalanine residue is buried in a hydrophobic pocket adjacent to this site ('DFG-in' conformation) [31]. Type I inhibitors tend to participate in similar interactions as the adenine ring of ATP and form 1-3 hydrogen bonds with the backbone amides of the hinge region. Since all kinases utilize ATP as a co-substrate, affinity and selectivity have to be achieved through specific interactions with hydrophobic pockets adjacent to the ATP-binding site [40].

Due to the inherent necessity to bind ATP, the active DFG-in conformation is very similar among kinases. Type II inhibitors target inactive conformations, which are more heterogeneous in nature [41].

Usually, in this inactive conformation, the DFG-motif is in a flipped orientation relative to the active form, with the phenylalanine residue rotated almost 180° and the aspartate side chain facing out of the active site ('DFG-out'), blocking access

of ATP. This rearrangement opens up an additional hydrophobic pocket that is addressed by type II inhibitors. Additionally, a characteristic set of hydrogen bonds with a conserved glutamate in the α C-helix and the backbone amide of the aspartate in the DFG-motif is often observed [31]. Exemplary binding modes as obtained for the tyrosine kinase Src are displayed in Fig. 2.

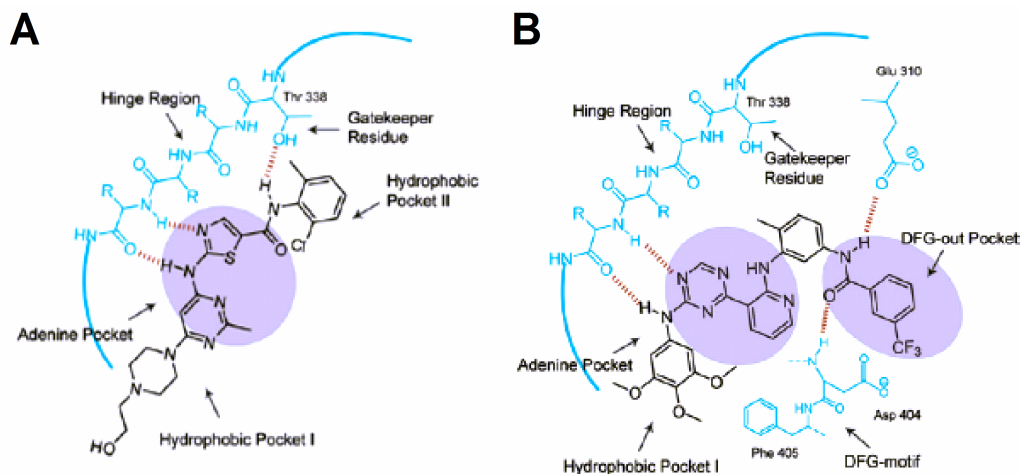


Fig. 2: Schematic representation of dasatinib, a type I inhibitor, bound to the tyrosine kinase Src (A). The adenine pocket is shown shaded. Dasatinib forms an additional hydrogen bond with the Thr gatekeeper residue in Src. On the right (B), a schematic representation of a type II inhibitor bound to the tyrosine kinase Src is shown. Two hydrogen bonds are formed with the hinge region of the kinase. The characteristic hydrogen bonds with the conserved glutamate residue in the α C-helix and the amide backbone of the aspartate of the DFG-motif are shown. The DFG-out pocket is shaded. Adapted with permission from [31]. Copyright 2010 American Chemical Society.

Type I inhibitors occupy the adenine pocket in the ATP binding cleft and form the typical hydrogen bonds with the amide backbone of the hinge region. For type II inhibitors, two hydrogen bonds with the hinge region of the kinase are formed. In addition, a characteristic set of hydrogen bonds with the conserved glutamate residue in the α C-helix and the amide backbone of the aspartate of the DFG-motif is typically formed. The DFG-out pocket that is generated by the movement of the phenylalanine residue of the DFG-motif is exploited by the inhibitor [31].

Although there are no experimental techniques that allow for determination of the relevant intracellular kinase conformations, the available crystal structures highlight the plasticity of the kinase active site and suggest the existence of a dynamic equilibrium [42].

Also, further addressable inactive kinase conformations have been reported, for instance the α C-helix-out conformation observed for EGFR in complex with lapatinib. This conformation retains the generally active DFG-in form but leads to inactivation by rotating and shifting the α C-helix outwards, revealing an additional pocket [43-44].

Like type I inhibitors, type II inhibitors usually form hydrogen-bonding interactions with the amide backbone of the hinge region and hydrophobic contacts with the adenine site. Currently, the number of kinases that are able to adopt the DFG-out conformation is not known, but for kinases structurally characterized in this conformation, the orientation of the DFG-motif is highly conserved [31]. Type II compounds typically have a lower dissociation constant (k_{off}) with extended residence time, which has a favorable impact on kinase inhibition [45-46].

However, drawing a distinction between type II and allosteric inhibitors is sometimes difficult, since even inhibitors that bind outside the ATP site can be ATP-competitive in kinetic studies. Compounds that bind to inactive states can be either ATP-competitive or uncompetitive depending on their binding mode. For example, lapatinib extends into the ATP region and is therefore considered type II, while other DFG-out and α C-out ligands do not reach the ATP site and have been described as allosteric [47].

Another approach for the general design of kinase inhibitors has been proposed by ZUCCOTTO et al., so called type I 1/2 inhibitors [48] (see Fig. 3). These inhibitors recognize the target kinases in their DFG-in conformation and, at the same time, extend to target the back cavity, establishing a defined set of conserved interactions with those residues characteristic for the type II design (DFG-out).

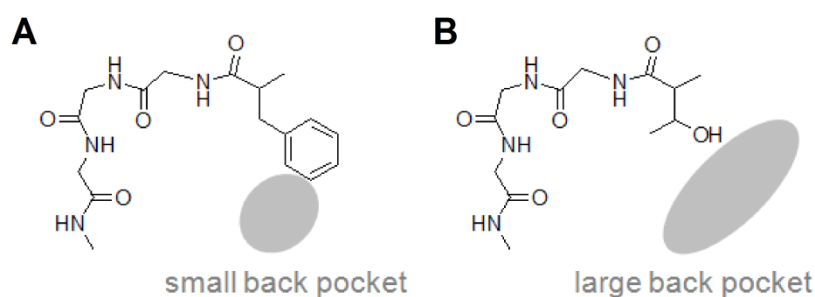


Fig. 3: Comparison of the hydrophobic back pockets (shaded) of kinases having a large Phe (e.g. Cdk2, A) or a small Thr (e.g. Myt1, B) gatekeeper residue. The size of the gatekeeper limits the dimensions of the back pocket. Figure adapted from ZUCCOTTO et al. [48] with permission. Copyright 2010, American Chemical Society.

The back cavity is mainly hydrophobic and is not occupied by the native cosubstrate ATP. Its size and shape are primarily controlled by the gatekeeper residue which is the first residue of the hinge region, connecting the C- and N-terminal lobes. If the gatekeeper is small, e.g. threonine, the side chain no longer limits the size of the cavity which expands towards β -sheet 5 and the α C-helix [48].

For targeting kinases with a small gatekeeper, it is clear that the exploitation of this cavity will increase affinity (i.e. potency) as well as selectivity. In contrast, those kinases having a large gatekeeper residue, e.g. phenylalanine, will have a much smaller back cavity which makes it more difficult to gain affinity there. Approximately 23% of all kinases have small gatekeeper residues with threonine being the most abundant one (18%), indicating the potential in terms of gaining selectivity [29]. In part, also mid-sized gatekeepers allow the occupation of the back cavity. For example, for methionine as a gatekeeper, it has been reported that its flexible side chain may move, hence opening the back pocket which can then indeed be targeted [49].

The first evidence that the back cavity can be exploited by an inhibitor was provided by TONG et al., who solved the crystal structure of mitogen-activated protein kinase 14 (MAPK14) in complex with an analogue of the highly potent inhibitor SB203580 and found the back cavity to be occupied [50-51]. Also other inhibitors, e.g. dasatinib, target this area.

The gatekeeper may also play a relevant role in general type II inhibition, as it might control which kinases can access the DFG-out conformation. Most kinases observed in DFG-out state have a small gatekeeper residue, particularly the Thr residue [48] which can be used as one of a number of means to introduce selectivity to kinase inhibition.

2.1.3. Selectivity in Kinase Inhibition

The term 'selectivity' is usually understood as the ratio of K_i or IC_{50} values for different kinases [52]. Having in mind that more than 500 kinases have been found, this measure does not seem to be suitable. To get a first impression of the inhibition pattern over the entire kinome, kinase dendrograms are often used but quantification remains difficult [2]. Mainly, two other measures have emerged and prevailed to quantify selectivity: The kinase selectivity score s ($0 \leq s \leq 1$, with 1 being completely unselective and values close to zero indicating selective inhibitors) [53] and the Gini coefficient G ($0 \leq G \leq 1$, with 0 being completely unselective and increasing selectivity as G approaches unity) [52]. These values give an overall idea of selectivity but they do not take into account the pattern of selectivity of a compound for a kinase family or subset [54]. Therefore, selectivity has to be considered on a case-by-case basis.

Defining and measuring inhibitor selectivity has become a critical activity both in the development of new drugs and the application of inhibitors as research tools for biological studies [54]. While research initially focused on specificity or high selectivity for therapeutic use, clinical experience and a growing understanding of kinase biology have indicated that compounds with a broader spectrum can be even more effective [34, 55].

However, selectivity is still important, as off-target kinase inhibition may cause additional toxicity [56-57]. Moreover, inhibitors that are used as biochemical research tools to understand biological systems should be as selective as possible to elucidate the actual function of the target kinase [58]. Measuring the selectivity and understanding the common features of kinase inhibitors may reinforce the development of less promiscuous agents or at least offer the possibility of prioritizing hits from library screening with regard to scaffolds with greater potential for a high degree of selectivity [59-60].

Besides efforts to assess inhibitor selectivity by simple chemical descriptors [61] or physical properties [62], more target-based, rational approaches have gained a lot of attention [63]:

- Shape complementarity between ligands and receptors is a fundamental aspect of molecular recognition and can be used to gain selectivity through specific interactions, even if only a single residue differs among closely related kinases [64].
- Electrostatic complementarity is a more complex concept but has also proven key in introducing selectivity, e.g. for the tyrosine kinases' counterpart, the tyrosine phosphatases [65].
- Explicit water molecules bound at the target site can provide key differences even in cases where the binding sites are highly similar [66]. For instance, these differences in water molecule locations, energetics, or both were able to explain experimentally observed kinase selectivity among Src kinases [67].
- Exploitation of allosteric pockets and non-competitive binding is a very promising concept and some examples have been described (e.g. [46, 68]). Among the best known allosteric inhibitors are MEK inhibitors, e.g. CI-1040, many of which are highly selective because of the uniqueness of

their binding site [69]. However, the approach is hampered by the inability to correctly predict such an inhibition and a general lack of examples in the PDB [34]. So far, there are no examples of predicting allosteric sites that were later confirmed experimentally [63].

- Conformational selection and flexibility is probably the most widely used approach to gain selectivity in kinase inhibitor development [11, 70].

The key notion for the latter is targeting of the inactive kinase state as described in the last section. While all kinases have the DFG-containing activation loop, the transition to the inactive DFG-out state has not been observed for all kinases, thereby offering a potential mechanism to gain selectivity. Generally, for inactive kinases, less is known about these conformations, so designing inhibitors becomes more of a challenge [42, 71].

At least for the Abl kinase, it was proposed through *in silico* modelling and, subsequently, experimentally shown that the incorporation of a large, lipophilic trifluoromethylbenzamide group at certain positions of known active conformation inhibitors can transform them into inhibitors binding the inactive conformation [72]. The relation between type I and type II inhibitors is clear, as the type I pharmacophore is a subset of the type II pharmacophore and they both display the same interactions in the adenine region of the ATP binding site [48].

Furthermore, a computational approach has been described to convert DFG-in kinase structures to the DFG-out form [73]. This method provides a chance to identify type II inhibitors in cases where only active kinase states are available as a crystal structure, although general energetic accessibility of the converted structure was not taken into account and has to be assessed individually.

However, the common belief that type II inhibitors are more selective does not hold true in every case [74].

Generally, the type II selectivity advantage may partly arise from the fact that not all kinases can adopt the required conformation. Aurora kinase inhibitors that preferentially bind active or inactive conformations have been described as showing good selectivity, suggesting that both conformations offer unique motifs that can be exploited [75]. However, a comprehensive analysis of kinase inhibitor selectivity confirmed a general trend that type II inhibitors are more likely to be selective than type I inhibitors, although a type II binding mode does not guarantee high selectivity, nor is it required [76]. In fact, some type I inhibitors

(e.g. tofacitinib) were as selective as any of the type II inhibitors, whereas some type II inhibitors (e.g. AST487) were among the least selective compounds [76].

2.1.4. Kinase Inhibitor Drug Resistance

As kinases have become increasingly more prevalent as drug targets, significant success has been achieved in targeting kinases involved in cancer. In many cases, clinical success has been shown to exist only within a narrow time frame. As most kinase inhibitors exert their effects by targeting a specific kinase or set of kinases, there is strong selective pressure for the development of mutations that prevent drug binding [42]. This problem is of particular importance when targeting inactive kinase conformations because they show a distinct susceptibility to loss of inhibitor sensitivity due to mutations. In active kinases, a mutation that prevents binding of an inhibitor will often cause loss of affinity towards ATP and abolish the kinase activity. In inactive kinase conformations, however, inhibitors bind to residues that are not necessarily involved in ATP binding. Mutations at these positions can cause loss of inhibitor sensitivity while remaining a functional kinase [54, 77]. As an example, an alteration of the Bcr-Abl gatekeeper residue (T315I), attributed to gene mutation, can cause complete loss of imatinib sensitivity [78]. There is a limited spectrum of mutations that are available to a kinase for developing resistance due to the necessity of maintaining the catalytic activity. The gatekeeper is not directly involved in ATP recognition so mutations do not affect the catalytic activity while the shape of the binding pocket is changed, preventing the inhibitor from binding. In order to overcome drug resistance caused by mutations, second-generation kinase inhibitors were developed that inhibit most of the resistant kinase mutants (e.g. nilotinib in case of imatinib resistance [79-80]).

2.2. Myt1, a Wee Family Kinase

In the following, the Myt1 kinase will be introduced. Starting from structural features and comparison to its closest relative, Wee1, the current knowledge concerning the physiological role of Myt1 will be discussed, finally leading to the rationale of utilizing Myt1 as a potential drug target.

2.2.1. Structural Features

In humans, the Wee kinase family consists of three kinases: Myt1 and two Wee1 kinases (Wee1, Wee1B). Both Wee1 kinases differ in temporal and spatial

expression and, in somatic cells, only Wee1 appears to be relevant [81]. Therefore, Wee1B is excluded in the following and only Wee1 and Myt1 are meant by the term 'Wee kinases'.

The central kinase domain of Wee kinases is atypical. Although tyrosine kinase activity for Wee1 and Myt1 is undisputed [82-83], sequence similarity searches do not place them in any of the tyrosine kinase subfamilies [84] and comparison with the full kinome led to formation of a separate kinase family consisting of these two kinases [2].

Overall, Wee kinases display a standard two-lobed kinase fold (as described in Section 2.1.1.). The active site region contains a catalytic segment that includes the essential catalytic aspartate (Wee1: Asp426, Myt1: Asp233) and the activation loop which provides a substrate binding platform and can undergo conformational changes to control the activation state (*vide supra*). Since the residue preceding the catalytic aspartate is not an arginine but rather nonpolar (Wee1: Met425, Myt1: Leu232), it has been suggested that Wee1 kinase does not need to be activated by phosphorylation of the activation loop [33, 85] and the same can be assumed for Myt1.

Sequence alignment of Wee family members of various species suggests several structurally conserved features across the whole kinase domain [85]. Superimposition studies for Wee1 revealed the closest structural matches to be Ser/Thr kinases, including the active forms of Cdk2 and Chk1. Notably, a tyrosine kinase is not encountered until the 14th hit [85]. Due to lack of structural data at that time, Myt1 was not included in the study. In addition to structural studies, also the sequence is more closely related to Ser/Thr kinases than to Tyr kinases, as illustrated by a simple BLAST comparison of catalytic kinase domains [85-86]. Taken together, Wee kinases may have evolved from Ser/Thr kinases and a few key mutations may have converted them to functional Tyr kinases [85]. This hypothesis is supported by the fact that Myt1, as a dual-specific kinase, has been observed to phosphorylate Tyr and Thr residues alike [83, 87].

Both Wee kinases target the same site, the glycine rich loop of Cyclin-dependent kinase 1 (Cdk1). Wee1 acts specifically to phosphorylate Tyr15, while Myt1 is dual-specific for Tyr15 as well as Thr14 [82-83, 87]. Considering the close relationship, where does the difference in substrate specificity come from? For Tyr15 phosphorylation, the features that allow correct orientation are given in

both Wee kinases. A single differing residue in their glycine-rich loop may account for the Thr kinase activity of Myt1 [85]: Thr14 modification requires the substrate to approach the glycine-rich loop of the phosphorylating kinase more closely. In Wee1, Glu309 at the tip of this loop may inhibit a closer approach in the same way that phosphorylation of Cdk1 is believed to interfere with substrate binding through steric hindrance [88]. Corresponding to Glu309 in Wee1, the Ser120 residue in Myt1 is less bulky and does not cause electrostatic repulsion as does the negative charge of the glutamate side chain. Therefore, in contrast to Wee1, a closer substrate approach is realized that may make effective threonine phosphorylation possible.

2.2.2. *Myt1 and its Physiological Role*

To understand the physiological role of Myt1, the cell cycle, particularly the transition from G2- to M-phase and its regulation will be introduced. Subsequently, Myt1 and its intracellular functions will be discussed in more detail, from its classical understanding as a Cdk1 regulatory kinase, to more recent insights covering Golgi fragmentation and checkpoint recovery. However, these sections only cover regulations carried out *by* Myt1. How Myt1 itself can be regulated and how all its functions can be meaningfully combined remains rather unclear.

Without knowing the resulting effects, Myt1 interacts with Pin1 [89], but only after Cdk1/CycB catalyzed phosphorylation [90]. Myt1 is an indirect downstream target of Mek1 [91] and a direct target of Plk1 (Polo-like kinase 1) [92]. Additionally, Myt1 appears to be a HSP90 client [93], since inhibition of HSP90 destabilized Myt1 [94]. In starfish (*Asterina pectinifera*) as well as mammals, Myt1 activity is downregulated by Akt-dependent phosphorylation [94-95].

For now, all of these findings stand for themselves and research has not succeeded in generating a meaningful combination of this data.

2.2.2.1. *Cell Cycle in General and G2/M in Particular*

Myt1 acts as a cell cycle regulating kinase. The cell cycle is organized into a series of intertwined pathways, whereby the initiation of each event depends upon successful completion of previous events [96]. Cell division (mitosis) starts the cycle, subsequently, the cells either go into a resting phase (called G0) or a presynthetic (gap) phase (called G1), in which enzyme production occurs in preparation for *de novo* nucleic acid synthesis. Production of DNA then occurs in

an S-phase (synthesis). The S-phase is followed by another gap-phase (G2), in which RNA, critical proteins, and the mitotic spindle apparatus are generated for the next mitotic (M) phase [97].

This ordered progression is guarded by cell cycle checkpoints, i.e. mechanisms by which the cell actively halts progression through the cell cycle until it is ensured that earlier processes, such as DNA replication or mitosis, are completed [98]. In response to endogenous and exogenous sources of DNA damage, these mechanisms are indispensable for maintaining genomic integrity [99]. Activation of DNA damage checkpoints is enabled by recognition of DNA-damage by sensors, followed by an ordered activation of upstream kinases (ATM/ATR) and effector kinases (Chk1/Chk2), the latter of which can directly target the major cell cycle machinery [100]. A cell cycle arrest or delay upon DNA damage can be induced intra S-phase and at the transitions from G1 to S and from G2 to M-phase [100].

The decision to enter mitosis primarily depends on the activity of Cyclin-dependent kinase 1 (Cdk1). Cyclin-dependent kinases are catalytically inactive in their monomeric forms and their concentrations remain quite constant throughout the cell cycle [101-102]. Association with activators (cyclins) leads to heterodimeric active kinase complexes that can phosphorylate hundreds of downstream targets [103-104]. Cyclins are proteins that oscillate in synchrony with the cell cycle, thereby regulating the activity of the respective Cdk exactly as needed for proper cell cycle progression. In mammalian cells, A- and B-type cyclins are synthesized and degraded around the time of mitosis and are regarded as mitotic cyclins. Importantly, Cyclin B accumulation and degradation occurs slightly later than Cyclin A, regulated at the levels of transcription and proteolysis [105]. After initiation of the G2/M transition by complexation of CycA and phosphorylation of various downstream targets [106], CycA is degraded and Cdk1 becomes part of the M-phase promoting factor (MPF), which is composed of Cdk1 and CycB [107-109]. Cdk1/CycB is, in turn, regulated by complex mechanisms.

In the inner feedback loops, Cdk1/CycB activity is controlled by the balance between Wee kinases and Cdc25 phosphatases that is responsible for the status of inhibitory phosphorylations at Thr14 and Tyr15 [110]. These kinases and phosphatases are in turn regulated by Cdk1 activity. Once activated, Cdk1/CycB

can phosphorylate Wee1 and Myt1 to promote their inactivation via different cascades [92, 111-112]. Additionally, Cdk1/CycB can activate Cdc25 phosphatases which shifts the equilibrium even more towards active Cdk1/CycB (autoamplification) [110]. In other words, through the inner feedback loops, Cdk1/CycB can stimulate its further activation by directly activating its activators and deactivating its inactivators [27].

The regulating network becomes even more complex, if outer feedback loops, i.e. indirect regulation mechanisms besides Thr14/Tyr15 phosphorylations, are taken into account [27]. These feedback loops are superimposed on the inner feedback loops but act via other mediating enzymes such as Plk1. Plk1, a direct and indirect target of Cdk1/CycB [113-114], can mediate indirect inhibition through phosphorylations of Wee kinases and, at the same time, activate the Cdc25 phosphatases [92, 112, 115].

These feedback loops not only promote an efficient activation of Cdk1/CycB but also ensure that other regulatory factors needed for successful cell division are activated in a coordinated manner. Supporting this notion, short-circuiting the inner feedback loop by expression of a Wee1/Myt1-insensitive Cdk1 mutant (T14A, Y15F) led to abnormal cell division [116]. Owing to the numerous feedback loops, Cdk1/CycB activation is considered a bistable process, meaning the majority of the complexes are inactive, active or approaching one of these states [117-119]. Therefore, a cell will or will not enter mitosis, but cannot rest in an intermediate state [27]. Since the inactivation threshold requires lower Cdk1/CycB concentrations than the activation threshold (hysteresis), successful mitotic entry is ensured and, at the same time, the cell is given an opportunity to block mitotic entry in case of premature activity fluctuations [119-120].

Another important matter in Cdk1/CycB control and mitotic entry is nucleocytoplasmic shuttling. With respect to various posttranslational modifications, subcellular trafficking of CycB and Cdk1/CycB is altered because modifications affect the affinity towards transport proteins that mediate traffic between nucleus and cytoplasm. Therefore, spatial sequestration can also prevent protein interactions if the requirements for cell cycle progression have not yet been met [27, 121-122].

Altogether, entry into mitosis is controlled not only by regulation of CycB accumulation but also by inner and outer feedback loops as well as spatial and

time-dependent sequestration of the respective proteins. Myt1 is involved in some of these mechanisms and its actual role will be clarified in the upcoming section.

2.2.2.2. *Myt1 in Regulation of Mitotic Entry*

The Myt1 kinase was discovered in 1995 as a membrane-associated kinase that is responsible for inhibitory Cdk1 phosphorylations [83]. The kinase activity towards Thr14 and Tyr15 of the Cdk1 protein is high in interphase and decreases due to hyperphosphorylation in M-phase [83, 92, 111]. In contrast to Wee1, Myt1 exhibits a more restricted substrate specificity, in that it phosphorylates Cdk1 but not Cdk2 complexes [111].

The direct Cdk1/CycB regulation consists of two independent mechanisms. First, there are inhibitory phosphorylations at Thr14 and Tyr15 [87, 123]. Importantly, phosphorylation of Cdk1/CycB at Thr161 of the Cdk subunit by Cdk activating kinase (CAK) is prerequisite for activation of the Cdk/Cyc complex [124-125]. The phosphorylation of Thr161 is, in turn, tightly coupled to Thr14 phosphorylation [126]. Fig. 4 displays the current understanding of the direct phosphorylation-driven regulation of Cdk1/CycB [126].

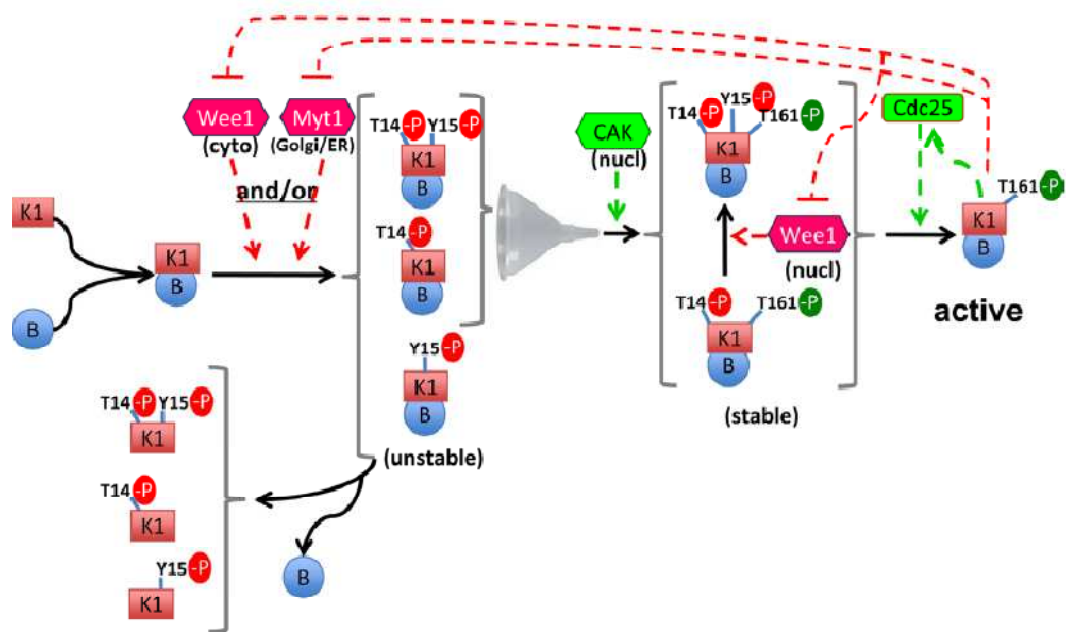


Fig. 4: Current understanding of direct phosphorylation-driven regulation of Cdk1/CycB. For description refer to the text. Reproduced with permission from [126], copyright 2011, Coulonval et al.

Cdk1/CycB is continuously shuttling but mostly cytoplasmic, due to its more active nuclear export [106, 127]. Upon binding to CycB, nonphosphorylated Cdk1 can be immediately phosphorylated at Thr14 and/or Tyr15 by Wee1 (mostly located to the nucleus, but also present in the cytoplasm to a lesser extent [128])

and/or Myt1, but not nuclear CAK [124]. In the absence of Thr161 phosphorylation, these Cdk1/CycB complexes are unstable and therefore release monomeric Cdk1 with its various possible phosphorylation patterns [129]. Nuclear trafficking pathways addressing pThr14-Cdk1/CycB are probably responsible for the observation that Thr161 modification is strictly associated with Thr14 modification. The actual activation is then mediated by nuclear Cdc25 phosphatases that hydrolyze the inhibitory phosphorylations while maintaining the required Thr161 modification. The tight coupling of Thr161 and Thr14 phosphorylation protects Cdk1/CycB from premature activation and ensures that it is only activated by dephosphorylation [126].

As a second mechanism to regulate Cdk1/CycB, there is a C-terminal domain within the Myt1 protein that interacts with Cdk1 complexes [90]. In contrast to the mostly nuclear Wee1, Myt1 is localized to endoplasmic reticulum and Golgi complex by a membrane-tether [87]. Binding of Cdk1 complexes by Myt1 sequesters them in the cytoplasm, thereby precluding entry into the nucleus and preventing cell cycle progression [90]. In a predictive mathematical model of the G2 checkpoint, Myt1 depletion led to nuclear accumulation of Cdk1/CycB [130]. Overexpression of Myt1 prevented entry into mitosis but the catalytic kinase activity was not essential for a cell cycle delay observed in human cells. Although the accumulation within the G2/M population was less efficient for catalytically inactive Myt1 than wild-type Myt1, the importance of the direct protein-protein interaction should not be underestimated [90]. These findings may partly explain the limited effects on mitotic entry of Myt1 knock-down by RNA interference [12, 91, 131] and highlight the need for small molecule inhibitors.

2.2.2.3. *Intracellular Membrane Dynamics and Mitotic Exit*

The idea that Myt1 might be involved in intracellular membrane dynamics came up quite recently [132]. Meanwhile, there is evidence that Myt1 plays a pivotal role in regulation of these processes. Myt1 depletion in somatic mammalian cells (HeLa) by RNA interference yielded a dramatically transformed morphology of the Golgi apparatus [131], namely condensed non-ribbon-like membranous structures near the nucleus. These cells showed a retarded proliferation rate and died within 10 d. These effects on Golgi reassembly were also observed when the Wee1 and Myt1 kinase inhibitor PD166285 was added to cycling cells [133].

In mammalian cells, the Golgi apparatus fragments into thousands of vesicles and tubules during prometaphase, and rapidly reassembles during telophase [134]. The Golgi fragmentation is thought to facilitate the equal partitioning of Golgi membranes between the two daughter cells during cell division [134] and has been reported to be an important step for mitotic progression [135-136]. Myt1 is not involved in maintenance of Golgi structure during interphase but is required for membrane fragmentation in G2 [91] as well as Golgi reassembly during telophase [131]. The Golgi apparatus is closely related to the endoplasmic reticulum (ER) [137]. The ER is a continuous membrane system enclosing a single luminal space and comprises fine tubular networks and cisternae throughout the cytoplasm [138-139]. Myt1 is also of major importance for the reassembly of the fine interphase-type ER meshwork during mitotic exit, as depletion led to disruption of the ER meshwork [131]. Importantly, these effects are caused by the kinase activity of Myt1, not by binding-mediated secondary effects [131]. Mitotic Golgi fragmentation in mammalian cells depends on Cdk1 [140] and by complete suppression of Cdk1/CycB kinase activity through inhibitory phosphorylations at the end of mitosis, Myt1 facilitates Golgi and ER assembly [131, 141]. The observed inhibitory Cdk1 phosphorylations at the end of mitosis are also part of an alternative mitotic exit mechanism in case of impaired CycB-degradation, which is the common way of transition from M to G1 [142-143]. In G1, inhibitory Cdk1 phosphorylations can lock Cdk1 in the inactive state [133]. A lack of these inhibitory Cdk1 phosphorylations, as observed by expressing an insensitive Cdk1(T14A,Y15F) mutant in somatic cells, makes the cells unable to properly lock the cell cycle at this stage, leading to rapid cell cycling with premature transition from G1- to S-phase or direct transition from G1- to M-phase [116].

Notably, the Myt1-mediated effects on Golgi fragmentation and G1 regulation are independent of Cdk1. Myt1 is inactivated in mitosis through hyperphosphorylation [83, 111], but is activated shortly after mitotic exit [133]. Specific *in vivo* targets for Myt1 besides Cdk1/Cyc complexes that allow a direct link to G1 regulation and membrane dynamics are still to be identified [91, 133].

2.2.2.4. Checkpoint Recovery and Maintaining G2-Arrest

When DNA damage occurs to a cell in G2-phase, the subsequent cell cycle arrest is achieved through posttranslational modifications as discussed above. Upon

repair of the damaged DNA, the cell can resume the cell cycle, a process that is referred to as checkpoint recovery [144].

Most recently, it was suggested that Myt1 plays a relatively minor role in unperturbed cell cycle and rather bears an essential function in G2 checkpoint recovery [15]. This Myt1 function in checkpoint recovery is completely independent of Wee1. It is hypothesized that the G2 DNA damage checkpoint maintains Cdk1 in a Thr14- and Tyr15-phosphorylated, inactive state, which is controlled by enhanced Wee kinase activity and reduced Cdc25 phosphatase activity [15]. As Plk1 is an important regulator of G2 checkpoint recovery, it mediates activation of Cdc25 and inactivation of Wee1 [144]. Because Myt1 is known to be negatively regulated by Plk1 through direct phosphorylations [92] and, moreover, found to be inactivated during checkpoint recovery, there might be a connection [15].

Downregulation of Myt1 accelerated checkpoint recovery and mitotic entry. Interestingly, in accordance with these findings, depletion of Myt1 potentiates with DNA damage to inhibit tumor growth, as observed in mouse xenograft models [15]. The involvement of Myt1 in checkpoint recovery was also predicted *in silico* using a mathematical model of the transition from G2- to M-phase [130].

2.2.2.5. Meiosis

Myt1 has a pivotal role in gametogenesis in various species such as *Xenopus laevis* [145], *Drosophila melanogaster* [146] and *Caenorhabditis elegans* [147]. As Myt1 is the only Cdk1 inhibitory kinase in prophase-arrested *Xenopus* oocytes, Myt1 is believed to be important in the meiotic cycle during early development [145]. With respect to lacking evidence in mammalian cells, this section is kept short. Future research will elucidate the role of Myt1 in this field and the significance for human cells.

2.2.3. Myt1 as a Potential Drug Target in Cancer Therapy

Mutations to p53, a protein of major importance to the G1 checkpoint, have been implicated in more than half of all human oncogenesis [148]. Due to mutations in the p53 network, many cancer cells have defective G1 checkpoint mechanisms [14, 148], which can result in increased DNA damage at the G2 checkpoint compared to normal cells [149]. Selective G2 checkpoint abrogation, disrupting a signal pathway not involved with p53, should not harm normal cells because they have another, p53-dependent pathway to halt the cell cycle at this point [13].

Therefore, a novel strategy of selective sensitization evolved, combining checkpoint abrogation with DNA damaging agents [150] or radiation [151].

The first (unintentionally) used G2 checkpoint abrogator was caffeine; the exact mechanism, however, still remains unclear [152-153].

Abrogation of the G2 checkpoint forces cells with unrepaired DNA damage into premature mitosis. This checkpoint abrogation can be induced by pharmacological manipulation, resulting in mitotic catastrophe and apoptosis when the extent of unrepaired DNA damage exceeds a varying threshold [150, 154-155]. Checkpoint abrogation is prerequisite for mitotic catastrophe [156], which results in apoptotic and non-apoptotic cell death [157]. Yet, apoptosis is not required for the lethal effect of mitotic catastrophe [158].

Cells with intact G1 checkpoint arrest, such as normal cells or cancer cells with intact p53 signaling, are less dependent on the G2 checkpoint arrest and are, therefore, not as sensitive towards G2 checkpoint abrogation [159].

Inhibitory Cdk1 phosphorylations are responsible for radiation-induced G2 arrest [160] and this checkpoint can be abrogated by expressing a non-phosphorylatable Cdk1 mutant [160].

Confirmed or suggested targets for G2 checkpoint abrogation and mitotic catastrophe are Wee1 [161], Myt1 [159], Chk1 [161] and Hsp90 [162].

Indeed, selective Wee1 inhibition by MK-1775 showed promising effects, just as predicted [16]: MK-1775 treated cells expressing short hairpin RNA against *p53* were much more sensitive towards gemcitabine, carboplatin or cisplatin [16].

In accordance with the theory, effects of MK-1775 monotherapy were only moderate. However, MK-1775 enhanced the cytotoxic effects of 5-fluorouracil (5-FU) in *p53*-deficient colon cancer cells and pancreatic cancer cells, but not in wild-type *p53* colon cancer cells [20]. Similar results were obtained in combination with gemcitabine [163], doxorubicin, carboplatin and cisplatin [20].

Similar to Wee1 knockdown, Myt1 knockdown increased the kinetics of G2/M transition, promoted early entry into mitosis [91] or led to total checkpoint abrogation [12]. Doxorubicin-induced G2 arrest in HeLa cells was abrogated when Myt1 was knocked down [12].

Downregulation of Myt1 shortened the time between checkpoint abrogation and mitotic entry which also increased the level of subsequent cell death. Therefore, Myt1 may be a useful target for anti-cancer therapy [15]. In xenograft models,

Myt1 revealed to be a particularly attractive target because it is of relatively minor importance for normal cell cycle progression [15]. Inhibitors of cell cycle components that are essential for normal cell cycle progression may be too toxic for normal cells and unsuitable for use in therapies [15].

So far, some other findings rather stand on their own but highlight the potential for Myt1 inhibition in cancer therapy: Myt1 was up-regulated by more than 10fold in seven tested ovarian cancer cell lines [164]; and gastric cancer cells were found to overexpress *Myt1* in response to the α -emitter Bi²¹³ prior to cell death [165].

In a RNAi screening across the entire kinome in combination with cytarabine in leukemias, *Chk1* and *Myt1* were the strongest sensitizers [166]. However, since a selective Myt1 inhibitor was not available, MK-1775 was used instead to inhibit Wee1 as the most closely related kinase. Leukemia cells were sensitized 97fold compared to cytarabine control [166], raising expectations with regard to Myt1 inhibition in future cancer therapy.

2.3. Target-Based Drug Discovery and Virtual Screening

In target-based drug discovery, the organism is seen as a series of genes and pathways and the goal is to develop drugs that affect only one molecular mechanism (i.e. the target) in order to selectively treat the deficit causing the disease while avoiding major side effects [167].

The strengths of the approach are high screening capacity and the ability to formulate clear requirements for the drug, which allows the implementation of ‘rational drug design’. Its weakness is that drugs can only be optimized against a small number of targets simultaneously. Therefore, this approach is inconsistent with ‘dirty’ drugs, i.e. drugs having multiple targets. Another weakness is the dissociation of physiology from the drug discovery process [167].

For the generation of novel lead structures, random screening of comprehensive compound collections (High throughput screening, HTS) can be considered a major source [168]. However, as the available compound sets become larger and larger and while the costs for such a screening rise, the hit rates actually decrease [169]. Screening of many thousands of compounds in HTS is financially difficult to afford for many companies and academic institutions [170]. Screening of a preselected subset, so called focused screening, is an alternate strategy to random screening [171]. Following this idea, information derived from the molecular structure of the desired target is used to filter libraries through a virtual screening

process. The goal of this procedure is to reduce the number of compounds for biological testing and, at the same time, to increase the probability of a focused library containing active compounds [172]. Due to the availability of X-ray crystal structures, virtual screening and 3D database searches, such approaches have been increasingly used in the pharmaceutical industry [173].

There are many possibilities to virtually screen compound libraries, including various two-dimensional (2D) and three-dimensional (3D) structural approaches, pharmacophore models, fingerprints and QSAR models [174-177]. Many successful examples of virtual screening approaches to target-based drug discovery are known, e.g. modulators of the retinoic acid receptor [178] or novel inhibitors of the human carbonic anhydrase [179].

When both receptor (protein) and ligand structures are known, the docking receptor-based approach is the most ideal situation [180-182]. The ligand can be docked into the receptor site and molecular mechanics can be used to simulate the respective ligand-receptor interactions and dynamics. Many software programs for the implementation of virtual screenings have been developed, e.g. GOLD [183], DOCK [184] or Glide [185], to name only a few.

Generally, a protein-based virtual screening flowchart comprises four essential steps [186]: The 2D database is filtered and suitable compounds are converted into 3D structures (Step 1). Then, each molecule is docked in the active site of the target protein (Step 2). The interaction between ligand and target protein is scored, if a docking solution has been found (Step 3). Finally, the data is extracted and the top scorers are post-processed to define a virtual screening hitlist (Step 4).

Databases can be filtered with respect to undesired properties of compounds. Common examples for such properties used as filter are accordance to the Lipinski 'Rule-of-Five' [187] or absence of highly-reactive chemical groups (acyl-halides, Michael-acceptors, etc.) [188]. In any case, the filter should be adapted to the size of the electronic database and the properties that are required [189].

As another practical aspect of virtual screening applications, the construction of known compound training databases is very important. Such a database usually contains a thousand compounds including up to 20 known active ligands and can be used to examine and refine the hypothetical query against the test database in terms of hit precision rate, false-negative rate and false-positive rate before searches in the large target database [173].

From theory to practice: How to carry out such a target-based drug discovery process? A general guideline including essential steps of such a process is presented in Fig. 5 [190-191].

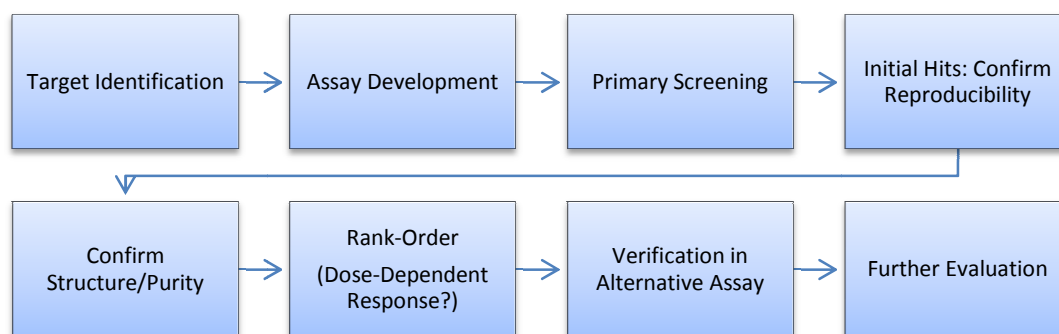


Fig. 5: A general workflow for a target-based drug discovery process.

As implied by the name of the approach, a target has to be selected in advance. This is a complex process guided by medical and strategic considerations together with a sound scientific rationale of the disease hypothesis linking a gene product to a disease state [192]. Examples for successful target approaches are inhibitors of angiotensin-converting enzyme (ACE) [193] and HIV protease [194].

In a next step, an appropriate assay has to be designed in order to screen a comprehensive or focused library. Assay development aims at delivering a test system to detect target modulation reproducibly and can be considered a critical step because the choice of an assay technology depends on many factors, including compatibility with given hardware (instrumentation) and available expertise but also assay sensitivity considerations and the susceptibility to possible assay artifacts [190]. Generally, the test quality is primarily determined by the ability of the assay to detect hit compounds which can be assessed by a number of statistical measures, e.g. the Z-factor [195].

After primary screening, retesting of primary hits under identical conditions is a mandatory step in any screening workflow [190]. If the compound acts reproducibly and structure/purity are known, a dose-dependence of the response must be investigated for two reasons: On the one hand, it helps rank the hits and, on the other hand, it verifies the assumed mode of action, as indicated by the development of the resulting dose-response curve [196].

As a further validation, the remaining compounds can be tested in an orthogonal assay system to exclude false-positive hits caused by artifacts.

Lead structures emerging from such a process can then be subjected to further evaluation and optimization.

3. Aim of the Work

As highlighted in former sections, Myt1 is a kinase that raises a lot of unanswered questions in the cellular context. Biochemical research tools are required to assess the true physiological role and druggability of this kinase.

At the beginning of this work, the inhibition profile of Myt1 was totally unclear. Very few reports existed, and these delivered inconsistent results, e.g. in terms of the effect of the pan-kinase inhibitor staurosporine [23-24].

To resolve these questions, the goal was to develop assay systems for the evaluation of potential inhibitors. Since Myt1 is, to date, not commercially available as an enzymatically active protein, it was proposed to generate Myt1 in a human expression system in cooperation with Dr. F. Erdmann (Institute of Pharmacy, Department of Pharmacology, MLU Halle-Wittenberg).

In 2005, ZHOU et al. reported glycolipids extracted from marine algae to be potent and selective Myt1 inhibitors [197]. The most potent compound was synthesized and derivatized in the working group of Dr. Schmidt/Prof. Sippl. It was proposed that this class of compounds should be evaluated based on the reliable biochemical assay methods developed.

Because the expertise of the working group around Prof. Sippl in virtual screening approaches should be used to discover formerly unknown inhibitors, investigations on the inhibition profile are of particular importance. *In silico* approaches require both positive and negative controls to validate theoretical models prior to the actual virtual screening. As an important part of the present work, the goal was to generate data for such a training set. Compounds suggested by subsequent virtual screenings were then assessed concerning their Myt1 inhibitory properties.

A few months after the beginning of this work, a crystal structure of the Myt1 kinase domain entered the protein databases (PDB: 3P1A [198]), significantly facilitating computational approaches.

Altogether, the goal was to generate recombinant human Myt1 kinase and set up suitable assays. Inhibition data generated by these assays was then used to get one step closer to the ultimate goal of a Myt1 inhibitor providing both potency and selectivity.

4. Materials and Methods

4.1. Devices and Equipment

Microplate readers

NOVOstar	BMG Labtech (Heidelberg, Germany)
Polarstar OMEGA	BMG Labtech (Heidelberg, Germany)
EnVision	Perkin-Elmer (Waltham, MA, USA)
Infinite M1000	Tecan (Männedorf, Switzerland)

Cell culture

Autoclave	ML2540	Tuttnauer (Breda, Netherlands)
Water bath	WB 7	Memmert (Schwabach, Germany)
Light microscope	CK2	Olympus (Hamburg, Germany)
Workbench	Tecnoflow	Integra Biosciences (Fernwald, Germany)
Pipette controller	Pipetboy plus	Integra Biosciences (Fernwald, Germany)
Flame burner	Fireboy eco	Integra Biosciences (Fernwald, Germany)
Incubator	Cellsafe	Integra Biosciences (Fernwald, Germany)
Benchtop centrifuge	Biofuge 13	Heraeus Instruments (Hanau, Germany)
Refrigerated centrifuge	Avanti 30 Centrifuge	Beckman (Krefeld, Germany)
Counting chamber	Neubauer-improved, bright line, 0.1 mm	Marienfeld (Lauda-Königshofen, Germany)

SDS-PAGE and Western blotting

Gel caster	Mighty Small Multiple Gel Caster SE250	GE Healthcare Life Sciences (Freiburg, Germany)
Transfer cell	Trans-Blot SD semi dry transfer cell	Bio-Rad (Munich, Germany)
X-ray film cassette	Hypercassette	Amersham Lifescience (Little Chalfont, UK)
Power supply	PowerPac 200	Bio-Rad (Munich, Germany)
Elektrophoresis chamber	Mighty Small II SF250	Hoefer (Holliston, MA, USA)

Chromatography

MPLC	PuriFlash 430	Interchim (Montluçon Cedex, France)
	Silica gel 60, 40e63 mesh column	Merck (Darmstadt, Germany)
HPLC, analytical (system 1)	1200 series Autosampler G1329A	Agilent technologies (Santa Clara, CA, USA)
	Pump G1312A	Agilent technologies
	Degasser G1379B	Agilent technologies
	Column Jupiter C18 250 x 4,6 mm	Phenomenex (Aschaffenburg, Germany)
	UV/Vis-Detector G1365B	Agilent technologies
HPLC, analytical (system 2)	Sampler 851-AS	Jasco (Tokyo, Japan)
	LiChroCART 125-4 (LiChrospher 100) RP-18 (5 µm) column	Merck (Darmstadt, Germany)
	Pump PU-980	Jasco (Tokyo, Japan)
	UV-Detector UV-975	Jasco (Tokyo, Japan)
	Fluorescence detectorFP-920	Jasco (Tokyo, Japan)

HPLC, analytical (system 3)	Autosampler SIL-HT	Shimadzu (Kyoto, Japan)
	Column XTerra RP18 3.5 μ m 3.9 x 100 mm	Waters (Milford, MA, USA)
	Pumps LC-10AD	Shimadzu (Kyoto, Japan)
	Detector (DAD) SPD-M10A VP PDA	Shimadzu (Kyoto, Japan)
HPLC, preparative	L-6200 Intelligent Pump	Merck-Hitachi (Darmstadt, Germany)
	250-25 mm LiChrospher 100 RP-8 (5 μ m) Column	HiBar (Urbach, Germany)
	L-4200 UV-Vis Detector	Merck-Hitachi
	D-2500 Chromato-Integrator	Merck-Hitachi

Devices for Microarray Studies

Fluorescence Scanner for microarray slides	GenePix 4000B	Molecular Devices (Sunnyvale, CA, USA)
Hybstation	HS400	Tecan (Männedorf, Switzerland)

Miscellaneous

Benchtop centrifuge	Force 7	Labnet (Woodbridge, NJ, USA)
Centrifuge (refrigerated)	Centrifuge 5804 R	Eppendorf (Hamburg, Germany)
Digital analytical balance	LE225D	Sartorius (Goettingen, Germany)
Gel documentation system	Gel Doc XR	Bio-Rad (Munich, Germany)
Orbital shaker	Polymax 1040	Heidolph (Schwabach, Germany)
pH meter	inoLab pH Level 1	WTW (Weilheim, Germany)
Pipette controller	Accu-Jet [®]	Brand (Wertheim, Germany)
Pipettes, single channel	Biopette [®] 10, 20, 200, 1000	Labnet (Woodbridge, NJ, USA)
	Research 100, 1000	Eppendorf (Hamburg, Germany)
	HandyStep [®]	Brand (Wertheim, Germany)
Repetitive pipette	Duomax 1030	Heidolph (Schwabach, Germany)
Rocking shaker	444-0274	VWR (Dresden, Germany)
Shaking incubator	NanoVue [®]	GE Healthcare Life Sciences (Freiburg, Germany)
Spectrophotometer	Savant-AES1010	Savant (Farmingdale, NY, USA)
SpeedVac [®]	Thermomixer comfort	Eppendorf (Hamburg, Germany)
Thermomixer	Transsonic T 460/H	Carl Roth (Karlsruhe, Germany)
Ultrasonic bath	REAX 2000	Heidolph (Schwabach, Germany)
Vortexer	DirectQ5	Millipore (Eschborn, Germany)
Water purification device	xCAD	TKA (Niederelbert, Germany)
Water purification device (Ultrapure)		

4.2. Consumables

384-Well plate, black	Optiplate [®] black opaque #6007270	Perkin-Elmer (Waltham, MA, USA)
384-Well plate, white	Optiplate [®] white opaque #6007290	Perkin-Elmer (Waltham, MA, USA)
6-, 24-, 96-Well tissue culture plates, F-bottom, sterile, clear	#92006, # 92024, # 92096	TPP (Trasadingen, Switzerland)
96-Well plate, F-bottom, black	#655 900	Greiner Bio-One (Frickenhausen, Germany)
96-Well plate, F-bottom, black, half-area, non binding surface	#3686	Corning (Corning, NY, USA)

96-Well plate, F-bottom, clear	#650 101	Greiner Bio-One (Frickenhausen, Germany)
Adhesive plate sealer	EasySEAL #676 001	Greiner BioOne (Frickenhausen, Germany)
Blotting paper	Blotting Pad 707	VWR (Dresden, Germany)
Canulae	Sterican® 0.6 x 30 mm	B. Braun (Melsungen, Germany)
Centrifuge tubes	15 ml, 50 ml	BD (Franklin Lakes, NJ, USA)
Cryo tubes	2 ml	Roth (Karlsruhe, Germany)
Dispense tips	PlastiBrand® PD-Tips 0.1, 0.5, 1.25 ml	Brand (Wertheim, Germany)
IMAC gravity columns	HiTrap® (1 ml)	GE Healthcare Life Sciences (Freiburg, Germany)
IMAC spin columns	His-Select®	Sigma (Schnelldorf, Germany)
Nitrocellulose membranes	Amersham HyBond®-ECL	GE Healthcare Life Sciences (Freiburg, Germany)
Pipette tips	0.1-10, 2-200, 100-1000	VWR (Dresden, Germany)
Pipettes, sterile, disposable	5 ml, 10 ml, 25 ml	VWR (Dresden, Germany)
PVDF membranes	0.2 µm, LC2002	Invitrogen (Madison, WI, USA)
Safe lock tubes	1.5, 2 ml	Eppendorf (Hamburg, Germany)
Syringe sterile filter	Pore size 0.2 µm	VWR (Dresden, Germany)
Syringes, disposable, Luer conus	Discardit® II 10 ml	Beckton Dickinson (Madrid, Spain)
Tissue culture dishes	10 cm, 20 cm	TPP (Trasadingen, Switzerland)
TLC	silica gel plates (E. Merck 60 F254)	Merck (Darmstadt, Germany)
Tubes	1.5 ml, amber PP farblos 0.5 ml, 1.5 ml, 2 ml Protein LoBind Safe-Lock 1,5 ml	Brand (Wertheim, Germany) Ratiolab (Dreieich, Germany) Eppendorf (Hamburg, Germany)

4.3. Reagents

Cell culture

Accutase®	PAA (Coelbe, Germany)
DMEM (with Phenolred)	PAA (Coelbe, Germany)
DMSO (HybriMax®)	Sigma (Schnelldorf, Germany)
Dulbecco's PBS (D-PBS)	PAA (Coelbe, Germany)
FCS (tetracycline negative)	PAA (Coelbe, Germany)
FCS GOLD®	PAA (Coelbe, Germany)
GlutaMAX® (L-Ala-L-Gln)	Gibco®, Life technologies (Carlsbad, CA, USA)
Lipofectamine® LTX & Plus Reagent	Invitrogen (Carlsbad, CA, USA)
OptiMEM® (without Phenolred)	Invitrogen (Carlsbad, CA, USA)
Trypan blue (C.I. 23850)	Applichem (Darmstadt, Germany)

Solid Phase Peptide Synthesis

Acetic anhydride	Merck (Darmstadt, Germany)
DIPEA	Merck (Darmstadt, Germany)
DMF (Synthesis grade, low in water < 150 ppm)	VWR (Dresden, Germany)
Fmoc-L-Arg(Pbf)-OH	AnaSpec (Fremont, CA, USA)
Fmoc-L-Asp(OtBu)-OH	GL Biochem (Shanghai, China)

Fmoc-L-Glu(OtBu)-OH	AnaSpec (Fremont, CA, USA)
Fmoc-L-Gly-OH	Alexis Corporations (Lausen, Switzerland)
Fmoc-L-His(Trt)-OH	GL Biochem (Shanghai, China)
Fmoc-L-Lys(Boc)-OH	AnaSpec (Fremont, CA, USA)
Fmoc-L-Met-OH	AnaSpec (Fremont, CA, USA)
Fmoc-L-Thr(tBu)-OH	AnaSpec (Fremont, CA, USA)
Fmoc-L-Tyr(tBu)-OH	AnaSpec (Fremont, CA, USA)
Fmoc-L-Val-OH	AnaSpec (Fremont, CA, USA)
Fmoc-Rink-Amide MBHA (0,45 mmol/g; 100-200 mesh; 75-200 µm)	Novabiochem® Merck (Darmstadt, Germany)
Piperidine	Merck (Darmstadt, Germany)
PyBOP	Sigma (Schnelldorf, Germany)
TFA	Uvasol® Merck (Darmstadt, Germany)

Chemicals

Acetonitrile (ACN, LiChrosolv®)	Merck (Darmstadt, Germany)
Acrylamide/Bisacrylamide (37.5:1) 40% (w/V)	Applichem (Darmstadt, Germany)
Agarose	Invitrogen (Carlsbad, CA, USA)
Ammonium persulfate (APS)	Sigma (Schnelldorf, Germany)
Ammonium sulfate	Applichem (Darmstadt, Germany)
Bicinchoninic acid (BCA)	Sigma (Schnelldorf, Germany)
Brij-35®	Applichem (Darmstadt, Germany)
BSA (blocking protein, RIA/EIA-grade)	Applichem (Darmstadt, Germany)
BSA (protein standard)	Fluka (St. Gallen, Switzerland)
CAPS	Applichem (Darmstadt, Germany)
3-[(3-Cholamidopropyl)-dimethyl ammonio]-1-propane sulfonate (CHAPS)	Sigma (Schnelldorf, Germany)
Coomassie®-Brilliant-Blue G-250	Applichem (Darmstadt, Germany)
DasAFITC	This work (4.18)
Dasatinib	LC Laboratories (Woburn, MA, USA)
1,8-Diazabicyclo[5.4.0]undec-7-ene (DBU)	Merck (Darmstadt, Germany)
1,6-Diphenyl-1,3,5-hexatriene (DPH)	Sigma (Schnelldorf, Germany)
Diphenyl phosphoryl azide (DPPA)	Sigma (Schnelldorf, Germany)
Disodium Ethylenediaminetetraacetic acid dihydrate (EDTA)	Sigma (Schnelldorf, Germany)
Dithiothreitol (DTT)	Sigma (Schnelldorf, Germany)
DMSO (for molecular biology)	Sigma (Schnelldorf, Germany)
DNA-Marker (GeneRuler 1 Kb Plus DNA Ladder)	Fermentas (St. Leon-Rot, Germany)
Ethidium bromide	Invitrogen (Carlsbad, CA, USA)
Ethyleneglycol-bis(2-aminoethyl ether)- <i>N,N,N',N'</i> -tetraacetic acid (EGTA)	Applichem (Darmstadt, Germany)
FITC isomer I	Sigma (Schnelldorf, Germany)
Fluorescein, sodium salt	Sigma (Schnelldorf, Germany)
Fluorescein-5-maleimide (F5M)	Pierce (Rockford, IL, USA)
Glycerol (molecular biology grade, >99%)	Sigma (Schnelldorf, Germany)
HEPES	Applichem (Darmstadt, Germany)
Imidazole	Sigma (Schnelldorf, Germany)
Kinase tracer 178(PV5593)	Invitrogen (Madison, WI, USA)
Kinase tracer 236 (PV5592)	Invitrogen (Madison, WI, USA)
Magnesium sulfate (MgSO ₄)	Applichem (Darmstadt, Germany)
Methanol (MeOH, HPLC-grade)	Applichem (Darmstadt, Germany)
Ninhydrin	Sigma (Schnelldorf, Germany)

Palladium on activated charcoal (Pd/C, 5% Pd basis)	Aldrich (Schnelldorf, Germany)
Photo-developer concentrate	Kodak (Stuttgart, Germany)
Photo-fixer concentrate	Kodak (Stuttgart, Germany)
Ponceau S (C.I. 27195)	Appllichem (Darmstadt, Germany)
Potassium hydrogencarbonate	Roth (Karlsruhe, Germany)
Protease inhibitor cocktail (Complete [®] EDTA-free)	Roche Diagnostics (Mannheim, Germany)
Protein marker for SDS-PAGE (Protein Marker III)	Appllichem (Darmstadt, Germany)
Protein marker for Western Blot (Protein Marker II, prestained)	Appllichem (Darmstadt, Germany)
Sodium azide (NaN ₃)	Sigma (Schnelldorf, Germany)
Sodium chloride (BioXtra [®] , NaCl)	Sigma (Schnelldorf, Germany)
Sodium dodecyl sulfate (SDS)	Appllichem (Darmstadt, Germany)
Sodium molybdate tetrahydrate	Appllichem (Darmstadt, Germany)
<i>N, N, N', N'</i> -Tetramethylethylenediamine (TEMED)	Sigma (Schnelldorf, Germany)
TGS-Puffer 10x	Appllichem (Darmstadt, Germany)
Trichloroacetic acid (TCA)	Appllichem (Darmstadt, Germany)
Trifluoroacetic acid (TFA)	Sigma (Schnelldorf, Germany)
Tris base (Trizma [®])	Sigma (Schnelldorf, Germany)
Triton [®] X-100 (TX100)	Sigma (Schnelldorf, Germany)
Tween [®] -20	Appllichem (Darmstadt, Germany)

Test compounds

0497595	Chembridge (San Diego, CA, USA)
1R-0035	Keyorganics (Camelford, UK)
1R-0046	Keyorganics (Camelford, UK)
2R-1301	Keyorganics (Camelford, UK)
3,7-Dihydroxyflavone-Hydrate	(Aldrich, Schnelldorf, Germany)
5665106	Chembridge (San Diego, CA, USA)
5679818	Chembridge (San Diego, CA, USA)
5924018	Chembridge (San Diego, CA, USA)
6643980	Chembridge (San Diego, CA, USA)
7507346	Chembridge (San Diego, CA, USA)
7651491	Chembridge (San Diego, CA, USA)
7705209	Chembridge (San Diego, CA, USA)
7706204	Chembridge (San Diego, CA, USA)
7928497	Chembridge (San Diego, CA, USA)
7938491	Chembridge (San Diego, CA, USA)
7G-003	Keyorganics (Camelford, UK)
8D-022	Keyorganics (Camelford, UK)
9L-564S	Keyorganics (Camelford, UK)
9N-661S	Keyorganics (Camelford, UK)
7769763	Chembridge (San Diego, CA, USA)
7697266	Chembridge (San Diego, CA, USA)
7871748	Chembridge (San Diego, CA, USA)
38874115	Chembridge (San Diego, CA, USA)
5849648	Chembridge (San Diego, CA, USA)
7960104	Chembridge (San Diego, CA, USA)
7773617	Chembridge (San Diego, CA, USA)
AC-Compounds	Synthesized by B. Sauer, MLU Halle-Wittenberg
Bisindolylmaleimid I	LC Laboratories (Woburn, MA, USA)
Bosutinib	LC Laboratories (Woburn, MA, USA)

BS-Compounds	Synthesized by B. Sauer [199]
CUDC-101	LC Laboratories (Woburn, MA, USA)
Daidzein	Sigma (Schnelldorf, Germany)
Dasatinib	LC Laboratories (Woburn, MA, USA)
Erlotinib	ChemieTek (Indianapolis, IN, USA)
Fisetin	Sigma (Schnelldorf, Germany)
Gefitinib	LC Laboratories (Woburn, MA, USA)
Genistein	Sigma (Schnelldorf, Germany)
Glycoglycerolipds	Synthesized by C. Göllner [200]
GS-Compounds	Synthesized by G. M. A. Al-Mazaideh [201]
HA-1077	LC Laboratories (Woburn, MA, USA)
Heptafluorbutyrate	Acros Organics (Geel, Belgium)
Imatinib	LC Laboratories (Woburn, MA, USA)
K252a	LC Laboratories (Woburn, MA, USA)
Kaempferol	Fluka (St. Gallen, Switzerland)
OSSK_670031	Chembridge (San Diego, CA, USA)
OSSK_670181	Chembridge (San Diego, CA, USA)
OSSL_110276	Chembridge (San Diego, CA, USA)
OSSL_164599	Chembridge (San Diego, CA, USA)
OSSL_438946	Chembridge (San Diego, CA, USA)
OSSL_048423	Chembridge (San Diego, CA, USA)
OSSK_318710	Chembridge (San Diego, CA, USA)
OSSL_410731	Chembridge (San Diego, CA, USA)
OSSL_396401	Chembridge (San Diego, CA, USA)
OSSL_719027	Chembridge (San Diego, CA, USA)
OSSL_393954	Chembridge (San Diego, CA, USA)
Lapatinib	LC Laboratories (Woburn, MA, USA)
Lestaurtinib (CEP-701)	LC Laboratories (Woburn, MA, USA)
Myricetin	Fluka (St. Gallen, Switzerland)
Naringenin (Racemate)	Sigma (Schnelldorf, Germany)
Neratinib	LC Laboratories (Woburn, MA, USA)
PD166285	Santa Cruz Biotechnology (Santa Cruz, CA, USA)
PD173952	Sigma (Schnelldorf, Germany)
PD180970	Sigma (Schnelldorf, Germany)
Phloretin	Sigma (Schnelldorf, Germany)
PKC-412 (Midostaurin)	LC Laboratories (Woburn, MA, USA)
Quercetin	Sigma (Schnelldorf, Germany)
Roscovitine	LC Laboratories (Woburn, MA, USA)
Saracatinib	LC Laboratories (Woburn, MA, USA)
SB203580	LC Laboratories (Woburn, MA, USA)
Silibinin	Sigma (Schnelldorf, Germany)
Staurosporine	LC Laboratories (Woburn, MA, USA)
Sunitinib	Pfizer (Groton, CT, USA)
Tivozanib	LC Laboratories (Woburn, MA, USA)
Tyrphostin AG 1478	LC Laboratories (Woburn, MA, USA)
U0126	LC Laboratories (Woburn, MA, USA)
Vatalanib	ChemieTek (Indianapolis, IN, USA)
Wee1-Inhibitor Calbiochem#681640	Merck (Darmstadt, Germany)

Peptides and Microarrays

A002-D_747 (DGHEYIYVDPMQL)	Thermo (Bonn, Germany)
Ac-Cdk1 ¹⁻²⁴	This work (4.22)
(Ac-MEDYTKIEKIGEGTYGVVYKGRHK-OH)	

Cdk1 ⁶⁻¹⁷ (KVEKIGEGTYVV)	ProBiodrug (Halle, Germany)
EFS_HUMAN_302 (GTDEGIYDVPLLG)	Thermo (Bonn, Germany)
eTY (EKIGEGTYGVVYKC)	ProBiodrug (Halle, Germany)
FPIA II Probe ((6-FAM)KI(pY)VV)	IKFZ (Leipzig, Germany)
H-Cdk1 ¹⁻²⁴	This work (4.22)
(H-MEDYTKIEKIGEGTYGVVYKGRHK-OH)	
INR1_HUMAN_548 (SSSIDEYFSEQPL)	Thermo (Bonn, Germany)
Phospho-PDGFRA-Y572 (SPDGHE(pY)IYVDPMQ)	Abgent (San Diego, CA, USA)
Phospho-TrkA-Y676 (FGMSRDI(pY)STDYYRV)	Abgent (San Diego, CA, USA)
Poly-AEKY (Ala:Glu:Lys:Tyr _{6:2:5:1})	Sigma (Schnelldorf, Germany)
pTpY (QKIGEG(pT)(pY)GVVYKC)	ProBiodrug (Halle, Germany)
pTY (QKIGEG(pT)YGVVYKC)	ProBiodrug (Halle, Germany)
TpY (QKIGEGT(pY)GVVYKC)	ProBiodrug (Halle, Germany)
TRKA_HUMAN_482 (GMSRDIYSTDYR)	Thermo (Bonn, Germany)
TY (QKIGEGTYGVVYKC)	ProBiodrug (Halle, Germany)

High-content peptide microarray slides were from JPT (Berlin, Germany) and kindly provided by Prof. Dr. M. Schutkowski (Institute of Biochemistry and Biotechnology, Martin-Luther-University Halle-Wittenberg).

Enzymes

Abl1	ProQinase (Freiburg, Germany)
Btk	ProQinase (Freiburg, Germany)
Cdk1	ProQinase (Freiburg, Germany)
Cdk1/CycB1	ProQinase (Freiburg, Germany)
Myt1 ⁷⁵⁻³⁶²	This work (4.5.2)
Myt1fl	This work (4.5.1)
Wee1 ²⁵⁰⁻⁶⁴⁶	ProQinase (Freiburg, Germany)
Wee1fl	Invitrogen (Carlsbad, CA, USA)

Antibodies

Anti-Cdk1	Cell Signaling (Danvers, MA, USA)
Anti-GAPDH (D16H11) XP	Cell Signaling (Danvers, MA, USA)
Anti-His	Cell Signaling (Danvers, MA, USA)
Anti-mouse IgG Dylight649 conjugate #35515	Pierce (Rockford, IL, USA)
Anti-Myt1	Cell Signaling (Danvers, MA, USA)
Anti-pThr (42H4)	Cell Signaling (Danvers, MA, USA)
Anti-pThr14-Cdk1	Cell Signaling (Danvers, MA, USA)
Anti-pTyr15-Cdk1	Cell Signaling (Danvers, MA, USA)
Eu-labeled anti-His tag antibody	Invitrogen (Madison, WI, USA)
HRP-conj. Affinipure Anti-Mouse	Jackson ImmunoResearch Laboratories (Westgrove, PA, USA)
HRP-conj. Affinipure Anti-Rabbit	Jackson ImmunoResearch Laboratories (Westgrove, PA, USA)

Kits

WesternBreeze chromogenic immunodetection kit	Sigma (Schnelldorf, Germany)
Plasmide Mega Kit	Qiagen (Hilden, Germany)
Enhanced Chemoluminescence Western Blot analysis system	GE Healthcare Life Sciences (Freiburg, Germany)

4.4. Buffers and Solutions

For all solutions mentioned in this section, ultrapure water was used as solvent.

BCA-Reagent I	1% BCA (sodium salt), 2% sodium carbonate monohydrate, 0.16% disodium tartrate, 0.4% sodium hydroxide, 0.95% sodium hydrogencarbonate, pH 11.25
BCA-Reagent II	40 g/l Copper-II-sulfate-pentahydrate
Bradford Reagent	40 mg/l Coomassie [®] Brilliant Blau G-250, 8,5% o-phosphoric acid, 10% EtOH
Complete cell culture medium	DMEM (with phenol red), 10 % FCS, 2 mM GlutaMAX
Fluorescein stock solution	1 mM Fluorescein, 20 mM CAPS pH 9.6
IMAC elution buffer (pH 7.5)	50 mM Tris-HCl pH 7.5; 150 mM NaCl; 3 mM MgCl ₂ ; 20% glycerol; 0.5% Triton X-100, 250 mM imidazole (pH 7.5)
IMAC equilibration buffer (pH 7.8)	50 mM Tris-HCl pH 7.8; 150 mM NaCl; 3 mM MgCl ₂ ; 20% glycerol; 0.5% Triton X-100
IMAC wash buffer (pH 7.8)	50 mM Tris-HCl pH 7.8; 150 mM NaCl; 3 mM MgCl ₂ ; 20% glycerol; 0.5% Triton X-100, 5 mM imidazole (pH 7.8)
Kinase binding assay buffer A (pH 7.5)	50 mM HEPES-NaOH, 10 mM MgCl ₂ , 1 mM EGTA, 0.01% Brij-35.
Kinase binding assay buffer B (pH 7.5)	50 mM HEPES-NaOH, 10 mM MgCl ₂ , 1 mM DTT, 0.03% CHAPS.
Lysis buffer	25 mM Tris-HCl pH 7.5, 150 mM NaCl, 3 mM MgCl ₂ , 1 mM DTT, 1% Triton X-100, 10% Glycerol, 1x Complete [®] EDTA-free
Lysis buffer (mild lysis)	50 mM Tris-HCl pH 7.8, 150 mM NaCl, 0.5 mM EDTA, 0.5% Triton X-100, 1x Complete [®] EDTA-free
Ponceau staining solution	0.2 g/l Ponceau S (2.6 mM), 30 g/l TCA
SDS-PAGE fixer	40% MeOH, 10% AcOH
SDS-PAGE loading buffer (pH 6.8)	0.004% bromo phenol blue, 400 mM DTT, 20% glycerol, 4% SDS, 125 mM Tris-HCl
SDS-PAGE running buffer (pH 8.3)	192 mM glycine, 25 mM Tris, 0.1% SDS
SDS-PAGE separating gel buffer	1.5 M Tris-HCl pH 8.8
SDS-PAGE stacking gel buffer	0.5 M Tris-HCl pH 6.8
SDS-PAGE staining solution A	50 g/l Coomassie Brilliant Blue G-250
SDS-PAGE staining solution B	20 g/l o-phosphoric acid, 100 g/l ammonium sulfate
Standard kinase buffer (pH 7.5)	50 mM Tris-HCl, 40 mM NaCl, 10 mM MgCl ₂ , 1 mM DTT, 0,04% Triton X-100, Complete EDTA-free.
TAE buffer (pH 8.3)	40 mM Tris, 40 mM acetate, 1 mM EDTA
TE buffer (pH 8.0)	10 mM Tris-HCl, 1 mM EDTA
Transfer buffer	14.35 g/l Glycin (191 mM), 3 g/l Tris (25 mM), 20% (V/V) Methanol
Tris buffered saline (TBS)	25 mM Tris pH 7.2, 137 mM NaCl
Tris buffered saline with Tween-20 (TBS-T)	25 mM Tris pH 7.2, 137 mM NaCl, 0.1% Tween 20
Trypan blue solution	5 g/l (5.2 mM) Trypan blue, 150 mM NaCl

4.5. Kinase Preparation

Generally, when working with a membrane-associated enzyme, there are two routes that can be used to obtain it. Either one has to solubilize a suitable full-length construct using a detergent [202] or a domain construct is required to overcome the solubilization step [203]. Both approaches were pursued in this work.

The generation of Myt1 was carried out in cooperation with Dr. F. Erdmann (MLU Halle-Wittenberg, Institute of Pharmacy, Department of Pharmacology).

4.5.1. Myt1 (full-length)

Full-length Myt1 was transiently expressed in the human cell line HEK293. Cell culture was handled under aseptic conditions using a clean workbench (Tecnoflow, Integra Biosciences).

4.5.1.1. Cell Culture

Cells were cultured in Dulbecco's modified Eagle's medium (DMEM), supplemented with 10% FCS and GlutaMAX at 37°C and 5% (V/V) CO₂ in a humidified incubator. Approximately 0.1 ml/cm² media was used for culture, independent of the respective cell culture vessel. When a confluent monolayer was reached, the cells were passaged. For this, the cells were washed with D-PBS, detached by Accutase following the instructions of the supplier and transferred into a 50 ml tube. After centrifugation (2000 RPM, 5 min, 20°C), the supernatant was removed and the pellet resuspended in media. A vital stain was conducted and the number of living cells was determined (*vide infra*). Subsequently, 500 cells per cm² were seeded in the respective vessel and cultured as described above.

4.5.1.2. Vital Stain and Cell Counting

To distinguish between dead and living cells, a vital stain by means of trypan blue was performed. As a negatively charged dye, it is not able to cross an intact cell membrane. Therefore, cells that are alive appear white in front of a blue background while dead cells are coloured blue due to the loss of membrane integrity. The procedure followed standard methodologies [204]. The cell suspension was diluted 5fold with D-PBS. To an aliquot of the resulting suspension, an equal amount of trypan blue staining solution (autoclaved before use) was added. After homogenisation, the mixture was incubated for 2 min at

37°C and transferred into Neubauer's improved counting chamber. The total number of cells N was determined by counting the cells using a light microscope and subsequent calculation following Eq. 1 (F : dilution factor; V : total volume cells were suspended in; Z : arithmetic mean value determined by counting).

$$N = Z * F * V * 10^4 \quad (\text{Eq. 1})$$

4.5.1.3. *Transfection and Harvesting*

Transfection was carried out with pcDNA3.1-Hismax-Myt1 expression plasmide (provided by Dr. F. Erdmann) by means of cationic lipids. Cationic lipids, neutral accessory lipids and DNA form complexes, so-called lipoplexes, that are able to fuse with the cell membrane. Fusion with the membrane releases the complexed DNA inside of the cell [205-206].

Cells were seeded onto tissue culture plates (diameter: 20 cm) and grown until approximately 80% confluence. Then, lipofectamine LTX and Plus reagent were used according to the recommendations of the supplier. As it is a transient expression system, cells will gradually lose the respective plasmide and stop producing the recombinant protein. Systematic expression experiments indicated 56 h after transfection to be the optimum time for harvesting. Cells were detached by Accutase, transferred into a 50 ml tube with D-PBS and harvested by centrifugation (2000 RPM, 5 min, 20°C).

4.5.1.4. *Isolation of Protein*

The pellet was resuspended in lysis buffer containing 25 mM Tris-HCl pH 7.8, 150 mM NaCl, 10 mM MgCl₂, 10% glycerol, 1% Triton X-100 and Complete EDTA-free protease inhibitor cocktail. Cells were finally lysed by shear stress using a 25 g needle and the lysate shaken on ice for 1 h. After centrifugation at 10 000 g for 15 min, the supernatant was loaded onto a HIS-Select column (Sigma) pre-equilibrated with IMAC equilibration buffer (50 mM Tris-HCl pH 7.8, 150 mM NaCl, 3 mM MgCl₂, 20% glycerol, 0.5% Triton X-100). The column was washed with IMAC wash buffer (equilibration buffer + 5 mM imidazole) and eluted with IMAC elution buffer (equilibration buffer + 250 mM imidazole). All steps were carried out at 4°C and the final eluate was supplemented with DTT (2 mM), frozen in ethanol/dry ice and stored at -80°C. The purification was controlled by coomassie stained SDS-PAGE analysis of all fractions. Determination of protein concentrations was conducted via BCA-assay

using BSA as protein standard. Identity of Myt1 was confirmed via anti-Myt1 and anti-His-tag western blotting experiments.

4.5.2. *Myt1 (kinase domain)*

The Myt1 kinase domain (comprising amino acids 75 to 362) was generally expressed and purified as described in [207]. The corresponding gene sequence of a Myt1 fragment (Myt⁷⁵⁻³⁶²) was cloned in pET28 plasmide and transformed into *E. coli* BL21(DE3) by electroporation. After inoculation of 1 l LB media, the cells were cultured at 37°C until OD₆₀₀ reached 0.6. Following subsequent cultivation at 22°C until OD₆₀₀ = 1.0, expression was induced by addition of IPTG (0.5 mM). Cells were harvested by centrifugation, the pellet re-suspended in binding buffer and frozen at -20°C. Thawed bacterial cells were disrupted by sonication on ice. Subsequently, after another centrifugation step, the supernatant containing the His₆-fusion protein was purified by affinity chromatography (1 ml Ni²⁺ HiTrap column, GE Healthcare) according to the recommendations of the manufacturer. Eluates were frozen in ethanol/dry ice and stored at -80°C. All steps were carried out on ice and analyzed in SDS-PAGE and ECL coupled western blotting system (anti-Myt1 and anti-His-tag). Determination of protein concentrations was conducted via BCA-assay.

4.6. Statistics and General Data Analysis

Quantitative data are expressed as arithmetic means unless stated otherwise and are derived from at least three independent experiments.

To examine the consistency of acquired data, the observations were tested for outliers on a regular basis. While for less than 30 observations, DIXON's test [208] was used, GRUBBS' test for outliers [209] was used for the examination of larger data sets (> 30 Observations).

Student's two-tailed *t*-tests were used to evaluate the statistical significance of differences between the means of paired data sets. Differences were considered significant when $p < 0.05$.

When calculating differences (e.g. Anisotropy Δr), the resulting statistical error Δy was calculated with respect to Gaussian error propagation:

$$\Delta y = \sqrt{|\Delta y_1|^2 + |\Delta y_2|^2} \quad (\text{Eq. 2})$$

Generally, data calculations were performed using Microsoft Office Excel 2007. Regression analysis was conducted by means of GraphPad Prism 5.01 (GraphPad

Software, Inc., La Jolla, CA, USA). IC₅₀ Curves were fitted via nonlinear regression (sigmoidal dose-response with variable slope) to equation 3:

$$y = y_{bottom} + \frac{y_{top} - y_{bottom}}{1 + 10^{\log_{10}(IC_{50} - x) * Hill\ Slope}} \quad (\text{Eq. 3})$$

Saturation binding curves were generated by nonlinear regression. For K_d estimations, data were fitted to equation 4:

$$y = \frac{y_{max} * x}{K_d + x} \quad (\text{Eq. 4})$$

To assess screening assay performance, the Z' factor [195] is preferred over other measures such as the signal window or the assay variability ratio [210]. Z' factor was calculated according to equation 5:

$$Z' = \frac{\mu^- - \mu^+ - 3 * (\sigma^- + \sigma^+)}{\mu^- - \mu^+} \quad (\text{Eq. 5})$$

where σ^+ and σ^- are the standard deviations of the positive and negative control wells. μ^+ and μ^- denote the average anisotropy values of those wells.

4.7. BCA-Assay

Since Myt1 isolation requires solubilization, a protein quantitation assay had to be used which is insensitive towards detergents. In contrast to other common methods such as the methodology described by BRADFORD [211], the BCA-Assay meets this requirement. In alkaline solution, copper-II is reduced to copper-I in presence of protein. Copper-I is subject to complexation by bicinchoninic acid (BCA), leading to formation of a purple colored complex that can be quantified photometrically. Because reducing agents such as thiols can strongly interfere with this assay, an aliquot of protein solution had to be removed for analytics prior to DTT supplementation.

The assay was performed in a modified procedure of the originally published version by SMITH et al. [212]. To 200 μ l standard working reagent (50 parts Reagent I + 1 part Reagent II; exact reagent constitutions are given in Section 4.4), 10 μ l sample was added in a transparent 96-Well plate (F-bottom, full area). The microplate was incubated at 60°C for 30 min at gentle shaking (400 RPM). After cooling down to room temperature, the plate was read in absorbance mode at a wavelength of 570 nm by a NOVOstar or PolarStar OMEGA platereader (BMG).

Blank controls and protein standards were carried along on the same microplate.

Bovine serum albumin (BSA, purchased from Fluka) was used as a protein standard. For protein concentrations ranging from 50 $\mu\text{g/ml}$ to 500 $\mu\text{g/ml}$ protein, this method showed excellent linearity.

4.8. Peptide Quantitation

Concentrations of all non-phospho peptide solutions used in fluorescence polarization assays were determined by measuring absorbance at 280 nm using a NanoVue Plus spectrophotometer (GE Healthcare Life Sciences). For each peptide, molar absorptivity (ϵ_{280}) was calculated according to the Edelhoch method [213], taking into account contributions from tyrosine and tryptophane present in the primary structure. Prior to calculation, nonprotein absorbance at 280 nm was subtracted as described in [214]. Tyrosine and tryptophane absorptivities amount to 1280 and 5690 $\text{M}^{-1}\cdot\text{cm}^{-1}$, respectively. This procedure is affected by an estimated error of 5% at most [215]. Phospho peptides were totally hydrolyzed by hydrochloric acid (5 M HCl, 24 h, 95°C) and the free amino acids were determined either by a ninhydrin-based assay as reported before [216] or by a HPLC-based method (HPLC system 1) as described by BÄBLER [217]. Both methods yielded equivalent results.

4.9. SDS-PAGE

SDS-PAGE was carried out as a discontinuous electrophoresis as described by LÄMMLI [218]. The gels were pipetted as shown in Table 1 and, after addition of TEMED and APS, the separating gel transferred between glass slides.

Table 1: Constitution of 12% separating gels and 4% stacking gels.

2 Gels	Separating gel	Stacking gel
Acrylamid-Bis 40%	4500 μl	975 μl
1,5 M Tris-HCl pH 8,8	3750 μl	---
0,5 M Tris-HCl pH 6,8	---	1875 μl
mQ-Wasser	6510 μl	4500 μl
SDS 10% (w/V)	150 μl	75 μl
APS 10% (m/m)	75 μl	37.5 μl
TEMED	15 μl	15 μl

After polymerization under n-BuOH (30 min), the butanol was removed, the surface washed three times with water and the stacking gel poured onto the

separating gel. After inserting the gel comb, polymerization proceeded for 45 min. The resulting gels can be stored at +4°C in a humidified bag for up to one week. Protein samples were diluted 1 : 2 with loading buffer and incubated at 95°C for 5 min at 1000 RPM. The protein separation was performed using 4% stacking gels and 12% separating gels (crosslinking C = 2.6%). Up to 20 µl per lane were loaded onto the gel (thickness 0.75 mm). The electrophoresis was run at a voltage of 80 V (stacking gel) and 160 V (separating gel) until the blue dye was migrated out of the gel. For analytical SDS-PAGE, an unstained protein ladder was used (Protein Marker III, Applichem), while for SDS-PAGE in preparation for western blotting, a stained protein marker (Protein Marker II, Applichem) was favored. For colloidal Coomassie staining, the gel was shaken for 1 h in fixer, washed twice with water and stained overnight in Coomassie staining solution (49 parts staining solution I + 1 part staining solution II, prepared at least 3 h in advance and shaken until use). Destaining was done with water. Gelanalyzer 2010a was used for densitometric evaluation.

4.10. Western Blot

After SDS-PAGE, the gel was equilibrated for 20 min in transfer buffer. Blotting on nitrocellulose membranes (HyBond) was carried out in a Trans-Blot SD semi dry transfer cell (Bio-Rad) for 90 min at 25 V for a single mini-gel. Blotting was controlled by Ponceau S staining of the membrane prior to blocking (5 min shaking in Ponceau staining solution, partly destained with water for visual inspection and, finally, completely destained with TBS-T). Blocking of the membrane was performed by adding 5% (w/V) BSA (EIA/RIA grade) in TBS-T for 1 h at ambient temperature on a shaker. After washing twice with TBS-T, the primary antibody diluted in TBS-T containing blocking protein (5%) was incubated overnight with the membrane (4°C). The next day, the membrane was rinsed three times and washed five times with TBS-T, before a dilution of suitable secondary antibody in TBS-T was added (incubation for 1 h at room temperature). Finally, three rinsing and five washing steps were conducted, before detection by enhanced chemoluminescence (ECL detection kit) was performed according to the recommendations of the supplier.

All antibodies that were used are listed in Section 4.3. Dilutions were made as recommended by the respective supplier.

4.11. Dot Blot

Dot blots were carried out using the WesternBreeze chromogenic immunodetection kit (Invitrogen). This kit makes use of the BCIP/NBT system (5-bromo-4-chloro-3-indolyl phosphate / nitro blue tetrazolium). The secondary antibody is conjugated to alkaline phosphatase that produces a blue purple product from BCIP/NBT [219].

After kinase reaction, samples were dried using a SpeedVac, redissolved and a volume of 5 μ l was spotted onto a PVDF membrane, air-dried and treated according to the instructions of the WesternBreeze manufacturer. Gel Pro Analyzer 3.1 was used for densitometric evaluation.

4.12. TCA Precipitation

Protein precipitations were carried out in Protein LoBind tubes (1.5 ml). The procedure was started by addition of trichloroacetic acid to a final concentration of 5%. The mixture was incubated on ice for 30 min and, subsequently, centrifugated (10.000 g, 10 min, 4°C). The supernatant was removed and the pellet washed with acetone (dried, degassed and precooled to -20°C). After another centrifugation step (*vide supra*) and removal of the supernatant, the pellet was washed again twice. Finally, solvent residues were evaporated *in vacuo*.

4.13. *In vitro* Kinase Reactions Utilizing Protein Substrates

Kinase reactions were carried out using 125 nM protein substrates and were started by addition of ATP to a final concentration of 250-400 μ M. Standard kinase buffer consisted of 50 mM Tris-HCl pH 7.5, 40 mM NaCl, 10 mM MgCl₂, 1 mM DTT, 2 mM molybdate, 0.04% Triton X-100, and EDTA-free protease inhibitor cocktail. The reaction mixture was incubated for 2 h at 30°C and the reaction terminated by addition of 20 μ l stop solution (100 mM EDTA in 50 mM Tris, pH 7.5). Recombinant Cdk1 and Cdk1/CycB1 complex were obtained as GST fusion proteins from ProKinase (Freiburg, Germany) and their phosphorylation monitored via western blotting. The protein was subjected to TCA precipitation and dissolved in loading buffer before subsequent SDS-PAGE and western blotting procedures were carried out.

4.14. Fluorescence Polarization: Background and Analysis

Fluorescence polarization (FP) is a ratiometric technique which depends on differing rotational properties between small and large molecules.

When an isotropically distributed fluorophore is excited by plane-polarized light, only those fluorophores which are appropriately oriented relative to the excitation plane can absorb the light, a process called photoselection [220].

However, these fluorescent molecules are not immobilized but undergo free diffusion and rotation (Brownian motion). When fluorescent molecules in solution are excited with polarized light, the degree to which the emitted light retains polarization reflects the rotation that the fluorophore underwent during the course of the excited state [221]. For a very slowly rotating molecule, the polarization of the exciting light is maintained during emission, while a quickly rotating molecule displays nearly isotropic emission upon polarized excitation. This phenomenon was first described by PERRIN in 1926 [222].

Fluorescence polarization is quantitated by measurement of the fluorescence intensity in two detection planes perpendicular to each other, parallel to the exciting light (I_{\parallel}) and perpendicular to the exciting light (I_{\perp}). The difference between both channels ($\Delta I = I_{\parallel} - I_{\perp}$) can be normalized against the sum of both channels ($I_{\parallel} + I_{\perp}$), leading to the entity polarization P , or against the total fluorescence intensity, leading to the entity anisotropy r . Both dimensionless entities have equal physical meaning, but anisotropy should be preferred due to reasons of additivity [223]. The total fluorescence intensity I_{total} is mathematically represented as follows [224]:

$$I_{\text{total}} = I_{\parallel} + 2 * I_{\perp} \quad (\text{Eq. 6})$$

The influences on FP can be described quantitatively by the Perrin-Equation [222]. In short, FP of a given molecule is positively correlated to the absolute temperature, and it is negatively correlated to the viscosity of the solution and the effective molar volume of the rotating unit. For a spherical protein, the unknown volume can be approximated by a term containing the molecular weight, the degree of hydration and the partial specific volume [220, 225]. Taken together, there is a correlation between FP and the molecular weight of the fluorescent molecule (or complex) that can be used analytically.

Fluorescence polarization was measured using a NOVOstar or a PolarStar OMEGA plate reader (BMG) at 485 nm excitation and 520 nm emission

wavelength using the suitable FP optics module. Prior to sample measurements, calibration by means of 30 nM fluorescein was performed and used to calculate a K-factor (Eq. 7), which was afterwards used to calculate the fluorescence polarization P of the respective sample (Eq. 8).

$$K = \frac{I_{\parallel} - P_{Fluorescein} * I_{\parallel}}{P_{Fluorescein} * I_{\perp} + I_{\perp}} \quad (\text{Eq. 7})$$

$$P = \frac{I_{\parallel} - K * I_{\perp}}{I_{\parallel} + K * I_{\perp}} \quad (\text{Eq. 8})$$

Prior to each calculation of fluorescence polarization, a background correction was carried out by subtracting the average fluorescence intensity of at least five appropriate control wells in each detection plane. Since fluorescence polarization does not behave additively, use of this unit will lead to tainted results [223]. Therefore, fluorescence polarization is reported as anisotropy r (Definition of anisotropy is shown in Eq. 9).

$$r = \frac{I_{\parallel} - I_{\perp}}{I_{\parallel} + 2 * I_{\perp}} \quad (\text{Eq. 9})$$

Polarization P can be converted into anisotropy r using equation 10.

$$r = \frac{2 * P}{3 - P} \quad (\text{Eq. 10})$$

In all FP assays, the total fluorescence intensity (Eq. 6) was monitored to reveal inconsistencies and identify false positives.

4.15. Fluorescence Polarization Immunoassay (FPIA)

Tyrosine kinase activity using synthetic Cdk1-derived peptides QKIGEGTYGVVYKC (TY), EKIGEGTYGVVYKC (eTY), QKIGEGpTYGVVYKC (pTY), QKIGEGTpYGVVYKC (TpY) and QKIGEGpTpYGVVYKC (pTpY) was analyzed via a fluorescence polarization immunoassay as a modified version of the one published in [24]. pTpY was labeled with fluorescein-5-maleimide to give the final probe pTpY-F5M. The labeling procedure and subsequent purification via HPLC (system 1) was conducted following the protocols developed by BÄBLER [217].

Myt1-Kinase (50 nM) in kinase buffer was pre-incubated with Cdk1-derived peptides (10 μ M) or 2 μ g/50 μ l Ala:Glu:Lys:Tyr_{6:2:5:1} (Poly-AEKY) in a total volume of 50 μ l in black half-area 96-well microplates. The reaction was started by addition of ATP (250 μ M) and proceeded for 2 h at 30°C. Subsequent

termination by 25 μ l stop solution was followed by addition of 25 μ l detection solution consisting of respective antibody and 20 nM pTpY labeled with fluorescein-5-maleimid (pTpY-F5M) in 25 mM Tris-HCl pH 7.5, 150 mM NaCl, 10 mM MgCl₂. After another incubation period (30 min), fluorescence polarization was measured. Antibodies utilized for this application were anti-pTyr15-Cdk1 antibody (8.8 nM final concentration) for the detection of Tyr - phosphorylated Cdk1-derived peptides and anti-pTyr antibody (135 nM final concentration) for the detection of phosphorylated Poly-AEKY.

4.16. pTyr FP Immunoassay (FPIA II)

Kinase reactions were carried out in 96-well half area non binding surface plates in a final assay volume of 40 μ l. Peptide substrate (20 - 200 μ M) was dissolved in the same buffer as used in microarray assays. ATP was present at 400 μ M. Kinase reactions were started by the addition of kinase (40 nM), proceeded for 2 h at 30°C (gentle shaking) and were terminated by addition of 10 μ l stop solution (100 mM EDTA, 50 mM Tris-HCl, pH 7.5). For the inhibitor studies, all dilutions were made from 10 mM stock solutions in DMSO and had a final assay concentration of 5 μ M with 0.5% DMSO in the assay buffer.

pTyr-peptide detection was performed by adding 10 μ l of a solution containing anti-pTyr antibody (pTyr-P-100) and (6-FAM)KI(pY)VV to a final concentration of 45 nM and 2.5 nM, respectively. After equilibration for 1 h at room temperature on a shaker, fluorescence polarization was measured as described in Section 4.14. Suitable background controls were carried along to allow for specific background correction.

4.17. LanthaScreen Binding Assay

TR-FRET binding assays were performed in white 384-well low volume plates at room temperature in sterile-filtered kinase buffer A (KBA) consisting of 50 mM HEPES-NaOH (pH 7.5), 0.01% Brij-35, 10 mM MgCl₂, and 1 mM EGTA.

4.17.1. Instrumentational Setup and Data Analysis

The LanthaScreen Eu kinase binding assay is a very demanding assay in terms of the instrumental requirements. In this work, three different plate readers were used for this assay. The instrumental settings used for each device are displayed in Table 2. The results obtained using these settings are of comparable quality.

A ratio of raw acceptor/donor intensities was calculated and normalized relative to wells containing fully bound or fully outcompeted tracer and reported as [relative percent tracer displaced].

Table 2: Time-resolved fluorescence settings for performing LanthaScreen kinase binding assays.

Plate Reader	PolarStar OMEGA (BMG) ^a	Infinite M1000 (Tecan)	EnVision (Perkin-Elmer)
Excitation filter	337/30 nm	317/20 nm ^b	340/30 nm
Emission filter 1 (acceptor)	TR 665 nm	665/12 nm ^b	665/10 nm
Emission filter 2 (donor)	TR 620 nm	620/12 nm ^b	615/10 nm
z-height	9 ^c	'optimal'	'optimal'
Delay	60 μs	100 μs	60 μs
Integration time	100 μs	200 μs	100 μs
Number of flashes	50	100 (100 Hz)	100
PMT gain	auto	auto	auto

^a Advanced Assay Technology TRF reading head required.

^b Tecan Infinite M1000 is a monochromator based plate reader, no filters are required.

^c The z-height has to be adjusted manually. In the present assay, z-height position 9 performed best.

4.17.2. Tracer Titrations

A serial dilution starting from 3000 nM tracer concentration was conducted in KBA. 5 μl of this solution was transferred to respective wells and, after addition of 5 μl positive control (30 μM PD166285 in KBA with 3% DMSO) or 5 μl vehicle control (3% DMSO in KBA), 5 μl solution containing 6 nM Eu-labeled antibody and 3-fold the desired kinase concentration in KBA was added. Final test concentrations were 2 nM Eu-labeled antibody, 10 μM PD166285, 1% DMSO and varying concentrations for tracer and Myt1. After centrifugation (500 g, 2 min), the plate was incubated at room temperature for 1 h while being shaken (500 RPM). After another centrifugation step, the plate was read as described in Section 4.17.1.

4.17.3. Inhibitor Studies

For all experiments with a kinase inhibitor, a dilution series of inhibitor was first prepared in 100% DMSO at 100fold the desired final assay concentration. From this master dilution series, inhibitors were diluted 33.3fold in kinase buffer for an intermediate concentration of inhibitor 3fold of that to be used in the assay

(containing 3% DMSO). To 5 μ L of each concentration of inhibitor to be tested, appropriate assay reagents (15 nM Myt1, 10 nM tracer, 2 nM Eu-labeled anti-His-tag antibody) were added to bring the final volume to 15 μ L and the final DMSO concentration to 1%. In general, all assays were performed with three replicates of each inhibitor concentration. Plates were centrifugated at 500 g for 2 min after pipetting and before reading (see 4.17.1).

4.18. Synthesis and Characterization of DasAFITC

All reagents were purchased and used without further purification unless stated otherwise. Solvents were dried according to standard procedures. All reactions were carried out under an atmosphere of dry argon. Mass spectra (MS) were recorded off-line with nano-ESI (Proxeon emitters, Odense, Denmark) on a LTQ-Orbitrap XL (Thermo Scientific). ^1H NMR and ^{13}C NMR spectra were recorded on a Varian Gemini 2000 and a Varian Inova 500; chemical shifts were referenced to residual solvent signals and reported in ppm (δ). Chromatography was performed on silica gel (Merck silica gel 60, 40e63 mesh) by MPLC (Interchim PuriFlash 430). As in-process control, TLC was carried out on silica gel plates (E. Merck 60 F254); spots were detected visually by ultraviolet irradiation (254 nm) or by spray detection (compound **3**, solution of 150 mg ninhydrin, 1.5 ml glacial acetic acid and 45 ml acetone) and heated to 130°C for 2 min.

The purity of the final compounds was determined by analytical HPLC (system 2) using a LiChroCART 125-4 (LiChrospher 100) RP-18 column (5 μ m). A slightly modified method as described previously was used [226]. Modifications included the use of MeOH:buffer 60:40 as an eluent and, additionally to UV-detection (Jasco UV-975), fluorescence detection (Jasco FP-920) at 480 nm (excitation) / 520 nm (emission).

Dasatinib **1** was from LC Laboratories (Woburn, MA, USA). The azide **2** was synthesized using a modified approach from ISAACS et al. [227-228]. Dasatinib (200 mg, 0.41 mmol) was dissolved in 5 ml THF and cooled to -5°C. Diphenylphosphoryl azide (DPPA; 137 μ l, 0.615 mmol) was added and stirred for 15 min. Subsequently, the base DBU (92 μ l, 0.615 mmol) was added dropwise. The reaction mixture was stirred for 16 h and allowed to warm to room temperature. NaN_3 (70 mg, 1.08 mmol) was added and the resulting suspension stirred for another 5 h. Saturated KHCO_3 -solution was added and the precipitate was filtered off. Purification was carried out by column chromatography using

chloroform/methanol on silica gel. The resulting organic azide **2** was instantly reduced by hydrogen using catalytic amounts of palladium (5%) on carbon. The azide **2** (184 mg, 0.36 mmol) was dissolved in 15 ml MeOH + 1 ml ethyl acetate. After addition of catalyst and connection to hydrogen at 1 bar, the reaction proceeded for 23 h giving the respective amine **3**. ^1H NMR (400 MHz, CD_3OD) δ 8.18 (s, 1H, thiazol-**H**), 7.39 (dd, $J = 7.3$; $J = 1.8$ Hz, 1H, chloroanilide-**H**), 7.32 – 7.21 (m, 2H, chloroanilide-**H**), 6.05 (s, 1H, pyrimidine-**H**), 3.77 – 3.60 (m, 4H, pyrimidine- $\text{N}(\text{CH}_2\text{-R})_2$), 2.93 (t, $J = 7.3$ Hz, 2H, $\text{R-CH}_2\text{-NH}_2$), 2.71 – 2.55 (m, 6H, $(\text{R}_{\text{alkyl}}\text{-CH}_2)_3\text{-N}$), 2.51 (s, 3H, pyrimidine- CH_3), 2.36 (s, 3H, chloroanilide- CH_3). MS (ESI) m/z 487 $[\text{M}+\text{H}]^+$, m/z 485 $[\text{M}-\text{H}]^-$.

N-[3',6'-dihydroxy-3-oxo-3*H*-spiro(2-benzofuran-1,9'-xanthen)-5-yl]-*N'*-(2-[4-{4-([*N*-{2-chloro-6-methylphenyl}-5-carboxamido]-thiazol-2-yl)amino-2-methylpyrimid-6-yl}piperazinyl]-ethyl)thiourea **4**, was synthesized using a modified procedure by LEE et al. [229]. The amine **3** (85 mg, 0.18 mmol) was dissolved in 5 ml THF/abs. EtOH (3:2) and cooled to 0°C. FITC isomer I (90 mg, 0.23 mmol), dissolved in 1 ml solvent, was added and the reaction was stirred for 6 h. The mixture was frozen in dry ice and lyophilized. The residue was purified by MPLC (chloroform/methanol gradient) to give the final fluorescent probe **4** (51 mg, 33%). The full characterization is given in Section 5.3.1. Fluorescence characterization by 3D scans and emission scans was conducted by means of Tecans's Infinite M1000 plate reader. Aqueous buffered solutions (10 μM compound in 50 mM Tris-HCl pH 7.5) were used.

Because the synthesized fluorophore **4** is a Dasatinib-derived Amine coupled to FITC, it is referred to as DasAFITC in the following.

4.19. CMC Determination Assays

When DasAFITC was used for CMC assays, the assay buffer consisted of 50 mM HEPES-NaOH pH 7.5 plus respective detergent. The assay volume was 60 μl with a final concentration of 5 nM fluorescent probe DasAFITC. After a 15 min incubation period at gentle shaking, FP was measured as described (Section 4.14). For investigations on association colloid formation of glycolipids and DasAFITC, two further methods were used, basically as described: a photometric assay based on inclusion of Coomassie Brilliant Blue G-250 [230], and a fluorimetric assay based on inclusion of 1,6-diphenyl-1,3,5-hexatriene (DPH) [231]. The fluorescence assay (filter settings: 355 nm Ex/ 460 nm Em) was

conducted in black half-area 96-Well plates (Corning) with a final assay volume of 60 μ l, while the absorbance assay (monitored at 450 nm and 620 nm) was performed in transparent 96-well plates (Greiner) with an assay volume of 250 μ l. DasAFITC did not interfere spectroscopically with either of the assays. As a reference, Triton X-100 had a CMC of 0.0096% and 0.008% (w/V), respectively.

4.20. DasAFITC Assay Procedure

The DasAFITC assay is an FP based kinase binding assay utilizing DasAFITC as a fluoroprobe. Wee1, Btk and Abl1wt were obtained from ProQinase as GST fusion proteins. The assays were carried out in black half-area 96-well plates (Corning). Fluorescence anisotropy was measured with a BMG PolarStar OMEGA or a BMG NOVOstar plate reader (Heidelberg, Germany) using a 485 nm excitation and 520 nm emission filter setup. Whenever dasatinib was used as a displacement control, it was included in the assay buffer at a concentration of 10 μ M.

4.20.1. Kinase Concentration and Incubation Time

For initial titrations, 5 nM ligand was incubated with increasing concentrations of the respective kinase (0-80 nM for Abl1, Btk and Wee1, 0-250 nM for Myt1). For each concentration, wells containing 10 μ M dasatinib were included as controls. The plates were gently shaken at room temperature and anisotropy r was measured after 30, 60 and 120 min. The difference between the values measured for sample and fully outcompeted sample at the respective concentration is displayed as Δr . All tests were carried out with 27 μ l assay volume. For long-term incubation tests (8 h), the assay volume was increased to 90 μ l in order to minimize evaporation effects.

4.20.2. Kinase Binding Assays

Kinase assays were conducted in sterile-filtered kinase binding assay buffer B (KBB). A final DMSO concentration of 1% was included at all times. For all experiments with potential inhibitors, a dilution series was prepared in DMSO at 100-fold the desired assay concentration. From this dilution series, inhibitors were diluted 33.3-fold in assay buffer, yielding 3-fold the desired assay concentration in 3% DMSO. To 9 μ l of each concentration of compound to be tested, 9 μ l tracer and 9 μ l kinase solution were added, giving a total assay volume of 27 μ l. Each

data point was performed at least in triplicate. Final tracer concentration (DasAFITC) used was 5 nM. Kinase concentrations were 15 nM (Abl1), 40 nM (Btk), and 100 nM (Myt1). Incubation periods before reading were 60 min for Abl1 and Btk, and 120 min for Myt1. For better comparability, anisotropy values were normalized against dasatinib controls (100% tracer displaced) and vehicle controls (0% displaced). Each plate contained at least five wells of both controls.

4.20.3. Anisotropy Data Analysis

Data processing was generally carried out as described before (Section 4.14).

To deduce K_i values from this fluorescence polarization based competition assay, displacement curves were fitted to the exact competitive binding model [232-233], as shown in Eq. 11:

$$r = \frac{r_f + \frac{[Myt1]}{K_d} * g * r_b}{1 + \frac{[Myt1]}{K_d} * g} \quad (\text{Eq. 11})$$

where $[Myt1] = -\frac{a}{3} + \frac{2}{3} * \sqrt{(a^2 - 3b)}$ * $\cos \frac{\theta}{3}$, with

$$a = K_d + K_i + [Tracer]_0 - [I]_0 - [Myt1]_0$$

$$b = K_i * ([Tracer]_0 - [Myt1]_0) + K_d([I]_0 - [Myt1]_0) + K_d * K_i$$

$$c = -K_d * K_i * [Myt1]_0$$

$$\theta = \arccos \frac{-2a^3 + 9ab - 27c}{2 * \sqrt{(a^2 - 3b)^3}}$$

K_d is the dissociation constant of the complex between the ligand and the enzyme, K_i is the dissociation constant of the complex between competitive inhibitor and enzyme. r_f and r_b are the anisotropies of free and bound labeled ligand, g equals the quantum yield enhancement factor with regard to wells without kinase but with tracer. The total inhibitor concentration is represented by $[I]_0$.

4.21. Microarray Assays

Two microarray slides were positioned face-to-face, separated by two spacers (0.3 mm). 350 μ l reaction mixture containing kinase (80 nM) in sterile filtered standard kinase buffer together with 250 μ M ATP was transferred bubble-free into the resulting reaction space between the two slides. Subsequently, the slide sandwich was incubated at 30°C for 2 h in a humid chamber. After incubation, the slides were washed five times with 50 ml TBS containing 0.1% Triton X-100 for 5 min followed by washing steps with deionized water. Finally, the microarray slides were spun dry at room temperature. For antibody detection, Tecan's Hyb

Station HS 400 was used in a semi-automatic procedure. All steps were carried out at 25°C and the protocol was as follows: After 2 washing steps with TBS-T (TBS + 0.1% Tween-20; 2 min wash, 2 min soak), a wash and soak step with TBS was performed. Subsequently, the primary antibody (Anti-pTyr P-100, at 10 µg/ml in TBS-T containing 3% BSA) was injected and hybridized for 1 h. After 5 washing steps with TBS-T and another step with TBS, the secondary antibody (Goat anti-mouse IgG #35515 as Dylight 649 conjugate (Pierce) at a concentration of 1 µg/ml in TBS-T containing 3% BSA) was injected and hybridized for 30 min. After five additional washing steps (TBS-T), the slides were rinsed with TBS and deionized water. Subsequent drying under a stream of gaseous nitrogen yielded slides ready for detection. For negative controls, the microarrays were subjected to the same procedure without addition of kinase.

The microarray slides were scanned at 635 nm (red channel) and 532 nm (green channel) using GenePix 4000B (Molecular Devices) at a PMT gain of 600. The response from the red channel was used to quantify the response, while the green channel was used to align the array grid in analysis. Images were saved electronically (TIFF and JPG formats) and analyzed utilizing the circular feature alignment of the GenePix Pro 6.1 software and GenePix Array List (GAL) files supplied by JPT (Berlin, Germany). Quality control conditions set were as described before [234]. GenePix results were saved and the median foreground and background intensities of the individual peptide spots were used for further analysis.

In the case of the radioactive assay, which was carried out in the working group of Prof. Schutkowski (Institute of Biochemistry and Biotechnology, MLU Halle Wittenberg), 300 µl of reaction mixture containing kinase in assay buffer together with 10 µM ATP and 500 µCi [γ -³³P]-ATP were transferred into the reaction space between the two slides. The incorporated radioactivity was detected by exposure of the microarrays for 2-8 d to imaging plates (Fuji BAS-MS) followed by readout with a phosphor imager (FujiFilm FLA-7000).

4.22. Solid Phase Peptide Synthesis

Peptides Cdk1¹⁻²⁴ (H-MEDYTKIEKIGEGTYGVVYKGRHK-OH) and Ac-Cdk1¹⁻²⁴ (Ac-MEDYTKIEKIGEGTYGVVYKGRHK-OH) were synthesized on Fmoc-Rink MBHA basically as described in [235] following a standard Fmoc/tBu based strategy. After final cleavage of side-chain protecting groups and cleavage

from the resin by TFA containing 2% water, the TFA was removed using a rotary evaporator. The crude product was precipitated by addition of cold diethyl ether, carefully filtered off and washed with cold ether. Solvent residues were removed *in vacuo* in an exsiccator. Purification was carried out by preparative RP-HPLC. A prepacked 250-25 mm LiChrospher 100 RP-8 (5 μ m) column from Hibar was used and the UV-Vis detector was set to 220 nm. A shallow gradient over 100 min from water containing 0.1% TFA to 50% ACN (0.1% TFA) was run and the eluate collected and fractionated.

Purities > 80% at 220 nm were achieved as indicated by analytical HPLC (system 3, water / ACN gradient): H-Cdk1¹⁻²⁴ (86.1%) and Ac-Cdk1¹⁻²⁴ (80.1%). Analysis was realized using a RP18 column. Identity was confirmed by Dr. Schierhorn from the Institute of Biochemistry and Biotechnology (MLU Halle-Wittenberg) using MALDI-MS with 2,5-Dihydroxybenzoic acid matrix. Spectra and chromatograms are given in the appendix (p. 146).

5. Results and Discussion

As assay development is central to this work, substrate studies were conducted to find out about a possible further progression. Since this turned out to be difficult, assay development focused on binding assays as a means of screening compounds without need for an *in vitro* substrate. Indeed, after development and establishment of binding assays, potential inhibitors were tested and also a postulated Myt1 inhibitor (a glyco-glycerolipid) was thoroughly reevaluated. Finally, the search for an *in vitro* substrate was taken up again and microarray experiments led to the identification of suitable substrates.

5.1. Substrate Studies

Identification of a molecule that can be phosphorylated by the isolated kinase is one of the most important parts of kinase assay development [223]. Therefore, a detailed analysis of different substrates was required. Initially, three general types of substrates were tested: a heterodimeric protein complex Cdk1/CycB1 representing the native substrate, the single Cdk1 protein and peptides derived from the phosphorylation sites Thr14 and Tyr15 within the Cdk1 primary structure. The phosphorylation status was monitored individually for each phosphorylation site in order to reveal differences or similarities.

In this study, full-length Myt1 (sometimes referred to as Myt1fl) was expressed in the human cell line HEK293 as His₆ fusion protein, solubilized and, subsequently, purified via immobilized metal ion affinity chromatography, as described in [236]. First of all, the question was whether Myt1 kinase shows the expected kinase activity. The native substrate Cdk1/CycB1 as well as monomeric Cdk1 were used in kinase reactions and phosphorylations at Thr14 and Tyr15 were monitored via western blot analysis using anti-pThr14-Cdk1- and anti-pTyr15-Cdk1-antibodies (Fig. 6).

Regarding Cdk1, a definite increase of pThr14 and pTyr15 in presence of Myt1 was detected. Results of controls with and without ATP were comparable concerning both phosphorylation sites. Using Cdk1/CycB1 as a substrate, the phosphorylation pattern changed, controls with and without ATP no longer matched. In fact, hyperphosphorylation at both sites of interest was detected, indicating autophosphorylation by the activated kinase complex. Under these conditions, the amounts of product formed in an autophosphorylation reaction are

similar to those mediated by Myt1 and the actual contribution of autophosphorylation and phosphorylation by Myt1 cannot be figured out clearly. However, the fact that Myt1 accepts Cdk1 cyclin complexes has been studied before using a catalytically inactive Cdk1(K33R) mutant [87].

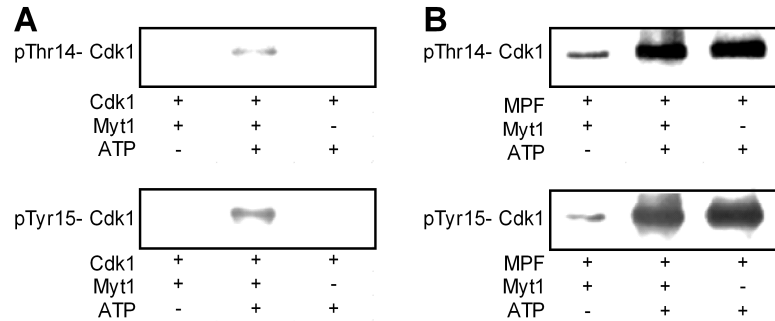


Fig. 6: Phosphorylation of Cdk1 (A) and Cdk1/CycB1 (MPF, B) by human Myt1 kinase. Shown are representative western blot images using anti-pThr14-Cdk1- (top) and anti-pTyr15-Cdk1- antibodies (bottom). Each panel consists of the respective sample surrounded by controls with and without ATP/enzyme.

The finding that Cdk/Cyc complexes are prone to autophosphorylation raises an issue with previous Myt1 inhibition data. It might interfere with a Myt1 kinase activity assay utilizing an active complex as a substrate, particularly because no control experiments without Myt1 were mentioned [24]. This issue and its implications will be discussed in more detail in upcoming sections.

Generally, a reasonable approach toward yielding a screening-amenable substrate is to use peptides derived from the native phosphorylation site or the use of randomly generated peptides [237].

Utilizing peptide substrates, tyrosine phosphorylations were investigated by means of a fluorescence polarization immunoassay (FPIA).

The assay is based on a labeled probe (low FP) that can be bound by an antibody, resulting in a high FP value. The general principle was introduced by DANDLIKER and FEIGEN in 1961 [238] and, decades later, adapted to kinases in a direct approach [239]. In order to save antibody and gain sensitivity, the assay principle was converted to a competitive FPIA shortly after [240]. Such a competitive approach was used in the following.

FPIA was performed as a modified version of the one published in [24]. Modifications include an increase in sensitivity by 10fold and monitoring of Tyr15 phosphorylation independent from the Thr14 status.

A bis-phosphorylated peptide derived from the native phospho-site (Cdk1⁸⁻²⁰) together with a C-terminally inserted cysteine (pTpY: QKIGEG(pT)(pY)GV-

VYKC) was labeled thiol-selectively with fluorescein-5-maleimide according to established protocols [217]. The fluorescent probe (pTpY-F5M) shows a rather low intrinsic fluorescence polarization which is increased upon addition of a suitable antibody. In solution, the antibody-antigen-complexes rotate more slowly than the antigen on its own, resulting in a higher FP value. The assay concentration for the probe should be as low as possible to set up a sensitive method. As indicated by pretests, a probe concentration of 5 nM is suitable to obtain sufficient signal to background ratios (S/B) and coefficients of variation for both channels ($CV < 5\%$). The pTyr targeting monoclonal antibodies used had satisfactory affinities towards the probe as indicated by antibody titrations: K_d values of 8.5 nM (anti-pTyr15-Cdk1) and 124 nM (anti-pTyr antibody) were obtained (data not shown). The respective assay concentrations were 8.8 nM (anti-pTyr15-Cdk1) and 135 nM (anti-pTyr antibody).

Using the specific anti-pTyr15-Cdk1 antibody, the assay makes the detection of low nanomolar concentrations of phosphorylated peptide possible. The EC_{50} lies around 18 nM, meaning a substrate turnover of 0.18% (at 10 μ M substrate) would result in a half maximum FP-decrease (Fig. 7). The differing height of the bottom plateaus could be explained by unspecific effects caused by increased amounts of BSA and glycerol that were brought into the assay when using the more specific antibody (purchased with a lower antibody concentration).

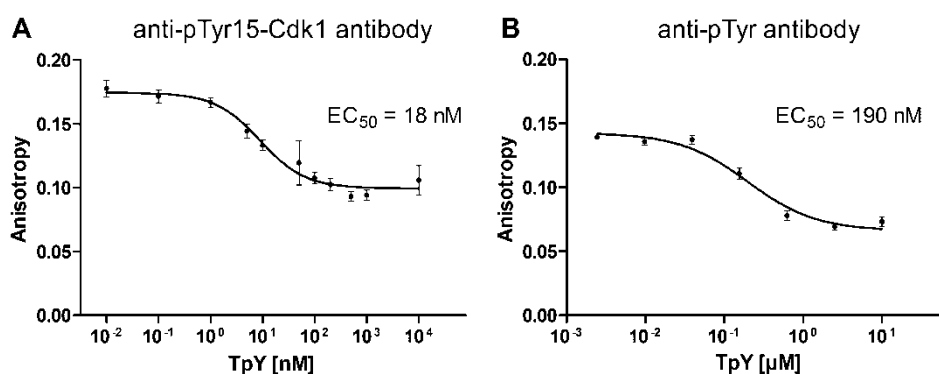


Fig. 7: To assess the analytical performance of both antibody setups with (A) anti-pTyr15-Cdk1-antibody and (B) anti-pTyr-antibody, TpY, imitating phosphorylation of the utilized peptides, was used to displace the probe from the antibody. pTpY showed the same properties concerning displacement of the probe, whereas TY, eTY and pTY did not lead to a decrease in fluorescence polarization (data not shown). Data shown here represent means \pm SD ($n=3$).

Initially, only QKIGEGTYGVVYKC (designated TY) was tested, a Cdk1 derived peptide as described in [24] which contains amino acids 9 to 20 of the native Cdk1, the additional cysteine at the C-terminus and a change in the first position from native Glu8 to Gln8. TY was not accepted as a substrate by Myt1 to a

detectable extent, so it was hypothesized that the N-terminal Gln might form pyroglutamic acid in a spontaneous manner affecting the kinase reaction in some way. The hypothesis that TY has a tendency to form a pyroglutamic acid derivative was supported by capillary electrophoresis studies, which showed a gradual loss of a single positive charge during incubation periods in absence of enzyme (data not shown). Apparently, this cyclisation did not affect the antibody binding, but to avoid any negative effect it was changed to the native amino acid Glu at the N-terminus (eTY: EKIGEGTYGVVYKC). However, still no kinase activity could be detected. Also the Thr14 monophosphorylated TY peptide (pTY), which proved to be a suitable substrate for Myt1's closest relative, Wee1 kinase, was not recognized as a substrate (Fig. 8).

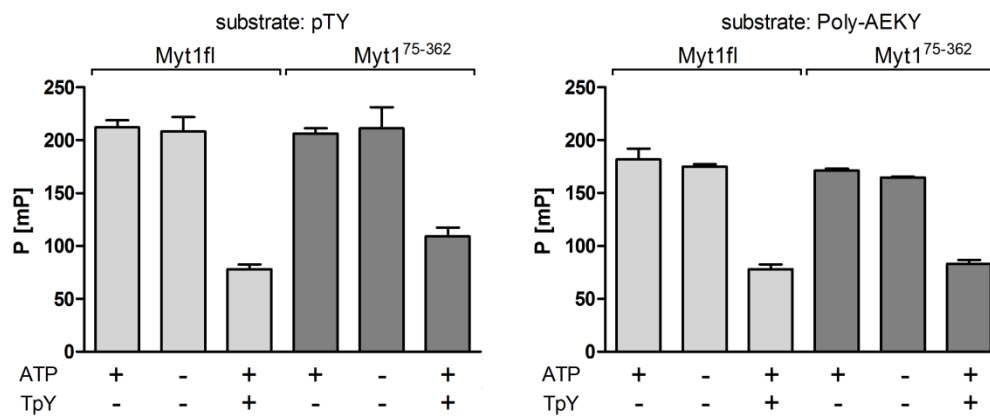


Fig. 8: Results of FPIA in terms of acceptance of peptidic substrates of Myt1fl and the kinase domain only (Myt1⁷⁵⁻³⁶²). For pTY (left) as well as Poly-AEKY (right), means of both samples differ highly significantly from TpY-containing positive controls ($p < 0.001$), indicating that no tyrosine phosphorylations occurred; utilizing TY or eTY as substrates resulted also in detection of no phosphorylated peptide (data not shown).

Since Cdk1 as a whole protein is accepted as a substrate, the possibility should be assessed that it might be an effect depending on the molecular mass only, because Cdk1-derived peptides have a much lower molecular weight compared to the entire Cdk1 protein, altering the interactions with the enzyme and the rigidity of the substrate. To answer this question, a polypeptide Poly-AEKY with an average molecular weight up to 30 kDa was tested as a substrate. This substrate was shown to be suitable as a tyrosine kinase substrate and, additionally, has been used successfully in Wee1 kinase assays [241-242]. In order to adapt the FPIA to this application, the antibody was simply changed to an unspecific pTyr-antibody, so any phosphorylated tyrosine can displace the fluorescent probe from the antibody (Fig. 7). No phosphorylation could be detected, indicating that this unspecific but large polypeptide is not suitable as a Myt1 substrate either (Fig. 8).

Determination of the threonine kinase activity turned out to be difficult, in part presumably due to the large neighbouring Tyr-moiety impairing binding of antibodies. Furthermore, pThr antibodies are often subjected to low affinity and narrow specificity [243]. Indeed, one monoclonal antibody (anti-pThr) failed to bind pTpY-F5M in fluorescence polarization as well as immunoblotting experiments (data not shown). A polyclonal antibody (anti-pThr14-Cdk1) was not suitable for FPIA but performed well in dot blot experiments. As can be seen in Fig. 9, no phosphorylation of Thr14 could be observed utilizing Cdk1-derived peptides as substrates in full-length Myt1 kinase activity experiments. Controls represent reaction mixtures without ATP where a defined amount of phosphopeptide was added to mimic product formation. If Myt1 catalyzed TY phosphorylation, it certainly would have been detected at substrate conversions down to 0.4%.

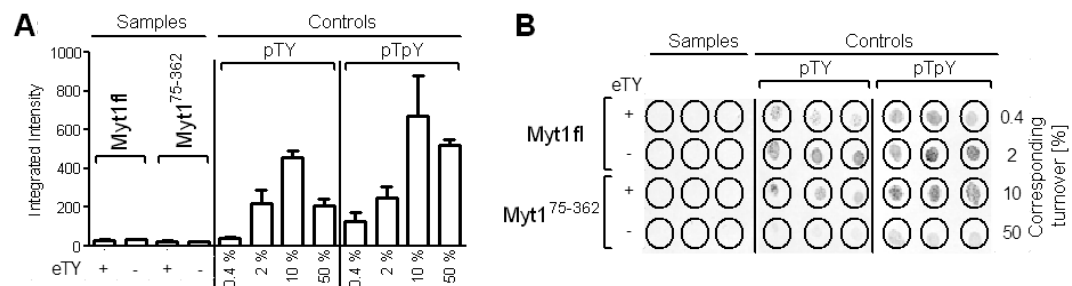


Fig. 9: Dot blot results using anti-pThr14-Cdk1 antibody as primary antibody. Panel A provides the densitometric evaluation derived from data shown in panel B. Neither Myt1fl nor Myt1⁷⁵⁻³⁶² showed any detectable phosphorylation activity utilizing eTY or TY (data not shown) as substrates. Positive controls show the expected signals for mono- and bisphosphorylated substrate at a turnover as indicated.

Since simplification of the substrate protein did not lead to any detectable kinase activity, the isolated kinase domain of the human Myt1 kinase was used as a model protein (Myt1⁷⁵⁻³⁶²). The C-terminal region (amino acids 437 – 499) is thought to be responsible for interaction with the Cdk1/CycB1 complex. Therefore, a protein lacking this sequence might be less restrictive in terms of substrate recognition [244]. In addition, the putative membrane association motif is not present anymore which remarkably facilitates purification procedures. Myt1⁷⁵⁻³⁶² was tested for Tyr and Thr kinase activity (see Fig. 8 for tyrosine and Fig. 9 for threonine kinase activity). Overall, the kinase domain showed no detectable kinase activity either in terms of Thr14 or Tyr15, leading to the conclusion that the recognition of the substrate by the full-length kinase might be of higher complexity.

The human Myt1 kinase was revealed to be a very restrictive enzyme concerning substrate acceptance. In fact, no simplified structure was identified that was phosphorylated by Myt1. The denial of phosphorylation is even more surprising considering the fact that Wee1, the closest relative of Myt1 within the human kinome, is known to accept all tested substrates (Table 3).

However, the tested protein substrates proved the kinase to be active in terms of Thr and Tyr kinase activity as expected.

Table 3: Comparison of Myt1 and Wee1 concerning substrate acceptance.

Substrate	Myt1 (Full-length)		Wee1 (Full-length)
	Thr kinase activity	Tyr kinase activity	Tyr kinase activity
Poly-AEKY	(No Thr residues contained)	-	+ [242]
Cdk1-derived peptides	-	-	+ [24, 82]
Cdk1	+	+	+ [82]
Cdk1/CycB1	(+) ^a	(+) ^a	+ [151]

^aContributions of autophosphorylation and phosphorylation by Myt1 cannot clearly be figured out, but acceptance has been shown before [87].

To achieve more insights into the interaction of Myt1 as well as Wee1 with their putative substrates, the X-ray structure of the related Cdk2 in complex with its substrate (PDB code: 1QMZ) was used to model all complexes. In silico studies were carried out by Dr. K. Wichapong (Department of Medicinal Chemistry, Institute of Pharmacy, MLU Halle-Wittenberg). Sequence alignment and protein modeling were performed using MOE2010.10 [245] and X-ray structures available in the Protein Data Bank (PDB code as indicated). For detailed information on the computational methods refer to [246]. Even though the percent sequence identity between each pair is relatively low (22.4% for Cdk2-Wee1, 28.6% for Cdk2-Myt1 and 35.3% for Myt1-Wee1, see appendix, Fig. 42), the overall 3D-structures are very similar as indicated by low root mean square deviations (RMSD) of about 2 Å for the kinase domain. Therefore, it is reasonable to use this Cdk2-substrate complex as a template to model the other complexes (Myt1-ATP-TY, Wee1-ATP-TY). The stability of the modeled complexes was investigated by molecular dynamics (MD) simulations which were carried out by means of Amber99SB [247]. Simulation time was set to 50 ns. The MD results show clearly that the Wee1-substrate was stable over the 50 ns with an interaction of Thr14/Tyr15 and the residues of the kinase phosphorylation site. In contrast,

the simulation of Myt1-ATP-TY shows the N-terminal part of the substrate moving out of the pocket in the case of Myt1 (Fig. 10).

This is also indicated by high fluctuation in the RMSD plots of the Myt1-substrate complex (around 5 - 6 Å) whereas the substrate in the Wee1 complex does not show significant movements (around 3 Å, see appendix, Fig. 43). The modeled kinase-substrate complexes (Fig. 10) suggest that the main difference among Wee1 and Myt1 and its substrate interaction may lie in the N-terminal part of the substrate from Gln8 to Thr14 as well as in the interacting residues at the Myt1 and Wee1 binding site.

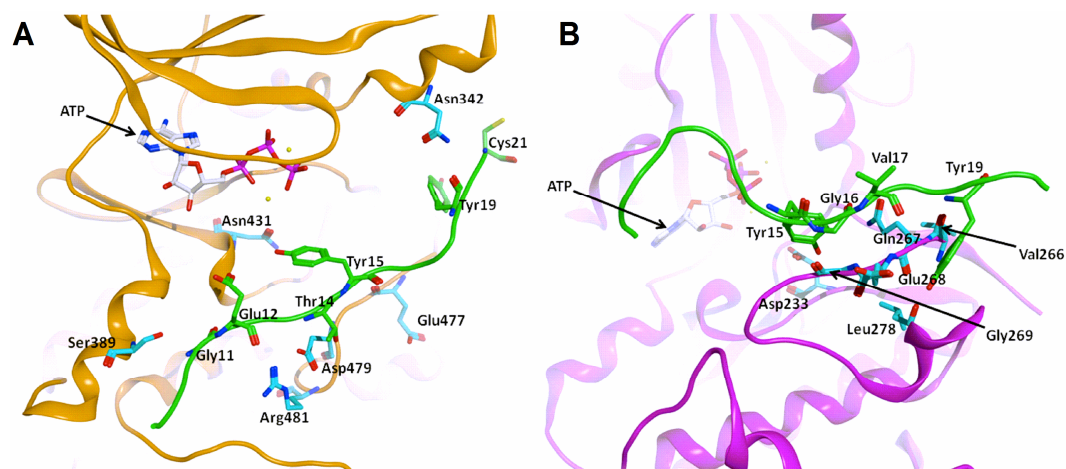


Fig. 10: Wee1-substrate (A) and Myt1-substrate complex (B) derived from the last snapshot (50 ns) of MD simulation. Protein structure is shown as orange ribbon for Wee1, magenta ribbon for Myt1 and amino acid residues of Wee1 and Myt1 are displayed as cyan stick. Substrate is represented by green ribbon.

In case of Myt1, Glu12 is surrounded by Gln195, Glu199 Asp270, Arg272, Tyr273 and Glu298, which introduce a strong negative electrostatic potential in the surrounding area (see appendix, Fig. 44), resulting in repulsion of the TY substrate as observed during the MD simulation. In the case of Wee1, Glu12 is surrounded by Ser389, Ala385, Cys509, Phe482, Asp479 and Arg483, which introduce a favorable positive electrostatic potential (see appendix, Fig. 44). Moreover, the Wee1-TY interaction is stabilized by two hydrogen bonds, one between Tyr392 of Wee1 (Gly202 in Myt1) and Gln8 (TY) and the second between Ser389 and Gly11 of TY. Hence, there are strong attracting interactions between the N-terminal part of the TY substrate and Wee1 explaining the substrate activity, whereas for Myt1 no favorable interaction could be observed. Which parts within the Cdk1 sequence are essential for Myt1 interaction and to what extent Cdk1 could be reduced in complexity in order to be recognized by Myt1 has to be clarified in further studies. The reader is referred to Section 5.5.

5.2. TR-FRET Based Binding Assay: LanthaScreen

Since the search for a suitable substrate turned out to be complex, a binding assay was used to obtain compound affinity data. The approach is guided by the assumption that a compound displacing ATP from the binding pocket will be an inhibitor of the respective kinase. This assumption mostly holds true, though exceptions are known [248]. In general, the use of binding assays in drug discovery is not necessarily accompanied by disadvantages. It has been shown that data gained by a kinase binding assay may provide a better correlation to cellular effects than a conventional enzyme activity assay. Moreover, the identification of hits targeting inactive kinase conformations is strongly facilitated compared to activity assays [249-250].

To generate a first inhibition profile, a TR-FRET based kinase binding assay as reported by LEBAKKEN et al. (LanthaScreen, [249]) was adapted to Myt1. In this assay, a fluorescently labeled ATP competitive kinase tracer binds to the kinase while a europium (Eu) labeled antibody binds to the purification tag of the recombinant kinase. The spatial proximity of Eu-labeled antibody and kinase tracer leads to Förster resonance energy transfer (FRET) to the fluorescence label (acceptor) upon excitation of the Eu (donor). Any non-inhibitor will not affect the binding to the kinase, therefore maintaining high FRET values, measured as ratio Emission (acceptor) to Emission (donor). If a compound displaces the tracer from the kinase, a spatial proximity between both labels will not exist anymore and the FRET will be lowered. Enabled by the lanthanoid label, a time-resolved measurement mode is used in this assay system to obtain improved signal to noise ratios.

5.2.1. Assay Development: LanthaScreen (Adaption to Myt1)

The development of an assay, particularly a binding assay, requires a known inhibitor. PD166285 was reported to be a potent Myt1 inhibitor ($IC_{50} = 72$ nM), although being more potent against Wee1 ($IC_{50} = 24$ nM) [151]. At the time the assay was implemented, it was the only known confirmed inhibitor [133, 251]. It is a very promiscuous inhibitor which targets many other kinases, such as c-Src and PDGFR [251] to mention only two, but it was used in early assay development as a positive control.

The LanthaScreen assay platform is validated by the supplier for 239 kinases including various kinase mutants (as of July 2013) but Myt1 has not been

described so far. Each kinase requires an affine commercially available tracer to set up such an assay and the suitable kinase-tracer pair has to be found on a case-by-case basis. Guided by kinase similarities, two promising tracers (chemical structures are not disclosed by the manufacturer) were chosen and tested. Binding of the tracer was tested by adding various dilutions of the respective tracer to a mixture of kinase and Eu-labeled anti His-tag antibody in presence or absence of PD166285 (10 μ M) at different concentrations of Myt1. Fig. 11 displays tracer titrations for both tested tracers at 15 nM Myt1.

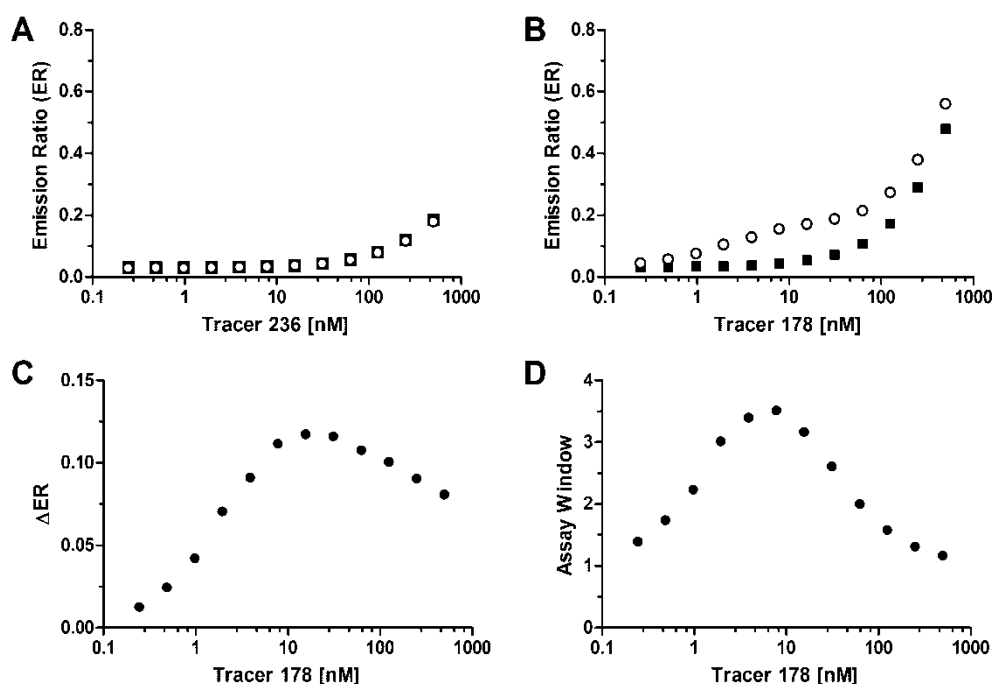


Fig. 11: Tracer titrations using tracer 236 (A) and tracer 178 (B) in presence of competitor PD166285 (squares) or vehicle (DMSO, open circles) at 15 nM Myt1fl. For tracer 178, the difference between bound and competitively displaced tracer shows a distinct local maximum (C) which comes out more clearly when plotting the assay window as an assay performance measure (D). Data represent means \pm SEM (n=3).

For tracer 236, no binding to Myt1 was detected since the FRET curves of competitor and control, measured as emission ratio (acceptor / donor), completely overlay. The increase of the curves at high tracer concentrations is caused by diffusion-enhanced FRET. Using tracer 178, both curves are clearly separated indicating binding of the tracer to Myt1 and enabling FRET. Again, at high concentrations of tracer, the extent of diffusion-enhanced FRET rises, narrowing the assay window remarkably [249, 252]. To determine a suitable tracer concentration for the actual screening assay, two main factors have to be considered: The tracer K_d and the assay window. It is recommended to use tracer concentrations as close to the K_d as possible in order to realize a sensitive assay

with IC_{50} values being close to the actual inhibition constant. The difference between FRET curves of the tracer titration in presence or absence of competitor should result in a saturation binding curve allowing K_d determination. However, the curve clearly shows a local maximum which precludes valid K_d estimations (Fig. 11C). Presumably, the decrease in the emission ratio difference (ΔER) is caused by diffusion-enhanced interference of Triton X-100, a detergent necessarily brought into the assay through the solubilisation step in Myt1fl preparation. Since the top plateau cannot be determined, the tracer K_d may be estimated roughly to be below 10 nM. The assay window, calculated as fold-increase of vehicle ER to competitor ER, shows a clear maximum at approximately 10 nM. Systematic experiments on assay performance were omitted due to low amounts of available protein. However, according to LanthaScreen validation data of the supplier, an assay window > 2 will typically yield a robust assay ($Z' > 0.5$) [253]. Concentrations of Eu-labeled antibody were kept constant at 2 nM throughout assay development to ensure relative excess of kinase and, therefore, nearly quantitative antibody binding. The final assay conditions were determined as follows: 10 nM tracer 178, 15 nM Myt1fl and 2 nM Eu-labeled antibody in a total assay volume of 15 μ l (384-well plate format). The exact protocol can be found in the methods section.

For a better comparability, all values were normalized against positive and negative controls (10 μ M PD166285 and 1% DMSO, respectively) and reported as [relative-% tracer displaced]. Using this procedure, the positive control PD166285 had an IC_{50} value of 7.2 nM (s. Fig. 12).

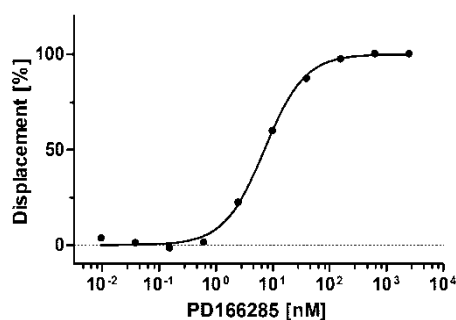


Fig. 12: Using the established assay protocol, the positive control PD166285 had an IC_{50} value of 7.2 nM. Data reported as means \pm SEM ($n=3$).

Throughout this work, IC_{50} curves were fitted to the data by GraphPad Prism 5.01 (San Diego, CA) using sigmoidal dose-response with a variable slope.

5.2.2. *LanthaScreen Inhibition Data*

Because common kinase inhibitors have not been tested against human Myt1 kinase so far, known promiscuous kinase inhibitors such as staurosporine as well as more selective tyrosine kinase inhibitors which have been approved and marketed, such as lapatinib and imatinib, were tested to obtain a first inhibition profile.

All compounds were tested three times at two different concentrations. Any substance binding > 50% at 10 μ M was subjected to further testing and IC₅₀ values were determined. Quantitative data are expressed as means \pm standard error. PD166285 was used as a positive control. Compounds and respective effects at a concentration as indicated are displayed in Table 4.

Table 4: Test of common kinase inhibitors for effects on the human Myt1 kinase. Binding of the respective compound is reported in [relative-% tracer displaced].

Compound	Displacement at 5 μ M [%]	Displacement at 10 μ M [%]	IC ₅₀ [nM]
Bisindolylmaleimide I	no displ. ^a	no displ.	n. t. ^b
Dasatinib	95.5 \pm 0.3	97.1 \pm 0.3	63.0 \pm 1.1
Erlotinib	7.1 \pm 1.7	8.2 \pm 0.7	n. t.
Gefitinib	no displ.	6.9 \pm 2.4	n. t.
HA-1077	no displ.	no displ.	n. t.
Imatinib	no displ.	no displ.	n. t.
K252a	no displ.	no displ.	n. t.
Lapatinib	no displ.	no displ.	n. t.
PD166285	n. t.	n. t.	7.2 \pm 1.1
Midostaurin	no displ.	no displ.	n. t.
SB 203580	no displ.	no displ.	n. t.
Staurosporine	n. t.	n. t.	no displ. up to 10 μ M
Sunitinib	no displ.	no displ.	n. t.
Tyrphostin AG 1478	24.8 \pm 0.7	39.5 \pm 1.5	n. t.
U0126	7.6 \pm 0.7	no displ.	n. t.
Vatalanib	no displ.	no displ.	n. t.

^a no displ.: no displacement (<5%) at the specified assay concentration

^b n. t.: not tested

Most of the tested compounds did not affect Myt1. The kinase was insensitive even towards highly promiscuous inhibitors such as staurosporine, sunitinib and bisindolylmaleimide I. The effects of erlotinib and gefitinib were negligible. Major effects could be determined for dasatinib and tyrphostin AG 1478. However, binding of the latter was too weak to determine IC₅₀ values due to limitations of the assay system (see upcoming Section 5.2.3). Dasatinib displaced the kinase tracer from Myt1 with an IC₅₀ of about 63 nM (Fig. 13).

Interestingly, staurosporine had no effect in concentrations up to 10 μ M (Fig. 13). Literature data concerning staurosporine effects on Myt1 were contradictory at that time. While FABIAN et al. found Myt1 to be insensitive towards staurosporine [23], other essays by KRISTJÁNSDÓTTIR et al. and ZHOU et al. reported IC₅₀ values against Myt1 [24, 197]. The data presented by ZHOU et al. are discussed in the upcoming Section 5.4, together with the reevaluation of glycolycerolipid inhibitors.

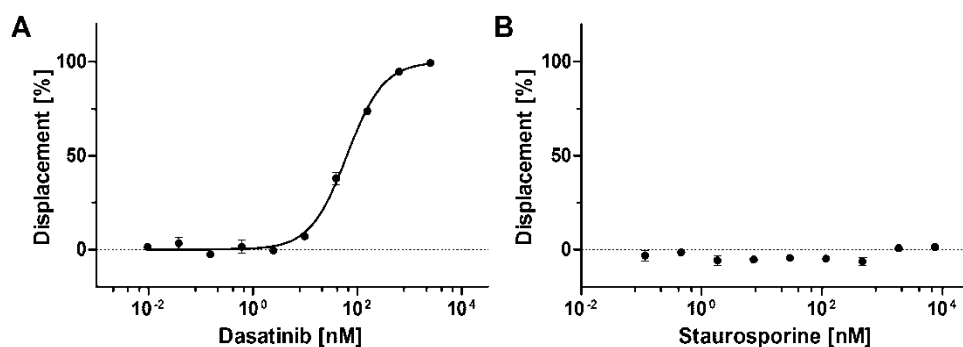


Fig. 13: Myt1fl inhibitor titrations with dasatinib (A) and staurosporine (B) in the LanthaScreen kinase binding assay. Dasatinib had an IC₅₀ value of approximately 63 nM while staurosporine showed no effect up to 10 μ M. Data displayed as means \pm SEM (n=3).

Here, staurosporine did not affect Myt1. This finding helps reveal potential inherent contradictions in the report of KRISTJÁNSDÓTTIR et al. Therein, the found inhibitor sensitivities differ vastly between Wee1 and Myt1 (for instance, Myt1 was highly sensitive to staurosporine whereas Wee1 was not at all). Altogether, the Myt1 inhibitor activities described correlate with known Cdk inhibitors rather than with Wee1 inhibitors. Thus, taking into account the autophosphorylation activities detected (see 5.1), the Myt1 inhibitor activities described may be incorrectly reported in parts. The compound effects detected might possibly be caused by Cdk-affecting mechanisms. No experiments or inhibitor pretreatments were mentioned to rule out this possibility. However, these facts do not at all affect the validity of the Wee1 results because these tests were carried out by the authors using a peptidic substrate instead of active Cdk/Cyc complexes.

The finding that staurosporine did not bind to Myt1 in the LanthaScreen assay is supported by a recent study with the Myt1 kinase domain which was expressed in *E. coli* [76] and is, furthermore, cross-validated by the fact that the staurosporine derivatives midostaurin and K252a did not show any effect in concentrations up to 10 μ M either. Also other compounds which usually inhibit a broad range of kinases (e.g. sunitinib) did not affect Myt1. Because assay development requires positive controls, i.e. known inhibitors, these unusual inhibition properties may be

jointly responsible for the lack of data so far. Three compounds displaced the kinase tracer from Myt1. The chemical scaffolds of these compounds share some structural similarity which can be seen in Fig. 14.

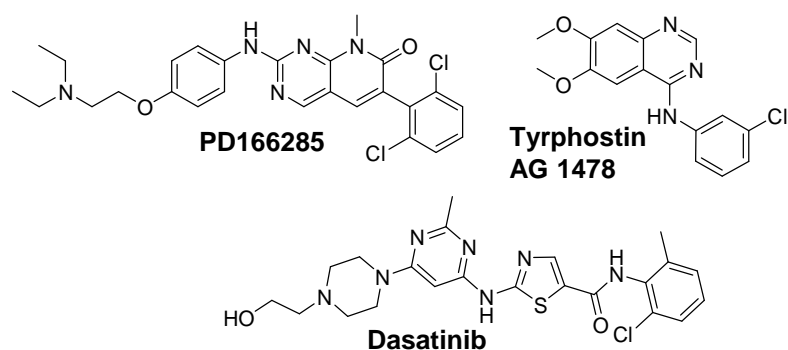


Fig. 14: Chemical structures of PD166285, tyrphostin AG 1478 and dasatinib.

Even the largest available kinase panels contain only a fraction of all kinases of the human kinome, and often the kinase domain only instead of the full-length protein. In addition, the panels are often highly biased by containing mostly kinases that can be easily purified and assayed. Additionally, as these kinases are typically purified from non-mammalian cells, they do not contain their naturally occurring post-translational modifications [6]. Myt1 is a difficult to obtain membrane-associated kinase which is, to the best knowledge, not commercially available as an enzymatically active protein so far. This kinase is of special interest because it is involved in pathways of major importance for development and survival of many cancer cells.

Myt1 was expressed in a human cell line, which means post-translational modifications are approximately as in the actual human target cells. The tested kinase preparation showed the typical catalytic activity towards Thr14 and Tyr15 of Cdk1, target sites specific for Myt1. Additionally, due to the fact that the epitope tag is present in the kinase of interest only, the assay system used is insensitive to contaminating kinases [249]. Together with the affirmation of PD166285 as a tightly binding compound, the results are valid.

Previously, Myt1 was suggested as a target of dasatinib using an MS-driven proteomics approach [254]. However, this approach used a chemically altered, immobilized dasatinib-derivative. Taking into account that former comparable studies did not reveal Myt1 to be a target of dasatinib [255], affirmation in a more specific way was needed. Dasatinib, having a Gini-coefficient of 0.74, is not a very selective inhibitor, though it is by far not as promiscuous as staurosporine ($G = 0.20$) or K252a ($G = 0.29$) [256].

In the *in vitro* test system used, dasatinib was found to affect Myt1 strongly, with an IC_{50} value of about 63 nM, leading to the conclusion that Myt1 may indeed be a target of dasatinib. However, the affinity of dasatinib towards its reported primary targets, Abl and Src, lies in the subnanomolar range [257] and is thus much higher compared to Myt1. Future work has to reveal whether Myt1 can be confirmed as a substantial target also in a cellular environment.

5.2.3. *LanthaScreen: Limitations and Drawbacks*

The LanthaScreen platform is a robust yet specific assay system. However, there are some drawbacks. As described in Section 5.2.1, a saturation binding curve for the tracer could not be derived. Therefore, the dissociation constant K_d cannot be estimated with sufficient certainty. Without tracer K_d , it is not possible to deviate inhibition constants (K_i) out of IC_{50} values. IC_{50} values are assay specific and need to be converted into K_i to yield a measure widely independent from the actual assay. That conversion is carried out mathematically by published equations, e.g. the Cheng-Prusoff equation, which includes parameters besides the IC_{50} such as tracer concentration and tracer K_d [258].

Furthermore, the assay is limited in terms of the concentrations of a given test compound. High compound concentrations cannot be tested due to non-specific diffusion enhanced FRET mechanisms as mentioned before. The presence of compounds containing aromatic systems, as are present in most kinase inhibitors, is therefore limited to about 10 μ M (assay concentration).

The reason for both drawbacks is likely the same and Fig. 15 may illustrate it:

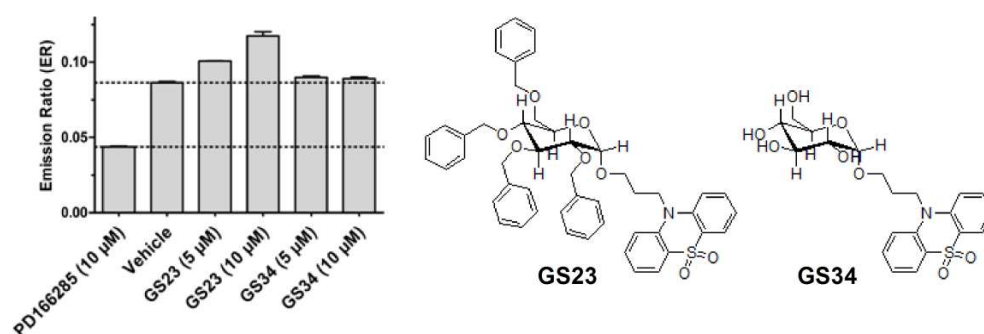


Fig. 15: Illustration of spectroscopic compound interference with the LanthaScreen assay. Data represent means \pm SEM (n=3).

The graph displays the actual FRET, indicated by the emission ratio acceptor/donor. Dashed lines mark the emission ratio for fully displaced (PD166285) and fully bound (vehicle) controls. Results for two test compounds as synthesized by AL-MAZAIDEH [201], each of them tested at two different concentrations, are shown. The compounds differ only in the degree of

benzylation. GS34, bearing no benzyl moieties, does not displace the tracer from Myt1, the FRET is comparable to vehicle control. The perbenzylated compound (GS23), however, affects the spectroscopic readout. It does not lead to a decreased FRET as expected for a binding compound, but rather enhances the FRET signal in a dose dependent manner.

Myt1, as a membrane-associated protein, must be solubilized out of the membrane by using detergents. Among five detergents commonly used for this purpose, Triton X-100 performed best in terms of solubilisation capacity as well as selectivity [236]. Triton X-100 is an alkyl-substituted phenol ether which may interfere with the assay readout exactly as some of the test compounds do.

Another drawback of the assay lies in its complexity. The tracer structure is unknown and the entire assay relies totally on the anti-His tag antibody utilized. A series of glycotriazoles, synthesized by SAUER [199], was tested and yielded two dose dependent hits (BS11 and BS12) with estimated IC_{50} values of about 17 - 18 μ M. The general structure as well as both screening hits are shown in Fig. 16.

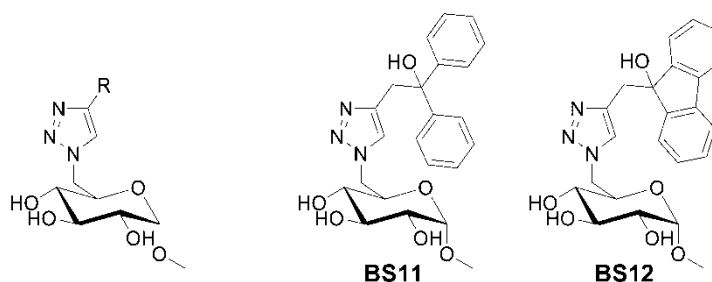


Fig. 16: General structure of the tested glycotriazole series and two screening hits thereof.

Due to the hydrophilic carbohydrate structure together with the aromatic triazole, the possibility that the effects measured are caused by displacement of the antibody instead of displacement of the tracer could not be excluded.

Indeed, the two hits might be false-positives, and another orthogonal secondary assay was needed to verify the results.

Additionally, at that time, the Institute of Pharmacy did not have suitable equipment for LanthaScreen because this assay is very demanding in terms of instrumentation. Experiments had to be run on plate readers of other institutes. Therefore, another assay was desired that can be performed using the given instruments.

Docking studies were carried out to identify potential starting points for the development of an orthogonal assay system.

5.2.4. Docking Studies

The potent inhibitors PD166285 and dasatinib were subjected to further *in silico* studies to investigate their putative interaction at the kinase binding site. *In silico* studies mentioned here were carried out by Dr. K. Wichapong.

First of all, the X-ray structure of Myt1 (PDB Code 3P1A) and Wee1 (PDB code 1X8B) was analyzed. Even though the sequence identity between Wee1 and Myt1 is rather low (35.3%), the overall 3D-structures, especially the binding pocket, are quite similar (see appendix, Fig. 45). Root mean square deviation (RMSD) between these two structures is 1.73 Å (backbone atoms). Therefore, it is reasonable to use the same protocol for Myt1 docking as for Wee1 docking. As discussed previously [259], the X-ray structures of Wee1-inhibitor complexes reveal the interaction between inhibitors and the residues Glu377 and Cys379 located at the hinge region. It is well known from other kinases that the residues at the hinge region play an important role for interacting with ATP-competitive inhibitors or ATP. Thus, the key residues where inhibitors and ATP bind are Glu188, Cys190 and the Thr187 gatekeeper residue of Myt1 (see also appendix, Fig. 45).

Previously, pyridopyrimidine derivatives were successfully docked into the binding pocket of Wee1 kinase [260]. The docking results showed a conserved binding, namely an H-bond interaction between the NH and N atom of the inhibitor's pyrimidine ring (the main scaffold) with the Cys379 residue. For the Myt1 kinase, the docking proposed the same binding mode, as displayed in Fig. 17A.

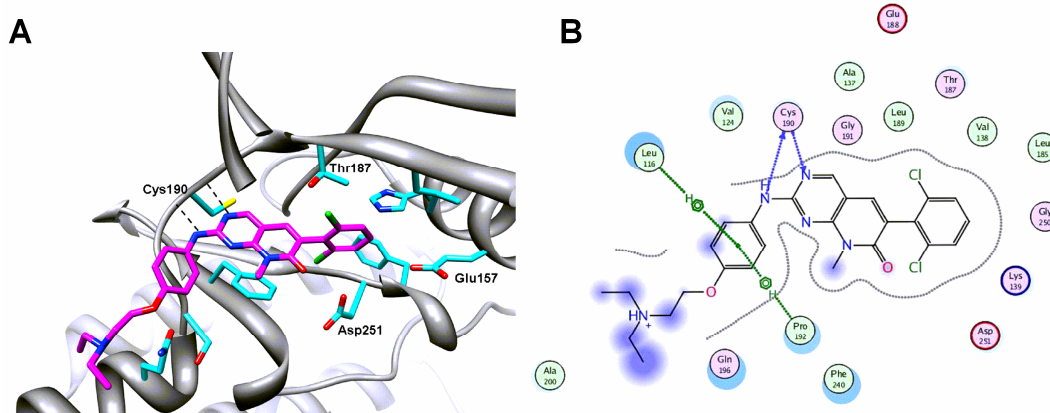


Fig. 17: GOLD docking solution of compound PD166285 (magenta stick) in the binding pocket of Myt1 (A) and a schematic representation of the interactions between compound PD166285 and the residues in the binding pocket of Myt1 (B). H-bonds are displayed as dashed lines.

The H-bond interactions were found between the NH atom and the pyrimidine ring of the inhibitor with Cys190. The benzene ring with the chloro substituent at the ortho position is located at the hydrophobic pocket. There is also another interaction between the benzene ring of the inhibitor with Pro192 and Leu116, as shown in Fig. 17.

Dasatinib is a well-known kinase inhibitor, and several X-ray structures of kinases (active conformation) complexed with dasatinib are available in the Protein Data Bank; for example PDB code 2GQG (Abl kinase), 3G5D (c-Src kinase), and 3K54 (Btk kinase). Superimposition of these X-ray structures reveals that dasatinib not only forms H-bonds with residues at the hinge region but also with the gatekeeper residue (see appendix, Fig. 46).

The molecular docking results for dasatinib and Myt1 (PDB code 3P1A, active conformation), as displayed in Fig. 18, yielded the same binding mode as for the other protein kinases. H-bond interactions were found between NH and the N atom of the thiazole ring with Cys190, and between the NH atom with Thr187 (gatekeeper residue). The additional interaction between dasatinib and Pro192 was also found, as shown in Fig. 18.

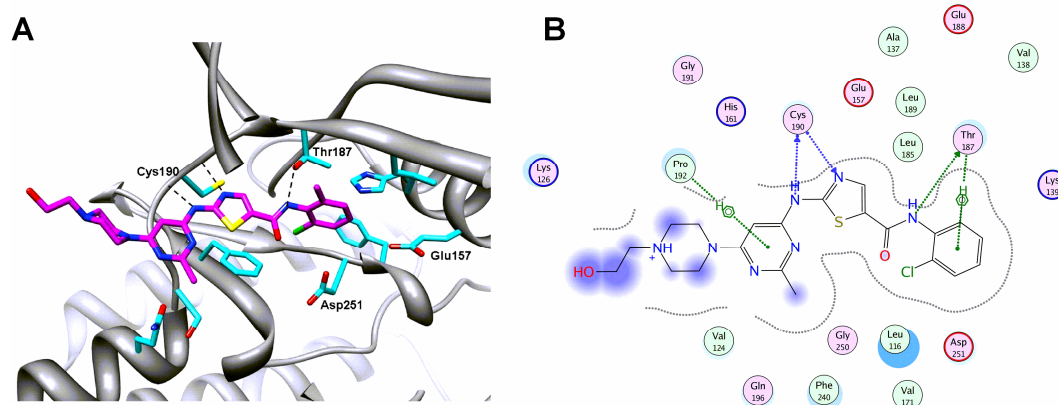


Fig. 18: GOLD docking solution of dasatinib (magenta stick) in the ATP-binding pocket of Myt1 (A) and a schematic representation of the interactions between dasatinib and the residues in the ATP-binding pocket of Myt1 (B).

According to their binding modes, both potent inhibitors exploit a hydrophobic pocket beyond the gatekeeper residue and not only the regions targeted by ATP, favored by the small threonine residue in this position. About 18% of all protein kinases contain a Thr-gatekeeper. As this residue is not very bulky, it provides the possibility to target the back pocket in a more specific way [48].

5.3. FP Based Kinase Binding Assay: DasAFITC-Assay

As mentioned before, dasatinib is a well-investigated approved drug in anti-cancer therapy that binds tightly to many kinases [76]. Due to advantages in terms of commercially available amounts and financial considerations, it was decided to focus on dasatinib instead of PD166285. As a starting point for the development of another Myt1 kinase binding assay, the molecular docking studies indicated the hydroxy-ethyl residue of dasatinib to be solvent exposed (see Fig. 18 and appendix, Fig. 46). Together with the fact that an alteration at this position, i.e. covalent linkage to a resin [255], maintained the ability to bind to several kinases, it was assumed that a chemical modification at this hydrophilic position would not have a major negative impact on the binding properties. Covalent linkage of a fluorophore at this position, i.e. formation of a molecular probe, might be the key to a fluorescence polarization (FP) based binding assay.

The assay principle is outlined in Fig. 19. It is based on a fluorescently labeled ATP-competitive inhibitor as a tracer.

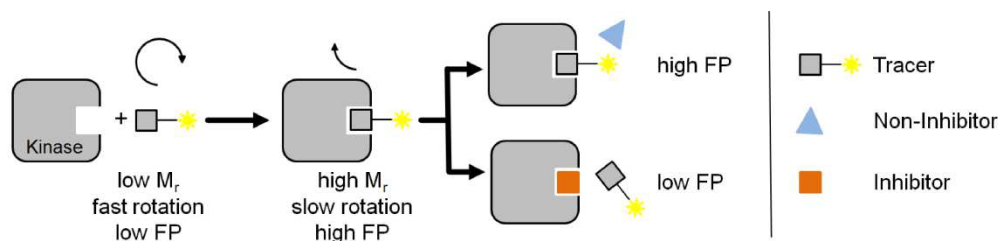


Fig. 19: The assay principle is based on a fluorescently labeled ATP-competitive compound (tracer) having a rather low intrinsic FP. Upon binding to the kinase, the increased size of the complex leads to slower rotation and, therefore, higher fluorescence polarization. While a non-inhibitor does not affect the kinase-tracer complex, an inhibitor displaces the tracer from the kinase, lowering the polarization.

Due to its rather low molecular weight, the probe moves very quickly in solution phase when excited by polarized light, leading to low fluorescence polarization values. However, if a suitable kinase is added, the molecular weight of the complex will be dramatically increased compared to the tracer itself. The rotational correlation time of the complex will therefore be increased (slower rotation) leading to increased polarization of the fluorescence emission. A non-inhibitor added to this complex will not affect the binding of the tracer and the high fluorescence polarization will be maintained. An inhibitor, however, will displace the tracer from the kinase which results in lowered FP values.

As a fluorophore, it was decided to use fluorescein due to its many available labeling derivatives, its excellent quantum yield and broadly available suitable instrumentation.

5.3.1. Synthesis and Characterization of a Suitable Tracer

Different synthetic plans were pursued using different labeling reagents such as aminofluorescein or thioacetamidofluorescein. The most successful derivative, however, was based on fluorescein isothiocyanate (FITC) as the defined single isomer I (fluorescein 5-isothiocyanate).

The synthesis route to the fluorophore-labeled dasatinib derivative **4**, *N*-[3',6'-dihydroxy-3-oxo-3*H*-spiro(2-benzofuran-1,9'-xanthen)-5-yl]-*N'*-(2-[4-{4-([*N*-(2-chloro-6-methylphenyl)-5-carboxamido]-thiazol-2-yl)amino-2-methylpyrimid-6-yl]piperazinyl]-ethyl)thiourea, is outlined in Fig. 20 (as a Dasatinib-derived Amine FITC-adduct, the final product is named DasAFITC).

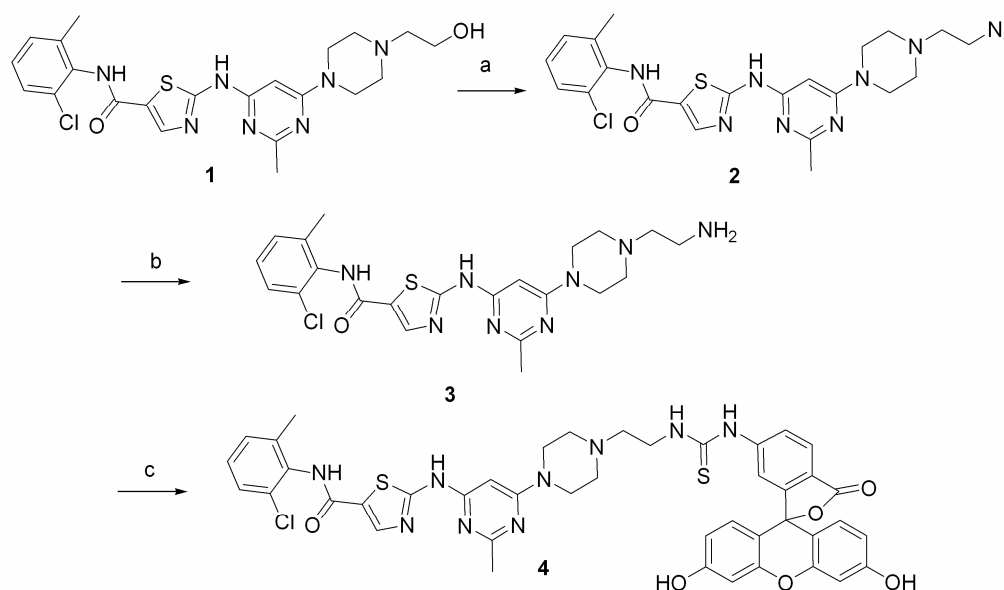


Fig. 20: Synthesis of a fluorescein-labeled dasatinib-derivative: (a) DPPA, DBU, NaN₃, THF, 5°C; (b) H₂, Pd/C, MeOH:EtOAc (15:1); (c) FITC isomer I, EtOH:THF (3:2), 0°C.

The primary hydroxyl-function was converted into an azide by means of diphenylphosphoryl azide (DPPA), yielding a 1:1 mixture of azide and diphenylphosphoryl ester. Addition of sodium azide led to full conversion from the ester to the desired azide (overall yield 87%). Reduction of this function was achieved by hydrogenation in presence of Pd/C with a yield of 90%. The resulting amine was coupled to fluorescein isothiocyanate isomer I in ethanol/THF forming a thiourea linker between fluorophore and pharmacophore (yield after purification: 33%), giving the final product DasAFITC **4**.

$C_{43}H_{38}ClN_9O_6S_2$: $M_p = 287^\circ C$; 1H NMR (400 MHz, DMSO- d_6) δ ppm 8.15 (d, $J = 1.9$ Hz, 1H, 4-fluoresceinyl-**H**), 8.14 (s, 1H, thiazole-**H**), 7.75 (dd, $J = 8.3$ Hz; $J = 2.0$ Hz, 1H, 6-fluoresceinyl-**H**), 7.34 (d, $J = 7.4$ Hz, 1H, 6-chloroanilide-**H**), 7.28 - 7.20 (m, 2H, 4-, 5-chloroanilide-**H**), 7.17 (d, $J = 8.3$ Hz, 1H, 7-fluoresceinyl-**H**), 6.70 - 6.65 (m, 4H, 1',4',5',8'-fluoresceinyl-**H**), 6.52 (dd, $J = 8.7$ Hz; $J = 2.4$ Hz, 2H, 2',7'-fluoresceinyl-**H**), 6.00 (s, 1H, pyrimidine-**H**), 3.66 (s, 4H, pyrimidine- $N(CH_2-R)_2$), 2.74 (t, $J = 6.1$ Hz, 2H, $R_2N-CH_2-CH_2-NHR'$), 2.72 - 2.61 (m, 4H, $(R-CH_2-CH_2)_2N-CH_2-R'$), 2.47 (s, 3H, pyrimidine- CH_3), 2.32 (s, 3H, chloroanilide- CH_3), 1.29 - 1.21 (m, 2H, $R_2N-CH_2-CH_2-NH-CS-R'$); ^{13}C NMR (125 MHz, DMSO- d_6) δ ppm 180.01, 168.36, 164.98, 162.36, 162.16, 159.73, 159.40, 156.77, 151.72, 141.26, 140.67, 138.63, 133.35, 132.78, 132.25, 128.81, 127.96, 126.80, 125.50, 123.93, 123.48, 112.44, 109.56, 102.05, 82.47, 62.90, 62.86, 59.69, 52.04, 43.40, 40.87, 25.40, 16.24, 15.80; HR-MS calculated for $[M+H]^+$ = 876.2148, found 876.2148 ($\Delta M = 0.0083$ ppm); UV/Vis (pH 7.5, aqueous buffer) $\lambda_{max1}(\epsilon = 29400 M^{-1}\cdot cm^{-1}) = 328$ nm, $\lambda_{max2}(\epsilon = 27400 M^{-1}\cdot cm^{-1}) = 498$ nm; $R_f(\text{MeOH}/\text{HCCl}_3 4:6) = 0.37$; HPLC $t = 5,8$ min, 98.64%.

Because DasAFITC was intended as a probe, the fluorescence properties were investigated in more detail. Fig. 21 shows the contour plot of a 3D scan of DasAFITC, i.e. the emission spectra for any given excitation were detected. Only Stokes fluorescence (emission wavelength > excitation wavelength) is shown.

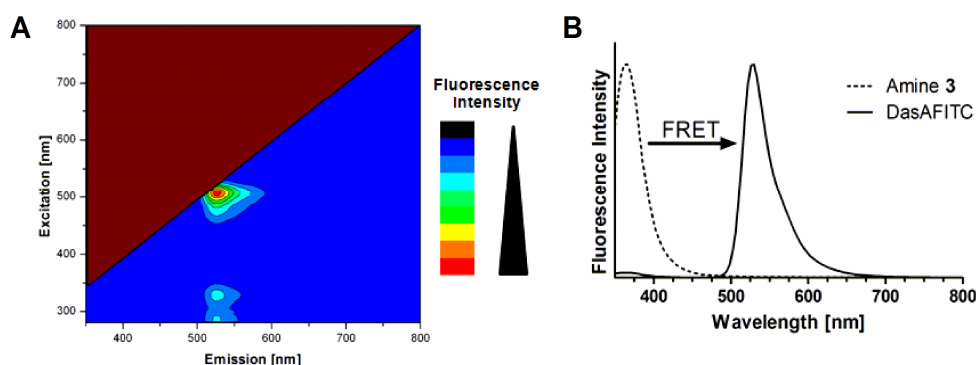


Fig. 21: Fluorescence characterization of DasAFITC by 3D scan in a contour plot (A). Emission scans at 330 nm indicate that DasAFITC has inherent FRET properties (B). Upon covalent linkage to FITC, the emission maximum of the dasatinib derived amine **3** shifts to the typical fluorescein maximum.

The dasatinib-like part of the molecule is fluorescent itself and emits light in the UV range. For DasAFITC, all detected fluorescence emission maxima are at the same wavelength of about 525 nm, the typical fluorescein emission. Apparently, DasAFITC is subject to inherent fluorescence resonance energy transfer. Emission

scans at 330 nm, a wavelength where the DasAFITC precursor **3** has properties comparable to dasatinib, reveal that after labeling with fluorescein, the emission wavelength dramatically shifts. Therefore, intramolecular FRET can be assumed. Due to intrinsic depolarization during FRET, this effect could not be exploited any further in this assay and common fluorescence at standard filter settings (485 nm Ex / 520 nm Em) was used in the development of the assay.

5.3.2. Assay Development: DasAFITC Assay

Fluorescence anisotropy is calculated as a ratio and can, therefore, be considered a natural constant of a compound in a defined environment. Since the anisotropy of the free fluoroprobe defines the bottom of the assay window, it was attempted to determine this value in kinase buffer A (50 mM HEPES pH 7.5, 10 mM MgCl₂, 1 mM EGTA, detergent 0.01% Brij-35). Detergents are commonly used in kinase buffers to increase the assay reproducibility and to reduce the number of false-positive hits [261]. The found value of about 0.180 (anisotropy) was unexplainably high for such a low molecular weight probe, which usually shows $r \ll 0.1$. To understand this phenomenon and exclude adsorption effects, various assay buffers containing different detergents and blocking proteins were tested. All measurements confirmed a high value, except a buffer containing CHAPS (data not shown). CHAPS is a detergent with a relatively high critical micelle concentration (CMC), which was not exceeded in the test buffer. This finding led to the idea that DasAFITC might have a strong amphiphilic character, so the lipophilic part is incorporated in micelles while the hydrophilic fluorescein part remains at the surface of the association colloid. This hypothesis would make it possible to develop a CMC determination assay based on the same tracer.

If values determined by this procedure were in accordance with CMC values reported in the literature, it would highlight the constitution of the assay buffer as a major critical point.

5.3.2.1. CMC Determination and Assay Buffer

The approach of using fluorescence anisotropy for CMC determination was reported in 2005 and the probe consisted of decanoylaminofluorescein [262], whose fatty acid residue appears to be much more lipophilic than the dasatinib-moiety of DasAFITC. To see whether the CMC was responsible for changes in the anisotropy, detergents from different classes were tested over a broad range of concentrations (Fig. 22A). At very low concentrations, a plausible r_0 of about 0.07

was observed and, as the respective CMC was approached, a sudden increase in anisotropy appeared. The Hill-slope of the fitted curves was $\gg 1$, meaning that the changes do not come from a reversible binding process, but rather from physical phenomena such as the formation of association colloids [263]. Interestingly, the tested detergents do not reach the same top plateau. The height of the plateau apparently correlates with dimensions and fluidity of the resulting colloidal structure. SDS forms rather small but clearly defined micelles, leading to a lower fluorescence anisotropy upon insertion of the probe than the bigger micellar structures of CHAPS. CMC determinations for cetyltrimethylammonium bromide (CTAB), as an example of a cationic detergent, were hardly possible, since the results showed bad reproducibility and achieved values far below literature (data not shown). This may be caused by the complementary electric charges of CTAB (positive) and the negatively charged carboxylate function of fluorescein.

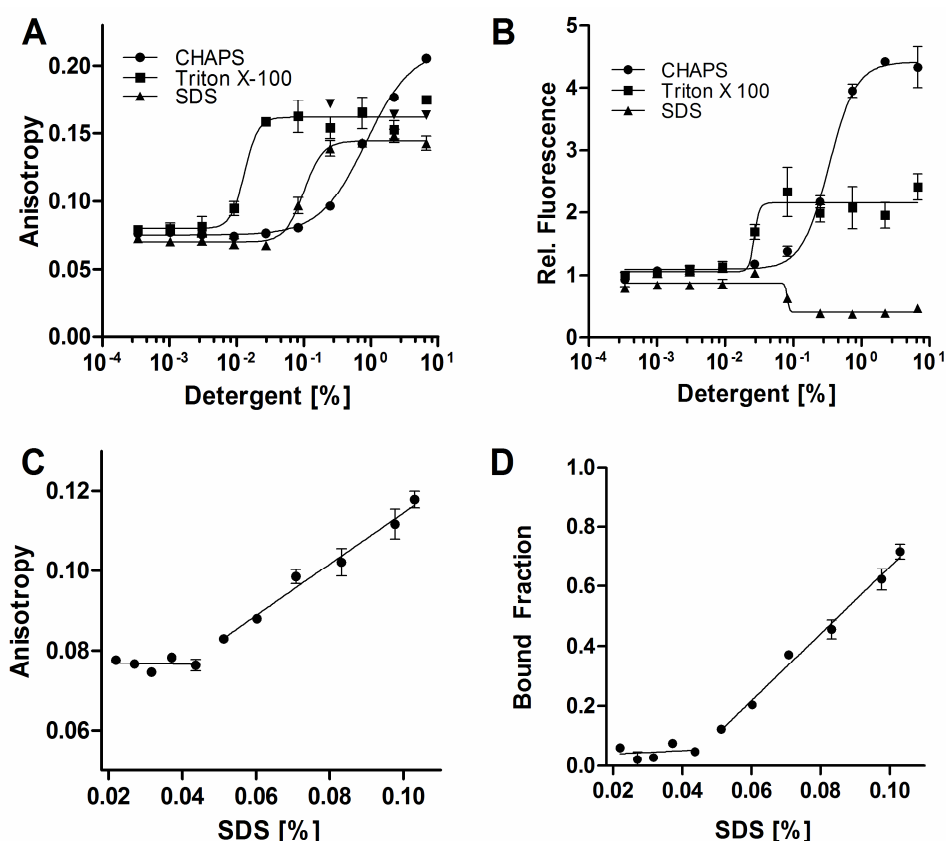


Fig. 22: Fluorescence anisotropy changes on insertion of the probe into micelles (A), but also the quantum yield may change dramatically (B). Direct deduction of the CMC from the anisotropy (C) therefore leads to wrong results. Calculation of the bound fraction, taking quantum yield changes into account, is needed for a correct determination (D).

Another important finding, which has not been mentioned in the previously described CMC determination anisotropy methodology [262], is the simultaneous change in quantum yields. Not only anisotropy changes upon insertion of the

fluoroprobe into micelles, also dramatic changes in overall fluorescence were observed for all tested detergents (Fig. 22B). These changes appear to be unpredictable and so the overall fluorescence intensity should always be calculated from the raw data ($I_{total} = I_{\parallel} + 2 * I_{\perp}$). The physical parameter measured (anisotropy) is only the apparent value that is formed additively out of bound and free fractions of fluoroprobe together with the respective intrinsic anisotropies. Alterations in the quantum yield prevent this assumption from being true and anisotropy can be translated into the bound fraction (f_b) using equation 12 [264]:

$$f_b = \frac{(r - r_f)}{r_b - r_f + (g - 1) * (r_b - r)} \quad (\text{Eq. 12})$$

wherein r_f and r_b represent the anisotropies of free or bound fluoroprobe and g is the quantum yield enhancement factor, simply calculated by dividing the fluorescence intensity of the respective sample with the fluorescence intensity of an equimolar sample of free fluorescent probe.

For CMC determination, two steps are necessary: Firstly, an experiment as mentioned before, covering many powers of ten (concentration), has to be performed to get an idea of the CMC (Fig. 22A). In a second step, a linear equidistant concentration series enclosing the CMC has to be carried out (for example, see Fig. 22C). The anisotropy remains constant (r_f) and, beginning with the CMC, anisotropy increases linearly. The intersection of both resulting lines should be equal to the CMC but is misleading due to alterations in quantum yield. A translation from r into f_b is necessary to get the correct CMC as intersection point (Fig. 22D), since fluorescence intensity changes upon insertion (Fig. 22B).

Table 5 shows CMC data determined with and without correction for quantum yield changes and compares the true values with previously reported CMCs.

Table 5: CMC values of selected detergents, resulting errors omitting quantum yield changes and comparison with CMC values from literature. CMC assays were conducted in 50 mM HEPES plus respective detergent.

Detergent	Apparent CMC (%) (anisotropy)	True CMC (%) (bound fraction)	True CMC (mM)	Systematic error ^a (%)	Literature CMC (mM)	Reference
Nonionic: Triton X-100 ^b	0.00733	0.00692	0.11	+6.0	0.22 (water)	[265]
Anionic: Dodecyl sulfate, sodium	0.0411	0.0453	1.57	-9.3	3.6 (25 mM HEPES) 0.72 (25 mM HEPES + 200 mM NaCl)	[262]
Betaine: CHAPS	0.14636	0.1562	2.54	+6.3	4 (10 mM HEPES + 50 mM NaCl)	[266]

^a error if CMC is calculated from anisotropy, omitting quantum yield changes.

^b this detergent is not a single defined substance, M = 625 g/mol was used for calculation of the molarity.

A systematic error can easily be avoided by taking g into account as discussed above. The determined values are in accordance with literature.

Another advantage of this methodology is the use of very low amounts of probe, thus minimizing the perturbation of micelle structure and formation by insertion of the probe. Due to that low concentration and the properties of DasAFITC, this method is able to measure CMC in a fully aqueous environment. Many published CMC determination procedures include organic solvents, e.g. THF [231] or ethanol [230], because of probe solubility issues.

It is to be noted that the development of the CMC assay was initially not intended. While trying to establish the kinase binding assay, serious problems concerning the anisotropy value of the free probe came up. Personal communication with Dr. Munoz, author of a report establishing a similar assay [250], revealed that they were facing similar problems when deriving a probe from SB203580, a highly potent p38 MAP kinase inhibitor. Therefore, the problem might be generic to FP based assays. In their assay, they finally made use of an assay buffer containing CHAPS to solve the problem, without understanding why this helped. However, to prove whether the high anisotropy value may be caused by insertion phenomena when the buffer contains detergents above the respective CMC, the probe was used to actually determine the CMC of reference detergents. The CMC determinations, matching literature values, provide evidence that this assumption is true and, indeed, should alert the practitioner to potential pitfalls when setting up an FP based assay.

The CMC assay itself can be considered an additional value to the probe and highlights the use of a quantum yield correction when applying such a methodology [262].

Having the amphiphilic character of DasAFITC in mind, an assay buffer containing a detergent concentration far below its CMC had to be used. Also the possibility that DasAFITC might form aggregates on its own, interfering with the assay principle, was examined. No formation of association colloids was observed in concentrations up to 10 μM using two different methods [230-231] (data not shown).

The final kinase binding assay buffer B (KBB) consisted of 50 mM HEPES-NaOH pH 7.5, 10 mM MgCl_2 , 0.03% CHAPS, 1 mM DTT.

5.3.2.2. *Microplates and Tracer Concentration*

Next, the choice of the optimal ligand concentration is a very essential step. One has to make a compromise between assay sensitivity, measurement error and kinase consumption. Since DMSO strongly affects the emissivity of fluorescein, 1% DMSO was included in any test, whether or not a compound was present. As indicated by pretests, 384-well plates did not provide an adequate signal-to-noise ratio at low concentrations, probably due to a rather low area of the well geometry. Therefore, 96-well plates were used instead, using a half-area well geometry to reduce the assay volume. Analytical pretests showed that, given the instrumentation, an assay volume of 27 μ l at a tracer concentration of 5 nM is well-suited to yield a signal-to-noise ratio of at least ten in both channels (data not shown), ensuring acceptable instrumental errors ($CV < 5\%$). This concentration was used in all further kinase experiments.

5.3.2.3. *Construction of Binding Isotherms*

The most important question at that stage was: What is the required affinity that allows for setting up an assay as intended? To be more quantitative, what K_d for dasatinib against a given kinase is sufficient?

To answer this question, four different kinases including Myt1 were chosen with respect to their reported binding affinity towards dasatinib. The kinases were Wee1 ($K_d = 7000$ nM), Myt1 ($K_d = 130$ nM), Btk ($K_d = 1.4$ nM) and Abl1 ($K_d = 0.038$ nM) [76]. For the generation of full-length Myt1 as a membrane associated protein, it is indispensable to use detergents for protein solubilization [236]. The use of detergents below their respective CMC may cause irreversible protein aggregation and has to be avoided. Since the dasatinib-derived fluorescent probe is not compatible with assay conditions including detergents above their CMC, the isolated Myt1 kinase domain was used in this assay. Lack of the membrane association motif allows for protein expression and purification without using detergents.

For a binding assay, it is crucial to know the K_d of the respective probe. In fluorescence anisotropy assays, the binding isotherm can be constructed by adding increasing amounts of protein to a constant concentration of fluorescent probe. 5 nM probe were incubated with defined amounts of four different kinases. Measurements were taken after incubation periods of 30 min, 60 min and

120 min. Fig. 23A shows the change in anisotropy compared to fully outcompeted, dasatinib-containing controls (Δr) after 120 min incubation.

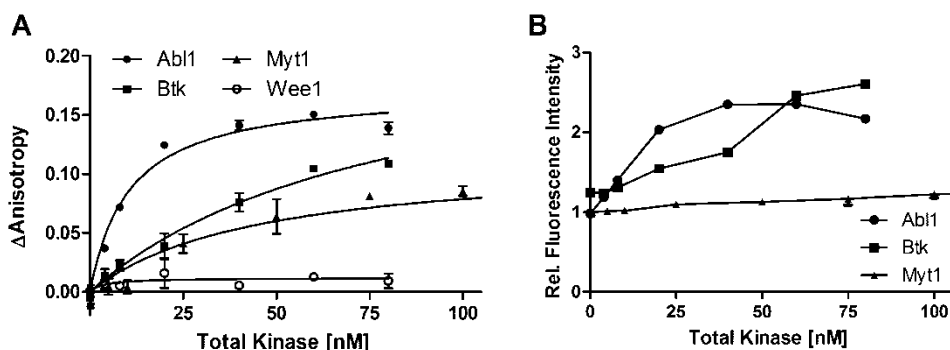


Fig. 23: Change in anisotropy upon kinase titration (A). All tested kinases except Wee1 bind the kinase tracer and the development reflects their affinity in the following order: Abl1 > Btk > Myt1 > Wee1. However, changes of the overall fluorescence intensity (B) necessitate a quantum yield correction. Data reported as means \pm SEM (n=4).

Wee1 does not bind the kinase tracer to a significant extent. Abl1, Btk and Myt1 do so and the concentrations at half the maximum increase reflect the expected affinity towards the tracer, which decreases in the order Abl1 > Btk > Myt1 > Wee1. The Δr plateau for Btk and Abl1 lies higher than for Myt1, values are given in Table 6. Responsible for this effect is mainly the molecular weight of the kinases, which directly affects the assay window. Abl1 and Btk have a GST-tag, which is many times heavier than the His₆ tag of Myt1. If one is planning to carry out fluorescence polarization experiments, it is advisable to use a GST-tag to increase the mass of the complex, leading to an increased r_{bound} and, therefore, a better assay window.

The curves shown in Fig. 23A, however, should not be used for the estimation of K_d , because, as mentioned for the CMC assay, dramatic changes in the overall fluorescence intensity (Fig. 23B) necessitate a correction for the quantum yield using the equation mentioned above. The estimated K_d values for the three binding kinases (apparent K_d : derived from anisotropy; true K_d : derived from the bound fraction) as well as quantum yield enhancement factors and maximum anisotropy differences between bound and free ligand are displayed in Table 6.

The K_d estimations using anisotropy and the calculated bound fraction differ vastly. Unacceptable systematic errors may occur and the error itself, even the tendency, is basically unpredictable and has to be monitored in every single case. However, the true K_d is in accordance with values reported in literature. The reference data by DAVIS et al. [76] was generated using quantitative PCR as readout principle. The affinities of the selected kinases are approximately

equidistant on a log-scale. Since there is no amplification in the present assay, the determined K_d values are equidistant on a linear scale and reflect the expected behaviour.

Table 6: Comparison of K_d estimations based on obtained anisotropy curves (apparent) and calculated bound fraction (true) with values reported in literature.

Kinase	Apparent K_d [nM]	True K_d [nM]	Systematic error ^a (%)	Literature K_d [nM] [76]	Quantum yield enhancement factor ^d	Δ anisotropy ^e	Molecular Mass (tested Protein) [kDa]
Abl1	10.5	16.5	-36%	0.038 ^b	2.21	0.172	76
Btk	81.2	55.1	+47%	1.4	2.10	0.229	77
Myt1	45.2	138	-67%	130	1.30	0.110	33
Wee1	n/a ^c	n/a ^c	n/a ^c	7000	n/a ^c	n/a ^c	75

^a error if CMC is calculated from anisotropy, omitting quantum yield changes.

^b K_d for Abl1wt was calculated as the arithmetic mean of phosphorylated and non-phosphorylated Abl1.

^c not applicable because no binding was detected.

^d calculated from fluorescence intensities of fully bound and fully displaced ligand.

^e difference between fully bound and fully displaced ligand. Equals the maximum measurement window.

With respect to assay window and estimated K_d , it was decided to perform further kinase assays at concentrations of 15 nM (Abl1), 45 nM (Btk), and 100 nM (Myt1). The kinase tracer used was not suitable for performing Wee1 kinase assays. The affinity of Wee1 to dasatinib as the starting compound was apparently not sufficient. However, the required affinity as a starting point for such an assay certainly lies beyond the 130 nM K_d of Myt1. This will hold true, particularly if the molecular mass of the kinase is big enough, which can be achieved by, for instance, using full-length kinases and/or high molecular weight purification tags such as GST.

5.3.2.4. Time Dependence and Assay Performance

In the kinase titration experiment, it was noticed that the Abl1 and Btk curves did not change between the measurements taken at 30 min and 120 min, while for Myt1 the anisotropy of the samples without dasatinib continued to increase.

Since special attention is given to Myt1, a more detailed analysis in terms of association times was carried out (Fig. 24). Vehicle control, containing 1% DMSO, and fully outcompeted samples containing dasatinib (10 μ M) were incubated over a long time period and measurements were taken repeatedly.

The assay window, represented by the difference between these two controls, needs at least two hours to develop a stable span. For the other two kinases, Abl1 and Btk, the binding process was fully completed after 5-10 min (data not shown).

All formed kinase-tracer-complexes showed excellent stability for at least 8 h, indicating a basically robust assay system. Ligand dissociation was not as slow as ligand association. Addition of dasatinib (10 μ M) to preequilibrated kinase-tracer-complex displaced the tracer with a dissociation half-life of $t_{1/2} = 2$ min, reaching equilibrium after approximately 10 min (equals $5 \cdot t_{1/2}$; data not shown).

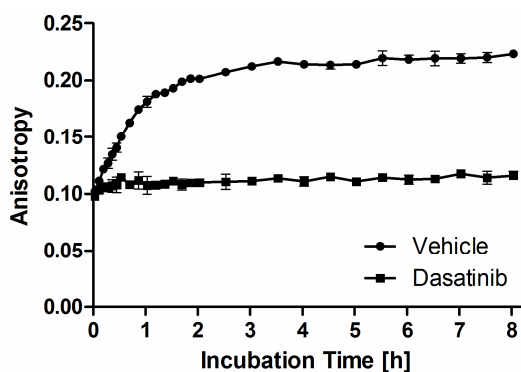


Fig. 24: Time course of the association of kinase tracer and Myt1. The assay window, represented by the difference between bound tracer (Vehicle control) and fully outcompeted tracer (Dasatinib), does not reach a stable plateau until at least two hours of incubation. For Abl1 and Btk, the binding process is completed after 5-10 min (data not shown). Data represent means \pm SEM (n=3).

The meeting of the incubation time criterion is particularly important in screening experiments. Usually, an equilibrium is reached after five association half-lives [267], which is approximately after 3 h in the present assay (association half-life $t_{1/2} = 0.6$ h). In practice, however, incubation times longer than 2 h did not lead to better Z' factors. Systematic Z' experiments yielded $Z' = 0.33$ after 1 h and 0.52 after 2 h. On the one hand, these numbers illustrate that a too short incubation time is necessarily accompanied by a loss of screening quality but, on the other hand, that if suitable incubation time criteria have been met, the assay is excellently suited to screening applications [33-34]. Fig. 25 shows a representative plate of such a systematical Z' experiment after 120 min incubation. Minus blank controls, half the plate (96-well) contained dasatinib and half the plate respective vehicle control.

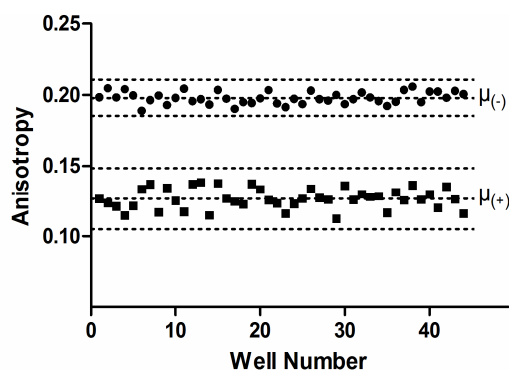


Fig. 25: A representative result of a plate containing dasatinib controls ($\mu_{(+)}$, n=44) and vehicle controls ($\mu_{(-)}$, n=44). Dashed lines indicate a distance of three standard deviations.

As can be seen, the vehicle controls show a higher anisotropy with an acceptable standard deviation, which allows for certain identification of hits. The span between mean values of the controls together with three times their standard deviations (dashed lines) is distinct, proving the suitability of the assay also for screening applications. In further inhibitor studies, 120 min for Myt1 and 60 min for Abl1/Btk were used as incubation periods before plate reading.

Using these optimized assay conditions, test data was always normalized against dasatinib control (100% displacement) and vehicle control (0% displacement) to allow for better comparability.

5.3.2.5. Assay Validation

Several compounds were assessed to compare the results with values reported in the literature and obtained from the LanthaScreen assay as described in Section 5.2.

For Abl1 and Btk, exemplary IC_{50} values were determined to show the general applicability of the assay. Some known inactive compounds were also included as a confirmation of the test system. See Fig. 26 for exemplary IC_{50} curves.

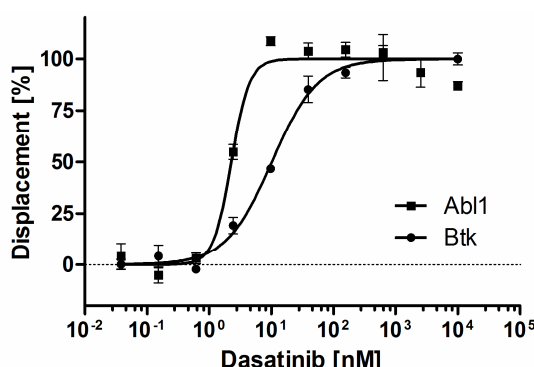


Fig. 26: Exemplary IC_{50} curves for dasatinib with Abl1 and Btk, proving analytical suitability of the described procedure. Data represent means \pm SEM of three experiments.

Table 7 summarizes the results for Abl1 and Btk.

Table 7: Determined inhibition profile for the kinases Abl1 and Btk, and comparison with literature data.

Compound	Abl1: IC_{50} [nM]	Literature K_i , K_d , IC_{50} [nM]	Btk: IC_{50} [nM]	Literature K_i , K_d , IC_{50} [nM]
Dasatinib	2.27	0.038 [76], 9 [255], 14 [268]	10.16	1.4 [76], 5 [268]
Lapatinib	No effect ^a	No effect [256]	No effect ^a	No effect [256]
SB203580	No effect ^a	No effect [76]	No effect ^a	No effect [76]
Roscovitine	No effect ^a	No effect [256]	No effect ^a	No effect [256]

^aMean displacement < 10% at 10 μ M

The data displayed for Abl1 and Btk corresponds with literature values, showing the general analytical suitability of the described procedure. The remarkable

slope-differences between both curves can be explained by the findings of SHOICHET [196]. Steep dose-response-curves can occur if the binding constant (compound to protein) is much lower than the actual enzyme concentration. The ratio (kinase concentration to K_d) is much higher for Abl1 (15 nM / 0.038 nM = 395) than for Btk (45 nM / 1.4 nM = 32), which explains well why the curve for Abl1 is remarkably steeper.

It can be assumed that the assay performances for Abl1 and Btk are even better compared to Myt1 due to the increased assay window as deduced from the kinase titrations. Therefore, and because the focus of this work clearly lies with Myt1, the compound series was expanded to include most compounds ever reported to inhibit Myt1. IC₅₀ curves are shown in Fig. 27 and all results obtained, including derived K_i values, are summarized in Table 8.

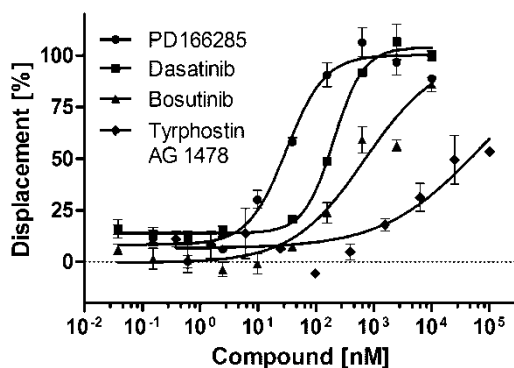


Fig. 27: IC₅₀ curves for identified Myt1 inhibitors. Data represent means \pm SEM (n=3).

Table 8: Inhibition profile of Myt1 obtained by the DasAFITC-assay.

Compound	Mean IC ₅₀ [nM]	K_i	Literature K_i , K_d , IC ₅₀ (nM) or inhibition at concentration
Dasatinib	202	73 \pm 16 nM	130 [76], 63 ^b
PD166285	31,1	2.0 \pm 1.5 nM	7.2 ^b , 72 [151]
Tyrphostin AG1478	55 μ M	26 \pm 8 μ M	25% at 5 μ M ^b , 40% at 10 μ M ^b
Bosutinib	704	304 \pm 71 nM	350 [76]
Roscovitine	No effect ^a	-	No effect [23]
Staurosporine	No effect ^a	-	No effect [76], ^b
Gefitinib	No effect ^a	-	No effect [76], ^b
Lapatinib	No effect ^a	-	No effect [76], ^b
SB203580	No effect ^a	-	No effect [76], ^b
Erlotinib	No effect ^a	-	No effect [76], ^b
HA-1077	No effect ^a	-	No effect ^b
Sunitinib	No effect ^a	-	No effect [76], ^b
Neratinib	No effect ^a	-	No effect [76]
Midostaurin	No effect ^a	-	No effect [76], ^b
K252a	No effect ^a	-	No effect ^b
U0126	No effect ^a	-	No effect ^b
CEP-701 (Lestaurtinib)	No effect ^a	-	No effect [76]

^a Mean displacement < 10%

^b as obtained by LanthaScreen kinase binding assay using Myt1 as full-length protein (see 5.2)

The test panel of kinase inhibitors contained not only known inhibitors. Also negative controls were included to see whether this assay utilizing the kinase domain of Myt1 leads to fully equivalent results compared to full-length Myt1 as tested in the LanthaScreen assay (Section 5.2).

The obtained K_i values are comparable to those reported in the literature and provide the possibility to rank the inhibitors reliably. This might be of particular importance for future virtual screening studies. The inhibition profile not only matches former studies with the kinase domain but also known full-length or functional data. Therefore, the use of the kinase domain instead of the full-length enzyme is a suitable model for Myt1 binding assays.

5.3.3. *Inhibitor Screening*

Altogether, more than 150 compounds were tested in the DasAFITC assay for their ability to affect Myt1. The compounds were chosen with respect to computational suggestions or general additions to the inhibition profile. Also, promising inhibitor classes such as flavonoids or glycotriazoles were tested. Structures of all compounds not common to general kinase research are given in the appendix (p. 140). Selected compounds will be discussed in the following.

5.3.3.1. *Identifying False-Positives: Flavonoids as Examples*

One of the classes screened against Myt1 were flavonoids. Flavonoids are polyphenolic compounds with a high degree of variation. Typically, they contain a C_{15} -scaffold and are structurally based on 1,3-diphenyl propane (flavonoids) or 1,2-diphenyl propane (isoflavonoids) [269]. More than 6500 structures are known, differing in hydroxylation, methylation, glycosylation and other modifications [270]. Flavonoids are known to have antiproliferative effects [269] and it has become clear that these effects are mediated by specific ligand-protein interactions [271]. In particular in the kinase field, flavonoids have gained a lot of attention [269, 271]. Therefore, a set of ten flavonoids¹ was chosen based on previously described kinase effects, occurrence in food and commercial availability. Importantly, genistein was included in the test set, an isoflavone that has previously been shown to inhibit many tyrosine kinases [274]. This compound

¹ Flavonoids chosen for testing (in alphabetical order), known kinase effects are exemplarily referenced: daidzein; 3,7-dihydroxy flavone (3,7-DHF); fisetin [272-273]; genistein [274]; kaempferol [275]; myricetin [276-277]; naringenin [278]; phloretin [279]; quercetin [277, 280] and silibinin [281].

is of particular importance because it was reported as a potential modulator of Myt1 in a biological study in TRAMP cancer cells [282].

Flavonoids, particularly their aglycones, appear as hits in many biological assays and are often referred to as *frequent hitters* [283-284]. However, these effects are often caused not by a specific mechanism, but rather by unspecific assay interference due to their many hydroxyl functions and spectroscopic properties (e.g. fluorescence). How to handle potential false-positives will be demonstrated in the following.

All flavonoids were screened at 10 μ M and 50 μ M in triplicates. Indeed, this class turned out to be analytically difficult. After primary screening, only daidzein, genistein, naringenin and silibinin could be certainly excluded as Myt1 effectors (mean displacement < 10% and absence of anomalies). The other compounds showed anomalies such as autofluorescence (fisetin >> myricetin > quercetin >> kaempferol) or remarkable displacement at 50 μ M while having no effect at 10 μ M. The inclusion of appropriate wells (containing no DasAFITC) in a secondary screening allowed for specific background correction and showed that quercetin and kaempferol did not bind to Myt1. The emissivity of fisetin and myricetin was very high and the respective background correction indicated fluorescence quenching effects as the absolute intensity of the probe was lowered by more than half compared to control wells. Therefore, the DasAFITC assay failed to assess these two compounds.

The two remaining compounds, phloretin and 3,7-DHF, were investigated by means of the Hill-slope as an analytical parameter. Starting from 100 μ M, four serial dilutions (1:2) were made and assayed (five data points, assayed in triplicates). Indeed, absolute Hill-slopes > 3 were obtained for both compounds after nonlinear regression (phloretin: 3.9; 3,7-DHF: 16.4). According to SHOICHET, there are three possible explanations for steep dose-response curves (absolute slope > 1.5) [196]: The enzyme concentration might be higher than the inhibition constant of the compound (1) or the respective enzyme might have several interaction sites (2). Both possibilities can be excluded due to micromolar compound concentrations and the specificity of the dasatinib-derived tracer and the use of the lone kinase domain. The remaining reason is a physical effect (3), common to so-called promiscuous inhibitors [285-286]: These compounds form aggregates with a size of 30-400 nm and insert proteins or probes, leading to

wrong results. Since these aggregates are not formed until a concentration threshold is reached, the dose-response curve obtained will be very steep. However, the occurrence of these aggregates is not predictable and is highly influenced by the exact assay conditions. Flavonoids have already been described as promiscuous inhibitors (e.g. quercetin [287]). Further photometric studies under assay conditions (data not shown) indicated that no precipitation occurred in the respective concentrations for phloretin, while 3,7-DHF showed distinct insolubilities $> 25 \mu\text{M}$. Taken together, the effects of phloretin and 3,7-DHF were caused by physical effects and not by specific interaction with Myt1. These compounds were identified as false positives in the primary screening, although only phloretin showed the characteristics of a promiscuous inhibitor in the sense of MCGOVERN [286].

None of the tested flavonoids were revealed to be a Myt1 inhibitor, though fisetin and myricetin could not be assessed due to their autofluorescent properties, a problem common to any screening based on fluorescence read-out [261]. This section, however, demonstrated how false-positive results can be identified without using an alternate assay.

5.3.3.2. *Virtual Screening*

Docking-based approaches are commonly implemented in prediction of the binding mode of a novel lead compound to a target protein. Although these docking-based approaches are usually able to reproduce the experimentally observed binding mode, accurate prediction of the binding affinity is still challenging [288].

Molecular docking is a fast and simple method and, therefore, frequently used for screening of compound databases. Simple scoring functions are often applied to estimate binding affinities but often show a poor correlation with experimental results [259, 289-290] and are, moreover, not accurate enough to discriminate active from inactive compounds.

The *in silico* studies described herein were carried out by Dr. K. Wichapong. The compounds tested in the TR-FRET based binding assay (see 5.2.2) were docked into the binding pocket of Myt1 (PDB: 3P1A). However, all of these compounds showed similar binding modes and H-bonds with key residues at the hinge region (Cys190 or Glu188). Comparison of the docking scores (GoldScore) revealed that active and inactive compounds were incorrectly ranked. For example, dasatinib

and PD166285 as affine binders yielded GoldScores of 52.0 and 51.4, while experimentally inactive compounds such as K252a or U0126 produced even higher scores (59.8 and 64.6, respectively). These results indicate that binding mode and docking score cannot be used to explain structure-activity relationships or to discriminate active from inactive compounds. In accordance with this finding a test set comprising twelve compounds selected from the Chembridge library with respect to molecular docking results did not have any effect in LanthaScreen or DasAFITC assay (Set: Chembridge I, see appendix (p. 140) for chemical structures).

Therefore, binding free energy calculations were used for postprocessing of protein-ligand docking poses as a more accurate method and QM/MM-GBSA (Quantum Mechanics/ Molecular Mechanics Generalized Born Surface Area) scoring using AMBER11 [291] performed best.

Only the top-ranked docking pose of every compound was rescored by calculating the binding free energy using this method and then ranked accordingly. Inactive compounds yielded positive values, indicating unfavorable binding to Myt1. By means of MD simulations and subsequent QM/MM-GBSA scoring of average MD snapshots, the method was also able to separate highly active (nanomolar affinity) from weakly active compounds (micromolar affinity).

As a validation of the methodology, external test sets were selected and screened in the DasAFITC assay. One set containing seven compounds from Key Organics was chosen as a negative control: Molecular docking implied binding to Myt1, while QM/MM-GBSA scoring predicted the compounds to be inactive (Set: Keyorganics, see appendix (p. 140) for chemical structures). Independently, a database containing 23 known kinase inhibitors was docked², binding modes compared to available crystal structure data and the poses refined using QM/MM-GBSA scoring. Three compounds were predicted to be active compounds (PD173952, PD180970 and CUDC-101) and two compounds were predicted to be weakly active (saracatinib and tivozanib).

As predicted, screening of the Keyorganics set at 10 μ M and 20 μ M did not lead to a significant displacement of the kinase tracer (data not shown).

²The kinase inhibitor set consisted of the following compounds (in alphabetical order): CHIR911, CUDC-101, GDC-0941, Go 6976, H-89, KU-0063794, LY 294002, MK1775, Mubritinib, OSU-03012, PD173074, PD173952, PD180970, PD325901, PD98059, PIK-75, PIK-90, Saracatinib, Tivozanib, Tyrphostin 48, Vargatef, Vemurafenib, VX-702, ZSTK474.

Using the same screening procedure, the five compounds predicted to be active were also tested. The results are summarized in Table 9.

Table 9: Results for five compounds suggested by virtual screening. Data was generated in the DasAFITC assay and is displayed as means \pm SEM (n=3).

Compound	Displacement at 10 μ M [%]	Displacement at 20 μ M [%]	Mean IC ₅₀	K _i
PD-173952	102 \pm 3	93 \pm 10	55 nM	8.1 \pm 3.6 nM
PD-180970	67 \pm 5	72 \pm 6	2700 nM	1.35 \pm 0.27 μ M
CUDC-101	No effect ^a	No effect ^a	-	-
Saracatinib	39.0 \pm 0,3	48 \pm 3	10.0 μ M	5.2 \pm 1.5 μ M
Tivozanib	No effect ^a	No effect ^a	-	-

^aMean displacement < 10%

Three out of the five compounds had major effects in the assay. The effects for both screening concentrations differ in a dose-dependent manner and no assay interference by autofluorescence occurred. For PD173952, it appears that both screening concentrations already lie in the displacement plateau. PD180970 and saracatinib showed dose-responses that could be resolved, meaning they are less potent than PD173952. CUDC-101 and tivozanib did not show significant effects and were wrongly predicted although possible effects at higher concentrations were not explored.

A critical step in the VS method used is the selection of the right binding mode. An incorrectly selected binding pose will result in a false prediction of the binding affinity. Moreover, as the entropy term in this approach is simply approximated from the number of rotatable bonds, highly flexible compounds such as CUDC-101 can lead to an overestimation of the entropy change upon binding, which can result in false positive results. Tivozanib was predicted to be a weakly active compound, which did not hold true.

To further investigate the dose-dependence for the three hit compounds and also to rank the compounds among other Myt1 inhibitors, IC₅₀ values were determined and used to derive inhibition constants (K_i). The dose-response curves obtained are displayed in Fig. 28, the data is included in Table 9. Hill-slopes showed no anomalies.

Saracatinib, predicted to be a weakly active compound, did indeed bind to Myt1 with micromolar affinity (K_i = 5.2 μ M) and, most importantly, both pyridopyrimidine derivatives predicted to be active showed remarkable affinities: PD180970 had a low micromolar inhibition constant of 1.35 μ M and PD173952

was revealed to be a highly affine compound, having a K_i value in the low nanomolar range (approximately 8 nM).

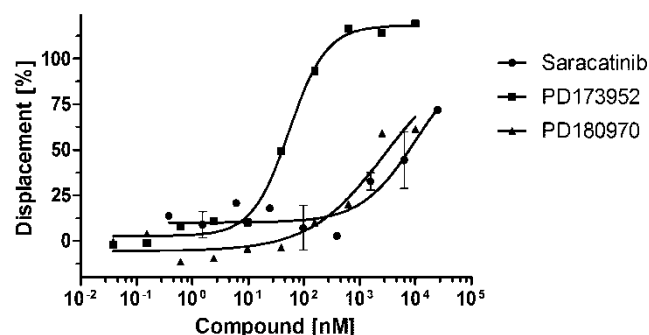


Fig. 28: IC_{50} curves for the three hit compounds derived from virtual screening. Data represent means \pm SEM (n=3).

With respect to questions raised in the literature, this is an interesting finding. PD173952 was found not to affect Wee1 and, moreover, acted as an S-phase blocking agent in MCF-7 and MDA-MB-468 cells, possibly due to unclear membrane effects [292]. Since Myt1 is involved in membrane dynamics (see 2.2.2.3), Myt1 inhibition might be partly responsible for the observed phenotype. The chemical structures of the three identified hit compounds are given in Fig. 29.

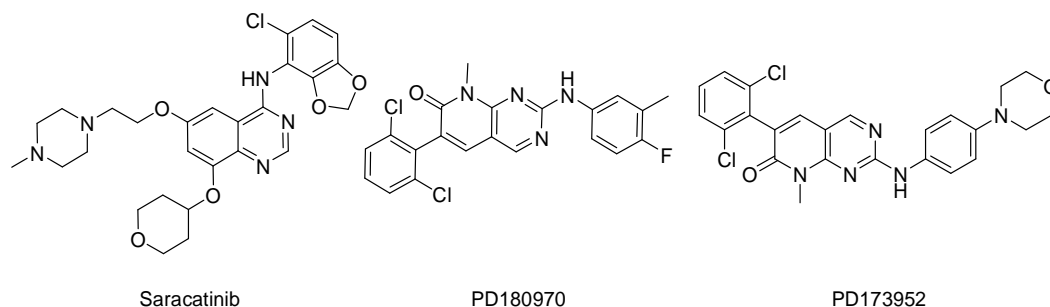


Fig. 29: Chemical structures of three hit compounds identified via virtual screening.

Furthermore, all Myt1 inhibitors mentioned in this work were investigated with regard to structural as well as binding mode similarities. Their chemical scaffold contains a thiazole (dasatinib), a quinazoline (tyrphostin AG 1478, saracatinib) or a pyridopyrimidine structure (PD compounds). The structures of the ligand-protein-complexes obtained after energy minimization revealed that these aromatic rings play an important role for interacting with Phe240 (π - π - interactions). For inactive compounds such as imatinib or bisindolylmaleimide I, such a π - π - interaction was not observed. The finding of Phe240 as a key interaction for Myt1 inhibition could be of particular importance to gain selectivity over other kinases. Many other kinases (Pim1, Cdk2, EGFR, Abl,...) do not include a phenylalanine at this position, but rather aliphatic side chains of Ala or Leu residues. Thus, for designing more selective inhibitors against Myt1,

aromatic ring systems should be inserted to gain interaction with the Phe240 residue.

Taken together, the *in vitro* screening of compounds suggested by VS confirmed the ability to identify hits in the DasAFITC assay.

Three hits out of five suggested compounds is not a hit rate to be expected for further screenings. As shown by BAMBOROUGH et al., when testing a library that only contains compounds known to affect kinases, the hit rates will dramatically increase, no matter which kinase is screened [74]. The identified structures may help learn about the ATP binding pocket of Myt1, though further screenings for the identification of less promiscuous and less extensively researched lead structures are necessary.

5.3.3.3. *Glycotriazoles*

The glycotriazole series was also tested in the DasAFITC assay (for chemical structures refer to the appendix, p. 142). Interestingly, the two hits from the LanthaScreen assay (BS11, BS12) could not be verified in concentrations up to 100 μ M. This finding supports the hypothesis that the compounds affect the antibody binding to the His-tag rather than actually displacing the tracer from the kinase in the LanthaScreen kinase binding assay.

The case of the glycotriazoles clearly shows that a suitable secondary assay can be considered essential for validation of novel lead structures and screening hits. Usually, a functional enzymatic assay is preferred for this task. In absence of such an assay, however, an orthogonally acting binding assay may also help verify or falsify results gained in the primary assay.

5.3.4. *DasAFITC Assay: Conclusion, Limitations, Drawbacks*

The present assay is a homogenous, single step assay without need for a special substrate. Basically, only kinase and labeled ligand are needed. This can be considered advantageous over other Myt1 binding assays such as LanthaScreen, because no capricious antibodies have to be used. The instrumentation to perform the assay is much less demanding and broadly available in many laboratories.

The effect that buffer additives strongly affect the dynamic range of such an assay does not only apply to detergents but has also been described for other buffer components, for instance blocking proteins such as BSA [293]. This effect generally limits the use of fluorescence anisotropy based methods in biological samples (blood, lysates, etc.).

A major point in any FP based competition assay is the affinity of the labeled ligand. Usually, it is advisable to use a ligand as affine as possible in order to expand the range of resolvable inhibitors [294-295]. Subnanomolar affinity probes have successfully been used in such assays [293]. An approximate estimate for the low end of K_i values that can be resolved is the K_d value of the fluorescent ligand [294]. This is one of the limitations of the assay described herein. Kinases with different affinities towards the tracer were tested and a Myt1 kinase assay (K_d approx. 130 nM) was still good in terms of assay performance (Z'). However, the lower tracer affinity compared to the other kinases leads to limitation in resolvable inhibitor potencies lying in the low nanomolar range. The statistical approach used, described by ZHANG et al. [232], improves the ability to rank compounds and may partly compensate this effect.

Another limitation lies in the fluorophore itself. Compound fluorescence is a common cause of assay interference. Heterocyclic compounds that dominate screening collections commonly fluoresce in the blue-green range. Therefore, fluorescein is susceptible to this type of optical interference [284]. Indeed, the assay was not able to analyze the binding properties of two flavonoids, myricetin and fisetin, due to their autofluorescence properties at the wavelength of the fluorophore.

Therefore, the use of a fluorophore that is excited with more red-shifted light will decrease assay interference and can be considered advantageous [296-297]. This might be a subject for future assay optimization.

5.3.5. *Affinity of ATP to Myt1*

One factor that limits the translation from *in vitro* assay data to a cellular context is the co-dependence of the inhibitor potency on the intrinsic affinity of the inhibitor and the kinetics of the enzyme with respect to its cofactor ATP [11]. In a typical functional assay for reversible, ATP-competitive inhibitors, inhibitor potency is expressed as an IC_{50} value which is a function of its intrinsic affinity (K_i) and the degree of competition from ATP [54].

Therefore, the binding affinity of ATP to Myt1 was investigated in the DasAFITC-assay. The IC_{50} acquired by displacing the probe through ATP is a good measure for the affinity and equals the apparent Michaelis-Menten constant ($K_{m,app}$). By applying the methodology by ZHANG et al. (see 4.20.3), the resulting $K_{i,ATP}$ equals the Michaelis-Menten constant ($K_{m,ATP}$).

Serial dilutions of ATP were performed and tested, starting from an assay concentration of approximately 7 mM. Higher assay concentrations led to fluorescence quenching effects and had to be excluded. The respective plates were read at different timepoints (15 min to 4 h) and the curve did not shift within this timeframe, indicating that ATP-degradation can be neglected as a source of error. In this experiment, a mixture of ATP and probe was given to the kinase. Since probe and kinase were not preincubated, sigmoidal curves having their inflection point at comparable concentrations were obtained. Fig. 30 shows the displacement curve for ATP after 120 min incubation.

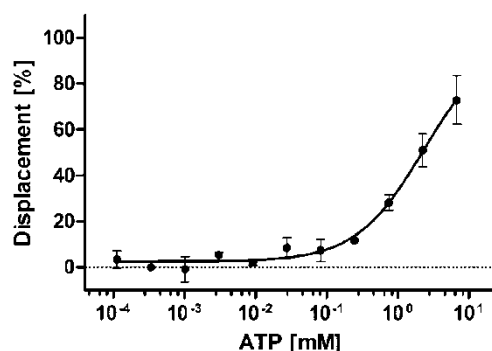


Fig. 30: Displacement curve for ATP obtained in the DasAFITC-assay. Data represent means \pm SEM (n=3). A sigmoidal dose-response with variable slope was applied, top was set to 100%.

The Hill-slope resulting from non-linear regression can be considered almost optimal (1.08), indicating competitive behaviour of ATP. The IC_{50} is equal to 2.3 mM. K_m was calculated to be 1.2 ± 0.2 mM. Importantly, this is the first estimation of ATP-affinity for Myt1.

Many kinases have $K_{m,ATP}$ in the range of 10-100 μ M. However, there are also significant outliers with millimolar values for $K_{m,ATP}$ [11]: For example, several phosphatidylinositol 4-kinases and mTOR have millimolar $K_{m,ATP}$ values [298-300].

Low affinities towards ATP do not preclude kinase activity because the cellular ATP concentration is high, typically 1-5 mM [301-302].

In cells, an inhibitor that has similar K_i values against several kinases will inhibit more potently those kinases that have a higher $K_{m,ATP}$. Analogously, although not found in a binding assay, a compound having a K_i in the mid-micromolar range might be a potent functional inhibitor. Such a compound could be missed in binding assays because the concentrations needed for displacement are not reachable due to solubility issues. In a functional assay however, it can compete with ATP and inhibit the kinase reaction.

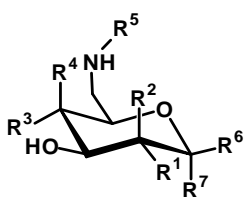
The isolated kinase domain may have differing affinity from the native enzyme, i.e. different $K_{m,ATP}$. The difference between protein constructs is particularly apparent when assaying allosteric kinase inhibitors. For example, potent allosteric Akt inhibitors require the presence of a specific domain of the kinase protein to show inhibitory activity [303]. Furthermore, $K_{m,ATP}$ can be affected by the substrate used, e.g. when comparing protein substrates to peptide substrates [304]. Taken together, the millimolar $K_{m,ATP}$ should be carefully interpreted, although it provides evidence that the inhibition profile obtained by binding assays should be ascertained in a functional assay in future research, since the binding affinity towards ATP is, apparently, only moderate.

5.4. Glycoglycerolipids as Myt1 Inhibitors?

Based on a report of ZHOU et al., the glycoglycerolipid 1,2-dipalmitoyl-3-(*N*-palmitoyl-6'-amino-6'-deoxy- α -D-glucosyl)-*sn*-glycerol (GGL1) is said to be a selective Myt1 inhibitor. That compound was synthesized [305] and derivatized to learn about the mechanism of action of this class. The chemical synthesis was carried out by Dr. C. Göllner and the structures for GGL1 and its tested derivatives are presented in Table 10.

Table 10: Glycoglycerolipids synthesized by Dr. Göllner. The carbohydrate core was varied from glucose (GGL1, GGL1 β) to galactose (GGL2 α , GGL2 β) and mannose (GGL3 α , GGL3 β). Using the glucoside, capryloyl chains were inserted instead of palmitoyl chains (GGL4 α).

	R ¹	R ²	R ³	R ⁴	R ⁵	R ⁶	R ⁷
GGL1	OH	H	OH	H	P ^a	H	DPG ^b
GGL1β	OH	H	OH	H	P	DPG	H
GGL2α	H	OH	OH	H	P	H	DPG
GGL2β	H	OH	OH	H	P	DPG	H
GGL3α	OH	H	H	OH	P	H	DPG
GGL3β	OH	H	H	OH	P	DPG	H
GGL4α	OH	H	OH	H	C ^c	H	DCG ^d



^a P: palmitoyl.

^b C: capryloyl.

^c DPG: 1,2-dipalmitoyl-*sn*-glycerol.

^d DCG: 1,2-dicapryloyl-*sn*-glycerol

Starting from GGL1, the carbohydrate core was varied (glucose (GGL1, GGL1 β), galactose (GGL2 α , GGL2 β) and mannose (GGL3 α , GGL3 β), in α - and β -anomeric configuration). As a further variation of GGL1, the side chains were shortened from palmitoyl to capryloyl moieties (GGL4 α).

Other working groups have also spent a lot of research effort on the synthesis of this compound class, but reliable Myt1 assay data are still missing [306-308]. Once again, this lack of Myt1 data might be caused by the difficulties in assaying this kinase such as membrane association, restrictivity in substrate acceptance, and unusual inhibition properties.

The glycoacylglycerolipids were tested three times in the LanthaScreen assay at 3 $\mu\text{g/ml}$ and 30 $\mu\text{g/ml}$. No effects on Myt1 could be determined. Only GGL2 α showed a negligible displacement (7.5%) of the kinase tracer at 30 $\mu\text{g/ml}$.

There are two possibilities why GGL1, which is reported to inhibit Myt1 quite potently (IC_{50} 0.12 $\mu\text{g/ml}$), did not show any effect in this assay. Either the results of the original work must be questioned, or this class unfolds its effect distant from the ATP-binding pocket.

Type III kinase inhibitors are compounds that bind exclusively to sites other than the ATP-binding site. Due to steric reasons caused by three fatty acid chains in the glycoacylglycerolipids, a mechanism of action outside the ATP-binding site is likely, making it type III instead of ATP-competitive. Even though most type III inhibitors do not directly bind to the ATP site, the majority must either alter the active site in a way that displaces the tracer or bind close to the active site. The glycoacylglycerolipids did not displace the tracer, although a maximum concentration up to 250-fold the reported IC_{50} was used. Considering the potency of GGL1 in an activity assay, the conclusion may, indeed, be drawn that the effect of this class is unfolded far from the active site. So far, there is only one known example of a type III inhibitor which could not be detected in a binding assay but in an activity assay. This compound inhibited p38 α depending on the substrate used [309-310].

The chemical structure of the tested compounds together with the cellular localization of Myt1, membrane-bound at the endoplasmic reticulum, give rise to another thesis. All tested GGLs are very hydrophobic and therefore practically insoluble in water. Not until solutizer (30% DMSO) or tenside were added could the compound be dissolved. Therefore, these compounds are likely to interact with more hydrophobic structures such as bilayers (membranes) and micelles. As can be seen in Fig. 31, the membrane association motif within the Myt1 protein sequence shows spatial proximity to both the kinase domain and the Cdk1 interaction site [90].

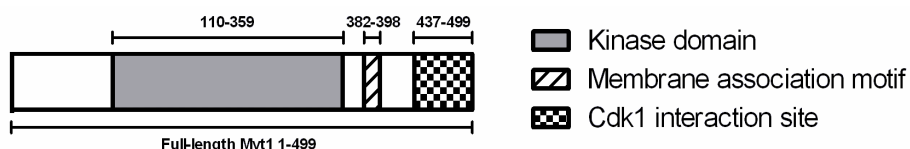


Fig. 31: Illustration of the full-length Myt1 sequence and respective function of selected regions.

Because an interaction of the GGLs with the kinase domain was not observed, GGL effects on the substrate (Cdk1) recognition of Myt1 might be responsible for their reported inhibitory potential.

To verify or falsify the results obtained in the LanthaScreen assay, GGL1 was also tested in the DasAFITC-assay. Here, only the Myt1 kinase domain was used for binding studies. Also with this anisotropy based binding assay, no effects could be determined (Fig. 32).

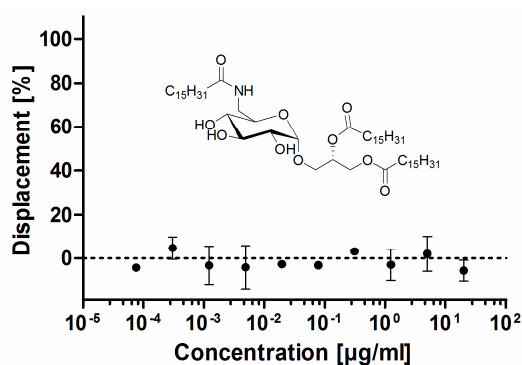


Fig. 32: Test of GGL1 in the DasAFITC-based binding assay. The reported Myt1 glycolipid inhibitor did not have any effect in this assay.

A closer look at the described assay procedure in the report by ZHOU et al. reveals some conceptual deficits. The description therein is kept short. An FPIA was conducted and KRISTJÁNSDÓTTIR et al. [24] is cited as a reference. However, the assay was run in a direct instead of a competitive approach using a labeled Cdk1-derived peptide substrate.

This leads to two general problems: Firstly, KRISTJÁNSDÓTTIR et al. as well as the results described in this thesis suggest that Myt1 does not accept short Cdk1-derived peptides as substrates. Secondly, direct fluorescence polarization assays carry some inherent limitations. A labeled substrate is directly phosphorylated and, subsequently, bound by an antibody. The resulting FP is increased compared to the free unbound probe. The measured fluorescence anisotropy is an additive entity based on the intrinsic anisotropies of free and bound fluorescent probe (r_b and r_f) together with their respective fractions (f_b and f_f):

$$r = f_b * r_b + f_f * r_f \quad (\text{Eq. 13})$$

Unphosphorylated peptide will not be bound by the antibody but it is still present in considerable amounts and, as it is labeled, it will interfere with the assay by narrowing the dynamic range [311]. As shown by WU, substrate conversions of at least 50% are required to overcome this effect and to yield an appropriate assay window [223].

If it is, furthermore, taken into account, that the substrate probe was used at a concentration of 2.5 nM, such a conversion is intrinsically limited by diffusion.

Altogether, the assay used to prove the inhibitory effects of GGL1 on Myt1 is not very trustworthy.

Assay interference by insertion of the labeled substrate into association colloids formed by GGL1 when dissolved in kinase buffer was excluded by CMC inclusion assays (see 4.19) for concentrations as used in the reported testing procedures.

To further examine whether the original publication by ZHOU et al. can be correct, a functional investigation was needed. Therefore, recombinant GST-Cdk1 (125 nM) was incubated with full-length Myt1 (80 nM) and ATP (250 μ M) as described in Section 4.13 in presence or absence of GGL1 (30 μ g/ml). Samples containing dasatinib (10 μ M) were carried along as inhibitor controls and samples without ATP were used as background controls. Myt1 was present in all samples. After incubation (2 h) the reaction was terminated by addition of EDTA. The protein was isolated by TCA precipitation and prepared for SDS-PAGE and subsequent western blotting. As primary antibodies, anti-pTyr15 Cdk1 antibody was used to visualize Myt1 kinase activity and anti-Cdk1 total antibody was used as loading control to exclude protein loss caused by work up and handling. Representative western blot results are displayed in Fig. 33.

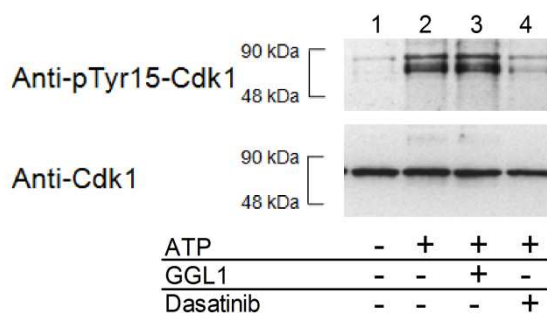


Fig. 33: Representative western blot results for investigations on the inhibitory properties of glycerolipid GGL1 on full-length Myt1.

As indicated by the anti-Cdk1 total antibody, an even loading of the samples can be assumed. Therefore, differences in the detected phosphorylation status can be

considered a result from the Myt1 kinase reaction. As expected, the control without ATP (lane 1) showed a low basal phosphorylation of Cdk1, while the kinase reaction (conversion control containing substrate, cosubstrate and kinase; lane 2) drastically altered the phosphorylation status. Addition of GGL1 (lane 3) did not reduce the formation of phospho-Tyr15 Cdk1 compared to the conversion control. The addition of dasatinib (lane 4), however, was indeed able to inhibit the kinase reaction. The amount of detected kinase reaction product remained close to the basal phosphorylation. The formation of phospho-product could not be totally suppressed which is mainly caused by the conditions used in this experiment (large excess of ATP and long incubation periods).

The concentration of GGL1 used here was about 250 times higher than the reported IC_{50} value. No relevant functional inhibition occurred. Apparently, GGL1 is not able to inhibit Myt1-mediated phosphorylation of Cdk1.

In summary, GGL1 did not affect full-length Myt1 in a kinase binding assay. Also, the kinase domain in another binding assay was not affected and even a functional assay with full-length Myt1 failed to reproduce the results obtained by ZHOU et al.

The glycolipid GGL1 is, apparently, no inhibitor of the human Myt1 kinase.

5.5. Advanced Substrate Studies

To finally identify a suitable *in vitro* substrate that allows for the development of a medium-throughput functional assay, the scope was widened to test a more diverse set of possible substrates. As a sophisticated technique, peptide microarrays allow for the screening of thousands of potential substrates at the same time, providing a unique possibility for kinase profiling [312].

5.5.1. Peptide Microarray Studies

As a starting point for the discovery of kinase substrates, two high content peptide microarrays as described in [243] were used, displaying, altogether, 2304 peptides derived from human protein sequences, arranged in three identical subarrays on chemically modified microscope slides. These peptides were extracted from the databases SwissProt [313] and Phosphobase [314] as sequences known to be phosphorylated in the human proteome. Each microarray was incubated with full-length Myt1 and full-length Wee1 in the presence of ATP and the resulting

phosphorylations were visualized by an anti phospho-tyrosine antibody and a fluorescent dye-labeled secondary antibody. Also, microarray controls were performed which were treated equally but in absence of kinase. In the first line, an immunological anti-pTyr method was used instead of radioactivity to visualize substrate phosphorylations. Fluorescence readout is favorable over a radioactive readout, since the resolution of phosphor imagers is dramatically lower than for fluorescence scanners. Additionally, incorporation of radioactivity in microarray studies leads more towards a yes/no answer, while fluorescence is much easier to quantitate, hence allowing statistical approaches to be used to identify the most promising peptides. Notwithstanding, the radioactive approach was used to verify the results from the antibody based experiments.

After fluorescence readout, the index I was calculated as a measure of response according to NAHTMAN et al. [315]. The index I is defined as follows, with \tilde{x} being the median of foreground intensity (actual spot) or background intensity (area around the actual spot having 3fold the diameter of the respective spot), as indicated:

$$I = \log_2 \left(\frac{\tilde{x}_{Foreground}}{\tilde{x}_{Background}} \right) \quad (\text{Eq. 14})$$

As a measure of response, the ratiometric index [315] is well defined even if background signal is higher than foreground signal (e.g. for empty spots as negative controls). Importantly, it provides the advantage of introducing homoscedasticity, facilitating statistical analysis. However, the importance of the visual inspection of every single spot cannot be overemphasized for such a ratiometric measure and has to be carried out carefully [234].

For the identification of false positives, control experiments without kinase were run. A graphical display index I vs. $\log_2(\tilde{x}_{background})$ was used for data evaluation, designated Nahtman-plot in the following. As shown in Fig. 34, a clear distinction is given between peptide spots with a reproducible response in all three blocks, and negative controls (no peptide spotted, empty). Using this methodology, for the two slides, nine reproducible false-positive peptides with high response indices could be identified (6+3). With respect to NGO et al. [234], these peptides can serve as positive controls in further experiments and, moreover, can be used to normalize readouts to allow for a better comparability between slides and kinase outcomes.

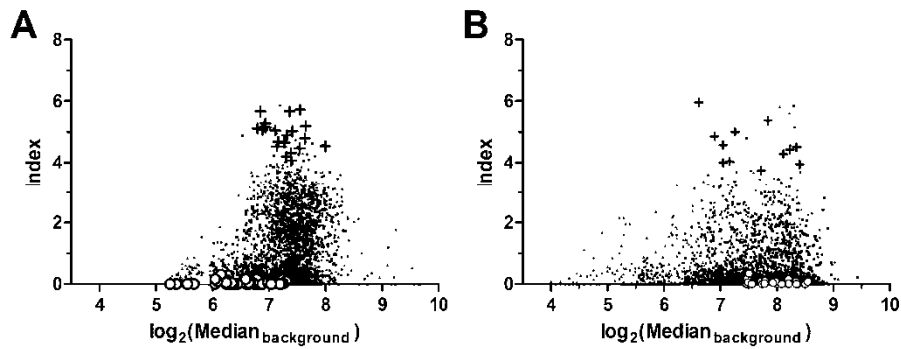


Fig. 34: Nahtman-plot for both microarrays I (A) and II (B) as a means of identifying false positives from antibody control slides. Reproducible false positives (plus signs) as well as negative controls (open circles) are indicated.

The two different slides were assessed individually and only the final results are presented together. After the kinase experiments, the responses were normalized using a two-step methodology. Firstly, the global median normalization was conducted [316]. Secondly, a positive control-guided normalization as described by NGO et al. was carried out [234]. Aligned dot plots of the normalized data for Myt1 and Wee1 are shown in Fig. 35. Both kinases were used in equal concentrations (80 nM) under identical conditions. The differences in range between Myt1 and Wee1 may arise from differences between the kinase activities of both preparations.

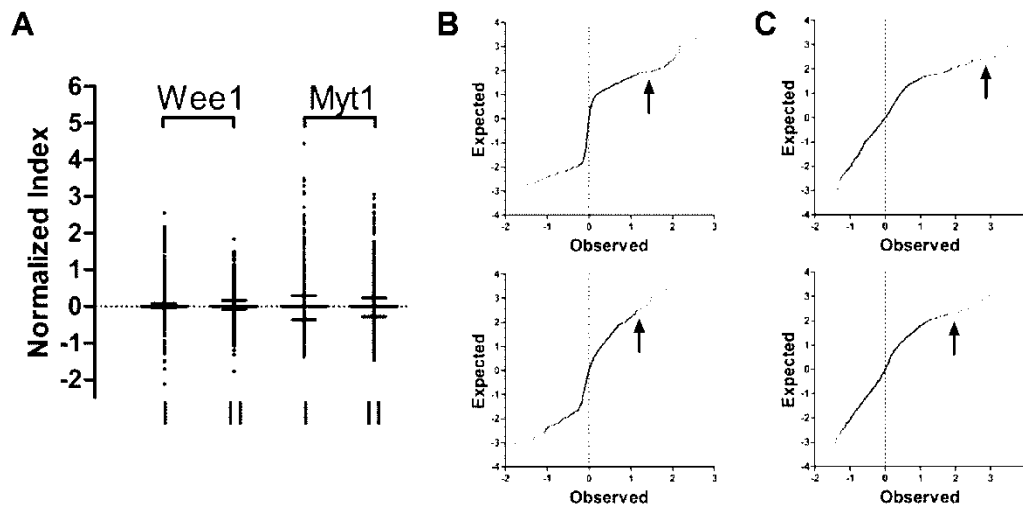


Fig. 35: Aligned dot plots of the normalized response index for the individually assessed microarray chips after incubation with Wee1 and Myt1 (A, displayed as Median \pm interquartile range). Quantile-quantile-plots for Wee1 (B) and Myt1 (C) are also shown: Slide I (upper panel) and slide II (lower panel). Arrows mark gaps in the QQ-plots. Indices beyond this gap were considered hits. Each set contains 1152 datapoints, calculated as mean index out of three replicates.

To identify promising hits, quantile-quantile-plots (QQ-plots, Fig. 35) were used as a simple means of cluster analysis for the two individual microarrays. Gaps in

the QQ-plot indicate discontinuity. Higher responses are unlikely to be part of the normally distributed population (the negative part of the dataset). More likely, higher responses constitute another, independent population of positives. Gaps at higher responses were identified visually and any index beyond the gap was considered a hit. The resulting hits were individually processed. Any peptides that appeared at least once in one of the antibody control experiments were removed, as well as peptides that contained a tyrosine only in terminal position or not at all in their sequences. Finally, a visual inspection of each individual spot was carried out to exclude false positives gained by artifacts.

Altogether, 21 top hits could be identified for Wee1, whereas Myt1 yielded 11 peptides. The overlap of both sets is represented by 4 peptides (Fig. 36).

This result was confirmed by a radioactive experiment using [γ - ^{33}P]-ATP and subsequent detection of incorporated radioactivity. All of these peptides were clearly positive in this radioactive approach (data not shown).

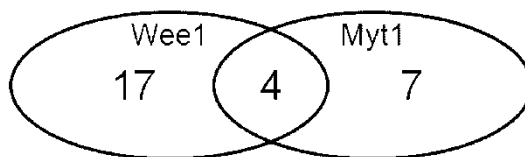


Fig. 36: Venn-plot of potential peptide substrates identified in microarray experiments for Wee1 and Myt1. For more information on the peptides refer to the upcoming tables.

A Venn-plot is shown in Fig. 36. Full information on the peptides as potential substrates can be found in Table 11 (Wee1) and Table 12 (Myt1). Peptide names consist of a protein abbreviation and an ID number, together unambiguously identifying the respective peptide. For the two peptide arrays, the top 50 highest response peptides for both kinases are provided in the appendix (see p. 148).

In order to identify a suitable Myt1 *in vitro* substrate, four of the identified peptides were selected for solution phase verification of these results: the highest response peptides (EFS_HUMAN_302 and A002-D_747) and two peptides from the overlap with Wee1 (TrkA_HUMAN_482 and INR1_HUMAN_548). To test these substrates for acceptance by Myt1, a suitable assay was required.

Table 11: Potential peptide substrates identified for Wee1 in alphabetical order. Peptides also positive for Myt1 are highlighted (grey).

Name	Uniprot ID [317]	Sequence	Full name
AD15_HUMAN_684	Q13444	VMLGAGYWYRARL	ADAM 15 (A disintegrin and metalloproteinase domain 15)
C79A_HUMAN_175	P11912	YEDENLYEGLNLD	Membrane-bound immunoglobulin associated protein (CD79a)
CDC2_HUMAN_287	P06493	KIGEGTYGVVYKG	Cell division control protein 2, Cyclin-dependent kinase 1 (Cdk1)
DDR1_HUMAN_369	Q08345	GMSRNLYAGDYR	Epithelial discoidin domain receptor 1 (Tyrosine kinase DDR1)
DDR1_HUMAN_371	Q08345	LYAGDYRQVQGRA	Epithelial discoidin domain receptor 1 (Tyrosine kinase DDR1)
EPB3_HUMAN_347	P54753	APGMKVYIDPFTY	Ephrin type-B receptor 3 (Tyrosine-protein kinase receptor HEK-2)
ERB4_HUMAN_376	Q15303	VAENPEYLSEFSL	ERBB-4 receptor protein-tyrosine kinase (p180erbB4) (cell surface receptor HER4).
FAK2_HUMAN_410	Q14289	YIEDEDYKASVT	Focal adhesion kinase 2 (FADK 2) (Proline-rich tyrosine kinase 2)
IG1R_HUMAN_542	P08069	DIYETDYRKGK	Insulin-like growth factor I receptor
IKKE_HUMAN_507	Q14164	DDEKFVSVYGTEE	Inhibitor of nuclear factor kappa-B kinase epsilon subunit (IkBKE) (IKK-epsilon)
INR1_HUMAN_548	P17181	SSSIDEYFSEQPL	Interferon-alpha/beta receptor alpha chain (IFN-alpha-REC)
INSR_HUMAN_509	P06213	GMTRDIYETDYR	Insulin receptor (IR)
JC4503_133	Q15546	WKYLRSPTDFMR	macrophage maturation-associated transcript dd3f protein
MK12_HUMAN_651	P53778	DSEMTGYVVTRWY	MAP kinase p38 gamma
PIG2_HUMAN_101	P16885	RDINSLYDVSRMY	Phospholipase C-gamma-2
RRPP_HRSV_983	P12579	NNEEESYSYEEI	RNA polymerase alpha subunit (Phosphoprotein P)
TRKA_HUMAN_16	P04629	DIYSTDYRVGGR	High affinity nerve growth factor receptor (TRK1, Trk-A)
TRKA_HUMAN_18	P04629	IYSTDYRVGGR	High affinity nerve growth factor receptor (TRK1, Trk-A)
TRKA_HUMAN_482	P04629	GMSRDIYSTDYR	High affinity nerve growth factor receptor (TRK1, Trk-A)
TRKB_HUMAN_117	Q16620	GMSRDVYSTDYR	BDNF/NT-3 growth factor receptor (Trk-B)
TRKB_HUMAN_180	Q16620	DVYSTDYRVGGH	BDNF/NT-3 growth factor receptor (Trk-B)

Table 12: Potential peptide substrates identified for Myt1 in alphabetical order. Peptides also positive for Wee1 are highlighted (grey).

Name	Uniprot ID [317]	Sequence	Full name
A002-D_747	P09619	DGHEYIYVDPMQL	Beta platelet-derived growth factor receptor
A051-F_442	P07949	YPNDSVYANWMLS	Proto-oncogene tyrosine-protein kinase receptor Ret precursor
EFS_HUMAN_302	O43281	GTDEGIYDVPLLG	Embryonal FYN-associated substrate (HEFS).
INR1_HUMAN_548	P17181	SSSIDEYFSEQPL	Interferon-alpha/beta receptor alpha chain (IFN-alpha-REC)
INSR_HUMAN_509	P06213	GMTRDIYETDYR	Insulin receptor (IR)
JC4503_133	Q15546	WKYLRSPTDFMR	Macrophage maturation-associated transcript dd3f protein
JH0826_968	Q16099	AFLLESTMNEYR	Glutamate ionotropic receptor EAA1 chain precursor
JS0648_1005	P35499	NPNYGYTSYDTFS	Sodium channel alpha chain
MK11_HUMAN_149	Q15759	DEEMTGYVATRWWY	MAP kinase p38 beta
MK14_HUMAN_150	Q16539	DDEMTGYVATRWWY	MAP kinase p38
TRKA_HUMAN_482	P04629	GMSRDIYSTDYR	High affinity nerve growth factor receptor (TRK1, Trk-A)

5.5.2. A Homogenous FP Based pTyr Assay (FPIA II)

For a specific verification of the peptides as Myt1 substrates, an assay aiming at phospho-tyrosines was required. Because separating and washing steps as well as radioactivity should be avoided, the methods to be used are limited. Direct measurement of phosphorylation, e.g. by fluorescent chemosensor peptides [318], requires a known and optimized substrate, which, so far, does not exist.

With respect to the expertise gained in former studies (see Section 5.1), it was decided to use a homogenous fluorescence polarization based immunoassay (FPIA). Because of its satisfying performance in the microarray studies, the same antibody should be used in the assay to detect phospho tyrosines. Phospho-tyrosine is the key motif for antibody binding, no matter what the surrounding sequence is. Therefore, the assay should be suitable for detecting any pTyr.

No peptidic Myt1 substrates have validly be reported so far which led to the expectation that sensitivity could be another important issue in this case. That is why a competitive FPIA was used instead of a direct one.

First of all, a suitable fluorescent probe was needed. As a requirement, the probe should have a molecular weight as low as possible (Fig. 37).

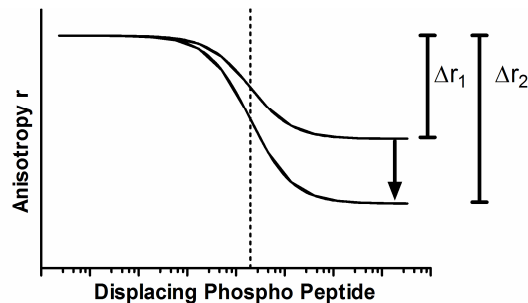


Fig. 37: Theoretical considerations in terms of molecular weight of the probe in FP-based immunoassays. The dynamic range Δr increases with decreasing mass of the probe, maintaining sensitivity as indicated by the dashed line that marks the EC₅₀ of both curves.

The lower the molecular weight of the probe, the better the dynamic range of the final assay. The free probe is determined to show a low FP due to fast rotation (Brownian motion). Association to the antibody dramatically increases the size compared to the free probe, leading to an increase in fluorescence polarization. If a mixture of antibody-probe complex (high FP) is added to a kinase reaction, any phospho-tyrosine residues formed will displace the tracer from the antibody, resulting in a lowered FP. Due to the high molecular mass of the antibody, the mass of the probe does not significantly affect the top plateau of a displacement curve. The bottom plateau, however, depends totally on the intrinsic anisotropy of

the probe. A heavy probe (consisting of many amino acids) will yield a narrow dynamic range (Δr_1), while a low molecular weight probe (containing only few amino acids) will yield an increased dynamic range (Δr_2), thereby improving the overall assay performance.

As a compromise between molecular weight and providing a suitable antibody epitope, a labeled pentapeptide was used as a probe.

All peptides identified for Myt1 that had only one central tyrosine residue were aligned to deduce a suitable pentapeptide XX(pY)XX with X being any amino acid. The formerly identified sequences were chosen, because, obviously, they could be bound by the antibody with sufficient affinity. The alignment led to the sequence XI(pY)VV (data not shown). Because there was no conserved residue for position one, N^{ϵ} -(6-Carboxyfluorescein)-L-lysine (6-FAM) was selected to insert the fluorescence label. Finally, (6-FAM)KI(pY)VV was used as a probe.

Briefly, the final assay was planned as follows: Kinase reactions should be carried out in 40 μ l assay volume and the reaction terminated by addition of 10 μ l stop solution containing EDTA. After addition of 10 μ l detection solution containing antibody and probe, measurements can be taken when equilibrium is reached.

All tests conducted at the assay development stage are directed to the planned procedure. Assay conditions (microplate, volumes, buffer constitutions...) were set in advance and followed accordingly.

Analytical pretests showed that FP of 2.5 nM (6-FAM)KI(pY)VV can be quantified with good certainty (CV < 5%). That concentration was used for all further tests. As a next step, a titration experiment with increasing amounts of antibody was carried out. Varying amounts of antibody were added to a solution containing 2.5 nM probe. Controls containing the phospho-peptide TpY (10 μ M, QLIGEGT(pY)GVVYKC), fully outcompeting the probe, were carried along. Results are shown in Fig. 38. In this assay, the K_d could be determined as 41 nM by nonlinear regression. As can be seen, the free probe has an intrinsic anisotropy of less than 0.05. In Section 5.1, a labeled tetradecapeptide was used for similar purposes, yielding an intrinsic anisotropy (free peptide) of approximately 0.08. As predicted (*vide supra*), the assay window utilizing the pentameric peptide tracer is noticeably increased. The maximum dynamic range (Δr_{max}) was 0.15 (anisotropy).

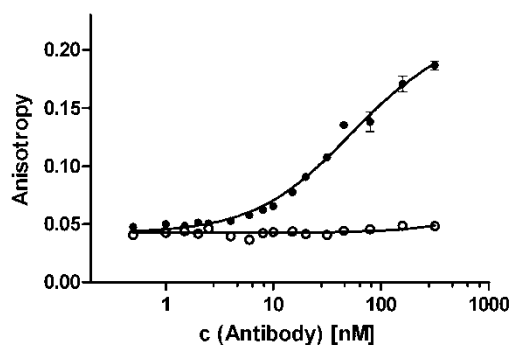


Fig. 38: Titration of the fluorescent probe with antibody. The antibody binds the probe resulting in increased fluorescence polarization (closed circles) and respective controls containing fully outcompeted probe (low fluorescence polarization, open circles). Nonlinear regression yielded a K_d of 41 nM. Data displayed as means \pm SEM ($n=3$).

For further assay development, a compromise between assay window (high antibody concentration) and sensitivity (low antibody concentration) had to be made. An antibody concentration slightly higher than the K_d -value yielded a sensitive yet robust assay. 45 nM antibody was used in further experiments, providing a difference between bottom and top of about 0.08 (anisotropy) which is equal to 123 mP (polarization).

To get an idea of the sensitivity of this setup, three different peptides containing phospho-tyrosine were used for exemplary displacement titrations.

These phospho peptides mimic phosphorylated substrate peptides and the displacement curves can help estimate the product formation required for detection. Phospho peptides used were TpY, TrkA pY676 (15-meric peptide) and PDGFRA pY572 (14-meric peptide). The resulting curves are shown in Fig. 39.

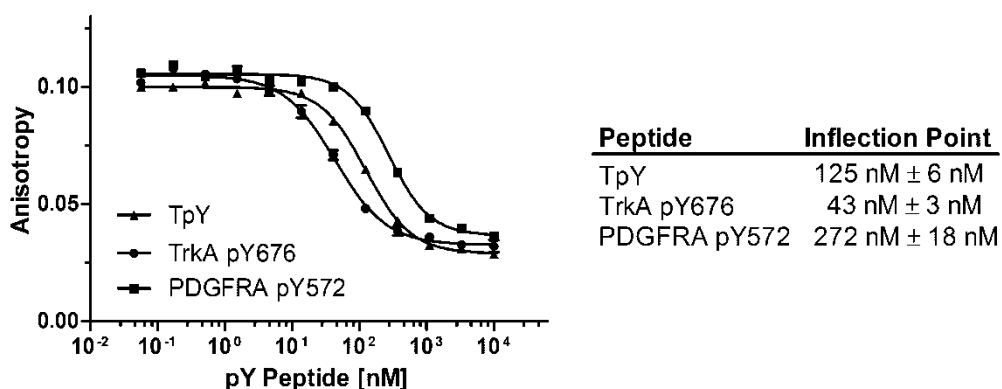


Fig. 39: Titration of antibody-probe complexes with different phospho peptides. The inflection points vary with regard to the respective pTyr-containing epitope but remain in a nanomolar scale indicating a sensitive assay system. Data represent means \pm SEM ($n=4$).

As can be seen from the decreasing curves, all of the phospho peptides did efficiently displace the probe from the antibody. The resulting EC_{50} is a good measure in terms of sensitivity and the values range from 43 nM for TrkA pY676

to 272 nM for PDGFRA pY572 (mean value for all peptides: 147 nM). These results indicate that the sensitivity of the monitored reaction, indeed, depends on the affinity of the formed product towards the antibody. However, all peptides could be detected in a submicromolar range with good certainty. Altogether, the general suitability for the detection of pTyr-containing peptides can be assumed which allows for the application of this system to the evaluation of peptide substrates. Refer to Section 4.16 for the exact assay protocol as used in upcoming sections.

5.5.3. *Solution Phase Verification of Peptidic Substrates*

For further solution phase substrate studies, not only the four peptides derived from microarray studies were tested, but also three other peptides. The previous work (see 5.1) showed that a peptide derived from the native phosphorylation site (Cdk1⁸⁻²⁰) was not modified by Myt1 *in vitro*. *In silico* studies suggested that the interaction N-terminal from the actual phosphorylation site might be important for substrate acceptance and that these interactions are not sufficient in the Cdk1⁸⁻²⁰ peptide. To prove or disprove this concept, a peptide containing the amino acids 6-17 (Cdk1⁶⁻¹⁷) was purchased to provide better N-terminal interactions. Furthermore, peptides containing amino acids 1-24 (Cdk1¹⁻²⁴) were synthesized by solid phase peptide synthesis to check whether the peptides tested in early substrate studies were simply too short to be recognized. As a posttranslational modification of this peptide, also acetylations of the N-terminus (Ac-Cdk1¹⁻²⁴) were introduced, as is the case in the native Cdk1 protein [319].

These seven peptides were tested at 20-200 μ M in kinase experiments containing 400 μ M ATP in standard kinase buffer. Typically, enzyme concentrations of 1-50 nM are used in such assays [320]. An important aspect to be considered is the limited specificity of the detection principle. Any phospho tyrosine brought into the assay will competitively displace the probe. Many posttranslational modifications including phosphorylations are reported for Myt1 [321-324]. One of these putative modifications is a tyrosine residue (Tyr97) [322] which might interfere with the assay by narrowing the assay window. To circumvent a large extent of such an interference, it was decided to test at 40 nM Myt1.

For monitoring the phosphorylation process, the homogenous assay as developed in the last section (5.5.2) was used and the results are summarized in Table 13.

Table 13: Evaluation of potential peptidic substrates in *in vitro* kinase reactions using the FPIA II. Data represent means \pm SEM (n=3).

Potential substrate	Extent assay window exploited [%] ^a	
	at 20 μ M peptide	at 200 μ M peptide
EFS_HUMAN_302	65.1 \pm 0.8	76.3 \pm 2.9
TRKA_HUMAN_482	No effect ^b	No effect ^b
INR1_HUMAN_548	No effect	No effect ^b
A002-D_747	54.3 \pm 3.3	63.8 \pm 2.5
Cdk1 ⁶⁻¹⁷	No effect ^b	No effect ^b
H-Cdk1 ¹⁻²⁴	No effect ^b	No effect ^b
Ac-Cdk1 ¹⁻²⁴	No effect ^b	No effect ^b

^a based on the dynamic assay range, calculated by controls without peptide and fully outcompeted controls containing 10 μ M TpY

^b mean effect < 10%

No relevant phosphorylations could be determined for the three Cdk1-derived peptides. Also with increased peptide concentration (200 μ M), no conversion was detected. In the case of the peptides derived from microarray studies, two out of four peptides were clearly modified at 20 μ M. For these two, the effect could even be enhanced by increasing the peptide concentration to 200 μ M. In control experiments without kinase, none of the seven peptides in concentrations up to 400 μ M affected the binding of the probe to the antibody. The peptides clearly phosphorylated by Myt1 were EFS_HUMAN_302 and A002-D_747 (for more information on these peptides refer to Table 12, p. 100).

For the putative Myt1 substrates, formation of the phosphorylated substrate peptides during kinase reaction was also qualitatively confirmed via ESI-MS (carried out by Dr. Schierhorn, Institute of Biochemistry and Biotechnology, MLU Halle-Wittenberg). Presence of both phospho-EFS_HUMAN_302 and phospho-A002-D_747 was proven in positive as well as negative ionization mode. Surprisingly, also for the other two peptides from the microarray approach, m/z values matching the respective phospho-peptides were found.

At least for TRKA_HUMAN_482, it can be assumed that a relevant formation of the pY676-containing peptide (equal to position 7 of the 13-meric peptide) would have been detected on a nanomolar scale, because the epitopes of the phospho-peptide is very closely related to the positive control used in displacement experiments during assay development (as seen in Fig. 39). The same applies to the Cdk1-derived peptides.

In contrast to EFS_HUMAN_302, the sequence of A002-D_747 contains two tyrosine residues quite close to each other. Based on the data gained so far, a certain determination of the exact position that was modified is not possible.

To solve the issues raised by the preliminary MS data and to doubtlessly identify the actual phosphorylation sites, MS-based fragmentation studies were conducted by Dr. C. Ihling from the working group of Prof. Sinz, Institute of Pharmacy, MLU Halle-Wittenberg.

Formation of both phospho-EFS_HUMAN_302 and phospho-A002-D_747 could be confirmed and, moreover, fragmentation proved the identity as tyrosine kinase reaction products as expected. For phospho-A002-D_747, the actual phosphorylation site could be resolved. The Tyr residue in position 7 of the peptide, equal to Tyr581 in the full-length protein, turned out to be modified.

Surprisingly, also for TRKA_HUMAN_482 and INR1_HUMAN_548, formation of the respective phospho-tyrosine containing products was confirmed. For these two peptides, however, also phosphorylation of serine residues was found. Mass spectra of relevant fragmented ionized phospho-peptides are given in the appendix (see p. 159).

Having in mind that these peptides were not recognized as tyrosine-phosphorylated in the FPIA II, there are different possibilities to explain these results. Since the conducted MS-studies did not lead to quantitative results, one might argue that the amount of pTyr-containing product is very low and, therefore, the displacement of the probe is not sufficient to enable an FP-change surmounting the normal background variation. Blocked access of the antibody to the epitope caused by the phospho-serine residues or the dramatical change of the peptide surface characteristics might be another explanation why the two phospho-peptides were not recognized in the FPIA II.

Myt1 is a dual-specific kinase that is generally characterized as a threonine and tyrosine modifying kinase. However, Myt1 is also known to modify serine residues, although this kind of posttranslational modification has only been described for Myt1 autophosphorylation so far [87].

The native Myt1 substrate contains both target sites next to each other. A substrate molecule that binds to Myt1 can therefore be modified at threonine, tyrosine or both. A sharp line between these three possibilities cannot be drawn. Whether the two general kinase activities (Ser/Thr kinase activity and Tyr kinase activity) can be separated is unknown. The present work focuses on tyrosine kinase substrates but the fact that Myt1 is also able to modify amino acids besides tyrosine has to be

emphasized. Further studies are required to elucidate Myt1 in terms of Ser/Thr kinase activity.

To validate the two identified Myt1 tyrosine substrates, the inhibition profile was examined. Since there is no selective Myt1 inhibitor available so far, specificity has to be gained from a combination of kinase inhibitors.

The Myt1 inhibitor analysis is based on the results of DAVIS et al. who set up inhibition profiles for > 80% of the human protein kinome [76]. It was found that, using dasatinib and CEP-701 (lestaurtinib) as inhibitors, only three tyrosine kinases showed the same inhibition profile as Myt1 (EPHA8, EPHB3 and ErbB2). Dasatinib inhibits Myt1, while the generally very promiscuous inhibitor CEP-701 should not affect the catalytic affinity of Myt1. Additionally, PD-173952, a pyrido [2,3-d] pyrimidine-based inhibitor closely related to PD-173955, should be used. This compound is approximately 10fold more potent toward Myt1 than dasatinib (K_i values 8 nM and 73 nM, respectively). Taking PD173952 into account, only two kinases should exhibit the same inhibition profile (EPHA8 and EPHB3). And only for Myt1, the inhibitory potency can be ordered as follows: PD173952 > dasatinib >> CEP-701.

Kinase reactions (200 μ M peptide, 400 μ M ATP) in the presence or absence of 5 μ M CEP-701, dasatinib or PD173952 were carried out with both EFS_HUMAN_302 and A002-D_747. Using these conditions, the assay window was exploited to an extent of approximately 64% (A002-D_747) and 76% (EFS_HUMAN_302), meaning that the assay was in its linear range and the change in fluorescence anisotropy should be directly proportional to product formation. Anisotropy values were converted into relative conversion using controls without substrate and conversion controls without inhibitor. The results are displayed in Fig. 40.

For both substrates, the conversion as seen in kinase reactions in the absence of inhibitor is dramatically decreased in presence of dasatinib. In presence of the even more potent inhibitor PD173952, the conversion drops down to baseline. The presence of CEP-701 does not considerably affect the conversion relative to conversion controls. Altogether, the results exactly match the inhibition profile as expected from the literature. So far, only Myt1 is known to show this inhibition profile.

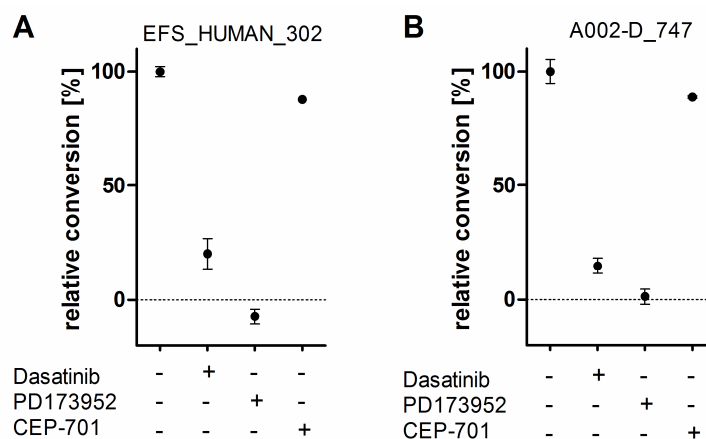


Fig. 40: Validation of substrates EFS_HUMAN_302 (A) and A002-D_747 (B) by inhibition profile. Values normalized against controls and displayed as means \pm SEM (n=3).

Wee1 (full-length) analytics by FPIA II failed due to high autophosphorylation activity, which narrowed the assay window in a way that did not allow substrate evaluation. Native Wee1 does not include tyrosine residues modified by phosphorylation. However, the GST-tag of the commercially obtained Wee1 includes 14 Tyr residues that are possibly modified during incubation.

To gain more insight into the substrate recognition process, the catalytic domains of both Wee1 and Myt1 (Myt1⁷⁵⁻³⁶², Wee1²⁵⁰⁻⁴⁶⁴) were tested with the seven peptidic substrates. The same conditions were used as in successful Myt1fl studies. Neither of the kinase domains mediated formation of phosphorylated peptide to a detectable extent. The commercially purchased kinase domain of Wee1 was also provided as fusion protein to GST. However, the assay window was not affected in any way compared to controls. The denial of the Myt1 kinase domain to mediate formation of phospho peptides might be explained by the findings of WELLS et al., who found the C-terminal domain of Myt1 (AA437-499) to be important for acceptance of protein substrates [90]. Possibly, this domain is also involved in the recognition of peptide substrates. However, the absence of a crystal structure of full-length Myt1 precludes further structural studies *in silico* and moves the answer to this question to future research.

The finding that Wee1 substrate recognition differs that strongly is somewhat surprising because many *in vitro* assays use the Wee1 single domain protein as tested here for activity-based screening assays (e.g. in [242]). Indeed, the Wee1 kinase domain exhibited ATP conversion independent from the presence or absence of Poly-AEKY substrate in a standard luciferase-based luminescence assay (data not shown). This issue emphasizes, once again, that data generated by

isolated domains instead of full-length proteins have to be evaluated carefully on a case-by-case basis.

Altogether, 2304 peptides (13-meric) derived from human phosphorylation sites [243] were utilized in kinase reactions via peptide microarray technology. 855 of these peptides contained potential phospho-tyrosine residues. The microarray experiments revealed 11 possible Myt1 substrates. Wee1 was revealed to have 21 possible substrates, having an overlap with potential Myt1 substrates of 4 peptides. Interestingly, the native phosphorylation site of both kinases, an N-terminal region of Cdk1, was identified as a substrate only for Wee1. This matches former reports [24] as well as data generated in this work (Section 5.1) wherein Wee1 but not Myt1 accepted peptidic substrates derived from this site (Cdk1⁸⁻²⁰).

Computer-driven approaches suggested that a lack of interaction N-terminal from the phosphorylation site might be responsible. To investigate this concept, peptides derived from an N-terminal shift of the peptide sequence (Cdk1⁶⁻¹⁷) as well as general prolongation with and without acetylation at the N-terminus (Cdk1¹⁻²⁴, Ac-Cdk1¹⁻²⁴) were tested. Additionally, to identify a peptidic Myt1 substrate, four peptides were chosen for solution phase verification and tested together with the Cdk1-derived peptides. For this purpose, an improved homogenous fluorescence polarization immunoassay was introduced which is broadly applicable to issues aiming at phospho-tyrosine modifications.

None of the Cdk1-derived peptides were phosphorylated by Myt1, leading to the conclusion that simply deducing a sequence from the native substrate, omitting the 3D structure of the protein, is not necessarily successful. Protein folding may lead to totally different surface characteristics compared to the isolated target site. However, other peptide sequences – though not associated with the native target protein – may mimic the native substrate and can, therefore, be efficiently phosphorylated. That is one of the reasons why peptide microarray technology helps learn about enzymes in general and kinases in particular.

Two substrates phosphorylated in the microarray experiments were not detected in a normal solution phase reaction. Various causes might be responsible for this discrepancy (*vide supra*) including general differences between the assays, such as effects of peptide immobilization on enzyme/antibody binding or other surface effects. The peptides EFS_HUMAN_302 and A002-D_747 could clearly be

verified as Myt1 substrates. Formation of the respective phosphorylation product was also confirmed via MS and also the exact phosphorylation site was identified by MS/MS studies. These substrates were validated by inhibition profiling using CEP-701 (lestaurtinib), dasatinib and PD173952. Based on data for 442 kinases, covering > 80% of the kinome [76], there is no tyrosine kinase but Myt1 showing an inhibition profile as observed here.

A common workflow in microarray experiments includes not only generation of a hit list, but also deduction of a consensus sequence based on the list of target peptides (e.g. [325]). Such a consensus sequence is often obtained by aligning the target peptides, or identification of substrate motifs (e.g. by WebLogos [326]).

Two of the four microarray derived peptides proved to be good substrates also in solution phase. Unfortunately, two peptides are not enough to deduce a valid consensus sequence. A verification of the other hit sequences from the microarray studies is necessary in order to allow for a meaningful alignment.

As analysis of the ensemble of hit sequences did not lead to meaningful results, the two identified peptidic tyrosine kinase substrates (Fig. 41B and C) were compared to the native phospho-site within the Cdk1 sequence (Fig. 41A).

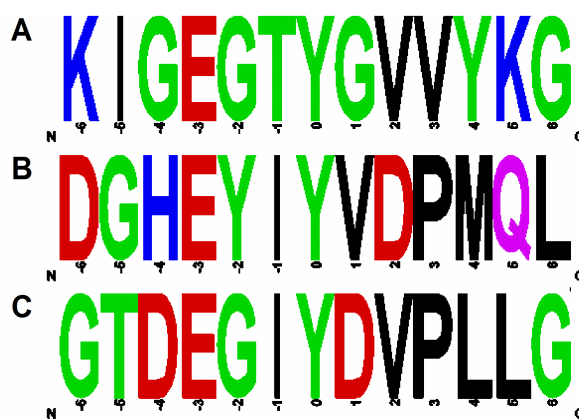


Fig. 41: Sequence comparison of a 13-meric peptide derived from Cdk1 (Cdk1⁹⁻²¹, A) with A002-D_747 (B) and EFS_HUMAN_302 (C). Colors denote the nature of the respective side chain: basic (blue), lipophilic (black), acidic (red), hydrophilic (green), primary amide structure (pink).

Importantly, only Tyr phosphorylations were investigated here. Both novel substrates share sequence features. The amino acid residues C-terminal to the actual phospho-site are quite lipophilic: Both share a Pro in position +3 and further hydrophobic positions in this region. Furthermore, a negative charge caused by Asp in position +1 or +2 is present in both substrates. In the N-terminal regions, all three peptides have a Glu in common (position -3). Taken together, the three peptides show quite similar characteristics: They are rather hydrophobic C-terminally, and have a negative charge N-terminally to the phospho Tyr.

However, the non-accepted Cdk1 substrates differ in a positively charged 'frame' around the phospho-site, having lysine residues in positions -6 and +5.

Lysine side chains are almost quantitatively protonated under physiological conditions ($pK_a = 10.8$ [327]), resulting in permanent positive charges around the Tyr-residue. For histidine, as in position -4 of A002-D_HUMAN_747, the side chain is protonated to less than 10% at pH 7.5 ($pK_a = 6$ [327]), leading to different surface characteristics compared to a Lys side chain. In the native whole protein, the phospho-site lies in the glycine-rich loop, a very flexible region of the protein. To allow for phosphorylation of Tyr, the positive charges are oriented away from Myt1: The regions N-terminal and C-terminal from Tyr15 form antiparallel β -sheets as observed for Cdk2 (PDB: 2DS1 and 1W8C, there is no available Cdk1 crystal structure, but Cdk2 offers 100% sequence identity in this region).

Therefore, the surface characteristics between protein (Cdk1) and protein-derived peptides (e.g. Cdk1⁸⁻²⁰) differ strongly, offering an explanation for the observed substrate acceptance. The required interactions may be mimicked by the identified peptide substrates, leading to formation of the respective phospho-product.

Of course, the identified peptides can be used to develop functional assays. Moreover, the proteins related to the substrate peptides identified on arrays are potential downstream targets of the profiled kinase [328]. Recently, a new cellular downstream target for Wee1 was discovered, vastly expanding its biological role [329]. Similarly, besides the assay development, the peptide studies presented herein may help to clarify cellular processes and further define the biological role of Myt1 and other proteins. For the two proteins that include the verified peptidic Myt1 target sequences, little is known about the role of respective phosphorylation sites. While A002-D is reported to modify its Tyr579 and Tyr581 residues by autophosphorylation [330-331], the kinase responsible for EFS modification at Tyr253 is unknown [317]. Future work has to resolve whether the results reported herein can be transferred to an actual cellular environment.

6. Summary and Perspectives

Even large pharmaceutical companies succeeded only in about 61% of their kinase screening projects, where success is defined as generation of enzyme, assay development and completion of the actual screening [332].

In the present work, the membrane-associated Myt1 kinase was generated based on a mammalian expression system. As a first step in assay development, substrate studies led to the conclusion that the approach of simply deducing a peptide from the cellular target sequence is not sufficient. Neither Thr, nor Tyr kinase activity evolved as monitored by immunoblotting experiments and fluorescence polarization immunoassays (FPIA). Myt1 revealed to be more restrictive in terms of substrate acceptance as compared to its most closely related Wee-kinase family member Wee1.

To overcome these problems, a TR-FRET based binding assay was established and, indeed, substantial contributions to the inhibition profile of this kinase were made. Interestingly, the approved drug dasatinib was found to be a highly affine Myt1 inhibitor while highly promiscuous compounds such as staurosporine did not affect Myt1. The inhibition data generated by the TR-FRET based binding assay provided a first training set which proved useful in the development of virtual screening protocols.

The identification of dasatinib led to the development of a fluorescence polarization based kinase binding assay for Myt1. However, the synthesized fluorescent probe, which was based on dasatinib, proved to be sensitive to detergents due to insertion phenomena. This problem might be generic to FP applications and was finally circumvented by using the isolated Myt1 kinase domain as expressed from *E. coli*. Since this protein lacks the membrane-association motif, the need for detergents above their CMC is eliminated. The results generated by this assay are in accordance with full-length data, confirming the kinase domain as an appropriate model protein for Myt1 in this assay.

Most of the compounds ever reported to inhibit Myt1 were tested and the derived inhibition constants help rank-order the inhibitors reliably, further facilitating computational approaches.

The assay showed excellent suitability to screening applications as indicated by Z' factors > 0.5 and it was used for the assessment of more than 150 compounds. The selection of compounds to be tested was mostly guided by virtual screening

suggestions, but also promising classes of potential inhibitors were investigated, such as flavonoids, glycotriazoles or available kinase inhibitors as a general contribution to the inhibition profile (e.g. lestaurtinib).

Additionally, a glycolycerolipid reported to inhibit Myt1 was thoroughly reassessed by binding studies with full-length Myt1, isolated kinase domain and functional investigations. These studies indicate that the aforesaid glycolycerolipid is not an inhibitor of Myt1.

Screening of compounds suggested by a QM/MM-GBSA virtual screening approach led, indeed, to the identification of three formerly unknown Myt1 inhibitors, remarkably expanding the number of available inhibitors. Although none of these compounds are specific toward Myt1, they will help to learn about the actual binding pocket and the key interactions required for high affinity. Driven by computational approaches, compound interactions with Phe240 or with the gatekeeper residue Thr187 appear to be promising starting points for the development of selective Myt1 inhibitors. The screening assays provided herein will act as invaluable tools for the identification of inhibitors in future research.

Taking up the idea of a peptidic Myt1 substrate again, the number of tested peptides for this purpose was vastly expanded by use of peptide microarray technology, a powerful means of kinase profiling. Wee1 and Myt1 were tested with hundreds of peptides, leading to a hit list of promising substrates. For Myt1, four peptides were tested in an improved FPIA aiming at phospho-tyrosines for solution phase verification, and two peptides were indeed phosphorylated in a dose-dependent manner. Formation of the respective phospho products was also confirmed via MS. The two identified peptides were further validated as Myt1 substrates using kinase inhibitors. Since no specific inhibitor is known so far, selectivity was gained from a combination of compounds and the resulting inhibition profile confirmed the peptides to be Myt1 substrates.

Future research can use these peptides not only for the development of a functional medium or high throughput assay, but also to derive substrate-site inhibitors or to identify new cellular downstream targets of Myt1. Identification of Histone 2B as a Wee1 target enormously expanded the understanding of this kinase [329]. As the biological role of Myt1 is not properly described yet, new targets in a cellular context may help elucidate its biological function.

Bibliography

1. Copeland, R.A., *Enzymes - a practical introduction to structure, mechanism and data analysis*. 1996, Weinheim: VCH Verlagsgesellschaft. pp. 1-10.
2. Manning, G., D.B. Whyte, R. Martinez, T. Hunter, and S. Sudarsanam, *The protein kinase complement of the human genome*. *Science*, 2002. 298(5600): pp. 1912-1934.
3. Nowell, P. and D. Hungerford, *A minute chromosome in human chronic granulocytic leukemia*. *Science*, 1960(132): p. 1497.
4. Nowell, P.C. and D.A. Hungerford, *Chromosome studies on normal and leukemic human leukocytes*. *J. Natl. Cancer Inst.*, 1960(85): pp. 85-109.
5. Rowley, J.D., *Ph1-positive leukaemia, including chronic myelogenous leukaemia*. *Clin. Haematol.*, 1980. 9(1): pp. 55-86.
6. Hantschel, O., U. Rix, and G. Superti-Furga, *Target spectrum of the BCR-ABL inhibitors imatinib, nilotinib and dasatinib*. *Leuk. Lymphoma*, 2008. 49(4): pp. 615-619.
7. Deininger, M., E. Buchdunger, and B.J. Druker, *The development of imatinib as a therapeutic agent for chronic myeloid leukemia*. *Blood*, 2005. 105(7): pp. 2640-2653.
8. Lugo, T.G., A.M. Pendergast, A.J. Muller, and O.N. Witte, *Tyrosine kinase activity and transformation potency of bcr-abl oncogene products*. *Science*, 1990. 247(4946): pp. 1079-1082.
9. Thiesing, J.T., S. Ohno-Jones, K.S. Kolibaba, and B.J. Druker, *Efficacy of STI571, an Abl tyrosine kinase inhibitor, in conjunction with other antileukemic agents against Bcr-Abl-positive cells*. *Blood*, 2000. 96(9): pp. 3195-3199.
10. Henderson, C.A., Jr., *Imatinib: The promise of a "magic bullet" for cancer fulfilled*. *J. Med. Assoc. Ga.*, 2003. 92(1): 12-4, 22.
11. Knight, Z.A. and K.M. Shokat, *Features of selective kinase inhibitors*. *Chem. Biol.*, 2005. 12(6): pp. 621-637.
12. Wang, Y., S.J. Decker, and J. Sebolt-Leopold, *Knockdown of Chk1, Wee1 and Myt1 by RNA interference abrogates G2 checkpoint and induces apoptosis*. *Cancer Biol. Ther.*, 2004. 3(3): pp. 305-313.
13. Kawabe, T., *G2 checkpoint abrogators as anticancer drugs*. *Mol. Cancer Ther.*, 2004. 3(4): pp. 513-519.
14. Saganuma, M., T. Kawabe, H. Hori, T. Funabiki, and T. Okamoto, *Sensitization of cancer cells to DNA damage-induced cell death by specific cell cycle G2 checkpoint abrogation*. *Cancer Res.*, 1999. 59(23): pp. 5887-5891.
15. Chow, J.P.H. and R.Y.C. Poon, *The CDK1 inhibitory kinase MYT1 in DNA damage checkpoint recovery*. *Oncogene*, 2013 32(40): pp. 4778-4788.
16. Hirai, H., Y. Iwasawa, M. Okada, T. Arai, T. Nishibata, M. Kobayashi, T. Kimura, N. Kaneko, J. Ohtani, K. Yamanaka, H. Itadani, I. Takahashi-Suzuki, K. Fukasawa, H. Oki, T. Nambu, J. Jiang, T. Sakai, H. Arakawa, T. Sakamoto, T. Sagara, T. Yoshizumi, S. Mizuarai, and H. Kotani, *Small-molecule inhibition of Wee1 kinase by MK-1775 selectively sensitizes p53-deficient tumor cells to DNA-damaging agents*. *Mol. Cancer Ther.*, 2009. 8(11): pp. 2992-3000.

17. ClinicalTrials.gov. *Clinical trials involving MK-1775 [8 studies listed]*. National Library of Medicine (US), Bethesda (MD) 29.02.2000 - today
Access date: 12.07.2013, available from:
<http://www.clinicaltrials.gov/ct2/results?term=mk-1775&Search=Search>.
18. Davies, K.D., P.L. Cable, J.E. Garrus, F.X. Sullivan, I. von Carlowitz, Y.L. Huerou, E. Wallace, R.D. Woessner, and S. Gross, *Chk1 inhibition and Wee1 inhibition combine synergistically to impede cellular proliferation*. *Cancer Biol. Ther.*, 2011. 12(9): pp. 788-796.
19. Ovejero-Benito, M. C. and J.M. Frade, *Brain-derived neurotrophic factor-dependent Cdk1 inhibition prevents G2/M progression in differentiating tetraploid neurons*. *PLoS ONE*, 2013. 5(6): e64890.
20. Hirai, H., T. Arai, M. Okada, T. Nishibata, M. Kobayashi, N. Sakai, K. Imagaki, J. Ohtani, T. Sakai, T. Yoshizumi, S. Mizuarai, Y. Iwasawa, and H. Kotani, *MK-1775, a small molecule Wee1 inhibitor, enhances antitumor efficacy of various DNA-damaging agents, including 5-fluorouracil*. *Cancer Biol. Ther.*, 2010. 9(7): pp. 514-522.
21. Krehling, J.M., J.Y. Gemmer, D. Reed, D. Letson, M. Bui, and S. Altiok, *MK1775, a selective Wee1 inhibitor, shows single-agent antitumor activity against sarcoma cells*. *Mol. Cancer Ther.*, 2012. 11(1): pp. 174-182.
22. Rajeshkumar, N.V., E. De Oliveira, N. Ottenhof, J. Watters, D. Brooks, T. Demuth, S.D. Shumway, S. Mizuarai, H. Hirai, A. Maitra, and M. Hidalgo, *MK-1775, a potent Wee1 inhibitor, synergizes with gemcitabine to achieve tumor regressions, selectively in p53-Deficient pancreatic cancer xenografts*. *Clin. Cancer Res.*, 2011. 17(9): pp. 2799-2806.
23. Fabian, M.A., W.H. Biggs, D.K. Treiber, C.E. Atteridge, M.D. Azimioara, M.G. Benedetti, T.A. Carter, P. Ciceri, P.T. Edeen, M. Floyd, J.M. Ford, M. Galvin, J.L. Gerlach, R.M. Grotzfeld, S. Herrgard, D.E. Insko, M.A. Insko, A.G. Lai, J.-M. Lelias, S.A. Mehta, Z.V. Milanov, A.M. Velasco, L.M. Wodicka, H.K. Patel, P.P. Zarrinkar, and D.J. Lockhart, *A small molecule-kinase interaction map for clinical kinase inhibitors*. *Nat. Biotech.*, 2005. 23(3): pp. 329-336.
24. Kristjánssdóttir, K. and J. Rudolph, *A fluorescence polarization assay for native protein substrates of kinases*. *Anal. Biochem.*, 2003. 316(1): pp. 41-49.
25. Brognard, J. and T. Hunter, *Protein kinase signaling networks in cancer*. *Curr. Opin. Genet. Dev.*, 2011. 21(1): pp. 4-11.
26. Domingo-Sananes, M.R., O. Kapuy, T. Hunt, and B. Novak, *Switches and latches: A biochemical tug-of-war between the kinases and phosphatases that control mitosis*. *Philos. T. R. Soc. B.*, 2011. 366(1584): pp. 3584-3594.
27. Lindqvist, A., V. Rodríguez-Bravo, and R.H. Medema, *The decision to enter mitosis: Feedback and redundancy in the mitotic entry network*. *J. Cell Biol.*, 2009. 185(2): pp. 193-202.
28. Pomerening, J.R., *Positive-feedback loops in cell cycle progression*. *FEBS Lett.*, 2009. 583(21): pp. 3388-3396.
29. Vulpetti, A. and R. Bosotti, *Sequence and structural analysis of kinase ATP pocket residues*. *Il Farmaco*, 2004. 59(10): pp. 759-765.

30. Traxler, P. and P. Furet, *Strategies toward the design of novel and selective protein tyrosine kinase inhibitors*. *Pharmacol. Ther.*, 1999. 82(2-3): pp. 195-206.
31. Krishnamurty, R. and D.J. Maly, *Biochemical mechanisms of resistance to small-molecule protein kinase inhibitors*. *ACS Chem. Biol.*, 2010. 5(1): pp. 121-138.
32. Madhusudan, P. Akamine, N.H. Xuong, and S.S. Taylor, *Crystal structure of a transition state mimic of the catalytic subunit of cAMP-dependent protein kinase*. *Nat. Struct. Biol.*, 2002. 9(4): pp. 273-277.
33. Johnson, L.N., M.E.M. Noble, and D.J. Owen, *Active and inactive protein kinases: Structural basis for regulation*. *Cell*, 1996. 85(2): pp. 149-158.
34. Morphy, R., *Selectively nonselective kinase inhibition: Striking the right balance*. *J. Med. Chem.*, 2010. 53(4): pp. 1413-1437.
35. Chapelat, J., F. Berst, A. L. Marzinzik, H. Moebitz, P. Drueckes, J. Trappe, D. Fabbro and D. Seebach, *The Substrate-Activity-Screening methodology applied to receptor tyrosine kinases: A proof-of-concept study*. *Eur. J. Med. Chem.*, 2012. 57: pp. 1-9.
36. Litman, P., O. Ohne, S. Ben-Yaakov, L. Shemesh-Darvish, T. Yechezkel, Y. Salitra, S. Rubnov, I. Cohen, H. Senderowitz, D. Kidron, O. Livnah, A. Levitzki, and N. Livnah, *A novel substrate mimetic inhibitor of PKB/Akt inhibits prostate cancer tumor growth in mice by blocking the PKB pathway*. *Biochemistry*, 2007. 46(16): pp. 4716-4724.
37. Blum, G., A. Gazit, and A. Levitzki, *Substrate competitive inhibitors of IGF-1 receptor kinase*. *Biochemistry*, 2000. 39(51): pp. 15705-15712.
38. Eglén, R.M. and T. Reisine, *Human kinome drug discovery and the emerging importance of atypical allosteric inhibitors*. *Expert. Opin. Drug. Discov.*, 2010. 5(3): pp. 277-290.
39. Bogoyevitch, M.A. and D.P. Fairlie, *A new paradigm for protein kinase inhibition: Blocking phosphorylation without directly targeting ATP binding*. *Drug. Discov. Today*, 2007. 12(15-16): pp. 622-633.
40. Liu, Y. and N.S. Gray, *Rational design of inhibitors that bind to inactive kinase conformations*. *Nat. Chem. Biol.*, 2007. 2(7): pp. 358-364.
41. Huse, M. and J. Kuriyan, *The conformational plasticity of protein kinases*. *Cell*, 2002. 109: pp. 275-282.
42. Liu, Y. and N.S. Gray, *Rational design of inhibitors that bind to inactive kinase conformations*. *Nat. Chem. Biol.*, 2006. 2(7): pp. 358-364.
43. Wood, E.R., A.T. Tuesdale, O.B. McDonald, D. Yan, A. Hassell, S.H. Dickerson, B. Ellis, C. Pennisi, E. Horne, K. Lackey, K.J. Alligood, D.W. Rusnak, T.M. Gilbmer, and L.A. Shewchuck, *unique structure for epidermal growth factor receptor bound to GW572016 (lapatinib): Relationships among protein conformation, inhibitor off-rate, and receptor activity in tumor cells*. *Cancer Res.*, 2004. 64: pp. 66452-66659.
44. Petrov, K.G., Y.M. Zhang, M. Carter, G.S. Cockerill, S. Dickerson, C.A. Gauthier, Y. Guo, R.A. Mook, D.W. Rusnak, A.L. Walker, E.R. Wood, and K.E. Lackey, *Optimization and SAR for dual ErbB-1/ErbB-2 tyrosine kinase inhibition in the 6-furanylquinazoline series*. *Bioorg. Med. Chem. Lett.*, 2006. 16: pp. 4686-4691.
45. Regan, J., C.A. Pargellis, P.F. Cirillo, T. Gilmore, E.R. Hickey, G.W. Peet, A. Proto, A. Swinamer, and N. Moss, *The kinetics of binding to p38MAP kinase by analogues of BIRB 796*. *Bioorg. Med. Chem. Lett.*, 2003. 13(18): pp. 3101-3104.

46. Pargellis, C., L. Tong, L. Churchill, P.F. Cirillo, T. Gilmore, A.G. Graham, P.M. Grob, E.R. Hickey, N. Moss, S. Pav, and J. Regan, *Inhibition of p38 MAP kinase by utilizing a novel allosteric binding site*. Nat. Struct. Biol., 2002. 9(4): pp. 268-272.
47. Getlik, M., C. Grutter, J.R. Simard, S. Kluter, M. Rabiller, H.B. Rode, A. Robubi, and D. Rauh, *Hybrid compound design to overcome the gatekeeper T338M mutation in cSrc*. J. Med. Chem., 2009. 52(13): pp. 3915-3926.
48. Zuccotto, F., E. Ardini, E. Casale, and M. Angiolini, *Through the "gatekeeper door": Exploiting the active kinase conformation*. J. Med. Chem., 2010. 53(7): pp. 2681-2694.
49. Scapin, G., S.B. Patel, J. Lisnock, J.W. Becker, and P.V. LoGrasso, *The structure of JNK3 in complex with small molecule inhibitors: Structural basis for potency and selectivity*. Chem. Biol., 2003. 10(8): pp. 705-712.
50. Tong, L., S. Pav, D.M. White, S. Rogers, K.M. Crane, C.L. Cywin, M.L. Brown, and C.A. Pargellis, *A highly specific inhibitor of human p38 MAP kinase binds in the ATP pocket*. Nat. Struct. Biol., 1997. 4(4): pp. 311-316.
51. Cuenda, A., J. Rouse, Y.N. Doza, R. Meier, P. Cohen, T.F. Gallagher, P.R. Young, and J.C. Lee, *SB 203580 is a specific inhibitor of a MAP kinase homologue which is stimulated by cellular stresses and interleukin-1*. FEBS Lett., 1995. 364(2): pp. 229-233.
52. Graczyk, P.P., *Gini Coefficient: A new way to express selectivity of kinase inhibitors against a family of kinases*. J. Med. Chem., 2007. 50(23): pp. 5773-5779.
53. Karaman, M.W., S. Herrgard, D.K. Treiber, P. Gallant, C.E. Atteridge, B.T. Campbell, K.W. Chan, P. Ciceri, M.I. Davis, P.T. Edeen, R. Faraoni, M. Floyd, J.P. Hunt, D.J. Lockhart, Z.V. Milanov, M.J. Morrison, G. Pallares, H.K. Patel, S. Pritchard, L.M. Wodicka, and P.P. Zarrinkar, *A quantitative analysis of kinase inhibitor selectivity*. Nat. Biotech., 2008. 26(1): pp. 127-132.
54. Smyth, L.A. and I. Collins, *Measuring and interpreting the selectivity of protein kinase inhibitors*. J. Chem. Biol., 2009. 2(3): pp. 131-51.
55. Klebl, B.M. and G. Müller, *Second-generation kinase inhibitors*. Expert. Opin. Ther. Targets, 2005. 9(5): pp. 975-993.
56. Zhang, X., A. Crespo, and A. Fernandez, *Turning promiscuous kinase inhibitors into safer drugs*. Trends Biotechnol., 2008. 26(6): pp. 295-301.
57. Hasinoff, B.B., D. Patel, and K.A. O'Hara, *Mechanisms of myocyte cytotoxicity induced by the multiple receptor tyrosine kinase inhibitor sunitinib*. Mol. Pharmacol., 2008. 74(6): pp. 1722-1728.
58. Andersen, C.B., Y. Wan, J.W. Chang, B. Riggs, C. Lee, Y. Liu, F. Sessa, F. Villa, N. Kwiatkowski, M. Suzuki, L. Nallan, R. Heald, A. Musacchio, and N.S. Gray, *Discovery of selective aminothiazole aurora kinase inhibitors*. ACS Chem. Biol., 2008. 3(3): pp. 180-192.
59. Aronov, A.M., B. McClain, C.S. Moody, and M.A. Murcko, *Kinase-likeness and kinase-privileged fragments: Toward virtual polypharmacology*. J. Med. Chem., 2008. 51(5): pp. 1214-1222.
60. Aronov, A.M. and G.W. Bemis, *A minimalist approach to fragment-based ligand design using common rings and linkers: Application to kinase inhibitors*. Proteins, 2004. 57(1): pp. 36-50.

61. Yang, Y., H. Chen, I. Nilsson, S. Muresan, and O. Engkvist, *Investigation of the relationship between topology and selectivity for druglike molecules*. *J. Med. Chem.*, 2010. 53(21): pp. 7709-7714.
62. Hughes, J.D., J. Blagg, D.A. Price, S. Bailey, G.A. DeCrescenzo, R.V. Devraj, E. Ellsworth, Y.M. Fobian, M.E. Gibbs, R.W. Gilles, N. Greene, E. Huang, T. Krieger-Burke, J. Loesel, T. Wager, L. Whiteley, and Y. Zhang, *Physicochemical drug properties associated with in vivo toxicological outcomes*. *Bioorg. Med. Chem. Lett.*, 2008. 18(17): pp. 4872-4875.
63. Huggins, D.J., W. Sherman, and B. Tidor, *Rational approaches to improving selectivity in drug design*. *J. Med. Chem.*, 2012. 55(4): pp. 1424-1444.
64. Wilson, K.P., P.G. McCaffrey, K. Hsiao, S. Pazhanisamy, V. Galullo, G.W. Bemis, M.J. Fitzgibbon, P.R. Caron, M.A. Murcko, and M.S. Su, *The structural basis for the specificity of pyridinylimidazole inhibitors of p38 MAP kinase*. *Chem. Biol.*, 1997. 4(6): pp. 423-431.
65. Iversen, L.F., H.S. Andersen, S. Branner, S.B. Mortensen, G.H. Peters, K. Norris, O.H. Olsen, C.B. Jeppesen, B.F. Lundt, W. Ripka, K.B. Moller, and N.P. Moller, *Structure-based design of a low molecular weight, nonphosphorus, nonpeptide, and highly selective inhibitor of protein-tyrosine phosphatase 1B*. *J. Biol. Chem.*, 2000. 275(14): pp. 10300-10307.
66. Scheffzek, K., W. Kliche, L. Wiesmuller, and J. Reinstein, *Crystal structure of the complex of UMP/CMP kinase from Dictyostelium discoideum and the bisubstrate inhibitor P1-(5'-adenosyl) P5-(5'-uridyl) pentaphosphate (UP5A) and Mg²⁺ at 2.2 Å: Implications for water-mediated specificity*. *Biochemistry*, 1996. 35(30): pp. 9716-9727.
67. Robinson, D.D., W. Sherman, and R. Farid, *Understanding kinase selectivity through energetic analysis of binding site waters*. *ChemMedChem*, 2010. 5(4): pp. 618-627.
68. Sadowsky, J.D., M.A. Burlingame, D.W. Wolan, C.L. McClendon, M.P. Jacobson, and J.A. Wells, *Turning a protein kinase on or off from a single allosteric site via disulfide trapping*. *Proc. Natl. Acad. Sci. U.S.A.*, 2011. 108: pp. 6056-6061.
69. Price, S., *Putative allosteric MEK1 and MEK2 inhibitors*. *Expert. Opin. Ther. Pat.*, 2008. 18(6): pp. 603-627.
70. Thaimattam, R., R. Banerjee, R. Miglani, and J. Iqbal, *Protein kinase inhibitors: Structural insights into selectivity*. *Curr. Pharm. Des.*, 2007. 13(27): pp. 2751-2765.
71. Fischer, P.M., *The design of drug candidate molecules as selective inhibitors of therapeutically relevant protein kinases*. *Curr. Med. Chem.*, 2004. 11(12): pp. 1563-1583.
72. Okram, B., A. Nagle, F.J. Adrian, C. Lee, P. Ren, X. Wang, T. Sim, Y. Xie, G. Xia, G. Spraggon, M. Warmuth, Y. Liu, and N.S. Gray, *A general strategy for creating "inactive-conformation" abl inhibitors*. *Chem. Biol.*, 2006. 13(7): pp. 779-786.
73. Kufareva, I. and R. Abagyan, *Type-II kinase inhibitor docking, screening, and profiling using modified structures of active kinase states*. *J. Med. Chem.*, 2008. 51(24): pp. 7921-7932.
74. Bamborough, P., D. Drewry, G. Harper, G.K. Smith, and K. Schneider, *Assessment of chemical coverage of kinome space and its implications for kinase drug discovery*. *J. Med. Chem.*, 2008. 51(24): pp. 7898-7914.

75. Pollard, J.R. and M. Mortimore, *Discovery and development of aurora kinase inhibitors as anticancer agents*. J. Med. Chem., 2009. 52(9): pp. 2629-2651.
76. Davis, M.I., J.P. Hunt, S. Herrgard, P. Ciceri, L.M. Wodicka, G. Pallares, M. Hocker, D.K. Treiber, and P.P. Zarrinkar, *Comprehensive analysis of kinase inhibitor selectivity*. Nat. Biotech., 2011. 29(11): pp. 1046-1051.
77. Noble, M.E.M., J.A. Endicott, and L.N. Johnson, *Protein kinase inhibitors: Insights into drug design from structure*. Science, 2004. 303(5665): pp. 1800-1805.
78. Gorre, M.E., M. Mohammed, K. Ellwood, N. Hsu, R. Paquette, P.N. Rao, and C.L. Sawyers, *Clinical resistance to STI-571 cancer therapy caused by BCR-ABL gene mutation or amplification*. Science, 2001. 293(5531): pp. 876-880.
79. Weisberg, E., P.W. Manley, W. Breitenstein, J. Bruggen, S.W. Cowan-Jacob, A. Ray, B. Huntly, D. Fabbro, G. Fendrich, E. Hall-Meyers, A.L. Kung, J. Mestan, G.Q. Daley, L. Callahan, L. Catley, C. Cavazza, M. Azam, D. Neuberg, R.D. Wright, D.G. Gilliland, and J.D. Griffin, *Characterization of AMN107, a selective inhibitor of native and mutant Bcr-Abl*. Cancer Cell, 2005. 7(2): pp. 129-141.
80. Kantarjian, H., F. Giles, L. Wunderle, K. Bhalla, S. O'Brien, B. Wassmann, C. Tanaka, P. Manley, P. Rae, W. Mietlowski, K. Bochinski, A. Hochhaus, J.D. Griffin, D. Hoelzer, M. Albitar, M. Dugan, J. Cortes, L. Alland, and O.G. Ottmann, *Nilotinib in imatinib-resistant CML and Philadelphia chromosome-positive ALL*. N. Engl. J. Med., 2006. 354(24): pp. 2542-2551.
81. Nakanishi, M., H. Ando, N. Watanabe, K. Kitamura, K. Ito, H. Okayama, T. Miyamoto, T. Agui, and M. Sasaki, *Identification and characterization of human Wee1B, a new member of the Wee1 family of Cdk-inhibitory kinases*. Genes Cells, 2000. 5(10): pp. 839-47.
82. McGowan, C.H. and P. Russell, *Human Wee1 kinase inhibits cell division by phosphorylating p34cdc2 exclusively on Tyr15*. EMBO J., 1993. 12(1): pp. 75-85.
83. Mueller, P.R., T.R. Coleman, A. Kumagai, and W.G. Dunphy, *Myt1: A membrane-associated inhibitory kinase that phosphorylates Cdc2 on both threonine-14 and tyrosine-15*. Science, 1995. 270(5233): pp. 86-90.
84. Robinson, D.R., Y.M. Wu, and S.F. Lin, *The protein tyrosine kinase family of the human genome*. Oncogene, 2000. 19(49): pp. 5548-5557.
85. Squire, C.J., J.M. Dickson, I. Ivanovic, and E.N. Baker, *Structure and inhibition of the human cell cycle checkpoint kinase, Wee1A kinase: An atypical tyrosine kinase with a key role in CDK1 regulation*. Structure, 2005. 13(4): pp. 541-550.
86. Altschul, S.F., T.L. Madden, A.A. Schaffer, J. Zhang, Z. Zhang, W. Miller, and D.J. Lipman, *Gapped BLAST and PSI-BLAST: A new generation of protein database search programs*. Nucleic Acids Res., 1997. 25(17): pp. 3389-3402.
87. Liu, F., J.J. Stanton, Z. Wu, and H. Piwnica-Worms, *The human Myt1 kinase preferentially phosphorylates Cdc2 on threonine 14 and localizes to the endoplasmic reticulum and Golgi complex*. Mol. Cell. Biol., 1997. 17(2): pp. 571-583.

88. Endicott, J.A., M.E. Noble, and J.A. Tucker, *Cyclin-dependent kinases: Inhibition and substrate recognition*. *Curr. Opin. Struct. Biol.*, 1999. 9(6): pp. 738-744.
89. Shen, M., P.T. Stukenberg, M.W. Kirschner, and K.P. Lu, *The essential mitotic peptidyl-prolyl isomerase Pin1 binds and regulates mitosis-specific phosphoproteins*. *Genes Dev.*, 1998. 12(5): pp. 706-720.
90. Wells, N.J., N. Watanabe, T. Tokusumi, W. Jiang, M.A. Verdecia, and T. Hunter, *The C-terminal domain of the Cdc2 inhibitory kinase Myt1 interacts with Cdc2 complexes and is required for inhibition of G(2)/M progression*. *J. Cell Sci.*, 1999. 112(19): pp. 3361-3371.
91. Villeneuve, J., M. Scarpa, M. Ortega-Bellido, and V. Malhotra, *MEK1 inactivates Myt1 to regulate Golgi membrane fragmentation and mitotic entry in mammalian cells*. *EMBO J.*, 2013. 9(32): pp. 72-85.
92. Nakajima, H., F. Toyoshima-Morimoto, E. Taniguchi, and E. Nishida, *Identification of a consensus motif for Plk (Polo-like kinase) phosphorylation reveals Myt1 as a Plk1 substrate*. *J. Biol. Chem.*, 2003. 278(28): pp. 25277-25280.
93. Burrows, F., H. Zhang, and A. Kamal, *Hsp90 activation and cell cycle regulation*. *Cell Cycle*, 2004. 3(12): pp. 1530-1536.
94. Schwock, J., N.-A. Pham, M. Cao, and D. Hedley, *Efficacy of Hsp90 inhibition for induction of apoptosis and inhibition of growth in cervical carcinoma cells in vitro and in vivo*. *Cancer Chemoth. Pharm.*, 2008. 61(4): pp. 669-681.
95. Okumura, E., T. Fukuhara, H. Yoshida, S. Hanada, R. Kozutsumi, M. Mori, K. Tachibana, and T. Kishimoto, *Akt inhibits Myt1 the signalling pathway that leads to meiotic G2/M-phase transitions*. *Nat. Cell. Biol.*, 2002. 4(2): pp. 111-116.
96. Bucher, N. and C.D. Britten, *G2 checkpoint abrogation and checkpoint kinase-1 targeting in the treatment of cancer*. *Brit. J. Cancer*, 2008. 98(3): pp. 523-528.
97. Roche, V.F., *Cancer and Chemotherapy*, in *Foye's Principles of Medicinal Chemistry*, T. Lemke, et al., Editors. 2008, Lippincott, Williams & Wilkins: Baltimore, MD, USA. pp. 1147-1192.
98. Hartwell, L.H. and T.A. Weinert, *Checkpoints: Controls that ensure the order of cell cycle events*. *Science*, 1989. 246(4930): pp. 629-634.
99. Kastan, M.B. and J. Bartek, *Cell-cycle checkpoints and cancer*. *Nature*, 2004. 432(7015): pp. 316-323.
100. Medema, R.H. and L. Macurek, *Checkpoint control and cancer*. *Oncogene*, 2012. 31(21): pp. 2601-2613.
101. Malumbres, M. and M. Barbacid, *Cell cycle, CDKs and cancer: A changing paradigm*. *Nat. Rev. Cancer*, 2009. 9(3): pp. 153-166.
102. Satyanarayana, A. and P. Kaldis, *Mammalian cell-cycle regulation: Several Cdks, numerous cyclins and diverse compensatory mechanisms*. *Oncogene*, 2009. 28(33): pp. 2925-2939.
103. Ubersax, J.A., E.L. Woodbury, P.N. Quang, M. Paraz, J.D. Blethrow, K. Shah, K.M. Shokat, and D.O. Morgan, *Targets of the cyclin-dependent kinase Cdk1*. *Nature*, 2003. 425(6960): pp. 859-864.
104. Ptacek, J., G. Devgan, G. Michaud, H. Zhu, X. Zhu, J. Fasolo, H. Guo, G. Jona, A. Breitkreutz, R. Sopko, R.R. McCartney, M.C. Schmidt, N. Rachidi, S.J. Lee, A.S. Mah, L. Meng, M.J. Stark, D.F. Stern, C. De Virgilio, M. Tyers, B. Andrews, M. Gerstein, B. Schweitzer, P.F. Predki,

- and M. Snyder, *Global analysis of protein phosphorylation in yeast*. Nature, 2005. 438(7068): pp. 679-684.
105. Fung, T.K. and R.Y.C. Poon, *A roller coaster ride with the mitotic cyclins*. Semin. Cell Dev. Biol., 2005. 16(3): pp. 335-342.
 106. Pines, J. and T. Hunter, *Human cyclins A and B1 are differentially located in the cell and undergo cell cycle-dependent nuclear transport*. J. Cell. Biol., 1991. 115(1): pp. 1-17.
 107. Gautier, J., C. Norbury, M. Lohka, P. Nurse, and J. Maller, *Purified maturation-promoting factor contains the product of a Xenopus homolog of the fission yeast cell cycle control gene cdc2+*. Cell, 1988. 54(3): pp. 433-439.
 108. Lohka, M.J., M.K. Hayes, and J.L. Maller, *Purification of maturation-promoting factor, an intracellular regulator of early mitotic events*. Proc. Natl. Acad. Sci. U.S.A., 1988. 85(9): pp. 3009-3013.
 109. Gautier, J., J. Minshull, M. Lohka, M. Glotzer, T. Hunt, and J.L. Maller, *Cyclin is a component of maturation-promoting factor from Xenopus*. Cell, 1990. 60(3): pp. 487-494.
 110. O'Farrell, P.H., *Triggering the all-or-nothing switch into mitosis*. Trends Cell Biol., 2001. 11(12): pp. 512-519.
 111. Booher, R.N., P.S. Holman, and A. Fattaey, *Human Myt1 is a cell cycle-regulated kinase that inhibits Cdc2 but not Cdk2 activity*. J. Biol. Chem., 1997. 272(35): pp. 22300-22306.
 112. Watanabe, N., H. Arai, Y. Nishihara, M. Taniguchi, T. Hunter, and H. Osada, *M-phase kinases induce phospho-dependent ubiquitination of somatic Wee1 by SCFbeta-TrCP*. Proc. Natl. Acad. Sci. U.S.A., 2004. 101(13): pp. 4419-4424.
 113. Elia, A.E., L.C. Cantley, and M.B. Yaffe, *Proteomic screen finds pSer/pThr-binding domain localizing Plk1 to mitotic substrates*. Science, 2003. 299(5610): pp. 1228-1231.
 114. Elia, A.E., P. Rellos, L.F. Haire, J.W. Chao, F.J. Ivins, K. Hoepker, D. Mohammad, L.C. Cantley, S.J. Smerdon, and M.B. Yaffe, *The molecular basis for phosphodependent substrate targeting and regulation of Plks by the Polo-box domain*. Cell, 2003. 115(1): pp. 83-95.
 115. Toyoshima-Morimoto, F., E. Taniguchi, N. Shinya, A. Iwamatsu, and E. Nishida, *Polo-like kinase 1 phosphorylates cyclin B1 and targets it to the nucleus during prophase*. Nature, 2001. 410(6825): pp. 215-220.
 116. Pomerening, J.R., J.A. Ubersax, and J.E. Ferrell, *Rapid cycling and precocious termination of G1 phase in cells expressing CDK1AF*. Mol. Biol. Cell, 2008. 19(8): pp. 3426-3441.
 117. Pomerening, J.R., *Uncovering mechanisms of bistability in biological systems*. Curr. Opin. Biotech., 2008. 19(4): pp. 381-388.
 118. Pomerening, J.R., E.D. Sontag, and J.E. Ferrell, *Building a cell cycle oscillator: Hysteresis and bistability in the activation of Cdc2*. Nat. Cell. Biol., 2003. 5(4): pp. 346-351.
 119. Lindqvist, A., W. van Zon, C. Karlsson Rosenthal, and R.M. Wolthuis, *Cyclin B1-Cdk1 activation continues after centrosome separation to control mitotic progression*. PLoS Biol., 2007. 5(5): pp. e123.
 120. Rodriguez-Bravo, V., S. Guaita-Esteruelas, N. Salvador, O. Bachs, and N. Agell, *Different S/M checkpoint responses of tumor and non tumor cell lines to DNA replication inhibition*. Cancer Res., 2007. 67(24): pp. 11648-11656.

121. Jackman, M., C. Lindon, E.A. Nigg, and J. Pines, *Active cyclin B1-Cdk1 first appears on centrosomes in prophase*. *Nat. Cell. Biol.*, 2003. 5(2): pp. 143-148.
122. Jackman, M., Y. Kubota, N. den Elzen, A. Hagting, and J. Pines, *Cyclin A- and cyclin E-Cdk complexes shuttle between the nucleus and the cytoplasm*. *Mol. Biol. Cell*, 2002. 13(3): pp. 1030-1045.
123. Mueller, P.R. and W.F. Leise, *Measurement of Wee Kinase Activity*, in *Methods in Molecular Biology: Cell Cycle Control*, T. Humphrey and G. Brooks, Editors. 2005, Humana Press. pp. 299-328.
124. Tassan, J.P., S.J. Schultz, J. Bartek, and E.A. Nigg, *Cell cycle analysis of the activity, subcellular localization, and subunit composition of human CAK (CDK-activating kinase)*. *J. Cell. Biol.*, 1994. 127(2): pp. 467-478.
125. Norbury, C., J. Blow, and P. Nurse, *Regulatory phosphorylation of the p34cdc2 protein kinase in vertebrates*. *EMBO J.*, 1991. 10(11): pp. 3321-3329.
126. Coulonval, K., H. Kooken, and P.P. Roger, *Coupling of T161 and T14 phosphorylations protects cyclin B-CDK1 from premature activation*. *Mol. Biol. Cell*, 2011. 22(21): pp. 3971-3985.
127. Gavet, O. and J. Pines, *Activation of cyclin B1-Cdk1 synchronizes events in the nucleus and the cytoplasm at mitosis*. *J. Cell. Biol.*, 2010. 189(2): pp. 247-259.
128. McGowan, C.H. and P. Russell, *Cell cycle regulation of human WEE1*. *EMBO J.*, 1995. 14(10): pp. 2166-2175.
129. Larochelle, S., K.A. Merrick, M.E. Terret, L. Wohlbold, N.M. Barboza, C. Zhang, K.M. Shokat, P.V. Jallepalli, and R.P. Fisher, *Requirements for Cdk7 in the assembly of Cdk1/cyclin B and activation of Cdk2 revealed by chemical genetics in human cells*. *Mol. Cell*, 2007. 25(6): pp. 839-850.
130. Kessler, K.J., M.L. Blinov, T.C. Elston, W.K. Kaufmann, and D.A. Simpson, *A predictive mathematical model of the DNA damage G2 checkpoint*. *J. Theor. Biol.*, 2013. 320(0): pp. 159-169.
131. Nakajima, H., S. Yonemura, M. Murata, N. Nakamura, H. Piwnicka-Worms, and E. Nishida, *Myt1 protein kinase is essential for Golgi and ER assembly during mitotic exit*. *J. Cell. Biol.*, 2008. 181(1): pp. 89-103.
132. Rabouille, C. and V. Kondylis, *Golgi ribbon unlinking: An organelle-based G2/M checkpoint*. *Cell Cycle*, 2007. 6(22): pp. 2723-2729.
133. Potapova, T.A., J.R. Daum, K.S. Byrd, and G.J. Gorbsky, *Fine tuning the cell cycle: Activation of the Cdk1 inhibitory phosphorylation pathway during mitotic exit*. *Mol. Biol. Cell*, 2009. 20(6): pp. 1737-1748.
134. Shorter, J. and G. Warren, *Golgi architecture and inheritance*. *Annu. Rev. Cell. Dev. Biol.*, 2002. 18: pp. 379-420.
135. Hidalgo Carcedo, C., M. Bonazzi, S. Spano, G. Turacchio, A. Colanzi, A. Luini, and D. Corda, *Mitotic Golgi partitioning is driven by the membrane-fissioning protein CtBP3/BARS*. *Science*, 2004. 305(5680): pp. 93-96.
136. Sutterlin, C., P. Hsu, A. Mallabiabarrena, and V. Malhotra, *Fragmentation and dispersal of the pericentriolar Golgi complex is required for entry into mitosis in mammalian cells*. *Cell*, 2002. 109(3): pp. 359-369.
137. Lippincott-Schwartz, J., T.H. Roberts, and K. Hirschberg, *Secretory protein trafficking and organelle dynamics in living cells*. *Annu. Rev. Cell. Dev. Biol.*, 2000. 16: pp. 557-589.

138. Voeltz, G.K., M.M. Rolls, and T.A. Rapoport, *Structural organization of the endoplasmic reticulum*. EMBO Rep., 2002. 3(10): pp. 944-950.
139. Shibata, Y., G.K. Voeltz, and T.A. Rapoport, *Rough sheets and smooth tubules*. Cell, 2006. 126(3): pp. 435-439.
140. Lowe, M., C. Rabouille, N. Nakamura, R. Watson, M. Jackman, E. Jamsa, D. Rahman, D.J. Pappin, and G. Warren, *Cdc2 kinase directly phosphorylates the cis-Golgi matrix protein GM130 and is required for Golgi fragmentation in mitosis*. Cell, 1998. 94(6): pp. 783-793.
141. Jin, P., S. Hardy, and D.O. Morgan, *Nuclear localization of cyclin B1 controls mitotic entry after DNA damage*. J. Cell. Biol., 1998. 141(4): pp. 875-885.
142. Glotzer, M., A.W. Murray, and M.W. Kirschner, *Cyclin is degraded by the ubiquitin pathway*. Nature, 1991. 349(6305): pp. 132-138.
143. Chow, J.P.H., R.Y.C. Poon, and H.T. Ma, *Inhibitory Phosphorylation of Cyclin-Dependent Kinase 1 as a Compensatory Mechanism for Mitosis Exit*. Mol. Cell. Biol., 2011. 31(7): pp. 1478-1491.
144. van Vugt, M.A., A. Bras, and R.H. Medema, *Polo-like kinase-1 controls recovery from a G2 DNA damage-induced arrest in mammalian cells*. Mol. Cell, 2004. 15(5): pp. 799-811.
145. Nakajo, N., S. Yoshitome, J. Iwashita, M. Iida, K. Uto, S. Ueno, K. Okamoto, and N. Sagata, *Absence of Wee1 ensures the meiotic cell cycle in Xenopus oocytes*. Genes Dev., 2000. 14(3): pp. 328-338.
146. Jin, Z., E.M. Homola, P. Goldbach, Y. Choi, J.A. Brill, and S.D. Campbell, *Drosophila Myt1 is a Cdk1 inhibitory kinase that regulates multiple aspects of cell cycle behavior during gametogenesis*. Development, 2005. 132(18): pp. 4075-4085.
147. Burrows, A.E., B.K. Scurman, M.E. Kosinski, C.T. Richie, P.L. Sadler, J.M. Schumacher, and A. Golden, *The C. elegans Myt1 ortholog is required for the proper timing of oocyte maturation*. Development, 2006. 133(4): pp. 697-709.
148. Levine, A.J., *p53, the cellular gatekeeper for growth and division*. Cell, 1997. 88(3): pp. 323-331.
149. Dixon, H. and C.J. Norbury, *Therapeutic exploitation of checkpoint defects in cancer cells lacking p53 function*. Cell Cycle, 2002. 1(6): pp. 362-368.
150. Zhou, B.B. and J. Bartek, *Targeting the checkpoint kinases: Chemosensitization versus chemoprotection*. Nat. Rev. Cancer, 2004. 4(3): pp. 216-225.
151. Wang, Y., J. Li, R.N. Booher, A. Kraker, T. Lawrence, W.R. Leopold, and Y. Sun, *Radiosensitization of p53 mutant cells by PD0166285, a novel G2 checkpoint abrogator*. Cancer Res., 2001. 61(22): pp. 8211-8217.
152. Mante, S. and K.P. Minneman, *Caffeine inhibits forskolin-stimulated cyclic AMP accumulation in rat brain*. Eur. J. Pharmacol., 1990. 175(2): pp. 203-205.
153. Cortez, D., *Caffeine inhibits checkpoint responses without inhibiting the ataxia-telangiectasia-mutated (ATM) and ATM- and Rad3-related (ATR) protein kinases*. J. Biol. Chem., 2003. 278(39): pp. 37139-37145.
154. Vogelstein, B., D. Lane, and A.J. Levine, *Surfing the p53 network*. Nature, 2000. 408(6810): pp. 307-310.

155. Castedo, M., J.L. Perfettini, T. Roumier, K. Andreau, R. Medema, and G. Kroemer, *Cell death by mitotic catastrophe: A molecular definition*. *Oncogene*, 2004. 23(16): pp. 2825-2837.
156. Castedo, M., J.L. Perfettini, T. Roumier, K. Yakushijin, D. Horne, R. Medema, and G. Kroemer, *The cell cycle checkpoint kinase Chk2 is a negative regulator of mitotic catastrophe*. *Oncogene*, 2004. 23(25): pp. 4353-4361.
157. Blagosklonny, M.V., *Mitotic arrest and cell fate: Why and how mitotic inhibition of transcription drives mutually exclusive events*. *Cell Cycle*, 2007. 6(1): pp. 70-74.
158. Roninson, I.B., E.V. Broude, and B.D. Chang, *If not apoptosis, then what? Treatment-induced senescence and mitotic catastrophe in tumor cells*. *Drug Resist. Update*, 2001. 4(5): pp. 303-313.
159. De Witt Hamer, P.C., S.E. Mir, D. Noske, C.J.F. Van Noorden, and T. Würdinger, *WEE1 kinase targeting combined with DNA-damaging cancer therapy catalyzes mitotic catastrophe*. *Clin. Cancer Res.*, 2011. 17(13): pp. 4200-4207.
160. Jin, P., Y. Gu, and D.O. Morgan, *Role of inhibitory CDC2 phosphorylation in radiation-induced G2 arrest in human cells*. *J. Cell. Biol.*, 1996. 134(4): pp. 963-970.
161. Ashwell, S., *Checkpoint kinase and Wee1 inhibition as anticancer therapeutics*, in *DNA repair in cancer therapy*, M.R. Kelley, Editor, Elsevier: Amsterdam. pp. 211-234.
162. Tse, A.N., T.N. Sheikh, H. Alan, T.C. Chou, and G.K. Schwartz, *90-kDa heat shock protein inhibition abrogates the topoisomerase I poison-induced G2/M checkpoint in p53-null tumor cells by depleting Chk1 and Wee1*. *Mol. Pharmacol.*, 2009. 75(1): pp. 124-133.
163. Mizuarai, S., K. Yamanaka, H. Itadani, T. Arai, T. Nishibata, H. Hirai, and H. Kotani, *Discovery of gene expression-based pharmacodynamic biomarker for a p53 context-specific anti-tumor drug Wee1 inhibitor*. *Mol. Cancer*, 2009. 8: 34.
164. Wong, K., R.S. Cheng, and S.C. Mok, *Identification of differentially expressed genes from ovarian cancer cells by MICROMAX™ cDNA microarray system*. *BioTechniques*, 2001(30): pp. 670-675.
165. Seidl, C., M. Port, K.-P. Gilbertz, A. Morgenstern, F. Bruchertseifer, M. Schwaiger, B. Röper, R. Senekowitsch-Schmidtke, and M. Abend, *213Bi-induced death of HSC45-M2 gastric cancer cells is characterized by G2 arrest and up-regulation of genes known to prevent apoptosis but induce necrosis and mitotic catastrophe*. *Mol. Cancer Ther.*, 2007. 6(8): pp. 2346-2359.
166. Tibes, R., J.M. Bogenberger, L. Chaudhuri, R.T. Hagelstrom, D. Chow, M.E. Buechel, I.M. Gonzales, T. Demuth, J. Slack, R.A. Mesa, E. Braggio, H.H. Yin, S. Arora, and D.O. Azorsa, *RNAi screening of the kinome with cytarabine in leukemias*. *Blood*, 2012. 119: pp. 2863-2872.
167. Sams-Dodd, F., *Target-based drug discovery: Is something wrong?* *Drug Discov. Today*, 2005. 10(2): pp. 139-147.
168. Mander, T., *Beyond uHTS: ridiculously HTS?* *Drug Discov. Today*, 2000. 5(6): pp. 223-225.
169. Lahana, R., *How many leads from HTS?* *Drug Discov. Today*, 1999. 4(10): pp. 447-448.

170. Lengauer, T., C. Lemmen, M. Rarey, and M. Zimmermann, *Novel technologies for virtual screening*. Drug Discov. Today, 2004. 9(1): pp. 27-34.
171. Valler, M.J. and D. Green, *Diversity screening versus focussed screening in drug discovery*. Drug Discov. Today, 2000. 5(7): pp. 286-293.
172. Hüser, J., *High Throughput-Screening in Drug Discovery*. Methods and Principles in Medicinal Chemistry. Vol. 35. 2006: Wiley VCH. p. 17.
173. Xie, X.Q., *Molecular Modeling and In Silico Drug Design*, in *Foye's Principles of Medicinal Chemistry*, T. Lemke, et al., Editors. 2008, Lippincott, Williams & Wilkins: Baltimore, MD, USA. pp. 54-98.
174. Sheridan, R.P., A. Rusinko, 3rd, R. Nilakantan, and R. Venkataraghavan, *Searching for pharmacophores in large coordinate data bases and its use in drug design*. Proc. Natl. Acad. Sci. U.S.A., 1989. 86(20): pp. 8165-8169.
175. Hopfinger, A.J., A. Reaka, P. Venkatarangan, J.S. Duca, and S. Wang, *Construction of a virtual high throughput screen by 4D-QSAR analysis: Application to a combinatorial library of glucose inhibitors of glycogen phosphorylase b*. J. Chem. Inf. Comput. Sci., 1999. 39(6): pp. 1151-1160.
176. Wolber, G. and T. Langer, *LigandScout: 3-D pharmacophores derived from protein-bound ligands and their use as virtual screening filters*. J. Chem. Inf. Model., 2005. 45(1): pp. 160-169.
177. Schapira, M., R. Abagyan, and M. Totrov, *Nuclear hormone receptor targeted virtual screening*. J. Med. Chem., 2003. 46(14): pp. 3045-3059.
178. Schapira, M., B. Raaka, H. Samuels, and R. Abagyan, *In silico discovery of novel Retinoic Acid Receptor agonist structures*. BMC Struct. Biol., 2001. 1(1): 1.
179. Gruneberg, S., B. Wendt, and G. Klebe, *Subnanomolar inhibitors from computer screening: A model study using human carbonic anhydrase II*. Angew. Chem. Int. Ed. Engl., 2001. 40(2): pp. 389-393.
180. Kitchen, D.B., H. Decornez, J.R. Furr, and J. Bajorath, *Docking and scoring in virtual screening for drug discovery: Methods and applications*. Nat. Rev. Drug Discov., 2004. 3(11): pp. 935-949.
181. Bissantz, C., G. Folkers, and D. Rognan, *Protein-based virtual screening of chemical databases. 1. Evaluation of different docking/scoring combinations*. J. Med. Chem., 2000. 43(25): pp. 4759-4767.
182. Humblet, C. and J.B. Dunbar Jr, *Chapter 29. 3D Database Searching and Docking Strategies*, in *Annual Reports in Medicinal Chemistry*, A.B. James, Editor. 1993, Academic Press. pp. 275-284.
183. Jones, G., P. Willett, R.C. Glen, A.R. Leach, and R. Taylor, *Development and validation of a genetic algorithm for flexible docking*. J. Mol. Biol., 1997. 267(3): pp. 727-748.
184. Kuntz, I.D., J.M. Blaney, S.J. Oatley, R. Langridge, and T.E. Ferrin, *A geometric approach to macromolecule-ligand interactions*. J. Mol. Biol., 1982. 161(2): pp. 269-288.
185. Friesner, R.A., J.L. Banks, R.B. Murphy, T.A. Halgren, J.J. Klicic, D.T. Mainz, M.P. Repasky, E.H. Knoll, M. Shelley, J.K. Perry, D.E. Shaw, P. Francis, and P.S. Shenkin, *Glide: A new approach for rapid, accurate docking and scoring. 1. Method and assessment of docking accuracy*. J. Med. Chem., 2004. 47(7): pp. 1739-1749.

186. Hölftje, H.-D., W. Sippl, D. Rognan, and G. Folkers, *Molecular Modeling - Basic Principles and Applications*. 2nd Edition. 2003, Weinheim: Wiley VCH. p. 146.
187. Lipinski, C.A., F. Lombardo, B.W. Dominy, and P.J. Feeney, *Experimental and computational approaches to estimate solubility and permeability in drug discovery and development settings*. *Adv. Drug Deliv. Rev.*, 2001. 46(1-3): pp. 3-26.
188. Oprea, T.I., *Property distribution of drug-related chemical databases*. *J. Comput. Aided Mol. Des.*, 2000. 14(3): pp. 251-264.
189. Hölftje, H.-D., W. Sippl, D. Rognan, and G. Folkers, *Molecular Modeling - Basic Principles and Applications*. 2nd Edition. 2003, Weinheim: Wiley VCH. p. 147.
190. Hüser, J., E. Lohrmann, B. Kalthof, N. Burkhardt, U. Brüggemeier, and M. Bechem, *High Throughput-Screening for targeted Lead Discovery*, in *Methods and Principles in Medicinal Chemistry: High Throughput-Screening in Drug Discovery*, J. Hüser, Editor. 2006, Wiley VCH. pp. 15-36.
191. Copeland, R.A., *Hit Validation and Progression*, in *Evaluation of Enzyme Inhibitors in Drug Discovery*. 2005, Wiley: Hoboken, NJ, USA. pp. 105-110.
192. Knowles, J. and G. Gromo, *A guide to drug discovery: Target selection in drug discovery*. *Nat. Rev. Drug Discov.*, 2003. 2(1): pp. 63-69.
193. Vane, J.R., *The history of inhibitors of angiotensin converting enzyme*. *J. Physiol. Pharmacol.*, 1999. 50(4): pp. 489-498.
194. Caporale, L.H., *Chemical ecology: A view from the pharmaceutical industry*. *Proc. Natl. Acad. Sci. U.S.A.*, 1995. 92(1): pp. 75-82.
195. Zhang, J.H., T.D. Chung, and K.R. Oldenburg, *A simple statistical parameter for use in evaluation and validation of high throughput screening assays*. *J. Biomol. Screen.*, 1999. 4(2): pp. 67-73.
196. Shoichet, B.K., *Interpreting steep dose-response curves in early inhibitor discovery*. *J. Med. Chem.*, 2006. 49(25): pp. 7274-7277.
197. Zhou, B.-N., S. Tang, R.K. Johnson, M.P. Mattern, J.S. Lazo, E.R. Sharlow, K. Harichd, and D.G.I. Kingston, *New glycolipid inhibitors of Myt1 kinase*. *Tetrahedron*, 2005. 61: pp. 883-887.
198. Chaikuad, A., J. Eswaran, O. Fedorov, C. Cooper, T. Kroeler, M. Vollmar, T. Krojer, G. Berridge, J.R.C. Muniz, A.C.W. Pike, F. von Delft, J. Weigelt, C.H. Arrowsmith, A.M. Edwards, C. Bountra, and S. Knapp. *Human protein kinase Myt1*. 30.09.2010, available from: http://www.thesgc.org/structures/structure_description/3P1A/.
199. Sauer, B., *Etablierung einer neuen Klasse ATP-kompetitiver Hemmstoffe der PKMYT1*, Diploma Thesis, Institute of Pharmacy (2011), Martin-Luther-University Halle-Wittenberg. 53 pages.
200. Göllner, C., *Neosynthese und Derivatisierung mariner Glycoglycerolipide als potentielle Inhibitoren der Myt1 Kinase*, Doctoral Thesis, Institute of Pharmacy (2012), Martin-Luther-University Halle Wittenberg. 132 pages.
201. Al-Mazaideh, G.M.A., *Development and Synthesis of New Potential ATP-Competitive Myt1 Kinase Inhibitors*, Doctoral Thesis, Institute of Pharmacy (2012), Martin-Luther University Halle-Wittenberg. 125 pages.
202. Bembenek, M.E., R. Roy, P. Li, L. Chee, S. Jain, and T. Parsons, *A homogeneous scintillation proximity format for monitoring the activity of*

- recombinant human long-chain-fatty-acyl-CoA synthetase 5*. *Assay Drug Dev. Technol.*, 2004. 2(3): pp. 300-307.
203. Vickers, C., P. Hales, V. Kaushik, L. Dick, J. Gavin, J. Tang, K. Godbout, T. Parsons, E. Baronas, F. Hsieh, S. Acton, M. Patane, A. Nichols, and P. Tummino, *Hydrolysis of biological peptides by human angiotensin-converting enzyme-related carboxypeptidase*. *J. Biol. Chem.*, 2002. 277(17): pp. 14838-14843.
204. Schmitz, S., *Zellbiologische und Routinemethoden*, in *Experimentator: Zellkultur*. 2011, Spektrum Akademischer Verlag: München. pp. 206-208.
205. Zuhorn, I.S., J.B. Engberts, and D. Hoekstra, *Gene delivery by cationic lipid vectors: Overcoming cellular barriers*. *Eur. Biophys. J.*, 2007. 36(4-5): pp. 349-362.
206. Miller, A.D., *Cationic Liposomes for Gene Therapy*. *Angew. Chem. Int. Ed. Engl.*, 1998. 37(13-14): pp. 1768-1785.
207. Chaikuad, A., J. Eswaran, O. Fedorov, C. Cooper, T. Kroeler, M. Vollmar, T. Krojer, G. Berridge, J.R.C. Muniz, A.C.W. Pike, F. von Delft, J. Weigelt, C.H. Arrowsmith, A.M. Edwards, C. Bountra, and S. Knapp. *Human protein kinase Myt1* (DOI: 10.2210/pdb3p1a/pdb). 30.09.2010, Materials and Methods available from: http://www.thesgc.org/structures/structure_description/3P1A/.
208. Dean, R.B. and W.J. Dixon, *Simplified statistics for small numbers of observations*. *Anal. Chem.*, 1951. 23: pp. 636-638.
209. Grubbs, F.E. and G. Beck, *Extension of sample sizes and percentage points for significance tests of outlying observations*. *Technometrics*, 1972. 14(4): pp. 847-854.
210. Iversen, P.W., B.J. Eastwood, G.S. Sittampalam, and K.L. Cox, *A comparison of assay performance measures in screening assays: Signal window, Z' factor, and assay variability ratio*. *J. Biomol. Screen.*, 2006. 11(3): pp. 247-252.
211. Bradford, M.M., *A rapid and sensitive method for the quantitation of microgram quantities of protein utilizing the principle of protein-dye binding*. *Anal. Biochem.*, 1976. 72: pp. 248-254.
212. Smith, P.K., R.I. Krohn, G.T. Hermanson, A.K. Mallia, F.H. Gartner, M.D. Provenzano, E.K. Fujimoto, N.M. Goeke, B.J. Olson, and D.C. Klenk, *Measurement of protein using bicinchoninic acid*. *Anal. Biochem.*, 1985. 150(1): pp. 76-85.
213. Edelhoch, H., *Spectroscopic Determination of tryptophan and tyrosine in proteins*. *Biochemistry*, 1967. 6(7): pp. 1948-1954.
214. Mach, H., C.R. Middaugh, and R.V. Lewis, *Statistical determination of the average values of the extinction coefficients of tryptophan and tyrosine in native proteins*. *Anal. Biochem.*, 1992. 200(1): pp. 74-80.
215. Gill, S.C. and P.H. von Hippel, *Calculation of protein extinction coefficients from amino acid sequence data*. *Anal. Biochem.*, 1989. 182(2): pp. 319-326.
216. Starcher, B., *A ninhydrin-based assay to quantitate the total protein content of tissue samples*. *Anal. Biochem.*, 2001. 292(1): pp. 125-129.
217. Bäßler, C., *Etablierung der humanen Myt1 Kinase als Zielstruktur moderner Arzneistoffentwicklung: Beiträge zu Expression und Assayentwicklung*, Doctoral Thesis, Institute of Pharmacy (2011), Martin-Luther-Universität Halle-Wittenberg. 180 pages.

218. Laemmli, U.K., *Cleavage of structural proteins during the assembly of the head of bacteriophage T4*. *Nature*, 1970(277): pp. 680-685.
219. Blake, M.S., K.H. Johnston, G.J. Russell-Jones, and E.C. Gotschlich, *A rapid, sensitive method for detection of alkaline phosphatase-conjugated anti-antibody on Western blots*. *Anal. Biochem.*, 1984. 136(1): pp. 175-179.
220. Jameson, D.M. and J.A. Ross, *Fluorescence Polarisation/Anisotropy in Diagnostics and Imaging*. *Chem. Rev.*, 2010(110): pp. 2685-2708.
221. Li, Y., W. Xie, and G. Fang, *Fluorescence detection techniques for protein kinase assay*. *Anal. Bioanal. Chem.*, 2008. 390(8): pp. 2049-2057.
222. Perrin, F., *Polarisation de la lumière de fluorescence. Vie moyenne des molécules dans l'état excité*. *J. Phys. Radium*, 1926. 7(12): pp. 390-401.
223. Wu, G., *Assay Development: Fundamentals and Practices*. 2010: John Wiley & Sons, Inc., Hoboken, New Jersey, USA. p. 182.
224. Lakowicz, J.R., *Principles of Fluorescence Spectroscopy*. 3rd Ed. 2006, Heidelberg: Springer. Chapter 10.4.6 (p. 364).
225. Soleillet, P., *Sur les paramètres caractérisant la polarisation partielle de la lumière dans les phénomènes de fluorescence*. *Ann. Phys. Biol. Med.*, 1929. 12: pp. 23-97.
226. Mhaske, D.V. and S.R. Dhaneshwar, *Stability indicating HPTLC and LC determination of dasatinib in pharmaceutical dosage form*. *Chromatographia*, 2007. 66(1-2): pp. 95-102.
227. Isaacs, R.C.A., M.G. Solinsky, K.J. Cutrona, C.L. Newton, A.M. Naylor-Olsen, J.A. Krueger, S.D. Lewis, and B.J. Lucas, *Structure-based design of novel groups for use in the P1 position of thrombin inhibitor scaffolds. Part I: Weakly basic azoles*. *Bioorg. Med. Chem. Lett.*, 2006. 16(2): pp. 338-342.
228. Isaacs, R.C.A., A.M. Naylor-Olsen, B.D. Dorsey, and C.L. Newton, *Thrombin inhibitors*, in *PCT Intl. Appl.* 1998. pp. 56/58.
229. Lee, W.S., C.-N. Im, Q.Y. Teng, Y.-T. Chang, D.-C. Kim, K.-T. Kim, and S.-K. Chung, *Synthesis and cellular uptake properties of guanidine-containing molecular transporters built on the sucrose scaffold*. *Mol. BioSystems*, 2009. 5(8): pp. 822-825.
230. Rosenthal, K.S. and F. Koussaie, *Critical micelle concentration determination of nonionic detergents with Coomassie Brilliant Blue G-250*. *Anal. Chem.*, 1983. 55(7): pp. 1115-1117.
231. Chattopadhyay, A. and E. London, *Fluorimetric determination of critical micelle concentration avoiding interference from detergent charge*. *Anal. Biochem.*, 1984. 139(2): pp. 408-412.
232. Zhang, R., T. Mayhood, P. Lipari, Y. Wang, J. Durkin, R. Syto, J. Gesell, C. McNemar, and W. Windsor, *Fluorescence polarization assay and inhibitor design for MDM2/p53 interaction*. *Anal. Biochem.*, 2004. 331(1): pp. 138-146.
233. Wang, Z.-X., *An exact mathematical expression for describing competitive binding of two different ligands to a protein molecule*. *FEBS Lett.*, 1995. 360(2): pp. 111-114.
234. Ngo, Y., R. Advani, D. Valentini, S. Gaseitsiwe, S. Mahdaviifar, M. Maeurer, and M. Reilly, *Identification and testing of control peptides for antigen microarrays*. *J. Immunol. Methods*, 2009. 343(2): pp. 68-78.

235. Coin, I., M. Beyermann, and M. Bienert, *Solid-phase peptide synthesis: From standard procedures to the synthesis of difficult sequences*. Nat. Protoc., 2007. 2(12): pp. 3247-3256.
236. Rohe, A., *Untersuchungen zur humanen Myt1 Kinase - Assayentwicklung und Enzympräparation*, Diploma Thesis, Institute of Pharmacy (2011), Martin-Luther-University Halle-Wittenberg. 62 pages.
237. Manning, B.D. and L.C. Cantley, *Hitting the target: Emerging technologies in the search for kinase substrates*. Sci. STKE, 2002(162): pe49.
238. Dandliker, W.B. and G.A. Feigen, *Quantification of the antigen-antibody reaction by the polarization of fluorescence*. Biochem. Biophys. Res. Commun., 1961. 5: pp. 299-304.
239. Seethala, R. and R. Menzel, *A homogeneous, fluorescence polarization assay for src-family tyrosine kinases*. Anal. Biochem., 1997. 253(2): pp. 210-218.
240. Seethala, R. and R. Menzel, *A fluorescence polarization competition immunoassay for tyrosine kinases*. Anal. Biochem., 1998. 255(2): pp. 257-262.
241. Zick, Y., G. Grunberger, R.W. Reesjones, and R.J. Comi, *Use of tyrosine-containing polymers to characterize the substrate-specificity of insulin and other hormone-stimulated tyrosine kinases*. Eur. J. Biochem., 1985. 148(1): pp. 177-182.
242. Bruyère, C., S. Madonna, G.V. Goietsenoven, V. Mathieu, J. Dessolin, J.-L. Kraus, F. Lefranc, and R. Kiss, *JLK1486, a Bis 8-hydroxyquinoline-substituted benzylamine, displays cytostatic effects in experimental gliomas through Myt1 and STAT1 activation and, to a lesser extent, PPAR γ activation*. Transl. Onc., 2011. 4(3): pp. 126-137.
243. Panse, S., L. Dong, A. Burian, R. Carus, M. Schutkowski, U. Reimer, and J. Schneider-Mergener, *Profiling of generic anti-phosphopeptide antibodies and kinases with peptide microarrays using radioactive and fluorescence-based assays*. Mol. Divers., 2004. 8(3): pp. 291-299.
244. Liu, F., C. Rothblum-Oviatt, C.E. Ryan, and H. Piwnicka-Worms, *Overproduction of human Myt1 kinase induces a G2 cell cycle delay by interfering with the intracellular trafficking of Cdc2-cyclin B1 complexes*. Mol. Cell. Biol., 1999. 19(7): pp. 5113-5123.
245. Chemical Computing Group, Inc., *MOE2010.10*. 2010: Montreal, Canada.
246. Rohe, A., F. Erdmann, C. Bäßler, K. Wichapong, W. Sippl, and M. Schmidt, *In vitro and in silico studies on substrate recognition and acceptance of human PKMYT1, a Cdk1 inhibitory kinase*. Bioorg. Med. Chem. Lett., 2012. 22(2): pp. 1219-1223.
247. Simmerling, C., V. Hornak, R. Abel, A. Okur, B. Strockbine, and A. Roitberg, *Comparison of multiple amber force fields and development of improved protein backbone parameters*. Proteins, 2006. 65(3): pp. 712-725.
248. Zhang, C., G. Habets, and G. Bollag, *Interrogating the kinome*. Nat. Biotech., 2011. 29(11): pp. 981-983.
249. Lebakken, C.S., S.M. Riddle, U. Singh, W.J. Frazee, H.C. Eliason, Y. Gao, L.J. Reichling, B.D. Marks, and K.W. Vogel, *Development and Applications of a Broad-Coverage, TR-FRET-Based Kinase Binding Assay Platform*. J. Biomol. Screen., 2009. 14(8): pp. 924-935.

250. Munoz, L., R. Selig, Y.T. Yeung, C. Peifer, D. Hauser, and S. Laufer, *Fluorescence polarization binding assay to develop inhibitors of inactive p38 alpha mitogen-activated protein kinase*. *Anal. Biochem.*, 2010. 401(1): pp. 125-133.
251. Hashimoto, O., M. Shinkawa, T. Torimura, T. Nakamura, K. Selvendiran, M. Sakamoto, H. Koga, T. Ueno, and M. Sata, *Cell cycle regulation by the Wee1 Inhibitor PD0166285, Pyrido [2,3-d] pyrimidine, in the B16 mouse melanoma cell line*. *BMC Cancer*, 2006. 6(1): 292.
252. Stryer, L., D.D. Thomas, and C.F. Meares, *Diffusion-enhanced fluorescence energy transfer*. *Annu. Rev. Biophys Bioeng.*, 1982. 11(1): pp. 203-222.
253. Invitrogen, *Technical Note PV5592: LanthaScreen kinase binding assay user guide*. 2010. Carlsbad, CA, USA.
254. Bantscheff, M., D. Eberhard, Y. Abraham, S. Bastuck, M. Boesche, S. Hobson, T. Mathieson, J. Perrin, M. Raida, C. Rau, V. Reader, G. Sweetman, A. Bauer, T. Bouwmeester, C. Hopf, U. Kruse, G. Neubauer, N. Ramsden, J. Rick, B. Kuster, and G. Drewes, *Quantitative chemical proteomics reveals mechanisms of action of clinical ABL kinase inhibitors*. *Nat. Biotech.*, 2007. 25(9): pp. 1035-1044.
255. Rix, U., O. Hantschel, G. Dürnberger, L.L. Rensing Rix, M. Planyavsky, N.V. Fernbach, I. Kaupe, K.L. Bennett, P. Valent, J. Colinge, T. Köcher, and G. Superti-Furga, *Chemical proteomic profiles of the BCR-ABL inhibitors imatinib, nilotinib, and dasatinib reveal novel kinase and nonkinase targets*. *Blood*, 2007. 110(12): pp. 4055-4063.
256. Anastassiadis, T., S.W. Deacon, K. Devarajan, H. Ma, and J.R. Peterson, *Comprehensive assay of kinase catalytic activity reveals features of kinase inhibitor selectivity*. *Nat. Biotech.*, 2011. 29(11): pp. 1039-1045.
257. O'Hare, T., D.K. Walters, E.P. Stoffregen, T. Jia, P.W. Manley, J. Mestan, S.W. Cowan-Jacob, F.Y. Lee, M.C. Heinrich, M.W.N. Deininger, and B.J. Druker, *In vitro Activity of Bcr-Abl Inhibitors AMN107 and BMS-354825 against Clinically Relevant Imatinib-Resistant Abl Kinase Domain Mutants*. *Cancer Res.*, 2005. 65(11): pp. 4500-4505.
258. Cheng, Y. and W.H. Prusoff, *Relationship between the inhibition constant (K_i) and the concentration of inhibitor which causes 50 per cent inhibition (I₅₀) of an enzymatic reaction*. *Biochem. Pharmacol.*, 1973. 22(23): pp. 3099-3108.
259. Wichapong, K., M. Lindner, S. Pianwanit, S. Kokpol, and W. Sippl, *Receptor-based 3D-QSAR studies of checkpoint Wee1 kinase inhibitors*. *Eur. J. Med. Chem.*, 2009. 44(4): pp. 1383-1395.
260. Wichapong, K., M. Lawson, S. Pianwanit, S. Kokpol, and W. Sippl, *Postprocessing of protein-ligand docking poses using linear response MM-PB/SA: Application to Wee1 kinase inhibitors*. *J. Chem. Inf. Model.*, 2010. 50(9): pp. 1574-1588.
261. Jadhav, A., R.S. Ferreira, C. Klumpp, B.T. Mott, C.P. Austin, J. Inglese, C.J. Thomas, D.J. Maloney, B.K. Shoichet, and A. Simeonov, *Quantitative analyses of aggregation, autofluorescence, and reactivity artifacts in a screen for inhibitors of a thiol protease*. *J. Med. Chem.*, 2010. 53(1): pp. 37-51.
262. Thorsteinsson, M.V., J. Richter, A.L. Lee, and P. DePhillips, *5-Dodecanoylaminofluorescein as a probe for the determination of critical*

- micelle concentration of detergents using fluorescence anisotropy*. Anal. Biochem., 2005. 340(2): pp. 220-225.
263. Copeland, R.A., *Concentration-Response Plots and IC₅₀ Determinations*, in *Evaluation of Enzyme Inhibitors in Drug Discovery*. 2005, Wiley: Hoboken, NJ, USA. pp. 113-121.
264. Jameson, D.M. and G. Mocz, *Fluorescence polarization/anisotropy approaches to study protein-ligand interactions - effects of errors and uncertainties*, in *Methods in Molecular Biology - Protein-Ligand Interactions*, G.U. Nienhaus, Editor. 2005, Springer. pp. 301-322.
265. Tiller, G.E., T.J. Mueller, M.E. Dockter, and W.G. Struve, *Hydrogenation of Triton X-100 eliminates its fluorescence and ultraviolet-light absorption while preserving its detergent properties*. Anal. Biochem., 1984. 141(1): pp. 262-266.
266. Schürholz, T., J. Kehne, A. Gieselmann, and E. Neumann, *Functional reconstitution of the nicotinic acetylcholine-receptor by CHAPS dialysis depends on the concentrations of salt, lipid, and protein*. Biochemistry, 1992. 31(21): pp. 5067-5077.
267. Motulsky, H.J. and L.C. Mahan, *The kinetics of competitive radioligand binding predicted by the law of mass action*. Mol. Pharmacol., 1984. 25(1): pp. 1-9.
268. Hantschel, O., U. Rix, U. Schmidt, T. Burckstummer, M. Kneidinger, G. Schutze, J. Colinge, K.L. Bennett, W.R. Ellmeier, P. Valent, and G. Superti-Furga, *The Btk tyrosine kinase is a major target of the Bcr-Abl inhibitor dasatinib*. Proc. Natl. Acad. Sci. U.S.A., 2007. 104(33): pp. 13283-13288.
269. Teillet, F., A. Boumendjel, J. Boutonnat, and X. Ronot, *Flavonoids as RTK inhibitors and potential anticancer agents*. Med. Res. Rev., 2008. 28(5): pp. 715-745.
270. Hollman, P.C. and M.B. Katan, *Dietary flavonoids: Intake, health effects and bioavailability*. Food Chem. Toxicol., 1999. 37(9-10): pp. 937-42.
271. Hou, D.X. and T. Kumamoto, *Flavonoids as protein kinase inhibitors for cancer chemoprevention: Direct binding and molecular modeling*. Antioxid. Redox Signal., 2010. 13(5): pp. 691-719.
272. Lu, X.H., J.I. Jung, H.J. Cho, D.Y. Lim, H.S. Lee, H.S. Chun, D.Y. Kwon, and J.H.Y. Park, *Fisetin inhibits the activities of cyclin-dependent kinases leading to cell cycle arrest in HT-29 human colon cancer cells*. J. Nutr., 2005. 135(12): pp. 2884-2890.
273. Lu, H., D.J. Chang, B. Baratte, L. Meijer, and U. Schulze-Gahmen, *Crystal structure of a human cyclin-dependent kinase 6 complex with a flavonol inhibitor, fisetin*. J. Med. Chem., 2005. 48(3): pp. 737-743.
274. Akiyama, T., J. Ishida, S. Nakagawa, H. Ogawara, S. Watanabe, N. Itoh, M. Shibuya, and Y. Fukami, *Genistein, a specific inhibitor of tyrosine-specific protein kinases*. J. Biol. Chem., 1987. 262(12): pp. 5592-5595.
275. Labbe, D., M. Provencal, S. Lamy, D. Boivin, D. Gingras, and R. Beliveau, *The flavonols quercetin, kaempferol, and myricetin inhibit hepatocyte growth factor-induced medulloblastoma cell migration*. J. Nutr., 2009. 139(4): pp. 646-652.
276. Kumamoto, T., M. Fujii, and D.X. Hou, *Akt is a direct target for myricetin to inhibit cell transformation*. Mol. Cell. Biochem., 2009. 332(1-2): pp. 33-41.

277. Walker, E.H., M.E. Pacold, O. Perisic, L. Stephens, P.T. Hawkins, M.P. Wymann, and R.L. Williams, *Structural determinants of phosphoinositide 3-kinase inhibition by wortmannin, LY294002, quercetin, myricetin, and staurosporine*. Mol. Cell, 2000. 6(4): pp. 909-919.
278. Harmon, A.W. and Y.M. Patel, *Naringenin inhibits phosphoinositide 3-kinase activity and glucose uptake in 3T3-L1 adipocytes*. Biochem. Biophys. Res. Commun., 2003. 305(2): pp. 229-234.
279. Yang, E.B., Y.J. Guo, K. Zhang, Y.Z. Chen, and P. Mack, *Inhibition of epidermal growth factor receptor tyrosine kinase by chalcone derivatives*. Biochim. Biophys. Acta, 2001. 1550(2): pp. 144-152.
280. Sicheri, F., I. Moarefi, and J. Kuriyan, *Crystal structure of the Src family tyrosine kinase Hck*. Nature, 1997. 385(6617): pp. 602-609.
281. Sharma, Y., C. Agarwal, A.K. Singh, and R. Agarwal, *Inhibitory effect of silibinin on ligand binding to erbB1 and associated mitogenic signaling, growth, and DNA synthesis in advanced human prostate carcinoma cells*. Mol. Carcinogen., 2001. 30(4): pp. 224-236.
282. Touny, L.H. and P.P. Banerjee, *Identification of both Myt-1 and Wee-1 as necessary mediators of the p21-independent inactivation of the cdc-2/cyclin B1 complex and growth inhibition of TRAMP cancer cells by genistein*. Prostate, 2006. 66(14): pp. 1542-1555.
283. Roche, O., P. Schneider, J. Zuegge, W. Guba, M. Kansy, A. Alanine, K. Bleicher, F. Danel, E.-M. Gutknecht, M. Rogers-Evans, W. Neidhart, H. Stalder, M. Dillon, E. Sjögren, N. Fotouhi, P. Gillespie, R. Goodnow, W. Harris, P. Jones, M. Taniguchi, S. Tsujii, W. von der Saal, G. Zimmermann, and G. Schneider, *Development of a virtual screening method for identification of "frequent hitters" in compound libraries*. J. Med. Chem., 2001. 45(1): pp. 137-142.
284. Inglese, J., R.L. Johnson, A. Simeonov, M.H. Xia, W. Zheng, C.P. Austin, and D.S. Auld, *High-throughput screening assays for the identification of chemical probes*. Nat. Chem. Biol., 2007. 3(8): pp. 466-479.
285. McGovern, S.L., B.T. Helfand, B. Feng, and B.K. Shoichet, *A specific mechanism of nonspecific inhibition*. J. Med. Chem., 2003. 46(20): pp. 4265-4272.
286. McGovern, S.L., E. Caselli, N. Grigorieff, and B.K. Shoichet, *A common mechanism underlying promiscuous inhibitors from virtual and high-throughput screening*. J. Med. Chem., 2002. 45(8): pp. 1712-22.
287. McGovern, S.L. and B.K. Shoichet, *Kinase inhibitors: Not just for kinases anymore*. J. Med. Chem., 2003. 46(8): pp. 1478-1483.
288. Klebe, G., *Virtual ligand screening: Strategies, perspectives and limitations*. Drug Discov. Today, 2006. 11(13-14): pp. 580-594.
289. Rapp, C., C. Kalyanaraman, A. Schiffmiller, E.L. Schoenbrun, and M.P. Jacobson, *A molecular mechanics approach to modeling protein-ligand interactions: Relative binding affinities in congeneric series*. J. Chem. Inf. Model., 2011. 51(9): pp. 2082-2089.
290. Lindstrom, A., L. Edvinsson, A. Johansson, C.D. Andersson, I.E. Andersson, F. Raubacher, and A. Linusson, *Postprocessing of docked protein-ligand complexes using implicit solvation models*. J. Chem. Inf. Model., 2011. 51(2): pp. 267-282.
291. Case, D.A.D., T. A.; Cheatham, I. T. E.; Simmerling, C. L.; Wang, J.; Duke, R. E.; Luo, R.; Crowley, M.; Walker, R. C.; Zhang, W.; Merz, K. M.; Wang, B.; Hayik, S.; Roitberg, A.; Seabra, G.; Kolossváry, I;

- Wong, K. F.; Paesani, F.; Vanicek, J.; Wu, X.; Brozell, S. R.; Steinbrecher, T.; Gohlke, H.; Yang, L.; Tan, C.; Mongan, J.; Hornak, V.; Cui, G.; Mathews, D. H.; Seetin, M. G.; Sagui, C.; Babin, V.; Kollman, P. A., *AMBER11*. 2010: University of California, San Francisco, CA, USA.
292. Mizenina, O.A. and M.M. Moasser, *S-phase inhibition of cell cycle progression by a novel class of pyridopyrimidine tyrosine kinase inhibitors*. *Cell Cycle*, 2004. 3(6): pp. 794-801.
293. Vaasa, A., I. Viil, E. Enkvist, K. Viht, G. Raidaru, D. Lavogina, and A. Uri, *High-affinity bisubstrate probe for fluorescence anisotropy binding/displacement assays with protein kinases PKA and ROCK*. *Anal. Biochem.*, 2009. 385(1): pp. 85-93.
294. Huang, X., *Fluorescence polarization competition assay: The range of resolvable inhibitor potency is limited by the affinity of the fluorescent ligand*. *J. Biomol. Screen.*, 2003. 8(1): pp. 34-38.
295. Nikolovska-Coleska, Z., R. Wang, X. Fang, H. Pan, Y. Tomita, P. Li, P.P. Roller, K. Krajewski, N.G. Saito, J.A. Stuckey, and S. Wang, *Development and optimization of a binding assay for the XIAP BIR3 domain using fluorescence polarization*. *Anal. Biochem.*, 2004. 332(2): pp. 261-273.
296. Swift, K., S.N. Anderson, and E.D. Matayoshi, *Advances in Fluorescence Sensing Technology V*. *Proc. SPIE*, 2001 (4252): pp. 47-58.
297. Zheng, W., S.S. Carroll, J. Inglese, R. Graves, L. Howells, and B. Strulovici, *Miniaturization of a hepatitis C virus RNA polymerase assay using a -102 degrees C cooled CCD camera-based imaging system*. *Anal. Biochem.*, 2001. 290(2): pp. 214-220.
298. Dennis, P.B., A. Jaeschke, M. Saitoh, B. Fowler, S.C. Kozma, and G. Thomas, *Mammalian TOR: A homeostatic ATP sensor*. *Science*, 2001. 294(5544): pp. 1102-1105.
299. Zhao, X.H., T. Bondeva, and T. Balla, *Characterization of recombinant phosphatidylinositol 4-kinase beta reveals auto- and heterophosphorylation of the enzyme*. *J. Biol. Chem.*, 2000. 275(19): pp. 14642-14648.
300. Downing, G.J., S. Kim, S. Nakanishi, K.J. Catt, and T. Balla, *Characterization of a soluble adrenal phosphatidylinositol 4-kinase reveals wortmannin sensitivity of type III phosphatidylinositol kinases*. *Biochemistry*, 1996. 35(11): pp. 3587-3594.
301. Gribble, F.M., G. Loussouarn, S.J. Tucker, C. Zhao, C.G. Nichols, and F.M. Ashcroft, *A novel method for measurement of submembrane ATP concentration*. *J. Biol. Chem.*, 2000. 275(39): pp. 30046-30049.
302. Traut, T.W., *Physiological concentrations of purines and pyrimidines*. *Mol. Cell. Biochem.*, 1994. 140(1): pp. 1-22.
303. Barnett, S.F., D. Defeo-Jones, S. Fu, P.J. Hancock, K.M. Haskell, R.E. Jones, J.A. Kahana, A.M. Kral, K. Leander, L.L. Lee, J. Malinowski, E.M. McAvoy, D.D. Nahas, R.G. Robinson, and H.E. Huber, *Identification and characterization of pleckstrin-homology-domain-dependent and iso-enzyme-specific Akt inhibitors*. *Biochem. J.*, 2005. 385(Pt 2): pp. 399-408.
304. Hawkins, J., S. Zheng, B. Frantz, and P. LoGrasso, *p38 map kinase substrate specificity differs greatly for protein and peptide substrates*. *Arch. Biochem. Biophys.*, 2000. 382(2): pp. 310-313.
305. Göllner, C., C. Philipp, B. Dobner, W. Sippl, and M. Schmidt, *First total synthesis of 1,2-dipalmitoyl-3-(N-palmitoyl-6'-amino-6'-deoxy-alpha-D-*

- glucosyl)-sn-glycerol--a glyco glycerolipid of a marine alga with a high inhibitor activity against human Myt1-kinase. Carbohydr. Res., 2009. 344(13): pp. 1628-1631.*
306. Li, C., Y. Sun, J. Zhang, Z. Zhao, G. Yu, and H. Guan, *Synthesis of 6'-acylamido-6'-deoxy- α -D-galactoglycerolipids. Carbohydr. Res., 2013. 376C: pp. 15-23.*
307. Sun, Y., J. Zhang, C. Li, H. Guan, and G. Yu, *Synthesis of glyco glycerolipid of 1,2-dipalmitoyl-3-(N-palmitoyl-6'-amino-6'-deoxy- α -D-glucosyl)-sn-glycerol and its analogues, inhibitors of human Myt1-kinase. Carbohydr. Res., 2012. 355: pp. 6-12.*
308. Wu, H.-J., C.-X. Li, G.-P. Song, and Y.-X. Li, *Synthesis of Natural α -6-Dehydroxy-6-aminoglucoglycerolipids. Chin. J. Chem., 2008. 26(9): pp. 1641-1646.*
309. Davidson, W., L. Frego, G.W. Peet, R.R. Kroe, M.E. Labadia, S.M. Lukas, R.J. Snow, S. Jakes, C.A. Grygon, C. Pargellis, and B.G. Werneburg, *Discovery and characterization of a substrate selective p38 α inhibitor. Biochemistry, 2004. 43(37): pp. 11658-11671.*
310. Lukas, S.M., R.R. Kroe, J. Wildeson, G.W. Peet, L. Frego, W. Davidson, R.H. Ingraham, C.A. Pargellis, M.E. Labadia, and B.G. Werneburg, *Catalysis and function of the p38 α circle MK2a signaling complex. Biochemistry, 2004. 43(31): pp. 9950-9960.*
311. Roehrl, M.H.A., J.Y. Wang, and G. Wagner, *A general framework for development and data analysis of competitive high-throughput screens for small-molecule inhibitors of protein-protein interactions by fluorescence polarization. Biochemistry, 2004. 43(51): pp. 16056-16066.*
312. Schutkowski, M., U. Reineke, and U. Reimer, *Peptide arrays for kinase profiling. ChemBioChem, 2005. 6: pp. 513-521.*
313. Boeckmann, B., A. Bairoch, R. Apweiler, M.C. Blatter, A. Estreicher, E. Gasteiger, M.J. Martin, K. Michoud, C. O'Donovan, I. Phan, S. Pilbout, and M. Schneider, *The SWISS-PROT protein knowledgebase and its supplement TrEMBL in 2003. Nucleic Acids Res., 2003. 31(1): pp. 365-370.*
314. Kreegipuu, A., N. Blom, and S. Brunak, *PhosphoBase, a database of phosphorylation sites: Release 2.0. Nucleic Acids Res., 1999. 27(1): pp. 237-239.*
315. Nahtman, T., A. Jernberg, S. Mahdaviifar, J. Zerweck, M. Schutkowski, M. Maeurer, and M. Reilly, *Validation of peptide epitope microarray experiments and extraction of quality data. J. Immunol. Methods, 2007. 328(1-2): pp. 1-13.*
316. Quintana, F.J., P.H. Hagedorn, G. Elizur, Y. Merbl, E. Domany, and I.R. Cohen, *Functional immunomics: Microarray analysis of IgG autoantibody repertoires predicts the future response of mice to induced diabetes. Proc. Natl. Acad. Sci. U.S.A., 2004. 101(Suppl. 2): pp. 14615-14621.*
317. The Uniprot Consortium, *Reorganizing the protein space at the Universal Protein Resource (UniProt). Nucleic Acids Res., 2012. 40(Database issue): pp. D71-75.*
318. Kamaruddin, M.A., P. Ung, M.I. Hossain, B. Jarasrassamee, W. O'Malley, P. Thompson, D. Scanlon, H.C. Cheng, and B. Graham, *A facile, click chemistry-based approach to assembling fluorescent chemosensors for protein tyrosine kinases. Bioorg. Med. Chem. Lett., 2011. 21(1): pp. 329-331.*

319. Oppermann, F.S., F. Gnad, J.V. Olsen, R. Hornberger, Z. Greff, G. Keri, M. Mann, and H. Daub, *Large-scale proteomics analysis of the human kinome*. Mol. Cell Proteomics, 2009. 8(7): pp. 1751-1764.
320. Hüser, J., ed. *High Throughput-Screening in Drug Discovery*. Methods and Principles in Medicinal Chemistry. Vol. 35. 2006, Wiley VCH: Weinheim. p. 101.
321. Nousiainen, M., H.H.W. Silljé, G. Sauer, E.A. Nigg, and R. Körner, *Phosphoproteome analysis of the human mitotic spindle*. Proc. Natl. Acad. Sci. U.S.A., 2006. 103(14): pp. 5391-5396.
322. Dephoure, N., C. Zhou, J. Villén, S.A. Beausoleil, C.E. Bakalarski, S.J. Elledge, and S.P. Gygi, *A quantitative atlas of mitotic phosphorylation*. Proc. Natl. Acad. Sci. U.S.A., 2008. 105(31): pp. 10762-10767.
323. Ruiz, E.J., M. Vilar, and A.R. Nebreda, *A two-step inactivation mechanism of Myt1 ensures CDK1/Cyclin B activation and meiosis I entry*. Curr. Biol., 2010. 20(8): pp. 717-723.
324. Daub, H., J.V. Olsen, M. Bairlein, F. Gnad, F.S. Oppermann, R. Körner, Z. Greff, G. Kéri, O. Stemmann, and M. Mann, *Kinase-selective enrichment enables quantitative phosphoproteomics of the kinome across the cell cycle*. Mol. Cell, 2008. 31(3): pp. 438-448.
325. Tinti, M., L. Kiemer, S. Costa, M.L. Miller, F. Sacco, J.V. Olsen, M. Carducci, S. Paoluzi, F. Langone, C.T. Workman, N. Blom, K. Machida, C.M. Thompson, M. Schutkowski, S. Brunak, M. Mann, B.J. Mayer, L. Castagnoli, and G. Cesareni, *The SH2 domain interaction landscape*. Cell Rep., 2013. 3(4): pp. 1293-1305.
326. Crooks, G.E., G. Hon, J.M. Chandonia, and S.E. Brenner, *Weblogo: A sequence logo generator*. Genome Res., 2004(14): pp. 1188-1190.
327. Copeland, R.A., *Physicochemical Properties of the Natural Amino Acids*, in *Enzymes - a practical introduction to structure, mechanism and data analysis*. 1996, VCH Verlagsgesellschaft: Weinheim. p. 37.
328. Schutkowski, M., U. Reimer, S. Panse, L. D., J.M. Lizcano, D.R. Alessi, and J. Schneider-Mergener, *High-content peptide microarrays for deciphering kinase specificity and biology*. Angew. Chem. Int. Ed. Engl., 2004. 43: pp. 2671-2674.
329. Mahajan, K., B. Fang, J.M. Koomen, and N.P. Mahajan, *H2B Tyr37 phosphorylation suppresses expression of replication-dependent core histone genes*. Nat. Struct. Biol., 2012. 19(9): pp. 930-937.
330. Mori, S., L. Ronnstrand, K. Yokote, A. Engstrom, S.A. Courtneidge, L. Claessonwelsch, and C.H. Heldin, *Identification of 2 Juxtamembrane Autophosphorylation Sites in the Pdgf Beta-Receptor - Involvement in the Interaction with Src Family Tyrosine Kinases*. EMBO J., 1993. 12(6): pp. 2257-2264.
331. Choi, M.H., I.K. Lee, G.W. Kim, B.U. Kim, Y.-H. Han, D.-Y. Yu, H.S. Park, K.Y. Kim, J.S. Lee, C. Choi, Y.S. Bae, B.I. Lee, S.G. Rhee, and S.W. Kang, *Regulation of PDGF signalling and vascular remodelling by peroxiredoxin II*. Nature, 2005. 435(7040): pp. 347-353.
332. Hüser, J., ed. *High Throughput-Screening in Drug Discovery*. Methods and Principles in Medicinal Chemistry. Vol. 35. 2006, Wiley VCH: Weinheim. pp. 95-97.

Appendix

Sequence Alignment and Modeling

```

CDK2-1QMZ 1 ---M-ENFQKVEKIGEGTYGVVYKAFNKLTGEVVALKKIRLDTETEGVPSTAIRESLL
Wee1-1X8B 291 MKSRYTTEFHELEKIGSGEGFVFCVKRDLGCIYAIKRSKKPLAGSVDEQNALREYVAH
Myt1-3P1A 102 PESFFQQSFQRLSRLGHGSYGEVFKVRSKEDGRLYAVKRSMSPFQPKDRARKLAEVGSH
      .*:.:*: * : * * * . : * : * : * :
      : * :

CDK2-1QMZ 56 KEL-NHPNIVKLLDVIHTENKLYLVFVFLH-QDLKKFMDASA--LTGIFLPLIKSYLFQL
Wee1-1X8B 351 AVLGQHSVVRVYFSAWAEDDHMLIQNEYCNGGSLADAISENYRIMSYFKEAELKDLLQV
Myt1-3P1A 162 EKVGOHPCCVRLECAWBEGGILYLQTELQCG-PSLOCHCEAWG--ASLPEAOVWGYLRDT
      : : * . * : . . . : : * . * . . : : . . . * :

CDK2-1QMZ 112 LQGLAFCHSHRVLHRDLKPNLLINTEGAIKLADFGLARAFVGPVRTYTHEVVTLWYRAP
Wee1-1X8B 411 GRGLRYIHSMSLVHMDIKPSNIFIS-KVMFKIGDLGHVTRIS----SPQVEEGDSRFLAN
Myt1-3P1A 218 LLALAHLSQGLVHLDVKPANI FLGPRGRCKLGDFFLLVELG-----VQEGDPRYMAP
      . * . * * : : * * * * * : : . . * : * * * : . : : *

CDK2-1QMZ 172 EI--LLGCKYVSTAVDIWSLGCIFAENVTRRALFPGDSEIDQLFRI FRTLDFSK--VVP
Wee1-1X8B 486 EV--LQENYTHLPKADIFALALTVVCAAGAEP LPRN----GDQWHEIRQGLRPR--IPQV
Myt1-3P1A 277 EL--LQGSYG--TAADVPSLGLTILEVACNMELPHG----GEGWQQLRQGYLPP-EPTAG
      * : * . . * : : * . . * . . : : : * : . .

CDK2-1QMZ 255 LD-EDGRSLLSQMLIHYDPNKRISAKAALAIHPFQDV
Wee1-1X8B 530 LS-QEFTTELLKVMIIHPDPERRPSAMALVKIISVL---
Myt1-3P1A 320 LS-SELRSVLVMMLEPDPKLRATAEALLALPVLRF
      * . . : . : * * : . * * : * * * : . . :

```

Fig. 42: Sequence alignment of Cdk2 (PDB code 1QMZ), Wee1 (PDB Code 1X8B) and Myt1 (PDB code 3PIA). Stars represent residues that are identical whereas dots and colons denote similar residues.

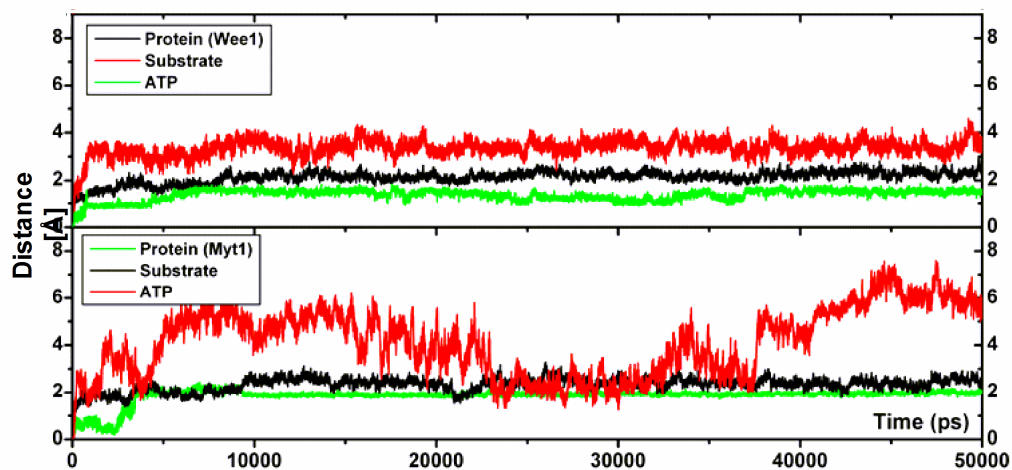


Fig. 43: RMSD plots obtained from MD simulation of Wee1-TY and Myt1-TY.

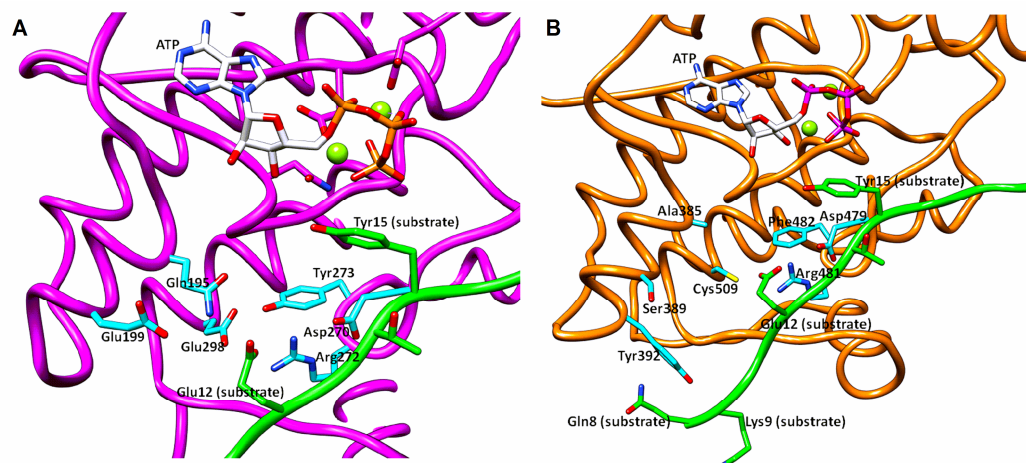


Fig. 44: Interaction of TY substrate residues (Gln8, Lys9, Glu12, Thr14 and Tyr15) with (A) Myt1 and (B) Wee1. Myt1 is shown as magenta ribbon and cyan stick, whereas the Wee1 is shown as orange ribbon and cyan stick. The TY substrate is represented as green ribbon and stick.

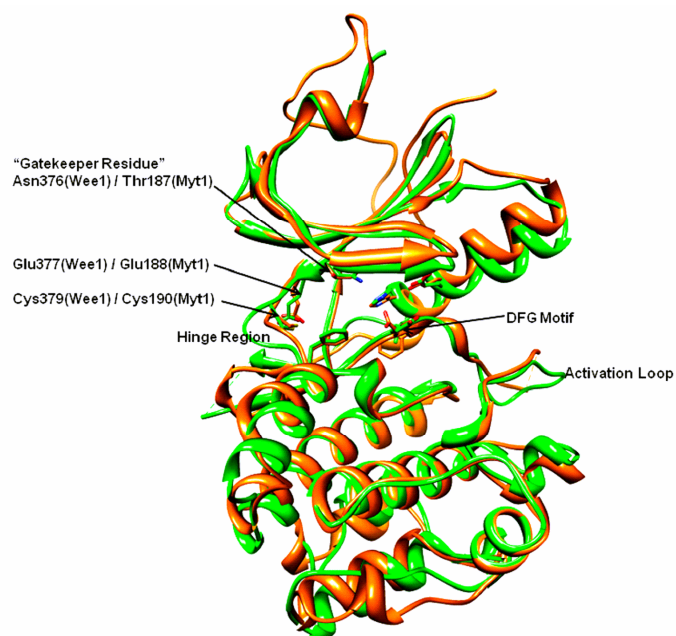


Fig. 45: Comparison of the overall structure of Wee1 (PDB Code 1X8B) and Myt1 (PDB: 3P1A). The structure of Wee1 and Myt1 are shown as green and orange ribbon, respectively.

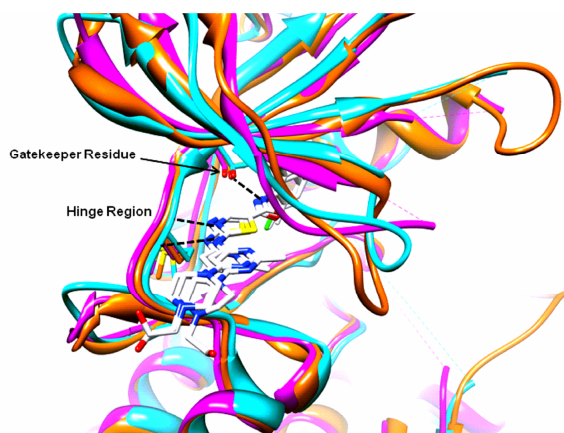
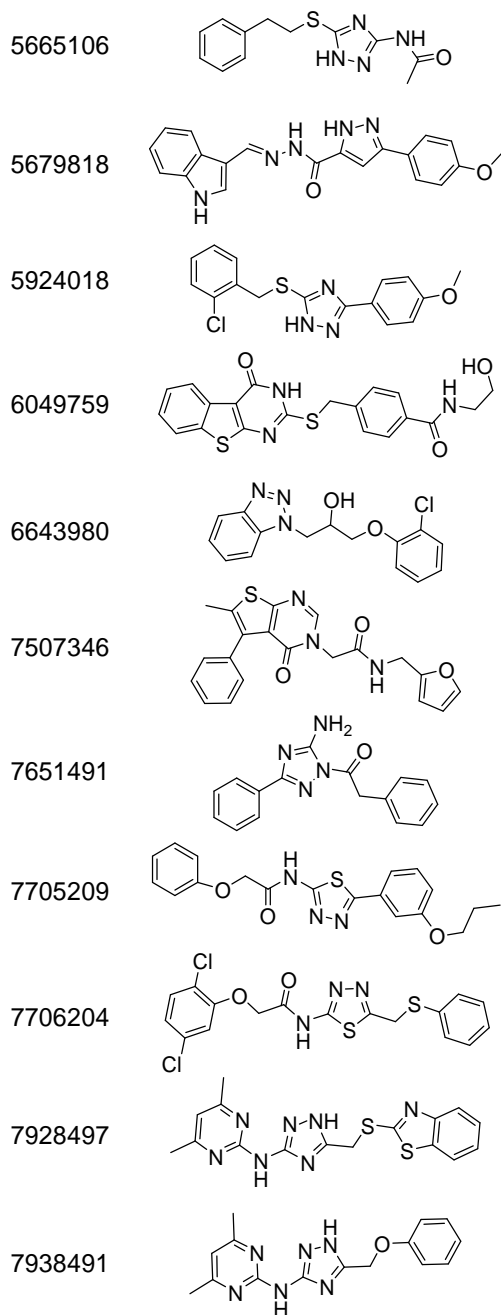


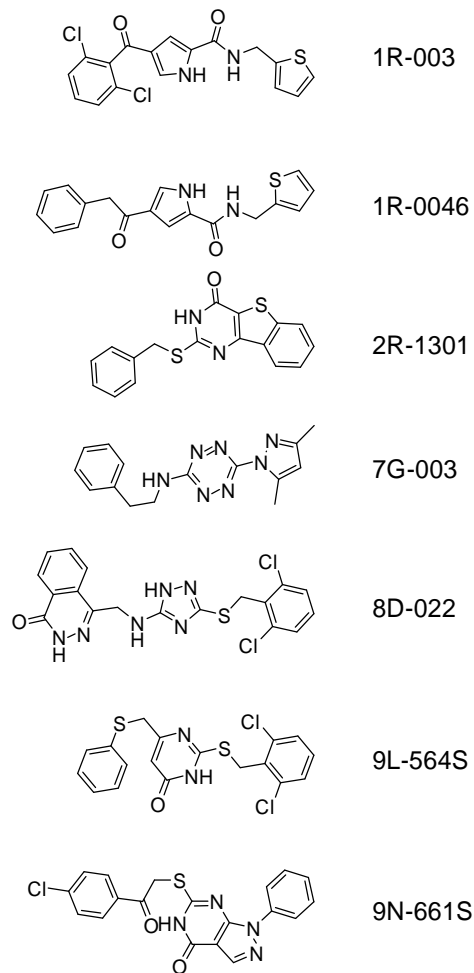
Fig. 46: Comparison of the binding mode of dasatinib (white stick) in the binding pocket of different kinases (Abl: orange-2GQG, c-Src: magenta-3G5D, and Btk: cyan-3K54).

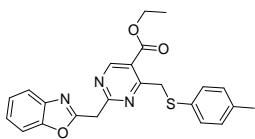
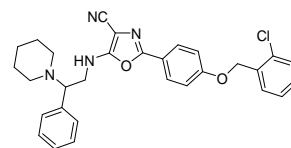
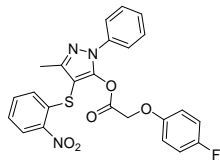
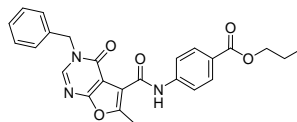
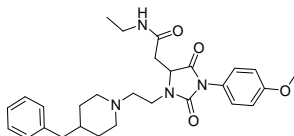
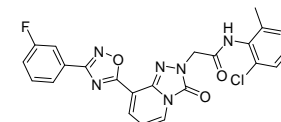
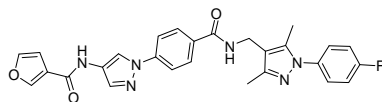
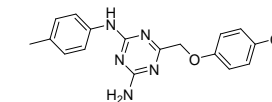
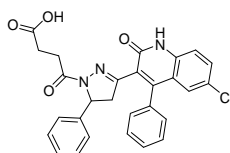
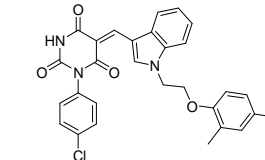
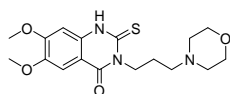
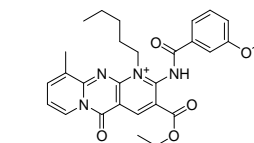
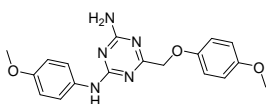
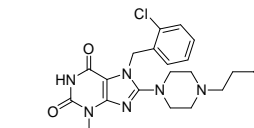
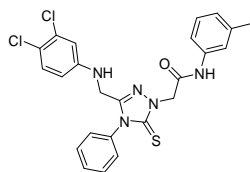
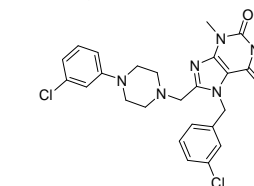
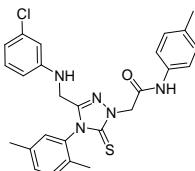
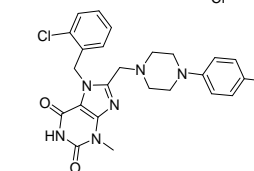
Chemical Structures of Selected Screening Compounds

Set Chembridge I



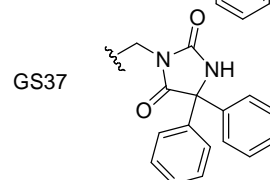
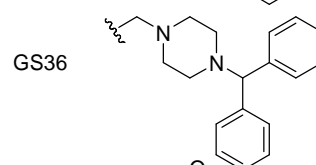
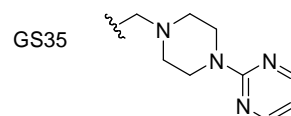
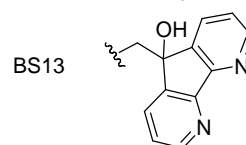
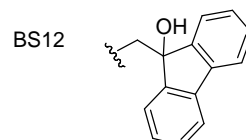
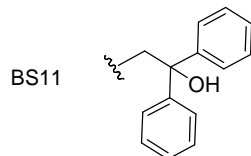
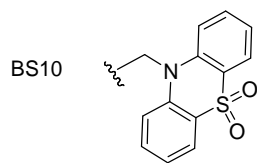
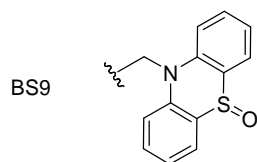
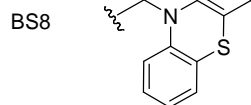
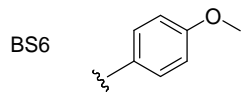
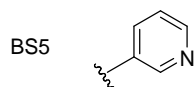
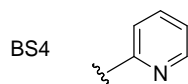
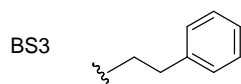
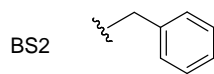
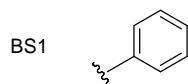
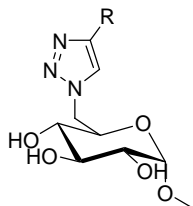
Set Keyorganics I



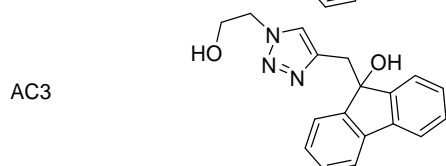
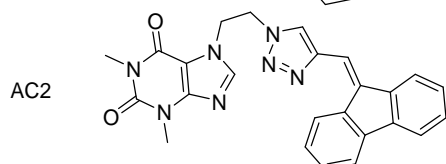
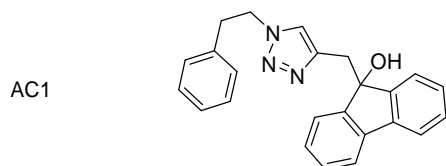
Set Chembridge II7769763 (KW1)
ZINC01425605OSSL_110276 (KW10)
ZINC326245517697266 (KW2)
ZINC02843127OSSL_164599 (KW11)
ZINC356724207871748 (KW3)
ZINC09850834OSSL_438946 (KW12)
ZINC6721930738874115 (KW4)
ZINC12025906OSSL_048423 (KW13)
ZINC172066295849648 (KW5)
ZINC13139806OSSK_318710 (KW14)
ZINC023000607960104 (KW6)
ZINC01061686OSSL_410731 (KW15)
ZINC203113817773617 (KW7)
ZINC18088912OSSL_396401 (KW16)
ZINC08996474OSSK_670031 (KW8)
ZINC16769432OSSL_719027 (KW17)
ZINC56918675OSSK_670181 (KW9)
ZINC16769666OSSL_393954 (KW18)
ZINC57016007

Glycotriazole series

a) Methyl glucosides

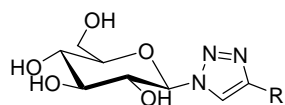


b) sugar-free BS12-derivatives

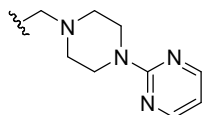


c) Triazolo glycosides

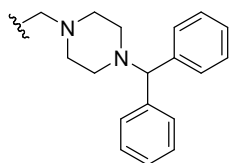
Triazolo glycosides



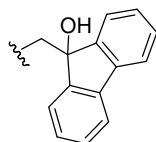
GS38



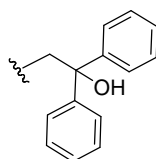
GS39



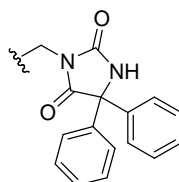
GS40



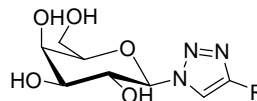
GS41



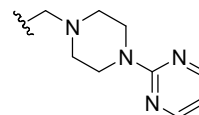
GS46



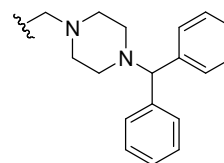
Triazolo galactosides



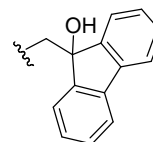
GS42



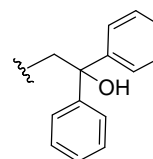
GS43



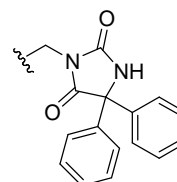
GS45



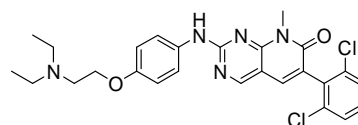
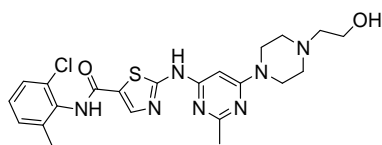
GS47



GS44

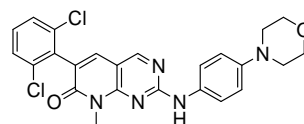
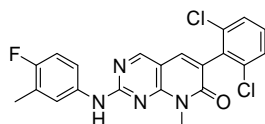
Myt1 kinase inhibitors in this work

Dasatinib



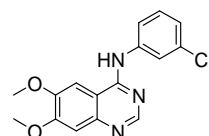
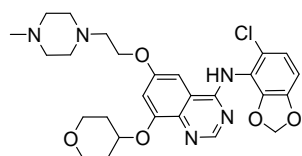
PD166285

PD180970

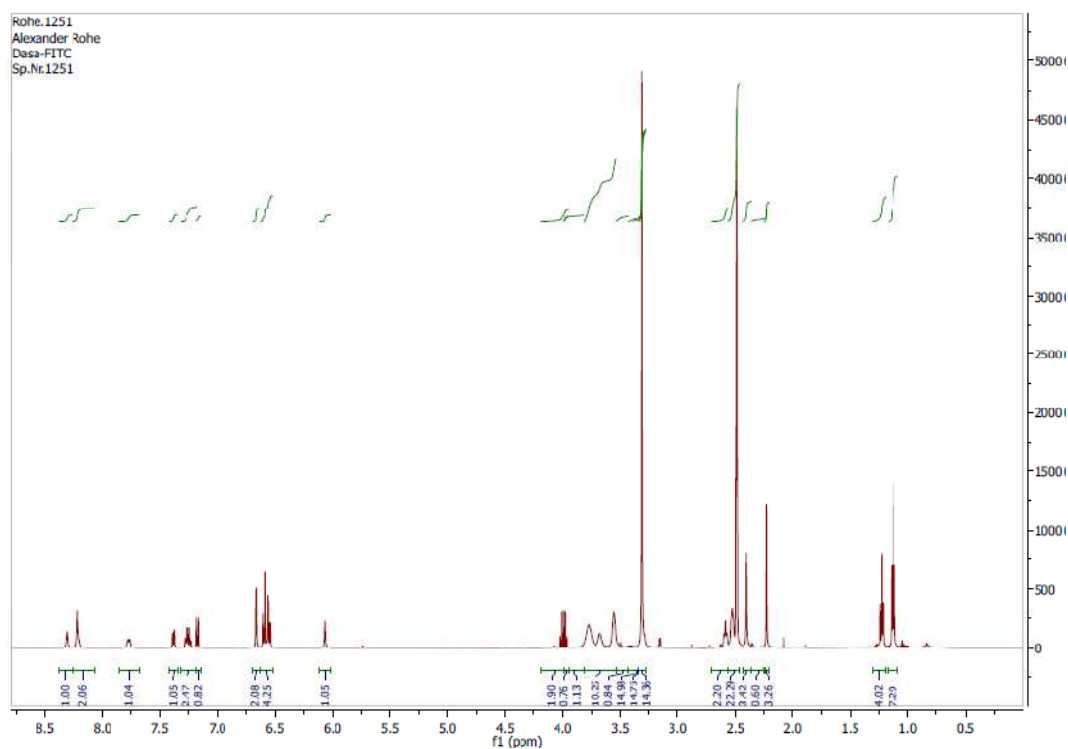


PD173952

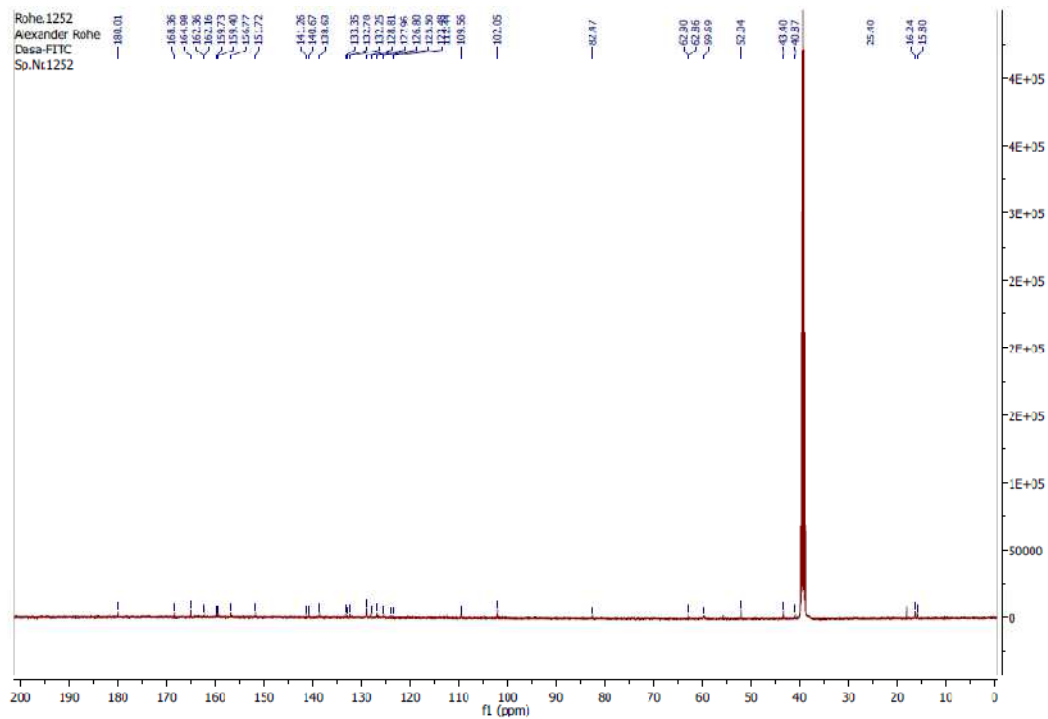
Saracatinib

Tyrphostin
AG 1478

DasAFITC: $^1\text{H-NMR}$

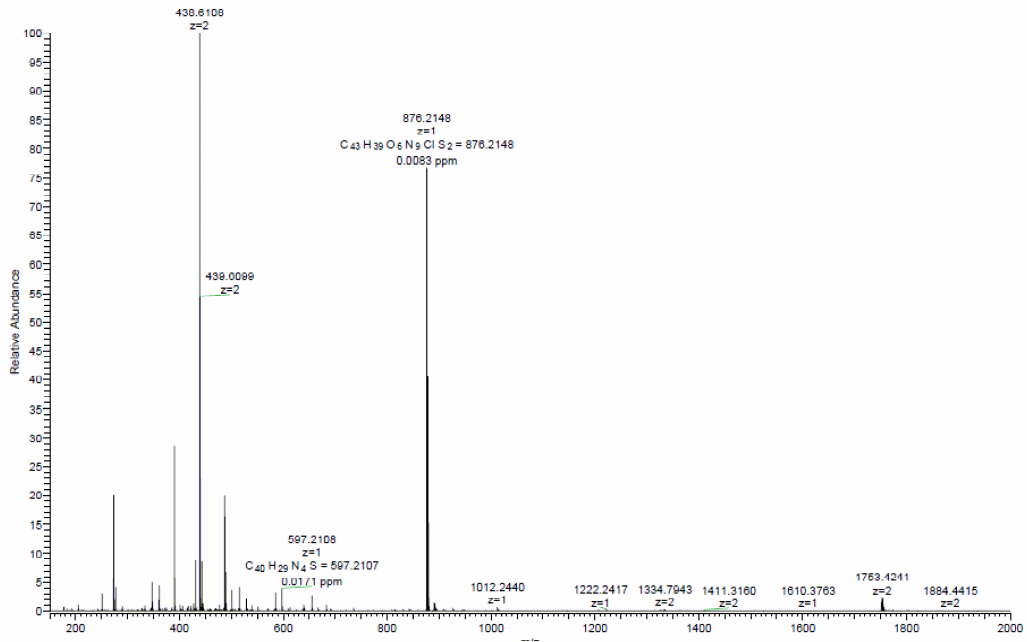
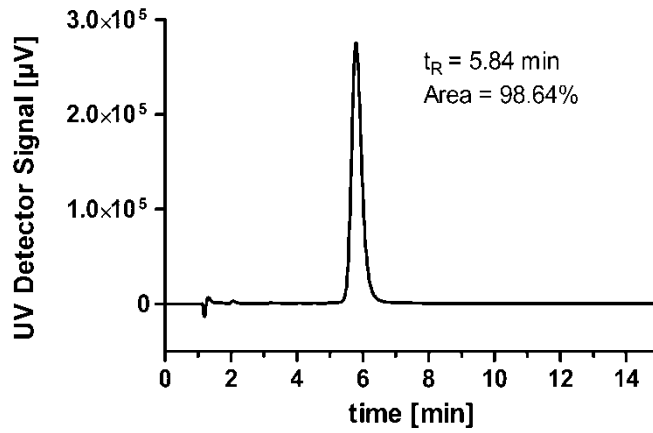


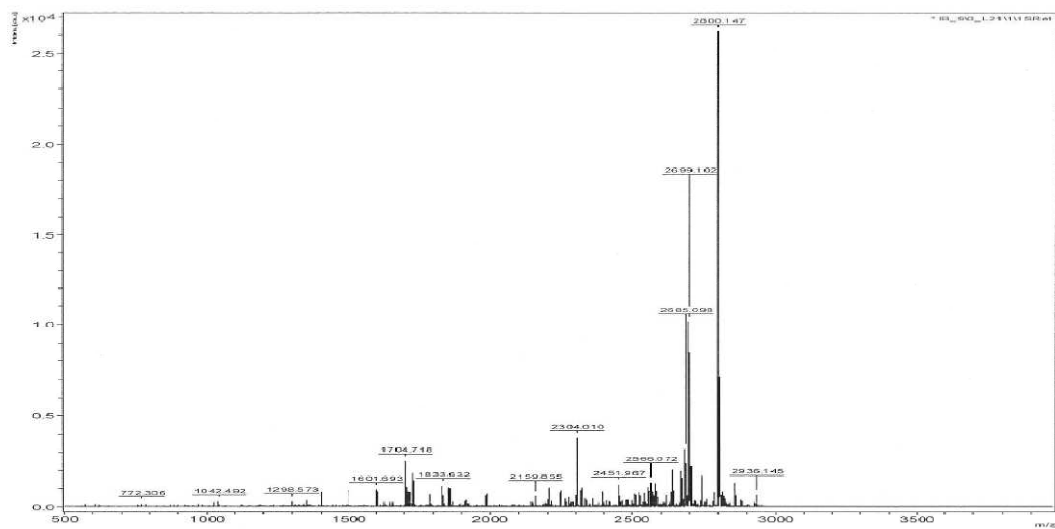
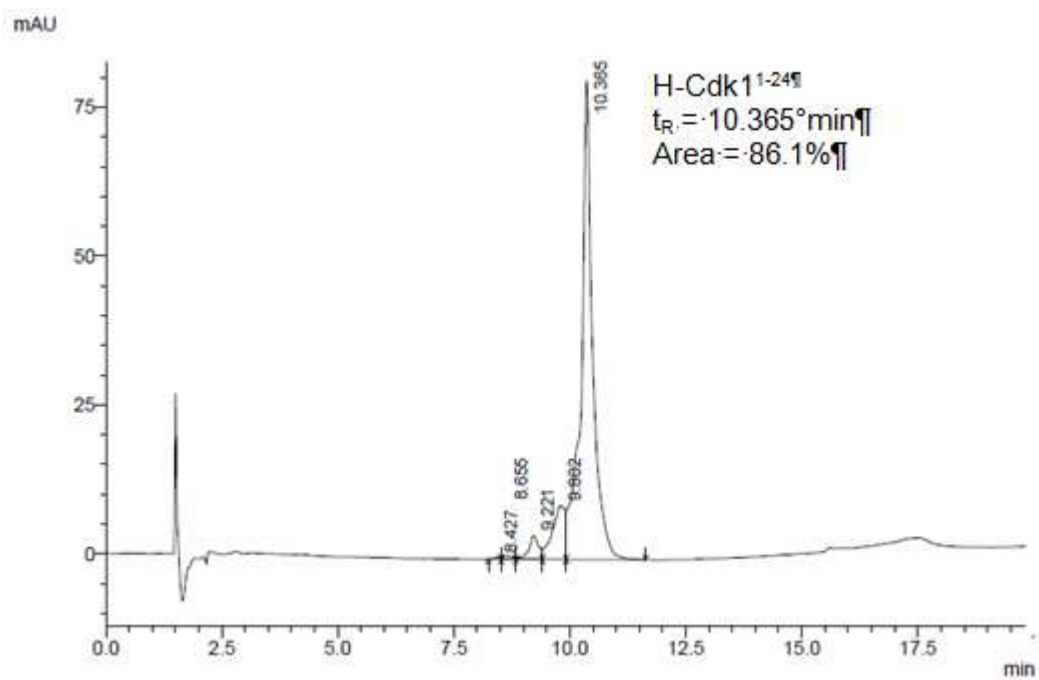
DasAFITC: $^{13}\text{C-NMR}$

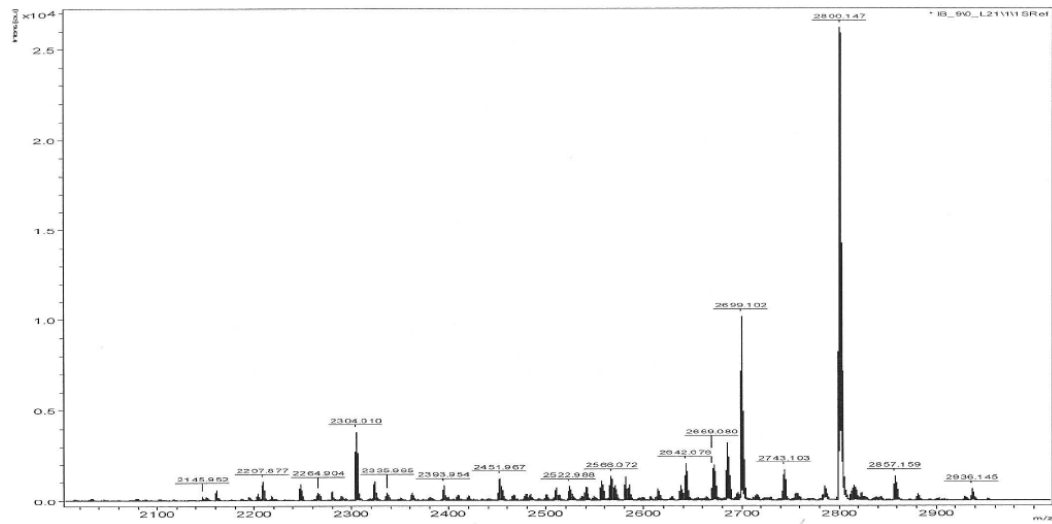
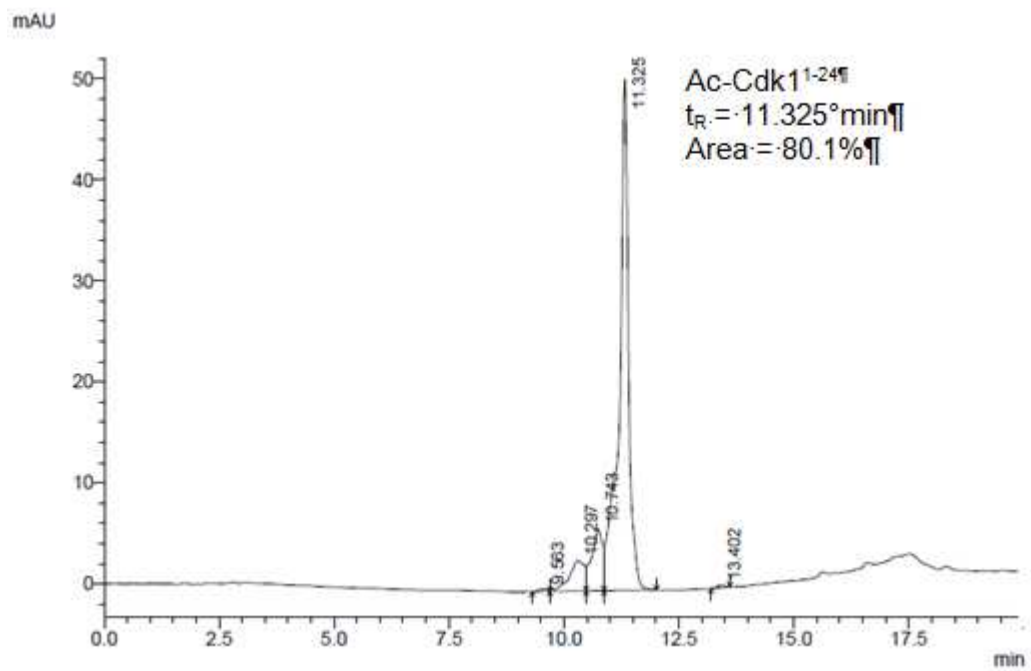
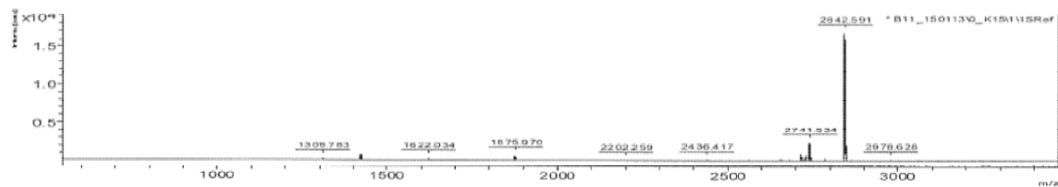


DasAFITC: HR-MS

L_120524144300#360 RT: 5.78 AV: 1 NL: 3.77E7
T: FTMS + p NSI Full m/z [150.00-2000.00]

**DasAFITC: HPLC**

Analytics of Peptides Synthesized in this Work: HPLC and MS**H-Cdk1¹⁻²⁴**

Ac-Cdk1¹⁻²⁴

Top 50 Peptides per Slide from Microarray Experiments

For top and bottom slide (I and II) from the microarray reaction chamber, the 50 highest response peptides are displayed for Myt1 and Wee1. Peptides are listed in four tables, providing informations on rank (#), ID, name, arithmetic mean response index, standard deviation (SD), number of observations (N), sequence and the full name of the corresponding protein. Numerical data reflects the response index I (Eq. 14, Section 5.5.1).

Myt Chip I

#	ID	Name	Mean Index	SD	N	Sequence	FullName
1	302	EFS_HUMAN	12,91	1,59	3	GTDEGIYDV- PLLG	embryonal FYN-associated substrate (HEFS)
2	509	INSR_HUMAN	7,04	1,03	3	GMTRDIYET- DYR	insulin receptor (IR)
3	659	MK09_HUMAN	6,49	1,20	3	NFMMPYV- VTRY	mitogen-activated protein kinase 9 (c-Jun N-terminal kinase 2, JNK2)
4	657	MK08_HUMAN	6,47	1,66	3	SFMMTPYV- VTRY	mitogen-activated protein kinase 8 (Stress-activated protein kinase JNK1) (c-Jun N-terminal kinase 1)
5	747	A002-D	5,19	0,95	3	DGHEYIYV- DPMQL	beta platelet-derived growth factor receptor
6	482	TRKA_HUMAN	5,06	0,94	3	GMSRDIYST- DYR	high affinity nerve growth factor receptor precursor (TRK1 transforming tyrosine kinase protein) (p140-TrkA) (Trk-A)
7	369	DDR1_HUMAN	4,09	0,21	3	GMSRNLYA- GDYR	epithelial discoidin domain receptor 1 precursor (Tyrosine-protein kinase CAK) (Cell adhesion kinase) (Tyrosine kinase DDR) (Discoidin receptor tyrosine kinase) (TRK E) (Protein-tyrosine kinase RTK 6) (CD167a antigen)
8	345	EPB2_HUMAN	3,76	1,04	3	TPGMKIYID- PFTY	ephrin type-B receptor 2 precursor (Tyrosine-protein kinase receptor EPH-3) (DRT) (Receptor protein-tyrosine kinase HEK5) (ERK)
9	111 4	KP58_HUMAN	3,74	0,40	2	RIEEGTYGV- VYRA	galactosyltransferase associated protein kinase p58/GTA (Cell division cycle 2-like 1) (CLK-1) (p58 CLK-1)
10	548	INR1_HUMAN	3,71	0,57	3	SSSIDEYFSE- QPL	interferon-alpha/beta receptor alpha chain precursor (IFN-alpha-REC)
11	341	EPB1_HUMAN	3,69	1,09	3	SPGMKIYID- PFTY	ephrin type-B receptor 1 precursor (Tyrosine-protein kinase receptor EPH-2) (NET) (HEK6) (ELK)
12	327	EPA4_HUMAN	3,35	1,06	3	NQGVRTYV- DPFTY	ephrin type-A receptor 4 precursor (Tyrosine-protein kinase receptor SEK) (Receptor protein-tyrosine kinase HEK8)
13	684	AD15_HUMAN	3,29	0,17	2	VMLGAGY- WYRRL	ADAM 15 precursor (A disintegrin and metalloproteinase domain 15) (Metalloproteinase-like)

14	115	FGR1_HUMAN	3,26	0,87	3	LTSNQEYLD-LSMP	basic fibroblast growth factor receptor 1 precursor (FGFR-1) (bFGF-R) (Fms-like tyrosine kinase-2) (c-fgr)
15	175	C79A_HUMAN	3,23	1,12	3	YEDENLYE-GLNLD	B-cell antigen receptor complex associated protein alpha-chain precursor (Ig-alpha) (MB-1 membrane glycoprotein) (Surface-Ig associated protein) (Membrane-bound immunoglobulin associated protein) (CD79a)
16	362	EPB4_HUMAN	3,21	1,01	3	GHGTKVYI-DPFTY	ephrin type-B receptor 4 precursor (Tyrosine-protein kinase receptor HTK)
17	101	PIG2_HUMAN	3,17	0,81	3	RDINSLYDV-SRMY	1-phosphatidylinositol 4,5-bisphosphate phosphodiesterase gamma-2 (Phospholipase C-IV)
18	710	TIE2_HUMAN	3,02	0,87	3	LYEKFTYA-GIDCS	angiopoietin 1 receptor precursor (Tyrosine-protein kinase receptor TIE-2) (Tyrosine-protein kinase receptor TEK) (P14TEK) (Tunica interna endothelial cell kinase)
19	653	MK13_HUMAN	3,01	0,53	3	DAEMTGYV-VTRWY	mitogen-activated protein kinase 13 (Stress-activated protein kinase-4) (Mitogen-activated protein kinase p38 delta) (MAP kinase p38 delta)
20	357	CDN1_HUMAN	2,96	1,02	3	GRKRRQTS-MTDFY	cyclin-dependent kinase inhibitor 1 (Melanoma differentiation associated protein 6) (MDA-6) (P21) (CDK-interacting protein 1)
21	651	MK12_HUMAN	2,73	0,43	3	DSEMTGYV-VTRWY	mitogen-activated protein kinase 12 (Extracellular signal-regulated kinase 6) (ERK-6) (ERK5) (Stress-activated protein kinase-3) (Mitogen-activated protein kinase p38γ) (MAP kinase p38γ)
22	656	MK07_HUMAN	2,73	0,28	3	QYFMTEYV-ATRWWY	mitogen-activated protein kinase 7 (Extracellular signal-regulated kinase 5) (ERK-5) (ERK4) (BMK1 kinase)
23	376	ERB4_HUMAN	2,67	1,11	3	VAENPEYLS-EFSL	ERBB-4 receptor protein-tyrosine kinase precursor (p180erbB4) (Tyrosine kinase-type cell surface receptor HER4)
24	410	FAK2_HUMAN	2,59	0,89	3	YIEDEDYK-ASVT	focal adhesion kinase 2 (FADK 2) (Proline-rich tyrosine kinase 2) (Cell adhesion kinase beta) (CAK beta)
25	117	TRKB_HUMAN	2,57	0,37	3	GMSRDVYS-TDYR	BDNF/NT-3 growth factors receptor precursor (TrkB tyrosine kinase) (GP145-TrkB) (Trk-B)
26	358	CDN1_HUMAN	2,54	0,16	2	RKRRQTS-MTDFYH	cyclin-dependent kinase inhibitor 1 (Melanoma differentiation associated protein 6) (MDA-6) (P21) (CDK-interacting protein 1)
27	899	A008-C	2,53	0,30	2	YEPETVYEV-AGAG	cortactin
28	347	EPB3_HUMAN	2,50	1,13	3	APGMKVYI-DPFTY	ephrin type-B receptor 3 precursor (Tyrosine-protein kinase receptor HEK-2)

29	542	IG1R_HUMAN	2,35	0,48	3	DIYETDYR- KGGK	insulin-like growth factor I receptor precursor
30	375	ERB4_HUMAN	2,35	1,14	3	TLQHPDY- LQEYST	ERBB-4 receptor protein-tyrosine kinase precursor (p180erbB4) (Tyrosine kinase-type cell surface receptor HER4)
31	468	A066-C	2,27	0,48	2	AFDNLYY- WDDQPP	ErbB-2 receptor protein-tyrosine kinase precursor
32	855	CDK2_HUMAN	2,25	0,65	3	KIGEGTYG- VYKA	cell division protein kinase 2 (p33 protein kinase)
33	168	CDC2_HUMAN	2,21	0,70	3	EKIGEGTYG- VVYK	cell division control protein 2 homolog (P34 protein kinase) (Cyclin-dependent kinase 1) (CDK1)
34	550	MINK_HUMAN	2,18	0,58	3	QARVLESY- RSCYV	IsK slow voltage-gated potassium channel protein (Minimal potassium channel) (MinK)
35	746	A002-C	2,15	0,86	3	SSDGHEYI- YVDPM	beta platelet-derived growth factor receptor precursor
36	745	TRKB_HUMAN	2,10	0,79	3	VYSTDYR- VGGHT	BDNF/NT-3 growth factors receptor precursor (Trk tyrosine kinase) (GP145-TrkB) (Trk-B)
37	101 4	STK9_HUMAN	2,03	0,12	3	NANYTEYV- ATRWY	serine/threonine-protein kinase 9
38	514	IRS1_HUMAN	1,99	0,35	3	LENGLN- YIDLVL	insulin receptor substrate-1 (IRS-1)
39	262	DCX_HUMAN	1,93	0,27	3	IVYAVSSD- RFRSF	doublecortin (Lissencephalin-X) (Lis-X) (Doublin)
40	105 2	SPIH_HUMAN	1,83	0,09	3	FDDDFHIY- VYDLV	spindlin homolog (Protein DXF34)
41	711	TIE2_HUMAN	1,81	0,08	3	MTCAEY- EKLPQG	angiopoietin 1 receptor precursor (Tyrosine-protein kinase receptor TIE-2) (Tyrosine-protein kinase receptor TEK) (P14TEK) (Tunica interna endothelial cell kinase)
42	113 5	TXK_HUMAN	1,72	0,35	3	YVLDDEY- VSSFGA	tyrosine-protein kinase TXK
43	43	ACHD_HUMAN	1,65	0,15	3	ISKAEEY- FLKSR	acetylcholine receptor protein
44	530	A061-A	1,65	0,12	3	LAVSEEY- LDLRLT	fibroblast growth factor receptor 4 precursor (FGFR-4)
45	182	CDK5_HUMAN	1,63	0,19	3	EKIGEGTYG- TVFK	cell division protein kinase 5 (Tau protein kinase II catalytic subunit) (TPKII catalytic subunit) (Serine/threonine-protein kinase PSSALRE)
46	113 3	ROR1_HUMAN	1,63	0,21	3	EIYSADY- YRVQSK	tyrosine-protein kinase transmembrane receptor ROR1 precursor (Neurotrophic tyrosine kinase)
47	983	RRPP_HRSV	1,51	0,20	3	NNEESSYS- YEEI	RNA polymerase alpha subunit (Phosphoprotein P)
48	138	A003-A	1,49	0,12	3	GASTGIY- EALCLR	alpha enolase
49	313	P53_HUMAN	1,48	0,37	3	LSQETFS- DLWKL	cellular tumor antigen p53 (Tumor suppressor p53) (Phosphoprotein p53)
50	256	DDR2_HUMAN	1,48	0,25	3	NLYSGDY- YRIQGR	discoidin domain receptor 2 precursor (Receptor protein-tyrosine kinase TKT) (Tyrosine-protein kinase TYRO 10) (Neurotrophic tyrosine kinase)

Myt1 Chip II

#	ID	Name	Mean Index	SD	N	Sequence	FullName
1	133	JC4503	4,93	0,64	3	WKYLYRSP-TDFMR	macrophage maturation-associated transcript dd3f protein
2	766	RHOA_HUMAN	4,70	1,69	3	ARRGKKKS-GCLVL	transforming protein RhoA (H12)
3	150	MK14_HUMAN	3,83	1,20	3	DDEMTGYV-ATRWW	mitogen-activated protein kinase 14 (Mitogen-activateprotein kinase p38) (MAP kinase p38) (Cytokine suppressive antiinflammatory drug binding protein) (CSAID binding protein) (CSBP(MAX-interacting protein 2) (MAP kinase MXI2)
4	1005	JS0648	3,45	0,49	3	NPNYGYTS-YDTFS	sodium channel alpha chain
5	1077	JC4812	3,35	0,50	3	GYATKYTS-RSRCY	hyaluronan synthase
6	442	A051-F	3,27	0,24	3	YPNDSVYA-NWMLS	proto-oncogene tyrosine-protein kinase receptor Ret precursor
7	149	MK11_HUMAN	3,25	1,01	3	DEEMTGYV-ATRWW	mitogen-activated protein kinase 11 (Mitogen-activateprotein kinase p38 beta) (MAP kinase p38 beta) (p38b) (p38-2) (Stressactivated protein kinase-2)
8	968	JH0826	2,96	0,67	3	AFLLESTM-NEYR	glutamate ionotropic receptor EAA1 chain precursor
9	654	STHM_HUMAN	2,87	1,10	3	AEERRKSHE-AEVL	stathmin (Phosphoprotein P19) (PP19) (Oncoprotein 18) (OP18(Leukemia-associated phosphoprotein P18) (PP17) (Prosolin(Metablastin) (PR22 protein)
10	211	JC2522	2,79	0,86	3	RKKLDESIY-DVAF	nuclear autoantigen
11	967	JH0826	2,53	0,69	3	QNSRYQTY-QRMWN	glutamate ionotropic receptor EAA1 chain precursor
12	536	TVHURS	2,43	0,16	3	GLARDIYKN-DYYR	kinase-related protein ros-1 precursor
13	469	KRAF_HUMAN	2,31	0,10	2	QRDSSYYW-EIEAS	RAF proto-oncogene serine/threonine-protein kinase (RAF-1) (C-RAF)
14	32	A46612	2,30	0,59	3	YATVKQSS-VDIYF	N-methyl-D-aspartate receptor chain 1 precursor
15	56	A040-I	2,27	0,71	3	LGFKRSYEE-HIPY	insulin receptor (IR)
16	496	A38197	2,13	0,07	3	GIIGEGTYG-QVYK	protein kinase cdc2-like
17	17	TRKA_HUMAN	2,11	0,55	3	IIENPQYFSD-ACV	high affinity nerve growth factor receptor precursor (TRK1 transforming tyrosine kinase protein) (p140-TrkA) (Trk-A)
18	147	MK01_HUMAN	2,11	0,57	3	TGFLTEYVA-TRWY	mitogen-activated protein kinase 1 (Extracellular signalregulated kinase 2) (ERK-2) (Mitogen-activated protein kinase 2) (MAkinase 2) (MAPK 2) (p42-MAPK) (ERT1)
19	1137	A46226	2,07	1,06	3	RVLLRPSRR-VRSQ	somatostatin receptor 3

20	835	HSHUP2	2,05	0,60	3	YRRRHCSR-RRLHR	sperm histone P2 precursor
21	16	TRKA_HUMAN	2,00	0,51	3	DIYSTDYR-VGGR	high affinity nerve growth factor receptor precursor (TRK1 transforming tyrosine kinase protein) (p140-TrkA) (Trk-A)
22	834	HSHUP1	1,97	0,64	3	RCCRSQSRS-RYYR	sperm histone P1
23	72	A54277	1,91	0,58	2	LYNRKTSR-VYKYC	transcription adaptor protein p300
24	18	TRKA_HUMAN	1,83	0,21	3	IYSTDYR-VGGRT	high affinity nerve growth factor receptor precursor (TRK1 transforming tyrosine kinase protein) (p140-TrkA) (Trk-A)
25	6	A009-B	1,82	0,64	3	DMYDKEYY-SVHNK	hepatocyte growth factor receptor precursor (HGF-SF receptor)
26	756	JC2522	1,77	0,27	2	QWWNMPS-SVDPY	nuclear autoantigen (striatin, calmodulin binding protein 3)
27	422	S68236	1,77	0,20	3	WKGVKSTG-KVVYF	betaine/GABA transport protein BGT-1
28	105	A49368	1,75	0,51	3	VRWLQESR-RSRKL	vesicle monoamine transporter
29	131	O60491	1,74	0,42	3	DQGDMTP-QFTPY	mitogen activated protein kinase activated protein kinase
30	969	A45100	1,74	0,36	3	GLNQSTPT-HAAG	mitogen-activated protein kinase kinase 1
31	965	JH0826	1,73	0,15	3	FLVARLTPY-EWYS	glutamate ionotropic receptor EAA1 chain precursor
32	971	A46612	1,72	0,32	2	QKCDLVTT-GELFF	N-methyl-D-aspartate receptor chain 1 precursor
33	41	B059-B	1,70	0,42	3	GGVKRISGL-IYEE	histone H4
34	531	TVHUTT	1,69	0,21	3	LAQAPPVYL-DVLG	nerve growth factor receptor
35	114 4	S68442	1,69	0,28	3	ASSQDCYDI-PRAF	Grb2-associated binder-1 protein
36	495	S71363	1,68	0,07	3	ALRRRRTL-ELYT	probable ATP-binding cassette transporter ABC-3
37	646	S39162	1,68	0,32	2	LYNRKTSR-VYKFC	transcription coactivator CREB-binding protein
38	428	JH0565	1,68	0,16	3	LLWLVSST-HRLL	calcium channel alpha-2b chain precursor
39	521	RBL2_HUMAN	1,67	0,52	3	MDAPPLSPY-PFVR	retinoblastoma-like protein 2 (130 kDa retinoblastoma-associateprotein) (PRB2) (P130) (RBR-2)
40	34	A46612	1,66	0,08	2	PRLRNPSDK-FIYA	N-methyl-D-aspartate receptor chain 1 precursor
41	63	JS0648	1,66	0,26	3	GLSVLRSFR-LLRV	sodium channel alpha chain
42	717	S74251	1,65	0,43	3	AFLRSGSVY-EPLK	phosphorylase kinase beta chain
43	384	KPCE_HUMAN	1,64	0,44	3	NGVTTTTFC-GTPD	protein kinase C
44	330	B159-B	1,64	0,12	3	RSKGQESFK-KQEK	nucleophosmin (nucleolar phosphoprotein B23)
45	106	A49368	1,64	0,26	2	LQESRRSRK-LILF	vesicle monoamine transporter
46	533	I73632	1,62	0,22	3	LGKATPIYL-DILG	neurotrophin-3 receptor precursor

47	1068	A47430	1,61	0,24	3	YVQLPRSRP-ALEL	gastrin/cholecystokinin receptor B
48	961	A46226	1,60	0,08	3	TGEKSSTMR-ISYL	somatostatin receptor 3
49	1113	JS0670	1,59	0,44	3	GPARLEYEY-ENEKK	insulin receptor substrate-1
50	1119	A57160	1,57	0,11	3	KYKRLRSM-TDVYL	chemokine (C-C) receptor 4

Weel Chip I

#	ID	Name	Mean Index	SD	N	Sequence	FullName
1	509	INSR_HUMAN	1,56	0,17	3	GMTRDIYET-DYYR	insulin receptor (IR)
2	577	LEPR_HUMAN	1,34	2,27	3	RQPFVKYA-TLISN	leptin receptor precursor (LEP-R) (OB receptor) (OB-R) (HuB219)
3	505	IKKA_HUMAN	1,34	1,87	3	KDVDQGS-CTSFV	inhibitor of nuclear factor kappa-B kinase alpha subunit (I kappa-B kinase alpha) (IkbKA) (IKK-alpha) (IKK-A) (IkkappaB kinase) (I-kappa-B kinase 1) (IKK1) (Conserved helix-loop-helix ubiquitous kinase) (Nuclear factor NFkappaB inhibitor kinase alpha) (NFKBIKA)
4	410	FAK2_HUMAN	1,33	0,04	3	YIEDEDYK-ASVT	focal adhesion kinase 2 (FADK 2) (Proline-rich tyrosine kinase 2) (Cell adhesion kinase beta) (CAK beta)
5	613	TAU_HUMAN	1,29	2,16	3	DRSGYSSP-SPGT	microtubule-associated protein tau (Neurofibrillary tangle protein) (Paired helical filament-tau) (PHF-tau)
6	983	RRPP_HRSV	1,28	0,17	3	NNEEESYS-YEEI	RNA polymerase alpha subunit (Phosphoprotein P)
7	357	CDN1_HUMAN	1,27	0,09	2	GRKRRQTS-MTDFY	cyclin-dependent kinase inhibitor 1 (Melanoma differentiation associated protein 6) (MDA-6) (P21) (CDK-interacting protein 1)
8	345	EPB2_HUMAN	1,25	0,10	3	TPGMKIYID-PFTY	ephrin type-B receptor 2 precursor (Tyrosine-protein kinase receptor EPH-3) (DRT) (Receptor protein-tyrosine kinase HEK5) (ERK)
9	341	EPB1_HUMAN	1,24	0,12	3	SPGMKIYID-PFTY	ephrin type-B receptor 1 precursor (Tyrosine-protein kinase receptor EPH-2) (NET) (HEK6) (ELK)
10	684	AD15_HUMAN	1,22	0,12	2	VMLGAGY-WYRRL	ADAM 15 precursor (A disintegrin and metalloproteinase domain 15) (Metalloproteinase-like)
11	653	MK13_HUMAN	1,20	0,11	3	DAEMTGY-VVTRWY	mitogen-activated protein kinase 13 (Stress-activated protein kinase-4) (Mitogen-activated protein kinase p38 delta) (MAP kinase p38 delta)
12	101	PIG2_HUMAN	1,18	0,19	3	RDINSLYDV-SRMY	1-phosphatidylinositol 4,5-bisphosphate phosphodiesterase gamma-2 (Phospholipase C-IV)

13	659	MK09_HUMAN	1,18	0,14	3	NFMMPYV-VTRY	mitogen-activated protein kinase 9 (Stress-activated protein kinase JNK2) (c-Jun N-terminal kinase 2) (JNK-55)
14	507	IKKE_HUMAN	1,17	0,02	3	DDEKFSV-VGTEE	inhibitor of nuclear factor kappa-B kinase epsilon subunit (I kappa-B kinase epsilon) (IkbKE) (IKK-epsilon) (IKK-E) (Inducible I kappa-B kinase) (IKK-i)
15	369	DDR1_HUMAN	1,15	0,31	3	GMSRNLYA-GDYR	epithelial discoidin domain receptor 1 precursor (Tyrosine-protein kinase CAK) (Cell adhesion kinase) (Tyrosine kinase DDR) (Discoidin receptor tyrosine kinase) (TRK E) (Protein-tyrosine kinase RTK 6) (CD167a antigen)
16	376	ERBB4_HUMAN	1,15	0,11	3	VAENPEYLS-EFSL	ERBB-4 receptor protein-tyrosine kinase precursor (p180erbB4) (Tyrosine kinase-type cell surface receptor HER4)
17	482	TRKA_HUMAN	1,14	0,23	3	GMSRDIYST-DYR	high affinity nerve growth factor receptor precursor (TRK1 transforming tyrosine kinase protein) (p140-TrkA) (Trk-A)
18	685	MPP8_HUMAN	1,13	1,89	3	SSVLNDSPF-PEDD	M-phase phosphoprotein 8 (Fragment)
19	168	CDC2_HUMAN	1,12	0,17	3	EKIGEGTYG-VVYK	cell division control protein 2 homolog (P34 protein kinase) (Cyclin-dependent kinase 1) (CDK1)
20	651	MK12_HUMAN	1,09	0,16	3	DSEMTGYV-VTRWY	mitogen-activated protein kinase 12 (Extracellular signal-regulated kinase 6) (ERK-6) (ERK5) (Stress-activated protein kinase-3) (Mitogen-activated protein kinase p38 gamma) (MAP kinase p38γ)
21	175	C79A_HUMAN	1,07	0,25	3	YEDENLYE-GLNLD	B-cell antigen receptor complex associated protein alpha-chain precursor (Ig-alpha) (MB-1 membrane glycoprotein) (Surface-IgM associated protein) (Membrane-bound immunoglobulin associated protein) (CD79a)
22	542	IG1R_HUMAN	1,05	0,04	3	DIYETDYR-KGGK	insulin-like growth factor I receptor
23	371	DDR1_HUMAN	1,04	0,10	3	LYAGDYR-VQGRA	epithelial discoidin domain receptor 1 precursor (Tyrosine-protein kinase CAK) (Cell adhesion kinase) (Tyrosine kinase DDR) (Discoidin receptor tyrosine kinase) (TRK E) (Protein-tyrosine kinase RTK 6) (CD167a antigen)
24	117	TRKB_HUMAN	1,02	0,06	3	GMSRDVYS-TDYR	BDNF/NT-3 growth factors receptor precursor (TrkB tyrosine kinase) (GP145-TrkB) (Trk-B)
25	548	INR1_HUMAN	1,02	0,23	3	SSSIDEYFS-EQPL	interferon-alpha/beta receptor alpha chain precursor (IFNα-REC)

26	757	NEUM_HUMAN	0,99	1,65	3	TETGESSQA-EENI	neuromodulin (Axonal membrane protein GAP-43) (PP46) (B-50) (Protein F1) (Calmodulin-binding protein P-57)
27	287	CDC2_HUMAN	0,96	0,03	2	KIGEGTYGV-VYKG	cell division control protein 2 homolog (P34 protein kinase) (Cyclin-dependent kinase 1) (CDK1)
28	180	TRKB_HUMAN	0,96	0,09	2	DVYSTDYI-RVGGH	BDNF/NT-3 growth factors receptor precursor (Trk tyrosine kinase) (GP145-TrkB) (Trk-B)
29	347	EPB3_HUMAN	0,96	0,02	3	APGMKVYI-DPFTY	ephrin type-B receptor 3 precursor (Tyrosine-protein kinase receptor HEK-2)
30	973	RBB8_HUMAN	0,94	1,51	3	DPGADLSQ-YKMDV	retinoblastoma-binding protein 8 (RBBP-8) (CtBP interacting protein) (CtIP) (Retinoblastoma-interacting protein and myosin-like) (RIM)
31	526	IRR_HUMAN	0,87	0,16	3	DVYETDYY-RKGGK	insulin receptor-related protein (IRR) (IR-related receptor)
32	291	DYRA_HUMAN	0,81	0,62	3	GQRIYQYIQ-SRFY	dual-specificity tyrosine-phosphorylation regulated kinase 1A (Protein kinase minibrain homolog) (MNBH) (HP86) (Dual specificity YAK1-related kinase)
33	262	DCX_HUMAN	0,77	0,61	3	IVYAVSSDR-FRSF	doublecortin (Lissencephalin-X) (Lis-X) (Doublin)
34	362	EPB4_HUMAN	0,76	0,55	3	GHGTKVYI-DPFTY	ephrin type-B receptor 4 precursor (Tyrosine-protein kinase receptor HTK)
35	937	KPYR_HUMAN	0,76	1,00	3	GYLRRASV-AQLTQ	pyruvate kinase
36	602	VINC_HUMAN	0,75	0,15	3	SFLDSGYRI-LGAV	vinculin (Metavinculin)
37	657	MK08_HUMAN	0,75	0,09	3	SFMMTPYV-VTRYI	mitogen-activated protein kinase 8 (Stress-activated protein kinase JNK1) (c-Jun N-terminal kinase 1) (JNK-46)
38	605	CCAC_HUMAN	0,75	0,08	3	SLGRRASF-HLECL	voltage-dependent L-type calcium channel alpha-1C subunit (Calcium channel)
39	981	RRPP_HRSV	0,74	0,62	3	EEESSYSYE-EIND	RNA polymerase alpha subunit (Phosphoprotein P)
40	514	IRS1_HUMAN	0,73	0,17	3	LENGLNLI-DLDLV	insulin receptor substrate-1 (IRS-1)
41	1009	SCG1_HUMAN	0,71	1,08	3	QINKRASG-QAFEL	SCG10 protein (Superior cervical ganglion-10 protein)
42	327	EPA4_HUMAN	0,71	0,54	3	NQGVRTYV-DPFTY	ephrin type-A receptor 4 precursor (Tyrosine-protein kinase receptor SEK) (Receptor protein-tyrosine kinase HEK8)
43	182	CDK5_HUMAN	0,71	0,67	3	EKIGEGTY-GTVFK	cell division protein kinase 5 (Tau protein kinase II catalytic subunit) (TPKII catalytic subunit) (Serine/threonine-protein kinase PSSALRE)

44	256	DDR2_HUMAN	0,68	0,49	3	NLYSGDYIY-RIQGR	discoidin domain receptor 2 precursor (Receptor protein-tyrosine kinase TKT) (Tyrosine-protein kinase TYRO 10) (Neurotrophic tyrosine kinase)
45	656	MK07_HUMAN	0,67	0,50	3	QYFMTEYV-ATRWY	mitogen-activated protein kinase 7 (Extracellular signal-regulated kinase 5) (ERK-5) (ERK4) (BMK1 kinase)
46	595	MGP_HUMAN	0,67	0,54	3	CYESHESM-ESYEL	matrix Gla-protein precursor (MGP)
47	1115	B165-A	0,66	0,13	2	RIRRRASQ-LKVKI	gamma-aminobutyric-acid receptor beta-1 subunit precursor
48	701	ACM4_HUMAN	0,65	0,19	3	NATFKKTF-RHLLL	muscarinic acetylcholine receptor M4
49	550	MINK_HUMAN	0,65	0,54	3	QARVLESY-RSCYV	IsK slow voltage-gated potassium channel protein (Minimal potassium channel) (MinK)
50	1114	KP58_HUMAN	0,65	0,87	2	RIEEGTYG-VVYRA	galactosyltransferase associated protein kinase p58/GTA (Cell division cycle 2-like 1) (CLK-1) (p58 CLK-1)

Wee1 Chip II

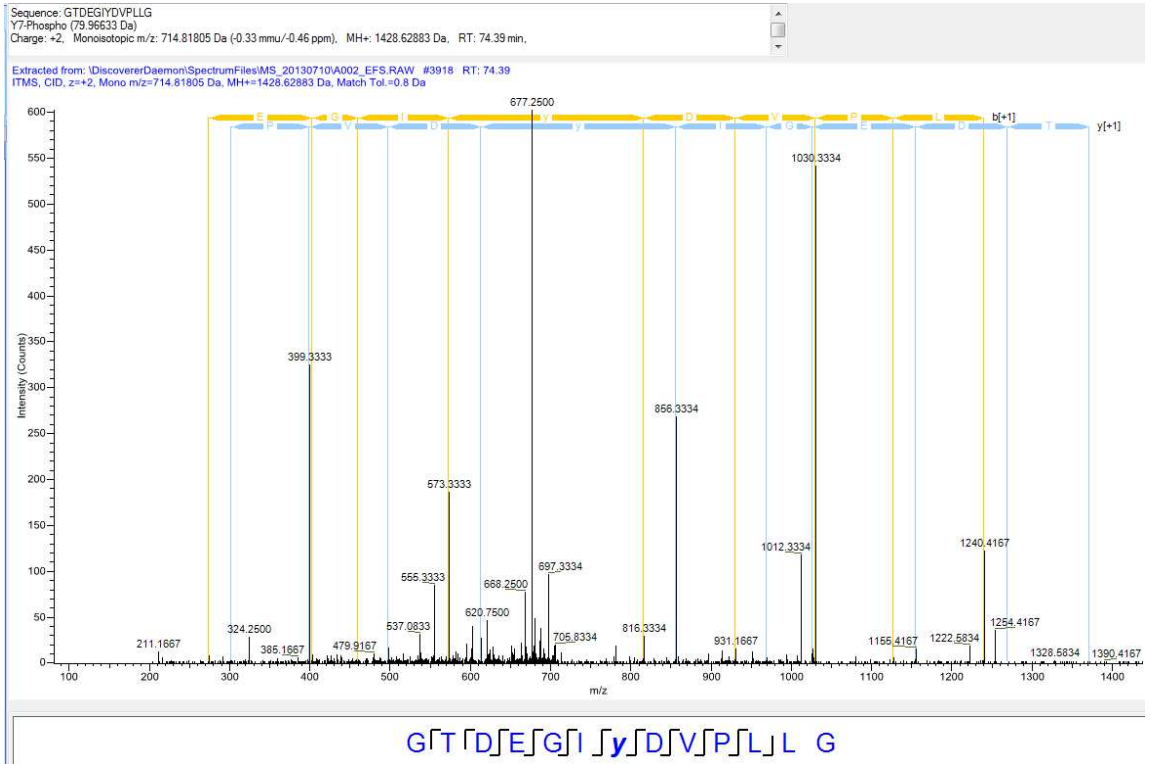
#	ID	Name	Mean Index	SD	N	Sequence	FullName
1	18	TRKA_HUMAN	1,05	0,17	3	IYSTDYIRV-GGRT	high affinity nerve growth factor receptor precursor (TRK1 transforming tyrosine kinase protein) (p140-TrkA) (Trk-A)
2	16	TRKA_HUMAN	0,87	0,10	3	DIYSTDYIRV-GGR	high affinity nerve growth factor receptor precursor (TRK1 transforming tyrosine kinase protein) (p140-TrkA) (Trk-A)
3	73	IRS1_HUMAN	0,86	0,10	2	HRLSTSSG-RLLY	insulin receptor substrate-1 (IRS-1)
4	502	JH0371	0,83	0,00	2	DGISYTTLR-FPEM	B-cell adhesion protein CD22 beta splice form precursor
5	34	A46612	0,81	0,01	2	PRLRNPSDK-FIYA	N-methyl-D-aspartate receptor chain 1 precursor
6	133	JC4503	0,76	0,08	3	WKYLYRSP-TDFMR	macrophage maturation-associated transcript dd3f protein
7	756	JC2522	0,74	0,15	2	QWWNMPS-PSVDPY	nuclear autoantigen (striatin, calmodulin binding protein 3)
8	330	B159-B	0,68	0,11	3	RSKGQESFK-KQEK	nucleophosmin (nucleolar phosphoprotein B23)
9	348	PVR2_HUMAN	0,68	0,07	3	GEEEEYLD-KINP	poliovirus receptor related protein 2 precursor (Herpes virus entry mediator B) (HveB) (Nectin 2) (CD112 antigen)
10	401	KPCT_HUMAN	0,67	0,09	3	GDAKTNTF-CGTPD	protein kinase C
11	131	O60491	0,67	0,26	3	DQGDLMTP-QFTPY	mitogen activated protein kinase activated protein kinase
12	41	B059-B	0,66	0,25	3	GGVKRISGL-IYEE	histone H4
13	121	A065-C	0,65	0,07	3	HAEEAALYK-NLLHS	mast/stem cell growth factor receptor precursor (SCFR)

14	534	A41527	0,65	0,11	3	DCLDGLYA-LMSRC	protein-tyrosine kinase axl precursor
15	504	PC4035	0,63	0,20	2	PYLRRRTT-MATRT	cell-cycle-dependent 350K nuclear protein
16	87	KLC2_HUMAN	0,63	0,16	3	KDKRRDSA-PYGEEY	kinesin light chain 2 (KLC 2)
17	484	RB_HUMAN	0,61	0,11	3	GGNIYISPL-KSPY	retinoblastoma-associated protein (PP110) (P105-RB)
18	108	A49368	0,60	0,05	2	VDLRHVSV-YGSVY	vesicle monoamine transporter
19	314	QRHUFT	0,59	0,08	3	YIHIYLTVR-NPNI	follicle-stimulating hormone receptor precursor
20	56	A040-I	0,57	0,47	3	LGFKRSYE-EHIPY	insulin receptor (IR)
21	17	TRKA_HUMAN	0,57	0,15	3	IENPQYFSD-ACV	high affinity nerve growth factor receptor precursor (TRK1 transforming tyrosine kinase protein) (p140-TrkA) (Trk-A)
22	378	KPC2_HUMAN	0,56	0,44	3	RHPPVLTPP-DQEV	protein kinase C
23	825	QRHUMT	0,56	0,17	3	PQERMFTID-PKVY	microtubule-associated protein 2
24	719	S71339	0,55	0,08	2	ASGKRVS-ALS-YSI	urea transport protein
25	211	JC2522	0,55	0,37	3	RKKLDESIY-DVAF	nuclear autoantigen
26	63	JS0648	0,54	0,11	3	GLSVLRSFR-LLRV	sodium channel alpha chain
27	1119	A57160	0,54	0,11	3	KYKRLRSM-TDVYL	chemokine (C-C) receptor 4
28	612	JS0648	0,54	0,03	2	AYVKKESGI-DDMF	sodium channel alpha chain
29	386	JN0268	0,53	0,15	3	RTGKRLTR-AQLIT	serotonin receptor 1B
30	32	A46612	0,51	0,10	3	YATVKQSS-VDIYF	N-methyl-D-aspartate receptor chain 1 precursor
31	287	A48222	0,51	0,08	2	LPIRRKTRS-LPDR	dematin 48K chain
32	392	JC2495	0,49	0,07	3	LKYRTKTR-ASATI	histamine H1 receptor
33	533	I73632	0,48	0,08	3	LGKATPIYL-DILG	neurotrophin-3 receptor precursor
34	95	B176-G	0,46	0,24	3	SVTVTRSY-RSVGG	lamin A (70 kD lamin)
35	602	S68236	0,46	0,17	3	PRQLRKSG-RRELL	betaine/GABA transport protein BGT-1
36	432	JS0648	0,46	0,27	2	NISALRTFR-VLRA	sodium channel alpha chain
37	601	JC2386	0,45	0,15	3	VWKGVKST-GKIVY	creatine transporter BS2M
38	395	A41795	0,45	0,02	2	ARYRRPTV-AKVVN	somatostatin receptor 1
39	450	AKT3_HUMAN	0,44	0,30	3	PHFPQFSYS-ASGR	RAC-gamma serine/threonine protein kinase (RAC-PK-gamma) (Protein kinase Akt-3) (Protein kinase B)
40	111	B176-K	0,44	0,31	3	GDDPLLYT-RFPPK	lamin A (70 kD lamin)
41	140	JC4389	0,44	0,09	3	RISIFLSMQ-DEIE	5-formyltetrahydrofolate cyclo-ligase

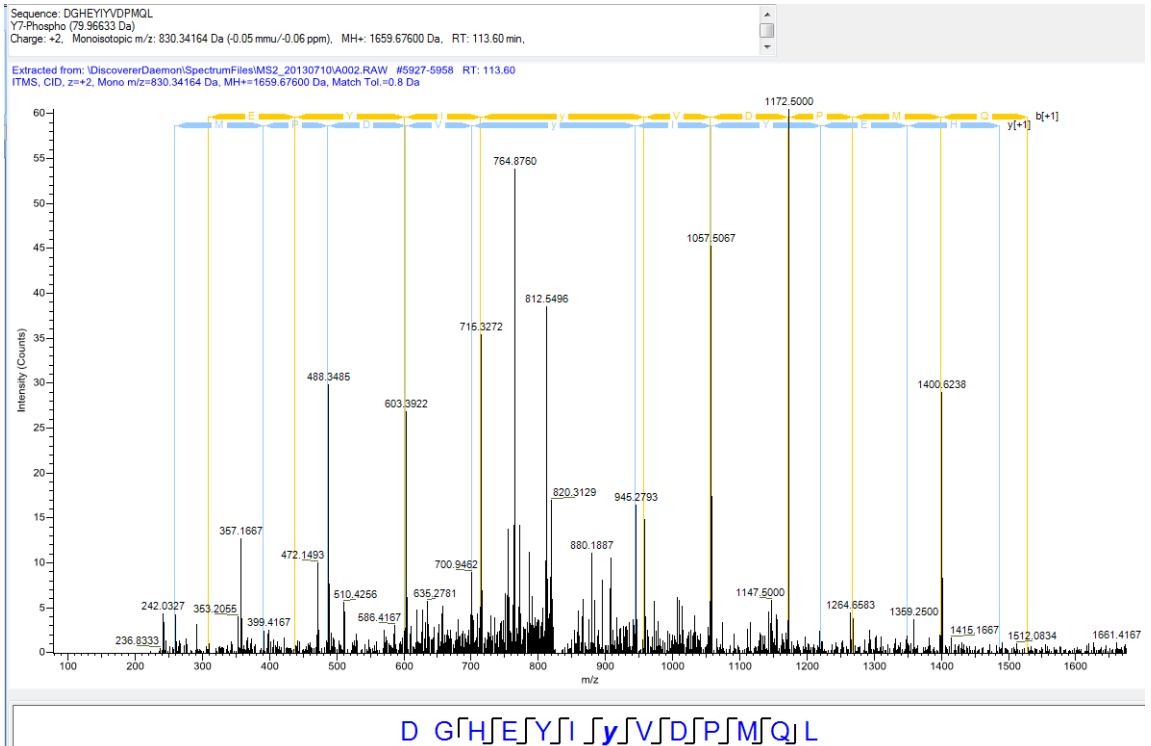
42	412	PTEN_HUMAN	0,44	0,09	3	PDHYRYSD- TTDSD	protein-tyrosine phosphatase PTEN (Mutated in multiple advanced cancers 1)
43	359	JC4776	0,44	0,04	2	WRHLTPTG- REFEG	limbic-system-associated membrane protein precursor
44	485	RB_HUMAN	0,44	0,34	3	IPHIPRSPYK- FPS	retinoblastoma-associated protein (PP110) (P105-RB)
45	35	A46612	0,44	0,13	2	VLEFEASQK- CDLV	N-methyl-D-aspartate receptor chain 1 precursor
46	531	TVHUTT	0,43	0,11	3	LAQAPPVYL- DVLG	nerve growth factor receptor precursor
47	269	O14974	0,43	0,08	3	REKRRSTGV- SFWT	myosin phosphatase target subunit 1
48	279	A34400	0,43	0,11	3	IKNKKGTDL- WLGV	ezzrin
49	613	CHK2_HUMAN	0,42	0,10	2	QPHGSVTQS- QGSS	serine/threonine-protein kinase Chk2 (Cds1)
50	178	A40409	0,42	0,11	2	LGGRALSN- RQHAS	G-0/G-1 switch regulatory protein 2

MS/MS: Phospho-Peptides

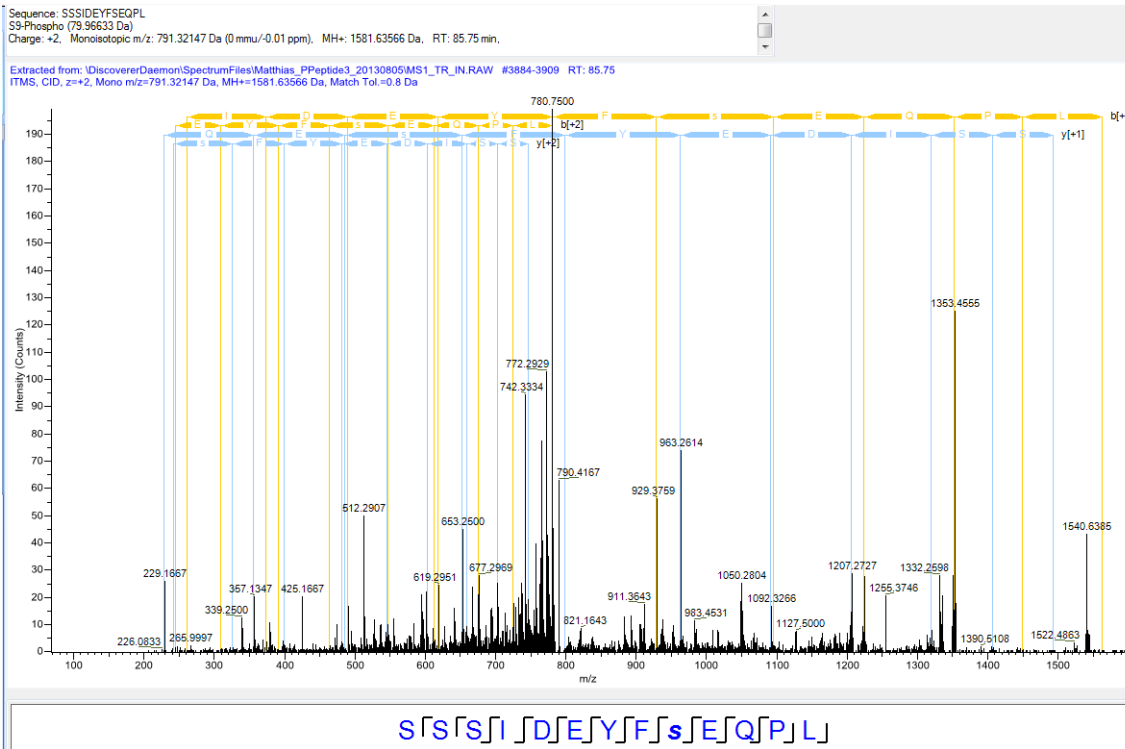
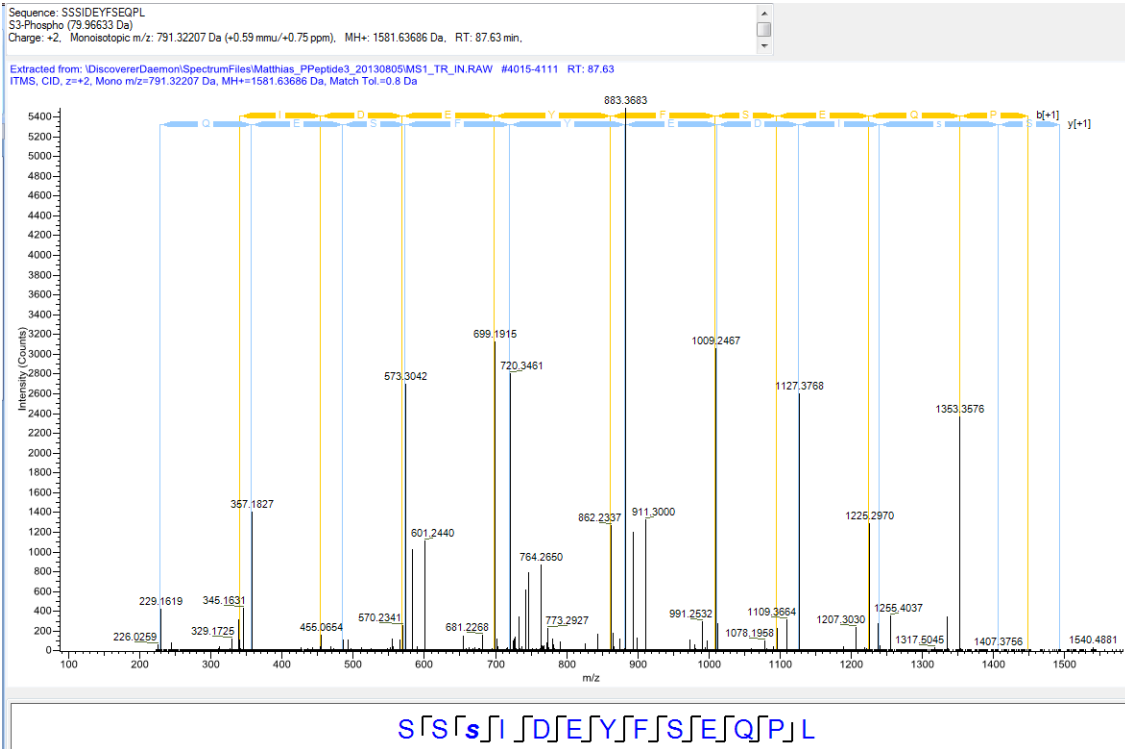
Phospho-EFS_HUMAN_302



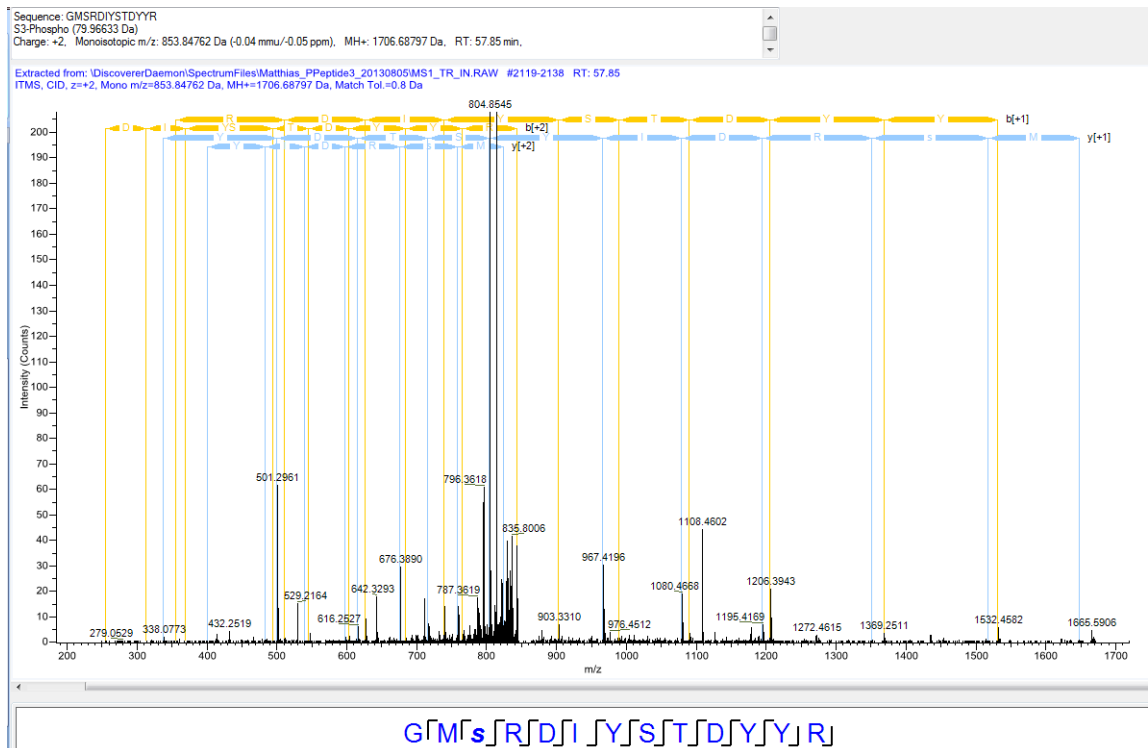
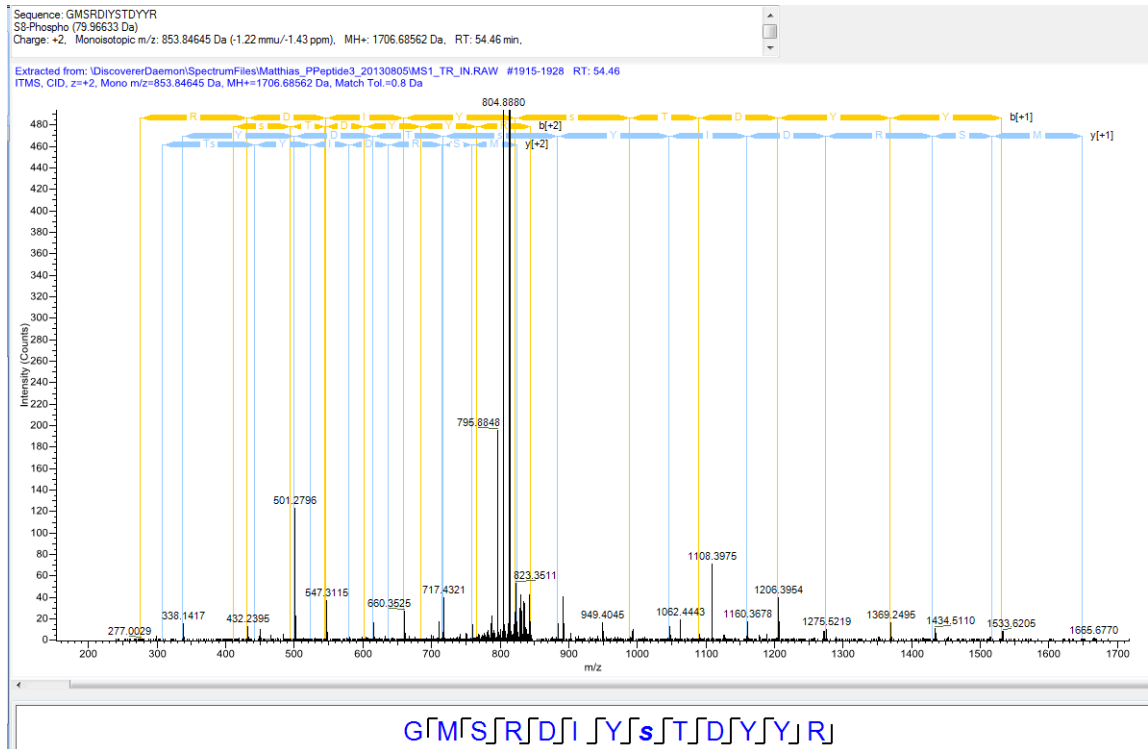
Phospho-A002-D_747



Phospho-INR1_HUMAN_548



Phospho-TRKA_HUMAN_482



Abstract / Zusammenfassung

English:

Myt1 is an important cell cycle regulating kinase. Herein, systematic substrate studies revealed the kinase to be restrictive in terms of substrate acceptance. While simplified proteins (peptides) were not accepted, full-length proteins were efficiently phosphorylated. Since protein substrates are problematic in screening assays, a kinase binding assay based on time-resolved fluorescence resonance energy transfer was established and a first inhibition profile for this kinase was obtained. As an alternate assay, a fluorescence polarization based kinase binding assay was developed and formerly unknown inhibitors were identified. Finally, peptide microarray studies helped resolve the Myt1 substrate issue. Indeed, two peptides derived from this approach could be verified and validated as Myt1 substrates also in solution phase.

Deutsch:

Die humane Myt1 Kinase ist an der Regulation des Zellzyklus beteiligt. Systematische Substratstudien in dieser Arbeit zeigten, dass dieses Enzym restriktiv in der Wahl seiner Substrate agiert. Während vereinfachte Proteine (Peptide) nicht phosphoryliert wurden, erwiesen sich die Vollproteine als gute Substrate. Da die Verwendung von Proteinsubstraten in Screeningassays viele Probleme mit sich bringt, wurde ein zeitaufgelöster Fluoreszenzresonanz-energieübertragung-basierter Kinasebindungsassay etabliert und ein erstes Inhibitionsprofil ermittelt. Als Assayalternative wurde zudem ein auf Fluoreszenzpolarisation basierender Bindungsassay entwickelt und neue, vormals unbekannte Hemmstoffe identifiziert. Schließlich wurden Peptid-Microarrays verwendet, um die Substratproblematik zu lösen. Tatsächlich konnten zwei Peptide aus dieser Herangehensweise auch in Lösung als Myt1 Substrate bestätigt und validiert werden.

Danksagung

Nach dem Hören einer Vorlesung über Assaymethoden in der Wirkstoffentwicklung und ersten kleineren Erfahrungen während eines Studentenpraktikums zu Beginn des Hauptstudiums war klar, dass ich nichts lieber täte, als in diesem Bereich eine eigenständige Forschungsleistung zu erbringen. Leider schien es so, als sei dies mit meinem weiteren Werdegang nicht vereinbar. Doch während des Wahlpflichtfachs Pharmazie, gegen Ende des Hauptstudiums, wurde ich von Dr. Jens Köhler, seinerzeit Postdoc im Arbeitskreis von Prof. M. Jung, angesprochen und auf die Abteilung Medizinische Chemie der MLU Halle-Wittenberg aufmerksam gemacht. Ihm danke ich sehr für diesen entscheidenden Hinweis.

Doch das wäre sinnlos gewesen, hätten nicht mein Doktorvater Prof. W. Sippl und mein direkter Betreuer Dr. M. Schmidt mir das Vertrauen entgegengebracht, hier tatsächlich anfangen zu können und arbeiten zu dürfen. Hierfür und für sämtliche Unterstützung möchte ich mich ausdrücklich bedanken.

Prof. M. A. Glomb vom Institut für Lebensmittelchemie der MLU Halle-Wittenberg danke ich dafür, die breite wissenschaftliche Aufstellung der Lebensmittelchemie wörtlich genommen und mir damit von Beginn an große Steine aus dem Weg geräumt zu haben.

Für immerwährenden Optimismus sowie steten Rat und stete Tat in allen Fragen der Proteinbiochemie, Zellkultur und Proteinexpression danke ich Dr. F. Erdmann (Abteilung Pharmakologie, Institut für Pharmazie, MLU Halle-Wittenberg), ohne den die Arbeit in dieser Form nicht hätte entstehen können.

Auch ohne bioinformatische Unterstützung und die durchgeführten Untersuchungen *in silico* wäre diese Arbeit nicht in ihrer jetzigen Form entstanden. Hierfür danke ich den Theoretikern der Arbeitsgruppe Sippl, wobei insbesondere Dr. K. Wichapong hervorzuheben ist, der immer wieder mit Ideen und großer Kompetenz die Arbeit bereicherte.

Ferner danke ich ausdrücklich Prof. M. Jung von der ALU Freiburg i. Br. und Prof. M. Schutkowski von der MLU Halle-Wittenberg, nicht nur für die Übernahme der Begutachtung, sondern auch für die inhaltliche Bereicherung dieser Arbeit durch Ideen (insbesondere in Sachen LanthaScreen bzw. Peptid-Microarrays) und Nutzungsmöglichkeiten von Geräten.

Dem gesamten Institutsbereich Pharmazeutische Chemie und Klinische Pharmazie des Instituts für Pharmazie möchte ich meinen Dank ausdrücken, da im Rahmen dieser Arbeit sicherlich jede Arbeitsgruppe mich in irgendeiner Form unterstützt hat, sei es durch Geräte (z.B. das NOVOstar Plattenlesegerät der Arbeitsgruppe Prof. P. Imming) oder durch wichtige Zuarbeiten (z.B. die von Dr. C. Ihling, Arbeitsgruppe Prof. A. Sinz, durchgeführten MS-Untersuchungen). Prof. A. Simm von der Abteilung Herz-Thorax-Chirurgie des Uniklinikums Halle danke ich für die Möglichkeit zur Nutzung des Tecan M1000 Plattenlesegerätes.

Dr. S. Pfeiffer und Dominik Schneider bin ich rund um Dot Blots zu Dank verpflichtet.

Für fachlichen Beistand, gute Zusammenarbeit und eine schöne Zeit danke ich den Mitgliedern der Arbeitsgruppe Langner/Dobner, insbesondere Christian Wölk, Patrick Kreideweiß und Nicole Erdmann. Für die Unterstützung in den Bereichen Microarray und Festphasenpeptidsynthese danke ich der Arbeitsgruppe um Prof. M. Schutkowski, insbesondere Antonia Masch, Dr. I. Born und Dr. A. Schierhorn.

Claudia Henze danke ich für die gute und fleißige Zuarbeit im Rahmen ihrer Diplomarbeit.

Auch nicht unerwähnt bleiben soll die Tätigkeit der Korrekturleser, wobei ich hier insbesondere Nora Bilowich zu großem Dank verpflichtet bin.

An der Schnittstelle zwischen Arbeit und Privatleben muss natürlich der Kern der Arbeitsgruppe Schmidt erwähnt werden: Dr. M. Schmidt, Tino Heimburg und Benjamin Sauer. Über weite Teile dieser Arbeit war genau diese Konstellation mit mir gemeinsam im Labor und hat durch geschickten Gebrauch von musikalischer Untermalung und Aroma Nero stets dafür gesorgt, dass Arbeit und Freizeit verschmolzen und zu einer unvergesslichen Zeit wurden.

Meinen Eltern und auch Großeltern kann ich nur danken für die Geduld im Ertragen meines Gejammers, meiner ständigen Abwesenheit und des beständig hohen Stresspegels. Wie viele Staatsexamina und Prüfungen noch kommen, habe ich immer wieder gern erläutert.

Mein größtmöglicher Dank geht an meine jetzige Frau und damalige Freundin Tanja, die 2010 den Weg von Baden-Württemberg nach Halle gegangen ist und mich vorher wie seitdem immer unterstützt und ertragen hat. Ohne sie wäre die Welt grau.

Publikationen

Veröffentlichungen mit Fachbegutachtung (peer-review):

A. Rohe, F. Erdmann, C. Bäßler, K. Wichapong, W. Sippl, M. Schmidt:
In vitro and in silico studies on substrate recognition and acceptance of human PKMYT1, a Cdk1 inhibitory kinase.

Bioorganic & Medicinal Chemistry Letters (2012), Volume 22,1219-1223.

A. Rohe, C. Göllner, K. Wichapong, F. Erdmann, G. M. A. Al-Mazaideh, W. Sippl, M. Schmidt:

Evaluation of potential Myt1 kinase inhibitors by TR-FRET based binding assay.

European Journal of Medicinal Chemistry (2013), Volume 61, 41-48.

A. Rohe, C. Henze, F. Erdmann, W. Sippl, M. Schmidt:

A fluorescence anisotropy based Myt1 kinase binding assay.

ASSAY and Drug Development Technologies (2013), DOI: 10.1089/adt.2013.534

Weitere Originalarbeiten sind in Vorbereitung, bzw. eingereicht.

Poster auf wissenschaftlichen Konferenzen:

DPhG Jahrestagung 04.10. - 07.10.2010, Braunschweig, Germany:

A. Rohe, C. Philipp, P. Balgarov, C. Göllner, G. Al-Mazaideh, F. Erdmann, W. Sippl, H. Rüttinger, M. Schmidt:

Development of a CE based assay for determination of human Myt1 kinase activity.

Joint Meeting DPhG/ ÖPhG 20.09. - 23.09.2011, Innsbruck, Austria:

A. Rohe, F. Erdmann, C. Philipp, G. Al-Mazaideh, C. Goellner, W. Sippl, M. Schmidt:

The human PKMYT1 as a target in G2/M transition: Discovery of new lead structures.

Advances in Microarray Technology, 05.03.2013 - 06.03.2013, Barcelona, Spain:

A. Masch, A. Rohe, M. Schmidt, W. Sippl, V. Schoeppler, J. Jansong, N. Pawlowski, U. Reimer, M. Schutkowski:

Characterizing 'Reader', 'Writer' and 'Eraser' of post-translational modifications by Histone Code Microarrays.

DPhG Annual Meeting 2013, 09.10.2013 - 11.10.2013, Freiburg i. Br., Germany:

A. Rohe, C. Henze, C. Platzer, F. Erdmann, W. Sippl, M. Schmidt:

A fluorescence anisotropy based Myt1 kinase binding assay

Curriculum Vitae

Angaben zur Person:

Name: Alexander Rohe
Geburtstag: 06.11.1985
Geburtsort: Saarbrücken
Staatsangehörigkeit: deutsch
Familienstand: verheiratet

Angaben zur Ausbildung:

1996 – 2005: Gymnasium Johanneum in Homburg/Saar
06/2005: Allgemeine Hochschulreife
07-2005 – 09/2005: Eintritt in die Bundeswehr und allgemeine Grundausbildung
10/2005 – 10/2009: Studium der Pharmazie,
Albert-Ludwigs-Universität Freiburg i. Br.
08/2007: Erster Abschnitt der Pharm. Prüfung
10/2009: Zweiter Abschnitt der Pharm. Prüfung
Abschluss: Staatsexamen
10/2009 – 04/2010: Praktikum nach AAppO, Weinberg-Apotheke, Halle (Saale)
04/2010 – 10/2010: Praktikum nach AAppO und Anfertigen einer Diplomarbeit
in der AG Medizinische Chemie des Instituts für Pharmazie,
Martin-Luther-Universität Halle-Wittenberg,
Leitung: Prof. Dr. Sippl, Abschluss: Diplom-Pharmazeut
11/2010: Dritter Abschnitt der Pharm. Prüfung,
im Anschluss: Erteilung der Approbation als Apotheker
10/2010 – 04/2013: Studium der Lebensmittelchemie,
Martin-Luther-Universität Halle-Wittenberg
Abschluss: Diplom-Lebensmittelchemiker
04/2010 – 05/2013: Promotionsstudent in der AG Medizinische Chemie des
Instituts für Pharmazie, Martin-Luther-Universität Halle-
Wittenberg, Leitung: Prof. Dr. Sippl
Seit 05/2013: Berufspraktische Ausbildung gemäß APVO LMChem in
der amtlichen Lebensmittel- und Bedarfsgegenstände-
überwachung am Landesamt für Verbraucherschutz und
Lebensmittelsicherheit des Landes Sachsen-Anhalt,
Halle (Saale)

Eigenständigkeitserklärung

Hiermit erkläre ich an Eides statt, dass ich die vorliegende Arbeit selbstständig und ohne fremde Hilfe angefertigt habe. Ich habe keine anderen als die angegebenen Quellen und Hilfsmittel benutzt und die den verwendeten Werken wörtlich oder inhaltlich entnommenen Stellen als solche kenntlich gemacht.

Ferner erkläre ich, dass ich mich mit der vorliegenden Dissertation erstmals um die Erlangung eines Doktorgrads bewerbe. Die vorliegende Arbeit ist weder im Inland noch im Ausland in gleicher oder ähnlicher Form einer anderen Prüfungsbehörde zum Zweck einer Promotion oder eines anderen Prüfungsverfahrens vorgelegt worden.

Halle (Saale), 28.08.2013

Alexander Rohe